Oxidation of Benzene in Supercritical Water: Experimental Measurements and Development of an Elementary Reaction Mechanism

by
Joanna L. DiNaro

B.S. Chemical Engineering
University of Colorado at Boulder, 1993

Submitted to the Department of Chemical Engineering
in partial fulfillment of the requirements for the degree of

DOCTOR OF PHILOSOPHY IN CHEMICAL ENGINEERING

at the

MASSACHUSETTS INSTITUTE OF TECHNOLOGY

September, 1999

Signature of Author: _____
Department of Chemical Engineering
September 3, 1999

Certified by: _____
Professor Jefferson W. Tester
Thesis Supervisor

Certified by: _____
Professor Jack B. Howard
Thesis Supervisor

Accepted by: _____
Professor Robert E. Cohen
St. Laurent Professor of Chemical Engineering
Chairman, Committee for Graduate Students

Oxidation of Benzene in Supercritical Water: Experimental Measurements and Development of an Elementary Reaction Mechanism

by
Joanna L. DiNaro

Submitted to the Department of Chemical Engineering on
September 3, 1999 in partial fulfillment of the requirements for the
degree of Doctor of Philosophy in Chemical Engineering

ABSTRACT

Supercritical water oxidation (SCWO) typically refers to a waste treatment or remediation process and derives its effectiveness from the unique solvent properties of water above its critical point. When organic compounds and oxygen are brought together in water well above its critical point of 221 bar and 374°C, the oxidation of the organic is rapid and complete to carbon dioxide and water with heteroatoms such as Cl, S and P converted to their corresponding mineral acids which can be neutralized using a suitable base. The research presented in this thesis addresses the general goal of characterizing the mechanisms and kinetics of reactions of model organic chemicals in supercritical water. This goal is achieved through a detailed experimental and theoretical investigation of the oxidation of benzene, a representative model aromatic compound, in supercritical water. Such basic research benefits the field by providing a better understanding of the SCWO process and can lead to better and more efficient designs of commercial waste treatment systems.

In preparation for experiments on the SCWO of benzene, an investigation was undertaken to characterize the effects of mixing and oxidant choice on laboratory-scale kinetic measurements. The apparent induction time, previously reported in SCWO kinetics of various model compounds measured in the MIT laboratory-scale tubular reactor system, was found to be influenced by the geometry and flow conditions within the mixing region at the reactor entrance. Redesign of this mixing region led to a reduction in the apparent induction time measured during methanol SCWO from 3.2 to 0.7 seconds. In order to realize higher concentrations of oxygen in the reactor, the use of hydrogen peroxide as an oxidant was explored. The oxidation rate of methanol was found to be the same using hydrogen peroxide or dissolved oxygen, thus demonstrating the use of aqueous hydrogen peroxide solutions as a viable means of introducing molecular oxygen *in situ* into the laboratory-scale SCWO reactor system.

Oxidation and hydrolysis reactions with benzene were thoroughly investigated in supercritical water using a laboratory-scale, plug-flow reactor system. Little to no conversion of benzene occurred in supercritical water at temperatures between 530 and 625°C by a hydrolysis pathway (in the absence of oxygen) for residence times up to 6 s. Oxidation reactions were studied at temperatures ranging from 479 to 587°C, pressures of 139 to 278 bar, reactor residence times from 3 to 7 s, and initial benzene concentrations of 0.4 to 1.2 mmol/L, and oxygen concentrations ranging from 40% of stoichiometric oxygen demand to 100% excess oxygen. The oxidation rate was found to be 0.40±0.06 order in benzene and 0.18±0.05 order in oxygen with an activation energy of 240±10 kJ/mol. The primary oxidation product at all reaction conditions and levels of benzene conversion was carbon dioxide. Other important oxidation products were carbon monoxide, phenol

and methane. Trace levels of additional light hydrocarbon gases and single- and multi-ringed aromatic species were detected as well.

Prior to the theoretical investigation of benzene SCWO using an elementary reaction mechanism (ERM), the effects of uncertainty in the input parameters of these ERMs on their predictive capabilities was explored for hydrogen oxidation in supercritical water. Two methods, the Deterministically Equivalent Modeling Method (DEMM) and Monte Carlo simulations, were applied for this purpose. Analysis revealed the presence of considerable uncertainty in the predicted species concentration profiles arising from the reported uncertainties in the forward rate constants and species enthalpies of formation. For example, at the point of maximum uncertainty, the predicted concentrations of hydrogen and oxygen deviated by ±70% from their median values at the upper 97.5% and lower 2.5% probability contours. Model predictions were found to be highly sensitive to two relatively uncertain parameters: the ΔH_f^0 of HO_2 radical and the rate constant for H_2O_2 dissociation.

An elementary reaction mechanism for the supercritical water oxidation of benzene was developed to provide mechanistic insights regarding key reaction pathways. An available, low-pressure combustion mechanism was adapted to the lower temperatures and higher pressures of SCWO through the addition of new reaction pathways and the calculation of the rate constants of pressure dependent reactions using quantum Rice-Ramsperger-Kassel (QRRK) theory. The resulting mechanism, after adjustment, accurately reproduces the experimentally measured benzene and phenol concentration profiles at 540°C and 246 bar with stoichiometric oxygen. Additionally, a comparison of the model predictions to benzene SCWO data measured at conditions other than those to which the model was fit revealed that the model qualitatively explains the trends of the data and gives good quantitative agreement at many conditions. For example, the model predicts the measured benzene conversion to better than ±10% conversion at temperatures between 515 and 590°C at 246 bar with stoichiometric oxygen and at pressures from 139 to 278 bar at 540°C with stoichiometric oxygen. The most important difference between this benzene SCWO mechanism and those previously developed for combustion conditions is the inclusion of reactions involving the C_6H_5OO radical. Without their inclusion, the predicted oxidation rate of benzene was too fast and the concentration of carbon monoxide was incorrectly predicted to exceed that of carbon dioxide.

Thesis supervisors:

Jefferson W. Tester
Herman P. Meissner Professor of Chemical Engineering
Director, MIT Energy Laboratory

Jack B. Howard
Hoyt C. Hottel Professor of Chemical Engineering

ACKNOWLEDGMENTS

Before coming to MIT I received a piece of advice from a professor at the University of Colorado (where I attended undergraduate) that, luckily, I chose to follow. He told me to select my advisor and not my area of research, for a good advisor would make me like any research topic. My research advisors, Professors Jefferson Tester and Jack Howard, created for me a supportive, challenging environment filled with never ending learning opportunities. As a direct result my experiences during the time I spent at MIT performing the research for this thesis were very positive and enjoyable. I will forever be grateful to them for taking me on as their student. Additionally, my tenure at MIT wouldn't have been nearly as enjoyable without the extracurricular activities they supported which included one hundred mile bike rides to Canada and ski trips to New Mexico.

I would like to thank the members of my thesis committee: Professor Paul Laibinis who, as not a researcher in SCWO, provided a much welcomed outside opinion of my work; Dr. William Peters who asked many thought-provoking, insightful questions and was consistently very supportive of my research; and Professor K.C. Swallow who taught me the analytical techniques necessary to complete my research and spent many hours with me in lab preparing samples and running analyses. Many of my research results are a direct result of her contributions. Although not members of my committee, I'd also like to thank Professors Bill Green and Ken Smith for their contributions to the kinetic modeling and the mixing studies in this thesis, respectively.

I'd particularly like to thank the following members of the support staff: Bonnie Caputo of the MIT Energy Laboratory and Elaine Aufiero and Janet Fischer of the Department of Chemical Engineering. These three people, who are instrumental in the day-to-day operations of their respective departments, were continuously a tremendous help to me, and I am very fortunate to have had the opportunity to know and work with them.

As I leave MIT and move on to the real world, as my friends like to call it, I'd like to acknowledge the past and present members of "Group Tester" who I worked with on a daily basis and made my time here much more enjoyable than I ever anticipated. Although we always had a good time working in the lab, the most enjoyable times we spent together were during the biking, hiking, skiing, rafting, and runs-to-Maine-for-lobster trips. I feel very fortunate that I worked with a group willing to participate in such numerous and diverse events outside of the academic arena, and I would like to make a few specific comments about these people.

I am grateful to Matthew DiPippo, Philip Marrone and Brian Phenix who, as senior lab members, taught me literally everything I needed to know in order to conduct research on my own. Matt DiPippo is one of the best teachers I've met, and I thank him for always knowing or knowing how to find the answers to my numerous questions, for pleasantly greeting me in the morning and usually sharing an interesting story, for continuing to provide us with pastries even after he graduated, and for giving me one of my most hilarious memories - that of the time he took out Jeff at Taos. I'm indebted to Phil Marrone for teaching me how to operate the reactor system, helping me interpret my experimental results, always setting aside time for me when I had questions, and for his incredible memory surrounding all of the old pitfalls that had become our reactor systems and the means used to solve them. Also, Phil joins me in my wonderment of why anyone who hates snow chooses to live in New England! I was very fortunate to have had the opportunity to work directly with Brian Phenix for four years. I cannot imagine how I would have completed this thesis without his guidance. Brian taught me how to question the way things were done in the past and the

value of investing a little time in improvements up front to yield great savings in time and effort down the road. I will always feel that I gained much more out of our working relationship than he did. Some of my funniest memories are a direct result of the time we spent together - most notably the paint-in-the-hamburgers incident and the hanging of the no-smoking sign which still remains on Sawin's lab door. Except for the unlikely event that one of his students reads this thesis, they will never discover the culprits.

I'd also like to thank the other members of the lab for their assistance and for creating a productive yet amusing work environment. The phrase "there's one in every crowd" applies to Randy Weinstein better than anyone I've met. Randy never ceased to entertain me, mostly at his own expense, and provided us with stories that we still laugh at when retelling for the twentieth time. Randy has since gone on to become a professor of chemical engineering, and I have no doubt he'll be as successful at that as he's been at everything else he's attempted. Josh Taylor is one of the most intelligent people I've ever met, but to his credit you wouldn't guess it just by talking to him - and that's not supposed to be an insult! I always enjoyed being around him in lab and could depend on him to join me for coffee or ice cream breaks and on the various excursions outside of lab. I wish him the best in his remaining time here, after which I'm going to try to keep him from moving back to California. I'd like to thank Jason Cline for educating me in the world of Unix, for joining me in my belief that Macs are superior to windows-based machines, for sharing with me all of his intriguing conspiracy theories and for being one of the most thoughtful people I have met. Matt Reagan also helped answer my countless questions regarding Unix, but more importantly Matt shares my love of hiking and skiing and was the only other group member who would ski Tuck's in the spring. Marc Hodes and I shared hours of interesting conversation, and he is the first person I turn to for advice on restaurants. Marc was especially helpful to me when I was searching for a job. Mike Kutney was a tremendous help to me when setting up our in-lab computer network, in the installation of new computer hardware and software, and with general computer maintenance. I respect him both for his intelligence and for taking the time to start a family while in graduate school. Mike Timko, Zhitao Cao and Neda Vukmirovic are the newest members of our lab. Mike is already off to a wonderful start and is much farther ahead of where I was at the same time in my Ph.D. tenure. I fully believe Mike will become famous for some great invention down the road. Zhitao has perhaps more energy than anyone I've ever met and, as a result, I know he'll be successful here at MIT. Neda is assuming the role as the sole female in the laboratory group. For that and in her research, I wish her luck! We were fortunate to have Dolors Salvatierra and Frederic Vogel join our group as post doctoral students. Dolors was the only other woman I had sustained contact with during my time at MIT. I greatly enjoyed her friendship and cherished the advice she gave me. Frederic and I worked together directly during the latter part of my research, and I benefited from his intelligence, technical judgment and from his positive attitude. I hope to visit him at his home in Switzerland some day. Finally, although not official members of Group Tester, Dave Kronholm, Carlo Procaccini and Henning Richter were all very helpful in different aspects of my research and also good friends to me.

Finally, I'd like to thank those people who are part of my other life. My wonderful friends from CU: MaryBeth, Traci, Adam, Mike B., Mike C., Larry and Robb give me that yearly ski trip to work for. My good friends Jess and Scott, Adrienne and Steve, and Jen and Steve (and Nicholas) make my life outside of MIT so enjoyable. Without the love, support and encouragement from my parents, Gail and Santo, I wouldn't have made it to where I am today, and I am especially grateful to them for keeping me "in the lifestyle to which I would like to become accustomed." Lastly, I'd like to thank my sister, Kimberly, for always being my biggest fan and my husband, Scott, for always thinking more of me than I think of myself.

~TABLE OF CONTENTS~

~LIST OF FIGURES~

~LIST OF TABLES~

Chapter 1.

Introduction and Background

1.1 Supercritical Fluids

The term "supercritical" simply means that a substance is above its critical temperature (T_c) and critical pressure (P_c). The shaded area of the generic P-T phase diagram in Figure 1-1 shows the supercritical region for a pure substance. To understand a supercritical fluid, first consider a pure liquid in equilibrium with its vapor phase in a closed container. This equilibrium system corresponds to any point on the vapor-liquid coexistence curve of Figure 1-1. Along the coexistence curve towards the critical point, the temperature and pressure both increase in order to maintain equilibrium. The density of the gas increases due to the increasing pressure, and the density of the liquid decreases slightly due to thermal expansion. The density of the liquid continues to decrease and that of the gas continues to increase until the critical point is reached. At the critical point, the density of the gas and liquid are equal, and there is no longer a distinction between the liquid and vapor as the phase boundary disappears. At higher temperatures and

Table 1-1. Critical parameters of common compounds

Compound	Critical Temperature (°C)	Critical Pressure (bar)
carbon dioxide	31.1	73.9
ethane	32.3	49.4
ethylene	9.3	51.2
propane	96.7	42.5
methanol	239.5	81.0
toluene	318.6	41.1
water	374.2	221.2

pressures, above T_c and P_c, a supercritical fluid state exists. The T_c and P_c vary significantly for different chemical species. Table 1-1 displays critical constants for some familiar compounds.

A substance's physical properties at or above the critical point can be much more complex than the apparently simple definition of a supercritical fluid ($T>T_c$, $P>P_c$) may imply. A substance above its critical point is neither considered a liquid nor a gas, but instead a dense fluid. A supercritical fluid remains in a single phase at any pressure and temperature combination above the T_c and P_c. In this region the substance's density and other physical properties vary widely with P and T, but usually are intermediate to those of a liquid and a gas at conditions of practical interest. Table 1-2 lists selected physical properties of supercritical fluids as compared to those of liquids and gases (Squires *et al.*, 1983). Supercritical fluids (SCFs) are about a factor of ten less dense than typical liquids, but still two orders of magnitude more dense than gases. SCFs have lower viscosities and higher diffusivities than liquids. Therefore, the density of SCFs is still high enough that they have liquid-like solvation power, yet the environment is gas-like with respect to mass-transfer rates. These properties make supercritical fluids attractive for chemical separations and reaction applications.

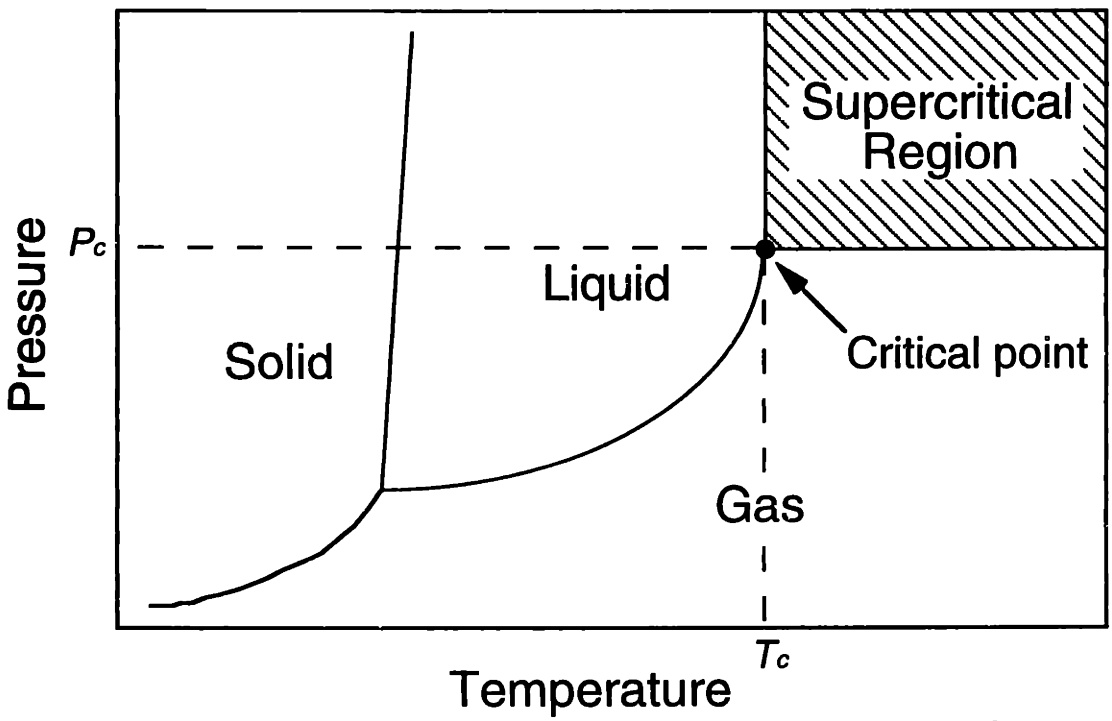

Figure 1-1 Generic pressure-temperature diagram of a pure substance with the supercritical region highlighted

Table 1-2. Comparison of the physical properties of gases, liquids and supercritical fluids (SCF)

Property	Phase		
	Gas	SCF	Liquid
Density (g/mL)	10^{-3}	10^{-1}	1
Viscosity (Pa s)	10^{-5}	10^{-4}	10^{-3}
Diffusivity (cm^2/s)	10^{-1}	10^{-4}	10^{-5}

Carbon dioxide is by far the most common SCF in industrial practice (McHugh and Krukonis, 1994). Supercritical CO_2 is most often used in extraction processes. In fact, the decaffeination of green coffee beans is accomplished using supercritical CO_2. The critical constants of CO_2 (31°C, 74 bar) are mild, CO_2 is cheap and nontoxic, and CO_2 has the advantage of being a gas at ambient conditions making it easy to separate CO_2 from the products. Recently, supercritical CO_2 started receiving attention as an environmentally benign replacement solvent for organic synthesis (for e.g., see DeSimone *et al.*, 1992; Weinstein *et al.*, 1996).

Like CO_2, water is an inexpensive, nontoxic solvent in its supercritical state. From Table 1-1 the critical temperature and pressure of water are high relative to other solvents. Since many organic compounds are thermally unstable at these conditions, supercritical water is not as good a medium for synthesis or extraction processes as is supercritical CO_2. Instead, the most promising application of supercritical water is as a medium for the destruction of hazardous organic chemicals by oxidation. Supercritical water (SCW) is usually a convenient solvent for hazardous waste remediation processes since many industrial wastes are in the form of aqueous solutions. Additionally, clean water is one of the final products and can be recycled or reused.

Supercritical water has disparate solvent properties from those of ambient water: while water readily dissolves salts but exhibits a low solubility towards hydrocarbons and gases at ambient conditions, hydrocarbons and gases are soluble in SCW in all proportions whereas salts are practically insoluble. As a result supercritical water commanded much attention over the past decades as applications for these unique properties were explored. What leads to these drastically different solvation properties? To understand the change in water's solvent properties in going from sub- to supercritical, it is instructive to first consider the structure of water at ambient conditions.

The molecular structure of water leads to complex solvating behavior. For example, water forms hydrogen bonds that consist of a dipole-dipole interaction between the H atom in a polar

bond (*e.g.*, O-H or N-H) and an electronegative atom such as O, N, or F. In ice, each O atom is bonded to four H atoms by two covalent bonds and two hydrogen bonds. This equality in the number of H atoms and lone pairs is not characteristic of NH_3, HF or any other molecule capable of hydrogen bonding. These other molecules can form rings or spheres, but not the highly-ordered, three-dimensional structures that water forms. In the three-dimensional structure of ice, the hydrogen bonding network keeps the water molecules further apart from each other than they are in liquid water, and as a result ice is less dense than liquid water. Were it not for the ability of water to hydrogen bond, water would be a gas at ambient conditions, bodies of water would freeze from the bottom up, and life as we know it on earth could not exist.

When ice melts water maintains a portion of this three-dimensional structure, and the average number of hydrogen bonds per water molecule is about 3.5. Because the hydrogen bonding network is maintained of, water under ambient conditions is a polar solvent. In order for a substance to dissolve in water, some hydrogen bonds between water molecules must be broken to make room for the solute, and this requires energy. Unless this energy is recovered in interactions with the solute, solubilization will not occur. Water exhibits a high solubility to alcohols because the -OH group can donate and accept hydrogen bonds. Ethers, which can only accept hydrogen bonds, are less soluble as only a portion of the energy is recovered in the solvation process. Alkanes and alkyl chlorides, which can neither accept nor donate hydrogen bonds, are only sparingly soluble in water.

Above the critical point where densities are lower than in the liquid state and temperatures are higher, each water molecule contains enough kinetic energy to disrupt the highly-ordered hydrogen bonding network. There is no longer an energetic constraint to dissolving hydrocarbons. Due to the loss of order, water no longer shields the charge on dissolved ions from one another and cannot solvate ions. As a result, salts exist as associated ion pairs and will precipitate from SCW.

These changing solvent properties are captured by two parameters: the static dielectric constant (ε) and the ion product of water (K_w). The static dielectric constant (Uematsu and Frank, 1980) and the ion product of water (Marshall and Franck, 1981) are plotted along with density (ρ) as a function of temperature at 250 bar in Figure 1-2 and Figure 1-3, respectively; 250 bar is a typical operating pressure of SCW processes. The ε, K_w, and ρ all undergo drastic changes in the transition region from sub- to supercritical. The ρ decreases from its ambient value of 1 g/mL to 0.1

g/mL or less in the supercritical region, ε decreases from 80 to 1-2, and K_w decreases approximately 10 orders of magnitude from $1x10^{-14}$ to $1x10^{-24}$ at supercritical conditions.

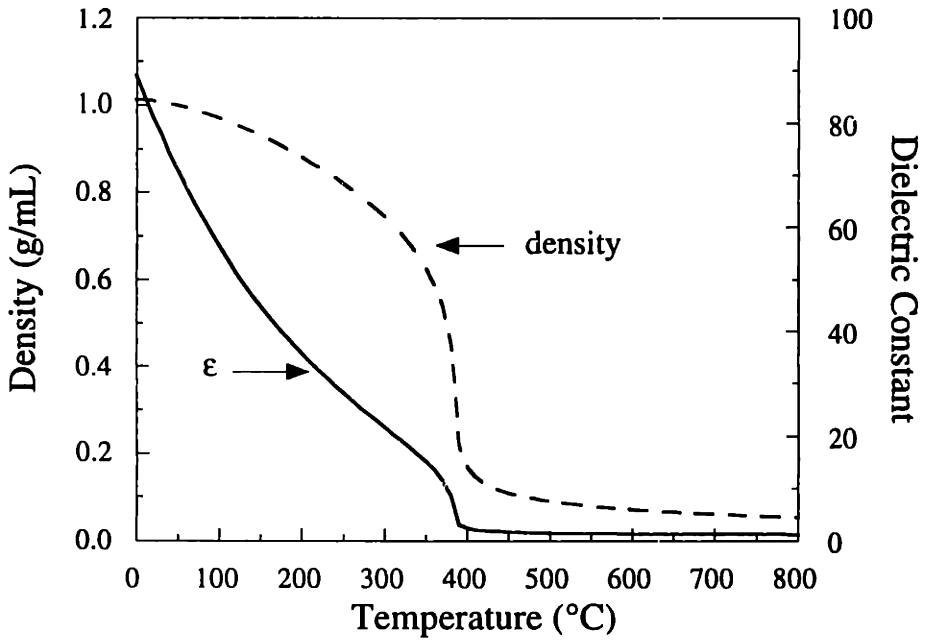

Figure 1-2 Static dielectric constant and density of water as a function of temperature at 250 bar

The static dielectric constant is a measure of the polarity of the solvent. As a rule of thumb, non-polar solvents have a dielectric constant below 20. The change in water from a polar to a non-polar solvent is apparent in Figure 1-2 during the transition from sub- to supercritical temperatures. Ambient water has a high ε due to its highly ordered structure resulting from the hydrogen bonding network. The drastic decrease of ε reflects the fact that SCW is largely a disordered fluid.

In addition to being a measure of solvent polarity, the dielectric constant is also a measure of a solvent's ability to separate ions. When ions dissociate in solution, each ion moves independent of every other in solution and is surrounded by several solvent molecules. A solvent dissolves ionic compounds by first separating the ions and then solvating them. The dielectric constant determines the ability of a solvent to separate these ions. With such a low dielectric constant, water can no longer separate charged species.

K_w is the product of $[OH^-]$ and $[H^+]$. The ten order of magnitude decrease in K_w demonstrates the inability of SCW to support individual charged ions. At ambient temperatures water has a $K_w=1x10^{-14}$ (hence, $[H^+]=1x10^{-7}$ and $pH=-\log[H^+]=7$). In the supercritical region

K_w=1x10^{-24}, and water is essentially in an undissociated, molecular form. Likewise, salts which are soluble in ambient water will not dissociate into their constituent ions under supercritical conditions and are insoluble. Acids, too, exist in molecular form. Since SCW will not solvate ions, free radical reactions are favored over ionic reactions.

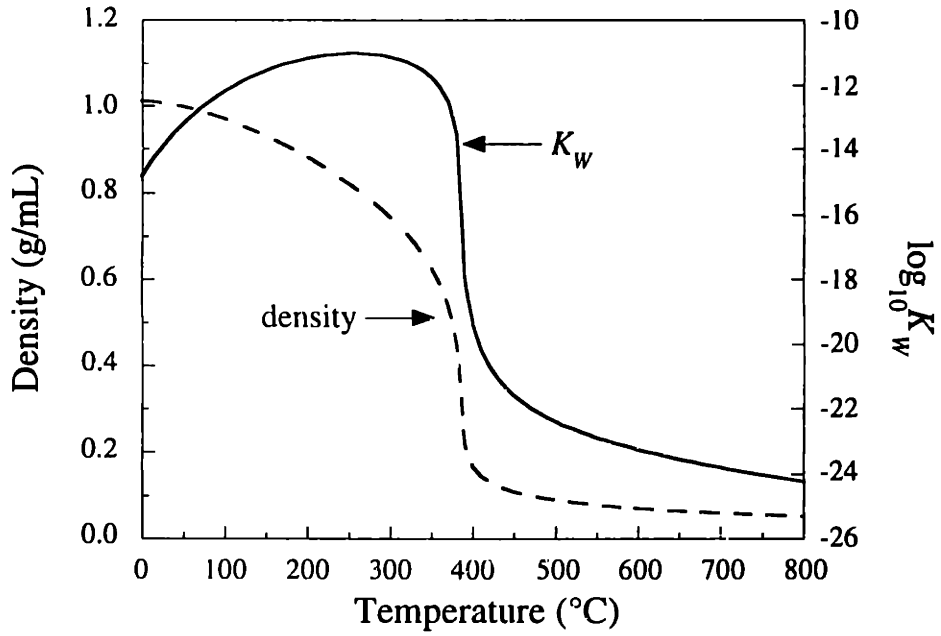

Figure 1-3 Density and the ion product of water as a function of temperature at 250 bar

1.2 The Supercritical Water Oxidation Process

The supercritical water oxidation (SCWO) process typically refers to a waste treatment or remediation process and derives its effectiveness from the unique solvent properties of water well above its critical point of 221 bar and 374°C. The process usually operates between 450 and 600°C and 250 to 280 bar. At these conditions, both organic compounds and oxygen are completely soluble, and the temperature is high enough that free radical oxidation reactions proceed rapidly. When organic compounds and oxygen are brought together in SCW, the organic oxidizes rapidly and completely (>99.99% destruction with less than one minute residence times) to CO_2 and H_2O. If any nitrogen is present, either introduced with the waste or if air is used as the source of O_2, the resulting product is N_2 or N_2O (Killilea and Swallow, 1992). NO_x and SO_x gases, typical undesired by-products of combustion processes, are not formed because the temperature is too low for these oxidation pathways to be favored. Any N_2O found can be catalytically converted to N_2.

Heteroatoms (*e.g.*, chlorine, phosphorous, sulfur) react to form their corresponding mineral acids. With the addition of a suitable base, acids are neutralized and form their corresponding salts which precipitate out of the reacting mixture allowing for their removal.

1.2.1 Applications

As noted previously, due to the severe critical parameters of water, supercritical water is not a feasible solvent for extraction or synthetic reactions, but instead its most promising application is as a medium for the oxidation of organic hazardous wastes. The supercritical water oxidation process resembles incineration in that free radical reactions are the primary mechanism for oxidation, and the final products are CO_2 and H_2O. The main benefits of SCWO over incineration are that the density is considerably higher and can allow complete containment of the reaction, SCWO requires a much lower fuel concentration to be self-sustaining, and NO_x gases are not produced. Additionally, justly or not, incineration has earned an unfavorable reputation, and the construction of new incinerators to handle the increasing load of hazardous wastes is often not acceptable to the public.

Traditionally, a large quantity of hazardous wastes have been landfilled, both in this country and abroad. Landfills are becoming less abundant, more expensive, and are often not an appropriate means of waste disposal. In Europe and Japan the landfill dilemma is even more severe than in this country. Due to the poor reputation of incineration and the need for an alternative to landfilling, SCWO has been under development as a means for hazardous waste destruction for the last two decades.

In economic terms, the market for SCWO is the treatment of difficult-to-dewater aqueous wastes containing 1-25 wt% organic. In-depth economic evaluations of SCWO are available (for e.g., see Thomason and Modell, 1984; Modell, 1989; Modell *et al.*, 1995). Below 1 wt% organic, bioremediation or activated carbon treatment are generally more economical than SCWO. The main cost associated with activated carbon treatment is incurred during the regeneration of the carbon. Since concentrated waste streams rapidly saturate the carbon, carbon treatment is only economically feasible for dilute aqueous wastes. The bioremediation process generally requires a well-characterized waste for optimal performance. If the waste contains chemicals that are incompatible with the bacteria used for bioremediation, the chemicals will not be destroyed or, worse, the bacteria

may die rendering the entire process ineffective. SCWO, on the other hand, indiscriminately oxidizes all organic compounds provided proper reactor conditions. Incineration has the economic advantage in treating concentrated wastes. Due to the strong public opposition toward incineration, SCWO may make sense particularly for very hazardous materials where by-products are of public concern even if the economics are not favorable.

The effectiveness of SCWO as a hazardous waste treatment technology has been proven by both academic and industrial researchers. These researchers showed that SCWO indiscriminately and rapidly destroys a broad spectrum of organic wastes. The chemical-related industries within the US generate more the 300 million tons per year of aqueous hazardous wastes, and more than 90% of the total hazardous waste generated by these industries is aqueous (Modell *et al.*, 1995). SCWO has been shown to be effective in treating toxic chlorinated chemicals such as polychlorinated biphenyls (PCBs) (Staszak *et al.*, 1987) and the pesticide DDT (Modell *et al.*, 1992), bacteria and dioxins (Thomason *et al.*, 1990), process waste waters (Li *et al.*, 1993a; Sawicki and Casas, 1993), and pharmaceutical and biopharmaceutical waste (Johnston *et al.*, 1988). Compounds which are problematic to recycle or dispose due to the formation of hazardous by-products and residues such as the polymer polyvinylchloride (PVC), the flame retardant tetrabromobisphenol A, and the chlorocarbons γ–hexachlorocyclohexane and hexachlorobenzene, are completely oxidized without hazardous by-product formation (Hirth *et al.*, 1998). The massive quantities of aqueous sludges resulting from wastewater treatment by bioremediation which are difficult to dewater beyond 30% solids (Modell *et al.*, 1995) have been traditionally landfilled. Municipalities and the pulp and paper industry generate the greatest amount of these sludges. Municipalities generate more than 7 million tons per year of dry solids in the US and another 7 million tons per year in the European Union, while the pulp and paper industry generates 28 million dry tons per year (Modell *et al.*, 1995). SCWO has been shown effective in the treatment of a highly contaminated activated sludge (Shanableh, 1995), municipal sludges (Shanableh and Gloyna, 1991; Tongdhamachart and Gloyna, 1991; Goto *et al.*, 1997), sludges from the pulp and paper industry (Modell, 1990; Modell *et al.*, 1992; Modell *et al.*, 1995), and a combination of sludge from a primary clarifier mixed with effluent from a bleach plant and a decant of pond sludge (Cooper *et al.*, 1997). Additionally, wastes which are typically treated by a bioremediation process, such as urea (Timberlake *et al.*, 1982), human

waste (Hong *et al.*, 1987; Hong *et al.*, 1988), and waste from manned space missions (Takahashi *et al.*, 1988) are all destroyed by SCWO.

While SCWO is shown effective in treating a wide range of organic wastes resulting from numerous processes, an important driving force in the development of the SCWO process has been the identification of SCWO as a promising alternative technology to incineration for the destruction of the nation's chemical weapons stockpile (NRC, 1993). Approximately 25,000 tons of chemical weapons is slated for destruction by 2006. Originally in 1982, these weapons were to be incinerated at each of the eight storage sites in the continental US (Umatilla DA, Oregon; Tooele AD, Utah; Pueblo DA, Colorado; Pine Bluff Arsenal, Arkansas; Newport AAP, Indiana; Lexington Blue Grass DA, Kentucky; Anniston AD, Alabama; and Aberdeen PG, Maryland)[1] and on Johnston Island in the Pacific. Due to operational problems at the Johnston Island incinerator, the increasingly poor public perception of incineration, and the unanticipated local public opposition to building new incinerators at the remaining storage locations, the Army was forced to consider alternative methods for destroying these weapons in the early 1990's (U.S. Congress, 1992). In this report, SCWO was selected as one of four possible alternative technologies. As a result of the need to assess the SCWO process, the US Army Research Office has funded basic research on SCWO at MIT and several other universities through the University Research Initiative (URI) program.

The nerve agents (organophosphates) VX ($C_{11}H_{26}NO_2PS$) and GB (Sarin; $C_4H_{10}FO_2P$) and the blister agents H, HD and HT mustard gas where H=$C_4H_8Cl_2S$ and T=$C_8H_{16}Cl_2OS_2$ are distributed amongst the eight storage locations in the continental US. About 42% of the total 25,000 tons of agent are located at the Tooele AD, about half of the 3,700 tons of propellant are between the Umatilla DA and Pine Bluff Arsenal, and the 1,558 tons of explosive are about equally distributed between the eight locations. Since it is generally regarded that the stockpiles from the eight separate locations cannot be consolidated at one facility due to the potential for a catastrophic accident during transport, treatment must occur on-site. Therefore, using one technology that can treat all of the constituents at a particular location would be ideal. Supercritical water oxidation has been shown effective for destroying the stockpiled chemical warfare agents (Downey *et al.*, 1995; Spritzer *et al.*, 1995; Snow *et al.*, 1996), propellants and energetics (Buelow, 1990; Buelow, 1992;

[1] AD=Army Depot, ADP=Army Ammunition Plant, DA=Depot Activity, PG=Proving Ground

Harradine *et al.*, 1993; Spritzer *et al.*, 1995), and military smokes and dyes (Robinson, 1992; Rice *et al.*, 1994; Lajeunesse and Rice, 1997).

Because of the ability of SCWO to destroy broad classes of organic wastes and its ability to destroy chemical warfare agents, the three branches of the military are building SCWO units for their purposes. The US Navy is developing compact SCWO units for the on-board treatment of hazardous wastes (Kirts, 1995). The US Army commissioned Foster Wheeler Development Corporation in conjunction with Sandia National Laboratories and Gencorp Aerojet to build a SCWO facility at the Pine Bluff Arsenal in Arkansas for destroying smokes, dyes, and pyrotechnics (Haroldsen *et al.*, 1996a; Haroldsen *et al.*, 1996b). The Army is also undergoing testing of an SCWO facility built by General Atomics in Toole, Utah for treating VX and GB. The US Air Force awarded a contract to General Atomics to design a plant for destroying solid rocket propellant (Hurley, 1996).

1.2.2 Process Description

The SCWO process typically operates between 450 and 600°C and around 250 bar. Figure 1-4 shows a schematic of a general SCWO process. The aqueous waste stream containing the organic is pressurized and preheated to reactor conditions. The oxidant stream, which can be an aqueous solution of hydrogen peroxide, pure oxygen, or air, is pressurized and mixed with the organic stream. The one-phase mixture of water, organic and oxidant enters the reaction zone, where the residence time is typically less than one minute. During the reaction, the organic is oxidized completely to CO_2, H_2O, and possibly N_2 and N_2O should any nitrogen be present in the feed. Because of the relatively low temperature, NO_x and SO_x gases are not formed. Any heteroatoms present in the feed can be precipitated as salts, and the solid salts must in some way be removed from the reactor. The single-phase effluent then enters a heat recovery system, whereby the heat generated from the highly exothermic oxidation reactions is recovered and used to preheat the reactor feeds. In most cases the SCWO process operates autothermally and needs no auxiliary fuel. The cooled effluent then goes through a pressure letdown system. The resulting gas and liquid product streams rarely require any post processing. In certain situations, they may undergo final effluent polishing to remove any suspended solids or conversion products.

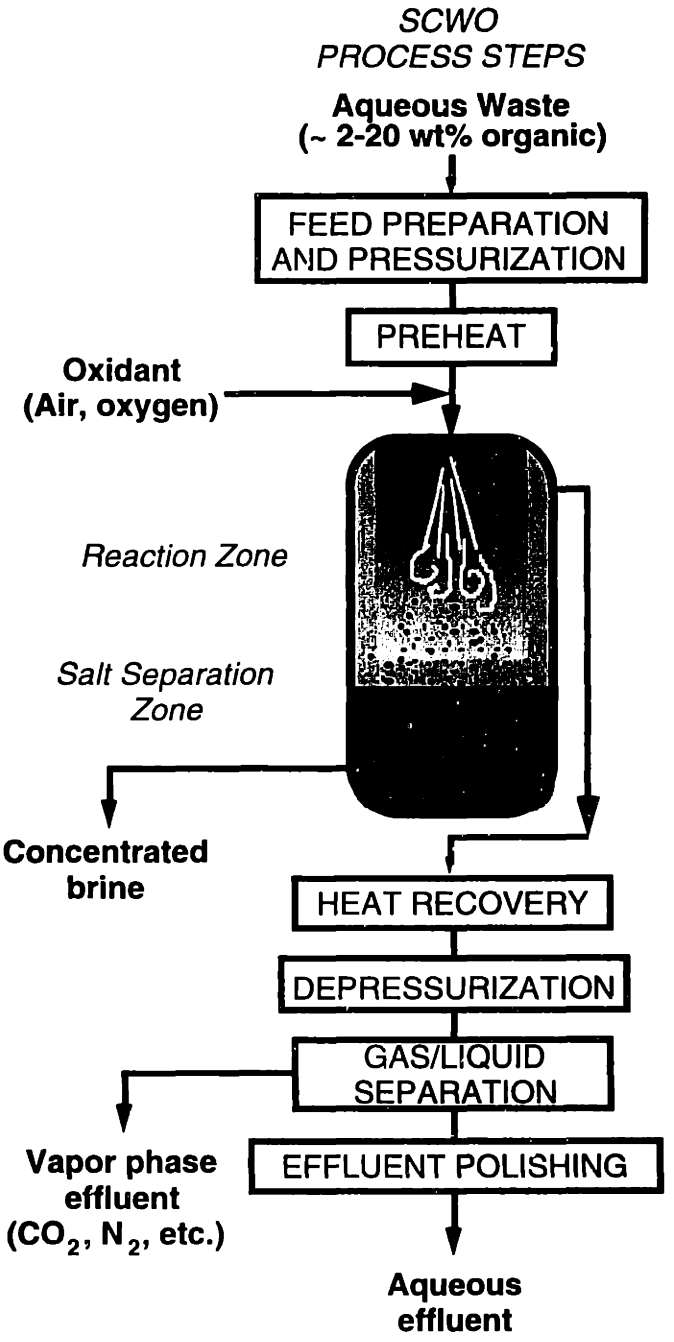

Figure 1-4 Schematic of a typical SCWO process

1.2.3 Industrial Status

The promotion of SCWO for treating industrial wastes has also met with limited success. MODAR, Inc., the first company to attempt to exploit the technology commercially, performed extensive studies of destruction efficiencies for organic compounds in the 1980's and early 1990's in an attempt to validate the SCWO process and develop large-scale reactor systems for treating industrial wastes. MODAR, Inc., was acquired by General Atomics in 1996, but General Atomics is currently only using the technology for treating military wastes. MODEC, Inc., another early company, designed a SCWO reactor system capable of avoiding the salt plugging problems and eliminating corrosion issues for many wastes. In 1994 Eco Waste Technologies started-up the world's first commercial SCWO facility for treating industrial wastewaters at Huntsman Corporation in Austin, Texas (McBrayer *et al.*, 1996). Eco Waste Technologies has since sold its SCWO design to a European company, but the Austin plant is still in operation.

The SCWO process does suffer from some significant, but not insurmountable, shortcomings. The main drawbacks are 1) the high operating pressures, 2) possible plugging of the reactors due to salt formation, 3) corrosive behavior under certain T-P-x_i conditions and 4) pre-commercial higher processing costs. With active research underway to understand and resolve the problems of plugging from salts and corrosion, the development of novel reactor designs to alleviate these problems and the disappearance of landfills, SCWO may yet become a viable waste treatment option for industrial wastes and find a niche market in the US or abroad. An even more serious problem facing SCWO having nothing to do with the process itself, is the unwillingness of US industries to invest in novel, and potentially superior, waste treatment technologies. This barrier will likely prove more difficult than the technical problems facing SCWO. Regulatory pressure does not suffer from these constraints, and changes in industrial effluent discharge regulations may be needed. The success of SCWO in treating the military wastes will be important for its industrial acceptance.

1.3 Overview of Previous Basic Research on SCWO

While both academic and industrial researchers have demonstrated that SCWO will completely oxidize a wide range of organics, such studies where the primary intent was to determine destruction efficiencies yielded little insight about the SCWO process at a molecular level. In

addition to the DRE studies referenced in Section 1.2, many researchers, primarily at universities and government research laboratories, are carrying out basic research on SCWO. Several of these researchers have published comprehensive surveys of the research on supercritical water and reactions in supercritical water and more generally in supercritical fluids. Tester *et al.* (1993a) reviews SCWO fundamentals, commercial development, critical engineering and performance issues (*e.g.*, salt formation, materials selection, ...), and the basic and industrial research on SCWO. Gloyna and Li (1995) overview the engineering aspects of SCWO. The review of Savage *et al.* (1995) covers reactions in supercritical fluids, and the recently published subsequent review (Savage, 1999) surveys organic reactions in SCW. For a detailed account of the SCWO literature, the interested reader is referred to these publications. The review of the literature that follows is provided to acquaint the reader with the focus of basic research and recognize the major contributors in the area of SCWO.

The research effort at MIT emphasizes the hydrolysis (reaction in the absence of oxygen) and oxidation of simple organic compounds in supercritical water. The simple organic compounds, referred to as "model compounds," were selected for study because they either common intermediates in the oxidation of more complex compounds, are simulants for hazardous chemical compounds, represent wide classes of organic chemical, or are characteristic chemical wastes. Comprehensive studies of oxidation and hydrolysis rates were performed on carbon monoxide (Helling and Tester, 1987; Helling and Tester, 1988; Holgate *et al.*, 1992; Holgate and Tester, 1994a; Holgate and Tester, 1994b), ethanol (Helling and Tester, 1988), ammonia (Helling and Tester, 1988; Webley *et al.*, 1990; Webley *et al.*, 1991), methane (Webley and Tester, 1991), methanol (Webley and Tester, 1989; Webley *et al.*, 1990; Webley *et al.*, 1991; Tester *et al.*, 1993b), hydrogen (Holgate and Tester, 1993; Holgate and Tester, 1994a; Holgate and Tester, 1994b), glucose (Holgate *et al.*, 1995), acetic acid (Meyer *et al.*, 1995), thiodiglycol (Lachance *et al.*, 1999), and methylene chloride (Marrone *et al.*, 1995; Marrone *et al.*, 1998a; Marrone *et al.*, 1998b). Many of these model compounds exhibited overall first-order kinetic behavior under oxidative conditions. Figure 1-5 shows our experimental SCWO data in the form of an assumed first-order Arrhenius plot for selected model compounds. Recently, Phenix (1998) reinvestigated methanol oxidation kinetics for the purposes of studying mixing effects, evaluating the use of hydrogen peroxide as an

alternative oxidant, and performing a direct comparison of kinetic data measured at MIT and independently gathered at Sandia National Laboratories.

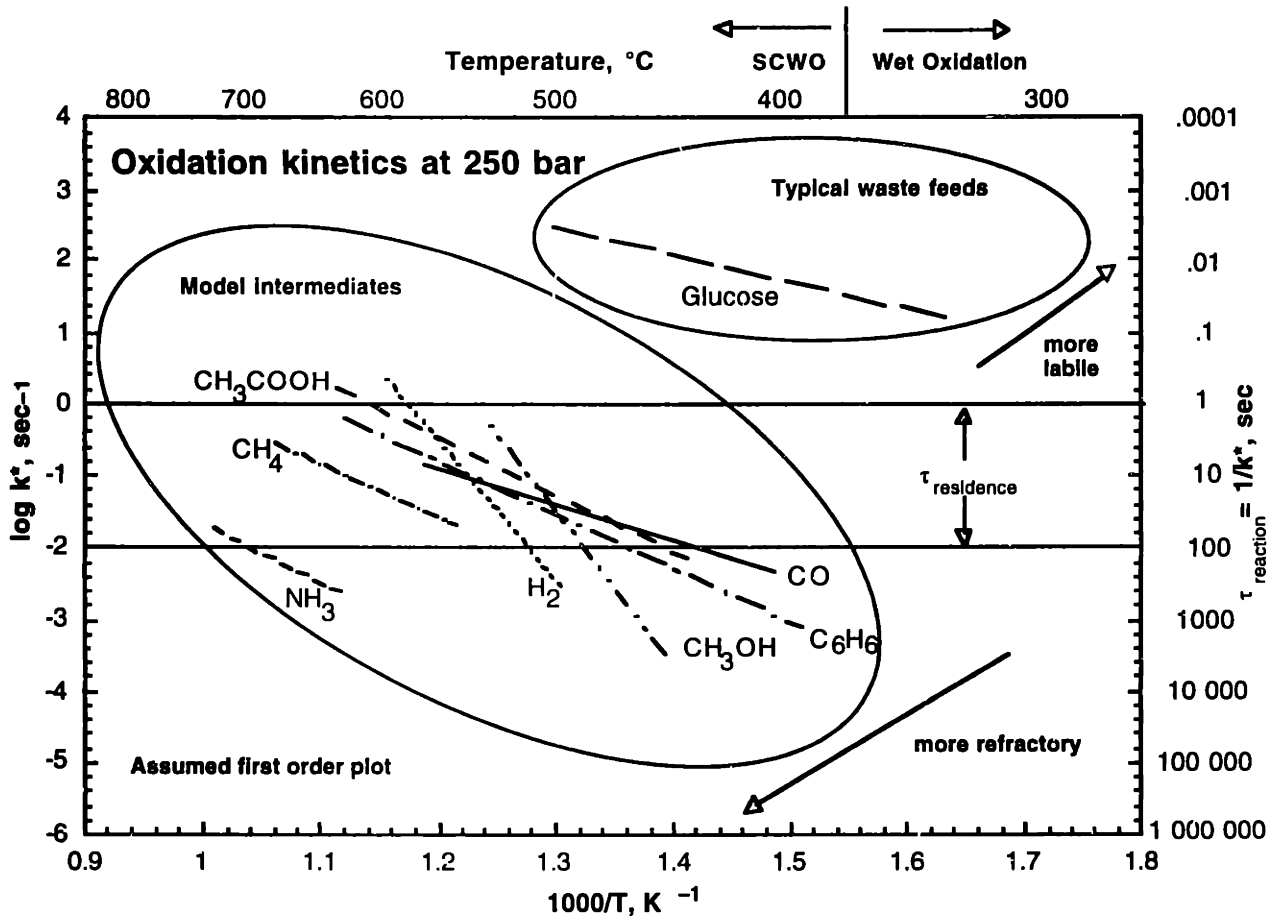

Figure 1-5 First-order Arrhenius plot for the SCWO of some typical model organic compounds

Our research on SCWO kinetics has three major objectives. First, we measure oxidation rates of the model compounds under well-defined conditions of temperature, pressure, concentration, and residence time and use these data to develop global reaction rate expressions. These rate expressions are useful in designing reactors. Second, we identify and quantify the partial and final oxidation products and determine how the distribution of species changes with the above mentioned experimental variables. Finally, we attempt to discern and model the complete reaction network, both on a global (Marrone *et al.*, 1998b) and elementary reaction level (Holgate and Tester, 1993; Holgate and Tester, 1994b; Phenix *et al.*, 1998). Our group also examines other critical aspects related to the commercialization of SCWO technology such as: salt formation and

deposition (Armellini *et al.*, 1994; DiPippo *et al.*, 1999); modeling the phase behavior of salt/water systems using *ab initio* calculations (Tester *et al.*, 1998; Reagan *et al.*, 1999); corrosion and materials selection (Peters, 1996); and SCW thermodynamic *PVT* property measurement and estimation (Kutney *et al.*, 1997).

Savage and coworkers at the University of Michigan have extensively studied the oxidation reactions of primarily aromatic, chlorinated and nitrogenated species in supercritical water, determining global rate expressions, performing extensive analyses of the reaction intermediaries, and discerning global and elementary reaction networks. Using data from their tubular-flow and batch reactors at near-critical and supercritical conditions, Savage *et al.* developed global rate expressions for the SCWO of phenol (Thornton and Savage, 1992; Gopalan and Savage, 1995b), 2-chlorophenol (Li *et al.*, 1993b), CH_3-, CHO-, OH-, OCH_3-, NO_2-, C_2H_5-, and CH_3CO-substituted phenols (Martino *et al.*, 1995; Martino and Savage, 1997b; Martino and Savage, 1997a; Martino and Savage, 1999b; Martino and Savage, 1999a), acetic acid (Savage and Smith, 1995), and methanol (Brock *et al.*, 1996). The thermal decomposition of formic acid was also studied (Yu and Savage, 1998). In addition to the development of these global models, Savage and company use elementary reaction mechanisms to model their oxidation data (Brock and Savage, 1995; Gopalan and Savage, 1995a; Brock *et al.*, 1996; Savage *et al.*, 1998). Savage's research group also uses molecular dynamics simulations to investigate hydrogen bonding in SCW (Mizan *et al.*, 1995; Mizan *et al.*, 1996) and to predict dielectric constants, self-diffusion coefficients for supercritical water, fugacity coefficients of radical species, and pressure-temperature-density relationships (Mizan *et al.*, 1996; Mizan *et al.*, 1997a; Mizan *et al.*, 1997b).

At the University of Delaware, Klein and coworkers study primarily hydrolysis reactions in SCW measuring apparent first-order rate constants and monitoring reaction products. Recently, they investigated the effects of the reactor surface-to-volume ratio, reactor usage history and reactor material on benzonitrile hydrolysis (Harrell *et al.*, 1999). They found that benzonitrile kinetics and product yields were not influenced by these factors leading to the conclusion that laboratory-deduced rate constants will provide accurate models which are scaleable to commercial conditions. Previously, they studied explosive simulants in SCW including nitroanilines (Wang *et al.*, 1995), 1-nitrobutane (Iyer *et al.*, 1996), and butyronitrile (Iyer and Klein, 1997). Additional studies include those on the hydrolysis of benzylphenylamine (a coal model compound) (Abraham and Klein,

1985; Abraham and Klein, 1987), phenyl ethers (Townsend *et al.*, 1988), and substituted anisoles (Klein *et al.*, 1992). Boock and Klein (1993) performed an oxidation study of C_1-C_3 alcohols and acetic acid in sub- and supercritical water. Reactivities and product spectra were monitored, and a detailed mechanism and lumped model were developed to represent the data. Also at the University of Delaware, Brill and coworkers are studying oxidation and hydrolysis in SCW using *in situ* spectroscopic techniques. This *in situ* monitoring of reactions allows measurement of real-time data and determination of the apparent activation energy, preexponential factor, induction times and product profiles. Urea (Kieke *et al.*, 1996), hydroxylammonium nitrate and ammonium carbonate (Schoppelrei *et al.*, 1996a), ethylenediammonium nitrate (Maiella and Brill, 1996a), guanidinium nitrate (Schoppelrei *et al.*, 1996b), and malonic acid (Maiella and Brill, 1996b) are among the model compounds investigated.

Houser *et al.* at Western Michigan University have focused on reactions in SCW without oxidant of various organic compounds containing heteroatoms to determine if, and under what conditions, SCW may aid in the removal of those atoms and lead to less hazardous and possibly useful by-products. Decomposition rates were studied for 1-chloro-3-phenylpropane, 2-chlorotoluene and 4-chlorophenol (Houser and Liu, 1996), several aromatic compounds (Tsao *et al.*, 1992), quinoline and isoquinoline (Houser *et al.*, 1986), and N, S, and O containing organic compounds (Houser *et al.*, 1993).

Several other universities have established research programs contributing to a fundamental understanding of reactions in SCW. Early research at the University of Illinois conducted by Yang and Eckert (1988) focused on the oxidation of *p*-chlorophenol with and without catalysts. Later, van Swol and Eckert (1990) conducted solubility and spectroscopic measurements on the supercritical fluid extraction of coal and coal model compounds. Gloyna's research group at the University of Texas at Austin have examined many aspects and phenomena associated with supercritical water, including the oxidation kinetics and/or destruction efficiencies of several model compounds including phenol and *n*-octanol (Li *et al.*, 1997), pyridine (Crain *et al.*, 1993), dimethyl methylphosphonate (McKendry *et al.*, 1994), dinitrotoluene (Li *et al.*, 1993a), acetamide (Lee and Gloyna, 1992), 2,4-dichlorophenol (Lee *et al.*, 1990), and acetic acid (Wilmanns and Gloyna, 1990; Frisch and Gloyna, 1992; Chang *et al.*, 1993). Abraham *et al.* have concentrated on SCWO in the presence of catalysts. For example, they examined the destruction of phenol (Ding *et al.*, 1995) and

1,4-dichlorobenzene (Jin *et al.*, 1990; Jin *et al.*, 1992) over V_2O_5 catalysts, the catalytic oxidation of pyridine (Aki and Abraham, 1999) and the partial oxidation of methane to methanol and formic acid (Aki and Abraham, 1994). Katritzky and coworkers have studied the hydrolysis reactions of a wide range of compounds in sub- and supercritical water including those of pyridine analogs and benzopyrroles (Katritzky *et al.*, 1994), nitrogen-containing heterocycles (Katritzky *et al.*, 1995), aryl sulfoxides and sulfones (Katritzky *et al.*, 1997a), and reactions of aromatic hydrocarbons, heteroaromatic *n*-oxides, and aryl carbonyl compounds (Katritzky *et al.*, 1997b). Johnston and coworkers at the University of Texas have examined solvent-solute interactions in SCW (Johnston *et al.*, 1995) and measured elementary reaction rates at supercritical conditions (Ferry and Fox, 1998) and pH and equilibrium constants under hydrothermal and supercritical conditions (Xiang *et al.*, 1996; Xiang and Johnston, 1997; Wofford *et al.*, 1998). Franck and coworkers, who primarily measure properties of pure water at sub- and supercritical conditions, have measured oxidation rates of methane, ethane and methanol at conditions that produce hydrothermal flames (Hirth and Franck, 1997).

Dr. Steven Rice heads basic research on SCWO at the Combustion Research Facility at Sandia National Laboratories in Livermore, California and has measured oxidation kinetics for methane (Steeper *et al.*, 1996), methanol (Rice *et al.*, 1996), isopropyl alcohol (Hunter *et al.*, 1996), and other organic compounds (Rice and Steeper, 1998). A SCW elementary reaction mechanism was developed for methane and methanol oxidation (Rice, 1997) and the elementary rate constant for hydrogen peroxide decomposition in supercritical water was measured (Croiset *et al.*, 1997). Additionally, collaborative research, which will be detailed in Chapter 4, has been ongoing under the SERDP program to examine the effect of mixing and oxidant selection on methanol oxidation in SCW (Phenix, 1998).

Los Alamos National Laboratory also has a SCWO basic research program. Under the direction of Dr. Steven Buelow, researchers have measured the SCWO rates of chlorinated hydrocarbons (Foy *et al.*, 1996) and the decomposition rate of hydrazine in SCW (Masten *et al.*, 1993) and examined the effect of using nitrates and nitrites as oxidants on the SCWO rates of methanol, acetic acid, EDTA, and phenol (Dell'Orco *et al.*, 1995b; Proesmans *et al.*, 1997) and ammonia (Dell'Orco *et al.*, 1997). In addition to their work on oxidation reactions, several studies

focused on the solubility of various sodium, lithium and potassium nitrate salts in SCW (Dell'Orco *et al.*, 1995a).

1.4 REFERENCES

Abraham, M.A. and M.T. Klein, "Pyrolysis of benzylphenylamine neat and with tetralin, methanol, and water solvents." *Ind. Eng. Chem. Prod. Res. Dev.* **24**, 300 (1985).

Abraham, M.A. and M.T. Klein, "Solvent effects during the reaction of coal model compounds." in *Supercritical Fluids: Chemical and Engineering Principles and Applications*, T. G. Squires and M. E. Paulaitis, Eds., ACS Symposium Series, **329**, American Chemical Society, Washington, D.C., 67 (1987).

Aki, S. and M.A. Abraham, "Catalytic partial oxidation of methane in supercritical water." *J. Supercrit. Fluids* **7**, 259 (1994).

Aki, S. and M.A. Abraham, "Catalytic supercritical water oxidation of pyridine: comparison of catalysts." *Ind. Eng. Chem. Res.* **38**(2), 358 (1999).

Armellini, F.J., G.T. Hong and J.W. Tester, "Precipitation of sodium chloride and sodium sulfate in water from sub- to supercritical conditions: 150° to 550°C, 100 to 300 bar." *J. Supercrit. Fluids* **7**, 147 (1994).

Boock, L.T. and M.T. Klein, "Lumping strategy for modeling the oxidation of C_1-C_3 alcohols and acetic acid in high-temperature water." *Ind. Eng. Chem. Res.* **32** (1993).

Brock, E., Y. Oshima, P. Savage and J. Barker, "Kinetics and mechanism of methanol oxidation in supercritical water." *J. Phys. Chem.* **100**, 15834 (1996).

Brock, E.E. and P.E. Savage, "Detailed chemical kinetics model for supercritical water oxidation of C_1 compounds and H_2." *AIChE Journal* **41**(8), 1874 (1995).

Buelow, S.J., "Destruction of propellant components in supercritical water." LA-UR-90-1338, Los Alamos National Laboratory, (1990).

Buelow, S.J., "Chemical reactions of nitrogen containing compounds in supercritical water." *Proceedings of Workshop on Federal Programs Involving Supercritical Water Oxidation*, Gaithersburg, MD, p. 7, July 6-7 (1992).

Chang, K.C., L. Li and E.F. Gloyna, "Supercritical water oxidation of acetic acid by potassium permanganate." *J. Hazard. Mater.* **33**(1), 51 (1993).

Cooper, S.P., H.G. Folster, S.A. Gairns and E.G. Hauptmann, "Treatment of lagoon sludge, primary clarifier sludge, and bleach plant effluent by supercritical water oxidation." *Pulp Pap. Can.* **98**(10), 37 (1997).

Crain, N., S. Tebbal, L. Li and E.F. Gloyna, "Kinetics and reaction pathways of pyridine oxidation in supercritical water." *Ind. Eng. Chem. Res.* **32**(10), 2259 (1993).

Croiset, E., S.F. Rice and R.G. Hanush, "Hydrogen peroxide decomposition in supercritical water." *AIChE Journal* **43**(9), 2343 (1997).

Dell'Orco, P., H. Eaton, T. Reynolds and S. Buelow, "The solubility of 1:1 nitrate electrolytes in supercritical water." *J. Supercrit. Fluids* **8**(3), 217 (1995a).

Dell'Orco, P., B. Foy, E. Wilmanns, L. Le, J. Ely, K. Patterson and S. Buelow, "Hydrothermal oxidation of organic compounds by nitrate and nitrite." in *Innovations in Supercritical Fluids*, K. W. Hutchenson and N. Foster, Eds., ACS Symposium Series, **608**, American Chemical Society, Washington, D.C., 179 (1995b).

Dell'Orco, P.C., E.F. Gloyna and S.J. Buelow, "Reactions of nitrate salts with ammonia in supercritical water." *Ind. Eng. Chem. Res.* **36**(7), 2547 (1997).

DeSimone, J.D., Z. Guan and C.S. Elsbernd, "Synthesis of fluoropolymers in supercritical carbon dioxide." *Science* **257**, 945 (1992).

Ding, Z.Y., S.N.V.K. Aki and M.A. Abraham, "Catalytic supercritical water oxidation: phenol conversion and product selectivity." *Environ. Sci. Technol.* **29**(11), 2748 (1995).

DiPippo, M.M., K. Sako and J.W. Tester, "Ternary phase equilibria for the NaCl-Na_2SO_4-H_2O system at 200 and 250 bar up to 400°C." *Fluid Phase Equil.* **157**(2), 229 (1999).

Downey, K.W., R.H. Snow, D.A. Hazlebeck and A.J. Roberts, "Corrosion and chemical agent destruction. Research on supercritical water oxidation of hazardous military wastes." in *Innovations in Supercritical Fluids*, K. W. Hutchenson and N. R. Foster, Eds., ACS Symposium Series, **608**, American Chemical Society, Washington, D.C., 313 (1995).

Ferry, J.L. and M.A. Fox, "Effect of temperature on the reaction of HO· with benzene and pentahalogenated phenolate anions in subcritical and supercritical water." *J. Phys. Chem.* **102**(21), 3705 (1998).

Foy, B.R., K. Waldthausen, M.A. Sedillo and S.J. Buelow, "Hydrothermal processing of chlorinated hydrocarbons in a titanium reactor." *Environ. Sci. Technol.* **30**, 2790 (1996).

Frisch, M.A. and E.F. Gloyna, "Supercritical water oxidation of acetic acid catalyzed by CeO_2/MnO_2." CRWR Technical Report 237, University of Texas at Austin, Austin, TX (1992).

Gloyna, E.F. and L. Li, "Supercritical water oxidation research and development update." *Environ. Prog.* **14**(3), 182 (1995).

Gopalan, S. and P.E. Savage, "Phenol oxidation in supercritical water. From global kinetics and product identities to an elementary reaction model." in *Innovations in Supercritical Fluids*, K. W. Hutchenson and N. R. Foster, Eds., ACS Symposium Series, **608**, American Chemical Society, Washington, D.C., 217 (1995a).

Gopalan, S. and P.E. Savage, "A reaction network model for phenol oxidation in supercritical water." *AIChE Journal* **41**(8), 1864 (1995b).

Goto, M., T. Nada, S. Kawajiri, A. Kodama and T. Hirose, "Decomposition of municipal sludge by supercritical water oxidation." *J. Chem. Eng. Jpn.* **30**(5), 813 (1997).

Haroldsen, B.L., D.Y. Ariizumi, B.E. Mills, B.G. Brown and D. Greisen, "Transpiring wall supercritical water oxidation reactor salt deposition studies." SAND96-8213 UC-702, Sandia National Laboratories, Livermore, CA (1996a).

Haroldsen, B.L., D.Y. Ariizumi, B.E. Mills, B.G. Brown and D.C. Rousar, "Transpiring wall supercritical water oxidation test reactor design report." SAND96-8213 UC-402, Sandia National Laboratories, Livermore, CA (1996b).

Harradine, D.M., S.J. Buelow, P.C. Dell'Orco, R.B. Dyer, B.R. Foy, J.M. Robinson, J.A. Sanchez, T. Sportarelli and J.D. Wander, "Oxidation chemistry of energetic materials in supercritical water." *Haz. Waste Haz. Mat.* **10**, 233 (1993).

Harrell, C.L., J.S. Moscariello and M.T. Klein, "The absence of wall effects during benzonitrile hydrolysis." *J. Supercrit. Fluids* **14**, 219 (1999).

Helling, R.K. and J.W. Tester, "Oxidation kinetics of carbon monoxide in supercritical water." *Energy and Fuels* **4**, 417 (1987).

Helling, R.K. and J.W. Tester, "Oxidation of simple compounds and mixtures in supercritical water: carbon monoxide, ammonia and ethanol." *Environ. Sci. Technol.* **22**(11), 1319 (1988).

Hirth, T. and E.U. Franck, "Oxidation and hydrothermolysis of hydrocarbons in supercritical water at high pressures." *Ber Bunsenges Phys. Chem.* **97**(9), 1091 (1997).

Hirth, T., L. Heck, S. Jahnke, B. Michelfelder and R. Schweppe, "Supercritical water oxidation - waste destruction and synthesis." *Koatsuryoku no Kagaku to Gijutsu* **7**(Proceedings of International Conference--AIRAPT-16 and HPCJ-38--on High Pressure Science and Technology, 1997), 1375 (1998).

Holgate, H.R., J.C. Meyer and J.W. Tester, "Glucose hydrolysis and oxidation in supercritical water." *AIChE Journal* **41**, 637 (1995).

Holgate, H.R. and J.W. Tester, "Fundamental kinetics and mechanisms of hydrogen oxidation in supercritical water." *Combust. Sci. Technol.* **88**, 369 (1993).

Holgate, H.R. and J.W. Tester, "Oxidation of hydrogen and carbon monoxide in sub- and supercritical water: reaction kinetics, pathways, and water-density effects. 1. Experimental results." *J. Phys. Chem.* **98**, 800 (1994a).

Holgate, H.R. and J.W. Tester, "Oxidation of hydrogen and carbon monoxide in sub- and supercritical water: reaction kinetics, pathways, and water-density effects. 2. Elementary reaction modeling." *J. Phys. Chem.* **98**, 810 (1994b).

Holgate, H.R., P.A. Webley, J.W. Tester and R.K. Helling, "Carbon monoxide oxidation in supercritical water: the effects of heat transfer and the water-gas shift reaction on observed kinetics." *Energy and Fuels* **6**, 586 (1992).

Hong, G.T., P.K. Fowler, W.R. Killilea and K.C. Swallow, "Supercritical water oxidation: treatment of human waste and system configuration tradeoff study." *Proceedings of 17th Intersociety Conference on Environmental Systems*, Seattle, WA, July 13-15 (1987).

Hong, G.T., W.R. Killilea and T.B. Thomason, "Supercritical water oxidation: space applications." *Proceedings of ASCE Space,* Albuquerque, NM, August 29-31 (1988).

Houser, T.J. and X. Liu, "Reactions of 1-chloro-3-phenylpropane, 2-chlorotoluene, and 4-chlorophenol in supercritical water." *J. Supercrit. Fluids* **9**(3), 167 (1996).

Houser, T.J., D.M. Tiffany, Z. Li, M.E. McCarville and M.E. Houghton, "Reactivity of some organic-compounds with supercritical water." *Fuel* **65**(6), 827 (1986).

Houser, T.J., Y. Zhou, C.C. Tsao and X. Liu, "Removal of heteroatoms from organic-compounds by supercritical water." in *Supercritical Fluid Engineering Science: Fundamentals and Applications*, E. Kiran and J. F. Brennecke, Eds., ACS Symposium Series, **514**, American Chemical Society, Washington, D.C., 327 (1993).

Hunter, T.B., S.F. Rice and R.G. Hanush, "Raman spectroscopic measurement of oxidation in supercritical water. 2. Conversion of isopropyl alcohol to acetone." *Ind. Eng. Chem. Res.* **35**(11), 3984 (1996).

Hurley, J.A., "Development of hydrothermal oxidation reactor technology for the destruction of hazard class 1.1 propellant." Presented at the Third International Conference on Advanced Oxidation Technologies for Water and Air Remediation, Cincinnati, OH, October 26-29 (1996).

Iyer, S.D. and M.T. Klein, "Effect of pressure on the rate of butyronitrile hydrolysis." *J. Supercrit. Fluids* **10**, 191 (1997).

Iyer, S.D., G.R. Nicol and M.T. Klein, "Hydrothermal reactions of 1-nitrobutane in high temperature water." *J. Supercrit. Fluids* **9**, 26 (1996).

Jin, L., Z.Y. Ding and M.A. Abraham, "Catalytic supercritical water oxidation of 1,4-dichlorobenzene." *Chem. Eng. Sci.* **47**(9-11), 2659 (1992).

Jin, L., Y.T. Shah and M.A. Abraham, "The effect of supercritical water on the catalytic oxidation of 1,4-dichlorobenzene." *J. Supercrit. Fluids* **3**, 233 (1990).

Johnston, J.B., R.E. Hannah, V.L. Cunningham, B.P. Daggy, F.J. Sturm and R.M. Kelly, "Destruction of pharmaceutical and biopharmaceutical wastes by the MODAR supercritical water oxidation process." *Biotechnology* **6**, 1423 (1988).

Johnston, K.P., P.B. Balbuena, T. Xiang and P.J. Rossky, "Simulation and spectroscopy of solvation in water from ambient to supercritical conditions." in *Innovations in Supercritical Fluids*, L. W. Hutchenson and N. Foster, Eds., ACS Symposium Series, **608**, American Chemical Society, Washington, D.C., 77 (1995).

Katritzky, A.R., R.A. Barcock, E.S. Ignatchenko, S.M. Allin, M. Siskin and C.W. Hudson, "Aqueous high-temperature chemistry of carbo- and heterocycles. 28. Reactions of aryl sulfoxides and sulfones in sub- and supercritical water at 200-460°C." *Energy & Fuels* **11**(1), 150 (1997a).

Katritzky, A.R., R.A. Barcock, M. Siskin and W.N. Olmstead, "Aqueous high-temperature chemistry of carbocycles and heterocycles. 23. Reactions of pyridine analogs and benzopyrroles in supercritical water at 460°C." *Energy & Fuels* **8**, 990 (1994).

Katritzky, A.R., E.S. Ignatchenko, S.M. Allin, R.A. Barcock, M. Siskin and C.W. Hudson, "Aqueous high-temperature chemistry of carbo- and heterocycles. 29. Reactions of aromatic hydrocarbons, heteroaromatic *n*-oxides, and aryl carbonyl compounds in supercritical water at 460°C." *Energy & Fuels* **11**(1), 160 (1997b).

Katritzky, A.R., P.A. Shipkova, S.M. Allin, R.A. Barcock, M. Siskin and W.N. Olmstead, "Aqueous high-temperature chemistry. 24. Nitrogen-containing heterocycles in supercritical water at 460°C." *Energy & Fuels* **9**(4), 580 (1995).

Kieke, M.L., J.W. Schoppelrei and T.B. Brill, "Spectroscopy of hydrothermal reactions. 1. The CO_2-H_2O system and kinetics of urea decomposition in an FTIR spectroscopy flow reactor cell operable to 725 K and 335 bar." *J. Phys. Chem.* **100**, 7455 (1996).

Killilea, W.R. and K.C. Swallow, "The fate of nitrogen in supercritical water oxidation." *J. Supercrit. Fluids* **5**(1), 72 (1992).

Kirts, R.E., "Destruction of Navy hazardous wastes by supercritical water oxidation." *Proceedings of Annual Meeting - Air Waste Management Association*, **9**, (1995).

Klein, M.T., Y.G. Mentha and L.A. Torry, "Decoupling substituent and solvent effects during hydrolysis of substituted anisoles in supercritical water." *Ind. Eng. Chem. Res.* **31**, 182 (1992).

Kutney, M.C., V.S. Dodd, K.A. Smith, H.J. Herzog and J.W. Tester, "A hard-sphere volume-translated van der Waals equation of state for supercritical process modeling: Part I, pure components." *Fluid Phase Equil.* **128**, 149 (1997).

Lachance, R., J. Paschkewitz, J. DiNaro and J.W. Tester, "Thiodiglycol hydrolysis and oxidation in sub- and supercritical water." *J. Supercrit. Fluids* (1999).

Lajeunesse, C.A. and S.F. Rice, "Case study on the destruction of organic dyes in supercritical water." *Chem. Oxid* **5**, 13 (1997).

Lee, D.S. and E.F. Gloyna, "Hydrolysis and oxidation of acetamide in supercritical water." *Environ. Sci. Technol.* **26**(8), 1587 (1992).

Lee, D.S., E.F. Gloyna and L. Li, "Efficiency of H_2O_2 and O_2 in supercritical water oxidation of 2,4-dichlorophenol and acetic acid." *J. Supercrit. Fluids* **3**, 249 (1990).

Li, L., P. Chen and E.F. Gloyna, "Pilot-plant validation of kinetic models for supercritical water oxidation." *Chem. Oxid.* **4**, 219 (1997).

Li, L., E.F. Gloyna and J.E. Sawicki, "Treatability of DNT process wastewater by supercritical water oxidation." *Water Env. Res.* **65**, 250 (1993a).

Li, R., P.E. Savage and D. Szmukler, "2-Chlorophenol oxidation in supercritical water: global kinetics and reaction products." *AIChE Journal* **39**(1), 178 (1993b).

Maiella, P.G. and T.B. Brill, "Spectroscopy of hydrothermal reactions. 3. The water-gas reaction, 'hot spots', and formation of volatile salts of NCO- from aqueous $[NH_3(CH_2)_nNH_3]NO_3$

(n=2,3) at 720 K and 276 bar by T-jump/FTIR spectroscopy." *Applied Spectroscopy* **50**, 829 (1996a).

Maiella, P.G. and T.B. Brill, "Spectroscopy of hydrothermal reactions. 5. Decarboxylation of malonic acid and monosodium malonate." *J. Phys. Chem.* **100**, 14352 (1996b).

Marrone, P.A., T.A. Arias, W.A. Peters and J.W. Tester, "Solvation effects on kinetics of methylene chloride reactions in sub and supercritical water: theory, experiment, and *ab initio* calculations." *J. Phys. Chem.* **102**, 7013 (1998a).

Marrone, P.A., P.M. Gschwend, W.A. Peters and J.W. Tester, "Product distribution and reaction pathways for methylene chloride hydrolysis and oxidation under hydrothermal conditions." *J. Supercrit. Fluids* **12**(3), 239 (1998b).

Marrone, P.A., R.P. Lachance, J.L. DiNaro, B.D. Phenix, J.C. Meyer, J.W. Tester, W.A. Peters and K.C. Swallow, "Methylene chloride oxidation and hydrolysis in supercritical water." in *Innovations in Supercritical Fluids: Science and Technology*, K. W. Hutchenson and N. Foster, Eds., ACS Symposium Series, **608**, American Chemical Society, Washington, D.C., Chapter 13 (1995).

Marshall, W.L. and E.U. Franck, "Ion product of water substance, 0-1000°C, 1-10,000 bars. New international formulation and its background." *J. Phys. Chem. Ref. Data* **10**(2), 295 (1981).

Martino, C.J. and P.E. Savage, "Supercritical water oxidation kinetics, products, and pathways for CH_3- and CHO-substituted phenols." *Ind. Eng. Chem. Res.* **36**(5), 1391 (1997a).

Martino, C.J. and P.E. Savage, "Thermal decomposition of substituted phenols in supercritical water." *Ind. Eng. Chem. Res.* **36**(5), 1385 (1997b).

Martino, C.J. and P.E. Savage, "Oxidation and thermolysis of methoxy-, nitro-, and hydroxy-substituted phenols in supercritical water." *Ind. Eng. Chem. Res.* **38**(1784-1791) (1999a).

Martino, C.J. and P.E. Savage, "Supercritical water oxidation kinetics and pathways for ethylphenols, hydroxyacetophenones, and other monosubstituted phenols." *Ind. Eng. Chem. Res.* **38**, 1775 (1999b).

Martino, C.J., P.E. Savage and J. Kasiborski, "Kinetics and products from *o*-cresol oxidation in supercritical water." *Ind. Eng. Chem. Res.* **34**(6), 1941 (1995).

Masten, D.A., B.R. Foy, D.M. Harradine and R.B. Dyer, "*In situ* Raman spectroscopy of reactions in supercritical water." *J. Phys. Chem.* **97**, 8557 (1993).

McBrayer, R.N., J.W. Griffith and A. Gidner, "Operation of the first commercial supercritical water oxidation industrial waste facility." *Proceedings of Int. Conf. Oxid. Technol. Water Wastewater Treat.*, **66**, (1996).

McHugh, M. and V. Krukonis, *Supercritical Fluid Extraction*. Butterworth-Heinemann, Stoneham, MA (1994).

McKendry, J.K., L. Li and E.F. Gloyna, "The effect of additives on the oxidation of dimethyl methylphosphonate in supercritical water." *Proceedings of Ind. Waste Conf.*, **49**, p. 365, (1994).

Meyer, J.C., P.A. Marrone and J.W. Tester, "Acetic acid oxidation and hydrolysis in supercritical water." *AIChE Journal* **41**(9), 2108 (1995).

Mizan, T.I., P.E. Savage and R.M. Ziff, "A molecular dynamics investigation of hydrogen bonding in supercritical water." in *Innovations in Supercritical Fluids*, ACS Symposium Series, **608**, Washington, D.C., 47 (1995).

Mizan, T.I., P.E. Savage and R.M. Ziff, "Temperature dependence of hydrogen bonding in supercritical water." *J. Phys. Chem.* **100**(1), 403 (1996).

Mizan, T.I., P.E. Savage and R.M. Ziff, "Critical point and coexistence curve for a flexible, simple point-charge water model." *J. Supercrit. Fluids* **10**(2), 119 (1997a).

Mizan, T.I., P.E. Savage and R.M. Ziff, "Fugacity coefficients for free radicals in dense fluids: HO_2 in supercritical water." *AIChE Journal* **43**(5), 1287 (1997b).

Modell, M., "Supercritical water oxidation." in *Standard Handbook of Hazardous Waste Treatment and Disposal*, H. M. Freeman, Ed., McGraw-Hill, New York, NY, 8.153 (1989).

Modell, M., "Treatment of pulp mill sludges by supercritical water oxidation." Final Report, DOE Contract No. FG05-90CE40914, (1990).

Modell, M., J. Larson and S.F. Sobczynski, "Supercritical water oxidation of pulp mill sludges." *Tappi J.*, 195 (1992).

Modell, M., S. Mayr and A. Kemna, "Supercritical water oxidation of aqueous wastes." *Proceedings of 56th Annual International Water Conference,* Pittsburgh, PA, p. 478, October 31 (1995).

NRC, "Alternative technologies for the destruction of chemical agents and munitions." National Research Council, Washington, D.C. (1993).

Peters, W.A., Ed., "Data needs to support modeling of supercritical water oxidation reactors and processes for chem demil applications." MIT-EL 96-002, Massachusetts Institute of Technology, Cambridge, MA (1996).

Phenix, B.D., "Hydrothermal oxidation of simple organic compounds." Ph.D. Thesis, Department of Chemical Engineering, Massachusetts Institute of Technology, Cambridge, MA (1998).

Phenix, B.D., J.L. DiNaro, M.A. Tatang, J.W. Tester, J.B. Howard and G.J. McRae, "Incorporation of parametric uncertainty into complex kinetic mechanisms: application to hydrogen oxidation in supercritical water." *Combust. Flame* **112**, 132 (1998).

Proesmans, P.I., L. Luan and S.J. Buelow, "Hydrothermal oxidation of organic wastes using ammonium nitrate." *Ind. Eng. Chem. Res.* **36**, 1559 (1997).

Reagan, M.T., J. Harris and J.W. Tester, "Molecular simulations of NaCl-H_2O mixtures from ambient to supercritical conditions." *accepted for publication to J. Phys. Chem.* (1999).

Rice, S.F., "Application of the GRI 1.2 methane oxidation model to methane and methanol oxidation in supercritical water." *Proceedings of The 4th International Symposium on Supercritical Fluids*, Sendai, Japan, p. 571, (1997).

Rice, S.F., T.B. Hunter, A.C. Ryden and R.G. Hanush, "Raman spectroscopic measurement of oxidation in supercritical water. 1. Conversion of methanol to formaldehyde." *Ind. Eng. Chem. Res.* **35**(7), 2161 (1996).

Rice, S.F., C.A. LaJeunesse, R.G. Hanush, J.D. Aiken and S.C. Johnston, "Supercritical water oxidation of colored smoke, dye, and pyrotechnic compositions." SAND94-8209, Sandia National Laboratory, (1994).

Rice, S.F. and R.R. Steeper, "Oxidation rates of common organic compounds in supercritical water." *J. Hazard. Mater.* **59**(2-3), 261 (1998).

Robinson, C., "Demilitarization R&D technology for conventional munitions via SCWO of colored smokes, dyes, and pyrotechnics." *Proceedings of Workshop on Federal Programs Involving Supercritical Water Oxidation*, Gaithersburg, MD, p. 160, July 6-7 (1992).

Savage, P.E., "Organic chemical reactions in supercritical water." *Chem. Rev.* **99**(2), 603 (1999).

Savage, P.E., S. Gopalan, T.I. Mizan, C.J. Martino and E.E. Brock, "Reactions at supercritical conditions: applications and fundamentals." *AIChE Journal* **41**(7), 1723 (1995).

Savage, P.E. and M.A. Smith, "Kinetics of acetic acid oxidation in supercritical water." *Environ. Sci. Technol.* **29**(1), 216 (1995).

Savage, P.E., J.L. Yu, N. Stylski and E.E. Brock, "Kinetics and mechanism of methane oxidation in supercritical water." *J. Supercrit. Fluids* **12**(2), 141 (1998).

Sawicki, J.E. and B. Casas, "Wet oxidation systems-process concept to design." *Environ. Prog.* **12**, 275 (1993).

Schoppelrei, J.W., M.L. Kieke and T.B. Brill, "Spectroscopy of hydrothermal reactions. 2. Reactions and kinetic parameters of $[NH_3OH]NO_3$ and equilibria of $(NH_4)_2CO_3$ determined with a flow cell and FT Raman spectroscopy." *J. Phys. Chem.* **100**, 7463 (1996a).

Schoppelrei, J.W., M.L. Kieke, X. Wang and T.B. Brill, "Spectroscopy of hydrothermal reactions. 4. Kinetics of urea and guanidinium nitrate at 200-300°C in a diamond cell, infrared spectroscopy flow reactor." *J. Phys. Chem.* **100**, 14343 (1996b).

Shanableh, A., "Destruction of sludge in supercritical water." *Water* **22**(3), 16 (1995).

Shanableh, A. and E.F. Gloyna, "Supercritical water oxidation - wastewater and sludges." *Water Sci. Tech.* **23**, 389 (1991).

Snow, R.H., W. Sabato, K. Taylor, G.C. Sresty, K. Downey, D. Hazlebeck and D. Jensen, "Demilitarization of chemical agents by hydrolysis and supercritical water oxidation." *Proceedings of ERDEC Scientific Conference on Chemical and Bioliological Defense Research*, p. 359, (1996).

Spritzer, M.H., D.A. Hazlebeck and K.W. Downey, "Supercritical water oxidation of chemical agents and solid propellants." *J. Energ. Mater.* **13**(3&4), 185 (1995).

Squires, T.G., C.G. Venier and T. Aida, "Supercritical fluid solvents in organic chemistry." *Fluid Phase Equil.* **10**, 261 (1983).

Staszak, C.N., K.C. Malinowski and W.R. Killilea, "The pilot-scale demonstration of the MODAR oxidation process for the destruction of hazardous waste materials." *Environ. Prog.* **6**(1), 39 (1987).

Steeper, R.R., S.F. Rice, I.M. Kennedy and J.D. Aiken, "Kinetics measurements of methane oxidation in supercritical water." *J. Phys. Chem.* **100**(1), 184 (1996).

Takahashi, Y.T., T. Koo and C. Koo, "Subcritical and supercritical water oxidation of CELSS model wastes." *Adv. Space Res.* **9**, 99 (1988).

Tester, J.W., H.R. Holgate, F.J. Armellini, P.A. Webley, W.E. Killilea, G.T. Hong and H.E. Barner, "Supercritical water oxidation technology: a review of process development and fundamental research." in *Emerging Technologies for Hazardous Waste Management III*, D. W. Tedder and F. G. Pohland, Eds., ACS Symposium Series, **518**, American Chemical Society, Washington, D.C., Chapter 3 (1993a).

Tester, J.W., P.A. Marrone, M.M. DiPippo, K. Sako, M.T. Reagan, T. Arias and W.A. Peters, "Chemical reactions and phase equilibria of model halocarbons and salts in sub- and supercritical water (200 to 300 bar, 100 to 600°C)." *J. Supercrit. Fluids* **13**, 225 (1998).

Tester, J.W., P.A. Webley and H.R. Holgate, "Revised global kinetic measurements of methanol oxidation in supercritical water." *Ind. Eng. Chem. Res.* **32**(1), 236 (1993b).

Thomason, T.B., G.T. Hong, K.C. Swallow and W.R. Killilea, "The MODAR supercritical water oxidation process." in *Innovative Hazardous Waste Treatment Technology Series, Volume 1: Thermal Processes*, H. M. Freeman, Ed., Technomic Publishing, Lancaster, PA, 31 (1990).

Thomason, T.B. and M. Modell, "Supercritical water destruction of aqueous wastes." *Haz. Waste* **1**(1), 453 (1984).

Thornton, T.D. and P.E. Savage, "Kinetics of phenol oxidation in supercritical water." *AIChE Journal* **38**(3), 321 (1992).

Timberlake, S.H., G.T. Hong, M. Simson and M. Modell, "Supercritical water oxidation for wastewater treatment: preliminary study of urea destruction." *Proceedings of 12th Intersociety Conference on Environmental Systems*, San Diego, CA, July 19-21 (1982).

Tongdhamachart, C. and E.F. Gloyna, "Supercritical water oxidation of anaerobically digested municipal sludge." CRWR Technical Report 229, University of Texas at Austin, Austin, TX (1991).

Townsend, S.H., M.A. Abraham, G.L. Huppert, M.T. Klein and S.C. Paspek, "Solvent effects during reactions in supercritical water." *Ind. Eng. Chem. Res.* **27**, 143 (1988).

Tsao, C.C., Y. Zhou, X. Liu and T.J. Houser, "Reactions of supercritical water with benzaldehyde, benzylidenebenzylamine, benzyl alcohol, and benzoic acid." *J. Supercrit. Fluids* **5**(2), 107 (1992).

U.S. Congress, O.T.A., "Disposal of Chemical Weapons: Alternative Technologies-Background Paper." OTA-BP-O-95, U.S. Government Printing Office, Washington D.C. (1992).

Uematsu, M. and E.U. Frank, "Static dielectric constant of water and steam." *The Journal of Physical Chemical Reference Data* **9**(4), 1291 (1980).

van Swol, F. and C.A. Eckert, "Supercritical fluid thermodynamics for coal processing: topical report." DOE/PC/88922-9, (1990).

Wang, X.G., L.U. Gron, M.T. Klein and T.B. Brill, "The influence of high-temperature water on the reaction pathways of nitroanilines." *J. Supercrit. Fluids* **8**, 236 (1995).

Webley, P.A., H.R. Holgate, D.M. Stevenson and J.W. Tester, "Oxidation kinetics of model compounds of human metabolic waste in supercritical water." *Proceedings of 20th International Conference on Environmental Systems*, Williamsburg, VA, July 9-12 (1990).

Webley, P.A. and J.W. Tester, "Fundamental kinetics of methanol oxidation in supercritical water." in *Supercritical Fluid Science and Technology*, K. P. Johnston and J. M. L. Penninger, Eds., ACS Symposium Series, **406**, American Chemical Society, Washington, D.C., 259 (1989).

Webley, P.A. and J.W. Tester, "Fundamental kinetics of methane oxidation in supercritical water." *Energy and Fuels* **5**, 411 (1991).

Webley, P.A., J.W. Tester and H.R. Holgate, "Oxidation kinetics of ammonia and ammonia-methanol mixtures in supercritical water in the temperature range 530-700°C at 246 bar." *Ind. Eng. Chem. Res.* **30**(8), 1745 (1991).

Weinstein, R.D., A.R. Renslo, R.L. Danheiser, J.G. Harris and J.W. Tester, "Kinetic correlation of Diels-Alder reactions in supercritical carbon dioxide." *The Journal of Physical Chemistry* **100**(30), 12337 (1996).

Wilmanns, E. and E.F. Gloyna, "Supercritical water oxidation of volatile acids." CRWR Technical Report 218, University of Texas at Austin, Austin, TX (1990).

Wofford, W.T., E.F. Gloyna and K.P. Johnston, "Boric acid equilibria in near-critical and supercritical water." *Ind. Eng. Chem. Res.* **37**(5), 2045 (1998).

Xiang, T. and K.P. Johnston, "Acid-base behavior in supercritical water: β-naphthoic acid-ammonia equilibrium." *J. Solution Chem.* **26**(1), 13 (1997).

Xiang, T., K.P. Johnston, W.T. Wofford and E.F. Gloyna, "Spectroscopic measurement of pH in aqueous sulfuric acid and ammonia from sub- to supercritical conditions." *Ind. Eng. Chem. Res.* **35**(12), 4788 (1996).

Yang, H.H. and C.A. Eckert, "Homogeneous catalysis in the oxidation of *p*-chlorophenol in supercritical water." *Ind. Eng. Chem. Res.* **27**, 2009 (1988).

Yu, J.L. and P.E. Savage, "Decomposition of formic acid under hydrothermal conditions." *Ind. Eng. Chem. Res.* **37**(1), 2 (1998).

Chapter 2.

Research Objective and Approach

This work addresses the general research goals of our group which are: 1) to further understand the chemical and physical nature of supercritical water; and 2) to characterize the mechanisms and kinetics of reactions of hazardous organic wastes in supercritical water. The specific goals of this thesis are to perform a detailed investigation of the oxidation of benzene in supercritical water and model its oxidation using an elementary reaction mechanism. The following summarizes the approach used to meet these goals:

1. *Characterize the effects of mixing and oxidant choice on laboratory-scale kinetic data.* In an effort to better understand the differences between the supercritical water oxidation kinetics measured in our and other laboratory-scale systems, a collaborative effort was undertaken with Brian Phenix to better understand the effects of mixing in our reactor system and to implement the use of hydrogen peroxide as an alternative oxidant. The objectives of the mixing study were to identify the extent mixing times contributed to the apparent induction times reported previously in the supercritical water oxidation kinetics of various model compounds measured in our laboratory-scale, tubular reactor system and to minimize the time required to mix the reactor feeds. The introduction of hydrogen peroxide as an alternative oxidant was targeted to overcome the limitation on reactor oxygen concentrations imposed by the oxygen saturator system used in all previous studies done with this system. Both investigations were performed using methanol as the model compound.

2. *Explore the effects of uncertainty in the input parameters on the predictive ability of a supercritical water hydrogen oxidation mechanism.* Also in collaboration with Brian Phenix, an investigation was performed to assess the level of uncertainty in the predictions of supercritical

water elementary reaction mechanisms given the uncertainty in the forward rate constants and species thermochemistry. The study was performed using the relatively well-understood combustion mechanism for hydrogen oxidation and was adapted to the temperatures and pressures of supercritical water oxidation.

3. *Generate kinetic data for the reaction of benzene in supercritical water under well-defined conditions.* Benzene is a hazardous chemical, a common environmental contaminant, and a known human carcinogen. The single aromatic ring of benzene is the building block for polyaromatic hydrocarbons and substituted aromatic compounds. Given the thermal and chemical stability of the aromatic benzene ring, it is likely that benzene will be a refractory intermediate in the oxidation of more complex aromatic compounds. Since benzene is both a problematic hazardous chemical and a model compound for other aromatic compounds, benzene was selected as a compound for experimental study. The specific objectives related to this research component were: 1) to determine of the effect of temperature, the fuel equivalence ratio, the initial feed concentrations and pressure on the reaction rate of benzene; 2) to develop a global rate expression from the data that would be used to design SCWO systems; and 3) to identify the major partial and final oxidation products.

4. *Model the oxidation of benzene in supercritical water using an existing elementary reaction network.* While global rate expressions are useful for designing reactors and predicting conversions inside the range of conditions over which they were developed, they yield little mechanistic insight. Benzene oxidation at combustion conditions has been relatively well modeled using detailed kinetic mechanisms, although there is still debate as to the proper mechanism. In an effort to gain a deeper understanding of benzene oxidation in supercritical water, the specific goals here are: 1) to adapt the most current benzene oxidation mechanism from the combustion literature for modeling benzene oxidation under supercritical water oxidation conditions which are considerably higher in pressure and lower in temperature than combustion conditions; and 2) to evaluate the ability of the model to predict benzene oxidation rates in supercritical water.

Chapter 3.

Equipment, Procedures and Analytical Methods.

3.1 Description of the Bench Scale SCWO System

All experiments were conducted in the bench-scale, tubular, plug flow reactor that has been used for all previous experimental studies in this laboratory. The reactor is similar to that used by Holgate (1993), but underwent modifications as detailed in Phenix (1998). The modified system, shown in Figure 3-1, is described below in detail. The reactor system consists of four sub-sections: feed preparation and pressurization, a preheating section, the reaction zone, and the letdown and sample collection section.

3.1.1 Feed Preparation and Pressurization

The feed preparation and pressurization section of the reactor system consists of organic and oxidant saturators, a water feed tank, a hydrogen peroxide feed tank, an organic feed tank, two HPLC pumps and associated tubing and gases (Figure 3-1). The purpose of this section of the reactor is to prepare separate aqueous solutions of the compound to be oxidized and the oxidant and then to separately pressurized these feeds to the operating pressure (up to 278 bar). All reactor feeds use deionized waterobtained by feeding house distilled water to a Barnstead Nanopure-A water purification system. The Barnstead system has four cartridges in the following order: a MACROpure cartridge (p/n D0836) designed to remove organics and colloids, an Ultrapure cartridge (p/n D0809) containing a mixed bed resin for cation/anion removal, an ORGANICfree cartridge (p/n D0820) for removal of TOC, and a 0.2 μm filter cartridge (p/n D0749).

There are two oxidant choices for this system: hydrogen peroxide or pure oxygen gas. The method of preparing the oxidant solution depends on which oxidant is used. For oxygen gas, a dissolved aqueous solution of oxygen is prepared in the stainless steel pressure vessel called the

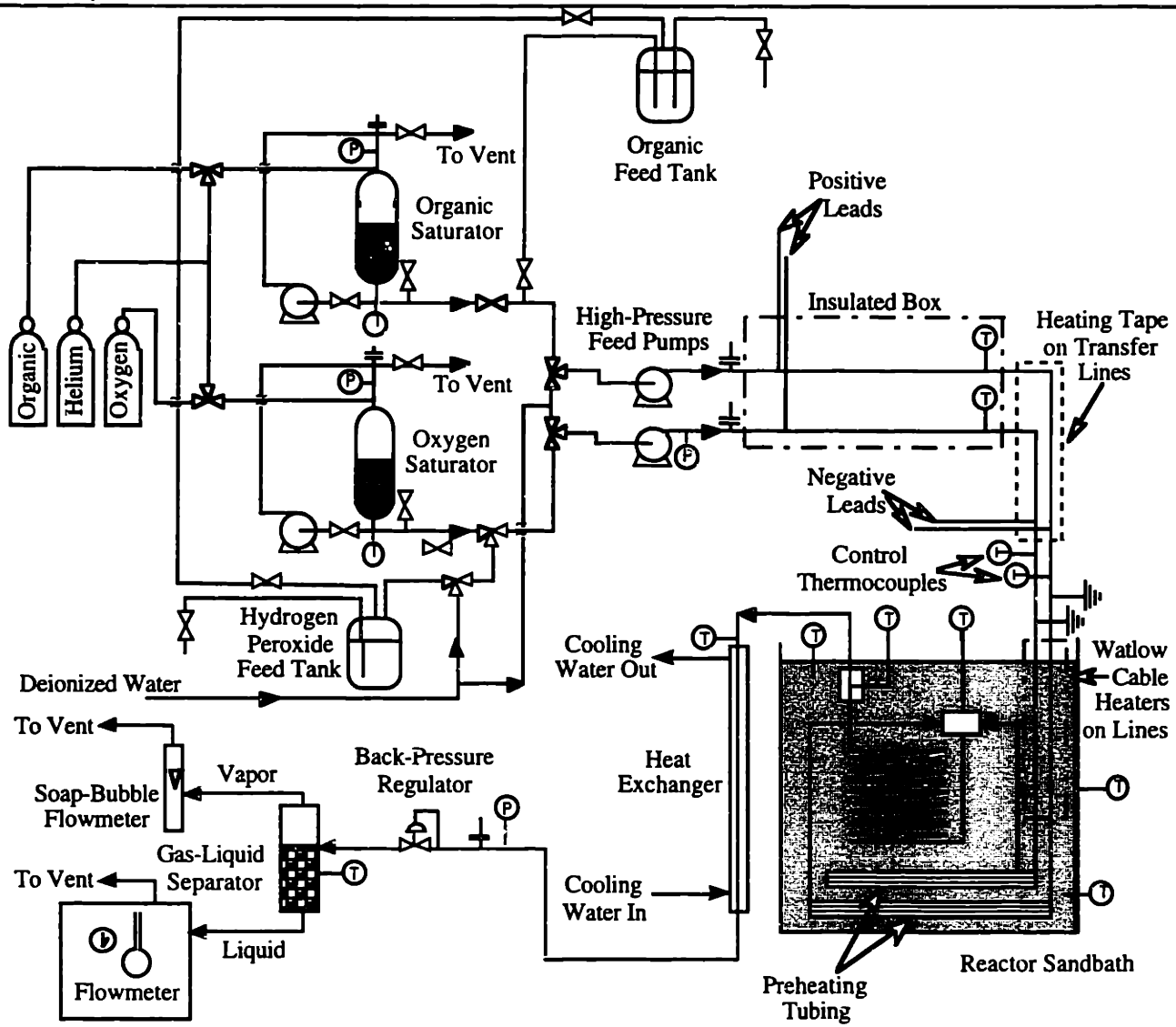

Figure 3-1 Bench-scale, tubular, plug flow reactor system

oxygen saturator. A 4 liter HDPE reservoir (Dionex, p/n 39164) holds the hydrogen peroxide feed solution.

The oxidizable waste can be a gas or liquid at ambient conditions. Since an aqueous solution of the waste must be prepared, the waste must exhibit an appreciable solubility in water to be studied in this system. The organic saturator is used to prepare an aqueous solution when the waste is a gas, and a 5 liter plastic-coated, glass container holds the aqueous waste feed when the waste is liquid.

Oxygen Saturator

The oxygen saturator is a 3 liter Hoke 304SS sampling cylinder (Hoke, Model 8HD3000, 1800 psig (125 bar) rating) used for preparing a dissolved aqueous oxygen solution. The saturator is filled with about 2.5 liters of deionized water. The remaining 0.5 liter headspace is pressurized and vented three times with oxygen to purge any residual gases from the saturator. After purging the saturator is loaded with the proper pressure of oxygen to yield the desired concentration of dissolved oxygen in the water when equilibrium is achieved. A Heise precision pressure gauge (CM series, 0-3000 psig (0-208 bar), accuracy of 0.1% of span) measures the saturator pressure. To ensure an equilibrium concentration of oxygen in the water, the water is recirculated at least 12 hours by withdrawing water from the bottom of the saturator and returning it to the top via a positive displacement pump (LDC Analytical minipump, Model 2396). During this period the water is turned over at least twice.

With a known partial pressure of oxygen in the saturator and assuming equilibrium of the gas and the liquid, the aqueous concentration of oxygen can be calculated using Henry's Law:

$$y_{O_2}\hat{\phi}_{O_2}(T,P,y_i)P = H_{O_2}(T,P)x_{O_2} \tag{3-1}$$

where y_{O_2} is the gas-phase mole fraction of oxygen, $\hat{\phi}_{O_2}(T,P,y_i)$ is the gas-phase fugacity coefficient of O_2, P is the measured pressure of the saturator, $H_{O_2}(T,P)$ is the Henry's Law constant for O_2 in water which is a function of both temperature and pressure, and x_{O_2} is the mole fraction of oxygen in the water. Since the headspace is pressurized with pure oxygen, $y_{O_2}=1$ and $\hat{\phi}_{O_2}(T,P,y_i) = \phi_{O_2}(T,P)$. When the pressure is near ambient, $\phi_{O_2} \cong 1$, but at pressures used in the saturator, $\phi_{O_2}(T,P)$ deviates from one and must be calculated using an equation of state. Here, the Peng-Robinson equation of state is used to calculate $\phi_{O_2}(T,P)$ (Peng and Robinson, 1976) with

parameters for O_2 from Reid *et al.* (1987). The pressure dependence of the Henry's Law constant is expressed as:

$$\left(\frac{\partial \ln H_{O_2}}{\partial P}\right)_T = \frac{\overline{V}_{O_2}^{\infty}}{RT} \tag{3-2}$$

where $\overline{V}_{O_2}^{\infty}$ is the partial molar volume of O_2 at infinite dilution. Integration of Eqn. (3-2) from the reference pressure (P_0) to the experimental pressure P assuming a constant $\overline{V}_{O_2}^{\infty}$ yields:

$$H_{O_2}(T,P) = H_{O_2}(T_0,P_0)\exp\left(\frac{\overline{V}_{O_2}^{\infty}(P-P_0)}{RT}\right) \tag{3-3}$$

Values of $H_{O_2}(T_0,P_0)$ are calculated from the correlation of Benson *et al.* (1979), and $\overline{V}_{O_2}^{\infty}$ in water is determined from that of Brelvi and O'Connell (1972). By incorporating Eqn. (3-3) into Eqn. (3-1), x_{O_2} can be calculated. The accuracy of Eqns. (3-1), (3-2), and (3-3) were verified by both Phenix (1998) and Holgate (1993).

The oxygen saturator is connected to the HPLC oxidant feed pump. A 1/4 in. (6.35 mm) O.D. section of 304SS tubing connects the bottom of the oxygen saturator to a three-way high pressure valve. The outlet of the valve leads directly to the pump via 316SS tubing. The three-way valve allows the feed to the pump to be switched between the oxygen saturator and the water feed tank.

Hydrogen Peroxide Feed Tank

At 25°C and 125 bar (the pressure rating of the oxygen saturator), the solubility of O_2 in water calculated by Eqns. (3-1)-(3-3) is 3930 wppm. The maximum attainable O_2 concentration in the reactor is limited by this solubility. By using an aqueous hydrogen peroxide solution instead of dissolved oxygen as a means of delivering oxygen to the reactor, higher reactor oxygen concentrations can be achieved. The use of hydrogen peroxide as an oxygen source in an SCWO system was first reported by Rice at Sandia National Laboratories. Hydrogen peroxide decomposes in the preheating section of the reactor system via the following global reaction producing oxygen and water:

$$2\,H_2O_2 \Leftrightarrow O_2 + 2\,H_2O \tag{3-4}$$

Experiments were conducted, which will be summarized in Chapter 4, to ensure complete decomposition of H_2O_2 to O_2 and H_2O in the preheater.

To prepare a hydrogen peroxide feed solution, a 30 wt% aqueous solution of A.C.S. grade H_2O_2 (Aldrich Chemical Co., p/n 21,676-3; VWR, p/n MK524004) is used as received and diluted with deionized water to the desired concentration. Once prepared, the concentration of H_2O_2 is verified using the ceric ion titration method described in Section 3.3. The hydrogen peroxide solution is transferred to the hydrogen peroxide feed tank, a 4 liter HDPE reservoir (Dionex, p/n 39164), shown in Figure 3-1. The headspace is pressurized with 1.7 bar of helium. A sampling line, made of teflon tubing and an on/off valve, extends from the hydrogen peroxide feed tank allowing for sampling of the solution. The reservoir is connected to the HPLC oxidant feed pump using 1/8 in. (3.2 mm) O.D. teflon tubing. Before the pump, there is a three-way valve that allows the pump feed to be switched between the H_2O_2 feed tank and the water feed tank. Since H_2O_2 decomposition is catalyzed by metals, the reservoir, tubing and valves for the hydrogen peroxide feed system before the pump are plastic (HDPE, ETFE, or PTFE) to minimize the breakdown of H_2O_2, and subsequent formation of O_2 bubbles, before the pump. Any O_2 bubbles in the feed before the pump would interfere with the ability of the pump to maintain a steady, precise flowrate.

Organic Saturator

The organic saturator system is identical to the described oxygen saturator system. When the reactant is a gas, a dissolved aqueous solution of the gas is prepared in the same manner as described for preparing a dissolved O_2 solution. The organic saturator was not used for the experiments reported in this thesis. For details on experiments conducted using the organic saturator, see Holgate (1993).

Organic Feed Tank

All experiments performed in this thesis used the organic feed tank for holding prepared aqueous solutions of the organic. The organic feed tank is a 5 liter plastic-coated glass feed vessel with a conical bottom (Kontes, p/n 953901-5002). The contents can be magnetically stirred. Aqueous solutions of organics that are highly soluble in water are prepared volumetrically using Class A glassware and a 2.5 or 5.0 mL syringe and then transferred to the feed vessel. This method was employed for the SCWO experiments on methanol which will be presented in Chapter 4. For

organics that are sparingly soluble in water, as is the case with benzene, a saturated aqueous organic solution was made by filling the 5 liter vessel with approximately 4.5 liters of deionized water and then adding the organic directly to the vessel in an amount which exceeds the solubility limit. The 2-phase solution was allowed to equilibrate, and the saturated aqueous solution of the organic used as the organic feed. The advantage of using saturated solutions for organics that are not highly water soluble is that, as long as sufficient time is given to achieve equilibrium, the aqueous organic concentration is always the solubility limit, and the difficulty of volumetrically preparing a given concentration of a hydrophobic organic in water is avoided.

The organic feed tank is connected to the HPLC organic pump via 1/8 in. (3.2 mm) O.D. teflon tubing. Before the pump, a three-way valve allows the pump feed to be switched between the organic feed tank and the water feed tank. The tank is capped and pressurized with 1.5 bar of helium to provide adequate head pressure to deliver the solution to the HPLC organic feed pump. A sampling line, made of 1/8 in. (3.2 mm) O.D. teflon tubing and an on/off valve, provides a means of withdrawing volumes of the organic solution for analysis.

Water Feed Tank

The water feed tank is a large reservoir for holding deionized water. During heatup and cooldown, pure water is pumped through the reactor from this tank. The water feed tank is connected by 340SS tubing to the three-way valves located prior to the pumps on the organic and oxidant feed lines. The valves the supply to the pumps to be switched from the organic or oxidant solutions to the water feed tank. During hydrolysis experiments (reaction of the organic in the absence of oxygen), the water feed tank delivers water through the oxidant feed pump throughout the experiment.

Feed Pumps

The organic and oxidant feeds are pressurized to the reactor pressure (typically 246 bar) and delivered to the system via two independent, digital HPLC pumps (Rainin, SD-200). Each pump has a 25 mL/min pump head which can increment flow at 0.001 mL/min. These pumps are rated for operation at 4,600 psig (318 bar) at maximum flow. Each pump also has a pulse-dampening pressure module. Using these pumps, the total pressure fluctuations measured downstream were only ±2 bar at the normal operating pressure of 246 bar (±0.8%). These pumps

are a new addition, modifying the systems of Holgate (1993) and Marrone (1998). The new pumps were added to increase the maximum achievable flowrate (the previous pumps had a maximum flowrate of 7 mL/min) and to decrease pressure pulsations. These pumps were also used in the methanol oxidation experiments of Phenix (1998), which will be partially summarized in Chapter 4.

The feed to the organic pump can be from the organic saturator or the organic feed tank, and that to the oxygen pump can be from the oxygen saturator or the hydrogen peroxide tank. Alternatively, both pumps can draw water from the water feed tank. The organic, hydrogen peroxide, and water feed tanks are each pressurized with 1.5-1.7 bar of helium, a sufficient head pressure to ensure the feeds are delivered to the suction-side of the pump faster than the pump draws the solution on the intake stroke of the pump's piston. Without sufficient head pressure, air bubbles will form in the piston chamber, and the pump will not deliver the desired flowrate. A Tefzel ferrule (Upchurch, p/n P-300) and an 1/8 in. Delrin nut (Upchurch, p/n P-301) connect the 1/8 in. O.D. teflon tubing from the organic and hydrogen peroxide feed tanks to the pump inlet. If either the organic or oxygen saturator is in use, the feed to the pump is under high-pressure (up to 125 bar). A super flangeless 1/16 in. ferrule with a lock ring (Upchurch, p/n P-250) and a 316SS nut (Upchurch, p/n F-160) connect 316SS 1/16 in. (1.6 mm) O.D. tubing to the pump in this case. Each pump has a pressure transducer which displays the pressure at the pump's exit. There is also a pressure gauge on the oxidant feed line just after the pump.

Although the HPLC pumps allow the flowrate to be set through the digital interface, it was observed that the actual flowrate was slightly higher than the setpoint when the pumps were installed in the reactor system. As a result, each pump was calibrated for use in the reactor system. The resulting pump calibration curves calculate the actual flowrate of each pump as a function of the pump setpoint, the total system pressure, and the suction-side pressure. These calibration curves were used to determine the flowrate delivered from the pumps in the design of experiments and for data analysis.

3.1.2 Preheating System

The preheating system separately heats the pressurized organic and oxidant lines to operating temperature before the two feeds are mixed at the reactor entrance. There are two subsections of the preheating system: the direct ohmic preheating section followed by preheating coils located in the sandbath which houses the reactor. The direct ohmic preheating section replaces

the preheater sandbath used by earlier investigators (Holgate and Tester, 1993; Marrone *et al.*, 1995) and is the same system used by Phenix (1998). The preheater sandbath was replaced because the direct ohmic system provides superior temperature control and allows preheating to higher temperatures than were achievable with the sandbath.

Direct Ohmic Heating

The direct ohmic heating (DOH) section of the preheater separately heats the aqueous organic and oxidant feeds to the reaction temperature using resistive heating. The system is an adaptation of the DOH system used at Los Alamos National Laboratory. Heating is accomplished by applying a voltage across independent 9.5 m lengths of 1/16 in. (1.6 mm) O.D. x 0.01 in. (0.25 mm) wall HC-276 tubing. Given that the resistance of the tubing of each preheater is 11 Ohms, up to 1300 Watts of power can be generated with application of the full 120 VAC, sufficient power to heat the feed streams to reaction temperature. Each 9.5 m tubing section is coiled and thermally and electrically insulated using two layers of high-temperature Nextel sleeving (Omega, p/n XC-116 and SXC-316). Electrical insulation is necessary to prevent both contact between the organic and oxidant DOH coils and the short circuiting of the individual coils that would occur if the successive coils of a preheater came into contact. These insulated coils are housed in a 20 cm x 36 cm x 66 cm insulated box made of Kaowool board and fiber bond cement (Lynn Ceramics). Loose, bulk alumina-silicate ceramic fiber (Lynn Ceramics) is packed around the coils and completely fills the box, providing additional insulation. The positive lead of a 120 VAC line is clamped to the upstream end of each 9.5 m coil, and the negative lead is clamped to the downstream end. A back-up ground is also attached to the tubing immediately after the negative lead to direct the electricity to ground in the event that contact is lost between the negative lead and the coil. At the beginning of each DOH preheater and immediately upstream of the contact point of the positive lead, there is a short section of high-pressure 1/8 in. (3.2 mm) O.D. x 0.04 in. (1.0 mm) I.D. PEEK tubing followed by a check valve (Nupro, p/n SS-53S4). The PEEK tubing electrically isolates the upstream section of the reactor, and the check valve prevents hot water from flowing back through the PEEK tubing should upstream pressure be lost. There are ungrounded 1/32 in. Type-K thermocouples located in the organic and oxidant flowstreams to monitor the fluid temperatures just before the DOH coils leave the insulated box. The last approximately 0.5 m of the 9.5 m DOH preheating coils, situated just before the preheaters drop into the sandbath housing the reactor, are

not located inside the insulated box due to the geometric constraints of the system. To prevent heat loss the preheating lines here are traced with Samox heat tape (Thermolyne, p/n BWH102060, 1 in. wide x 6 ft. long, 904 W). The power to the heat tape is controlled by a Thermolyne Percentage Power Controller (Thermolyne, Type CN45500, 120 VAC, 15 A), and the power setting is normally on "HI."

Temperature regulation of the DOH system is accomplished by controlling the supplied voltage levels, which are specified by thermocouples (1/32 in. Type-K thermocouples) located immediately after the negative leads and the back-up grounds on each preheater. The thermocouple tips are centered in the flow streams, and their output is routed to Omega PID temperature controllers (Omega, p/n CN9141A). Zero-voltage-switched, silicon controlled rectifier (SCR) power controllers (Omega, p/n CR71Z-230, 240 VAC, 30 A) regulate the percentage of complete sine waves delivered to the preheaters based on the signal from the Omega PID controllers.

There is about a 30 cm section of preheater tubing on each of the feed streams just after the control thermocouple and before the feeds enter the fluidized sandbath. These 30 cm sections are actively heated by resistive cable heaters (Watlow, p/n 62H24A6X, 1/16 in. (1.6 mm) O.D. x 2 ft. (61 cm) long, 10 V, 240 W max) which are wrapped around the preheater tubing. The tubing and cable heaters are insulated with Zetex insulating wrap (1 in. wide). The power to the cable heaters is controlled by variable transformers (Powerstat, p/n 3PN117C, 0-120 V, 12 A).

Preheating in the Fluidized Sandbath

Additional preheater tubing is located in the fluidized sandbath (Techne, FB-08) which contains the reactor. Once the organic and oxidant streams enter the sandbath, each stream passes through an additional 5.2 m coiled length of 1/16 in. (1.6 mm) O.D. x 0.01 in. (0.25 mm) wall HC-276 tubing. This additional tubing serves to ensure that the feeds enter the reactor at the desired temperature.

3.1.3 Reactor System

As most of the preheating load is accomplished by the DOH system, the main purpose of the Techne FB-08 fluidized sandbath is to provide an isothermal environment for the reactor. The sandbath operates at temperatures up to 700°C, and the temperature is controlled by a Eurotherm PID controller which uses a Type K thermocouple located in the sand as its sensing element. The

sand temperature at the bottom and the top of the sandbath is measured with 1/16 in. Type K thermocouples. With proper fluidization, the temperatures measured by the three thermocouples are within 2-3°C of each other.

Mixing of the organic and oxidant streams is accomplished in a specially modified 1/8 in. HC-276 cross from High Pressure Equipment (p/n 60-24HF2). The feed streams enter the cross in opposed flow configuration. The internal diameters of the two arms of the cross through which the organic and oxidant feeds enter were reduced from their original 1/16 in. (1.6 mm) I.D. to 0.01 in. (0.25 mm) I.D. to increase the velocities of the organic and oxidant feeds and thus increase the rate of mixing by press fitting short lengths of 1/16 in. (1.6 mm) O.D. x 0.01 in. (0.25 mm) I.D. 316SS tubing into those arms. Details of the mixing cross can be found in Phenix (1998) and will be summarized in Chapter 4. A 1/16 in. Type K thermocouple is seated in the top port of the cross, and its tip extends into the fluid. A HC-276 1/8 in. to 1/4 in. adapter (High Pressure Equipment, p/n 60-21HF4HM2) occupies the fourth port which connects the 1/4 in. (6.35 mm) O.D. reactor to the cross.

The reactor itself is a 1/4 in. (6.35 mm) O.D. x 0.067 in. (1.7 mm) I.D. 4.71 m coiled length of Inconel 625 tubing with an internal volume of 10.71 cm^3. At the end of the reactor there is another 1/4 in. to 1/8 in. adapter connected to an 1/8 in. HC-276 tee from High Pressure Equipment (p/n 60-23HF2). A second 1/16 in. Type K thermocouple is seated in the tee, and its tip is positioned in the flowstream to allow temperature monitoring at the end of the reactor. The temperature at the entrance and exit of the reactor are typically within 2-3°C of each other at the normal operating temperatures of 450 to 600°C. A third 1/8 in. to 1/4 in. adapter connects the outlet of the tee to a 26 cm length of 1/4 in. (6.35 mm) O.D. x 1/16 in. (1.6 mm) I.D. insulated HC-276 tubing which rises out of the sand and connects to the heat exchanger. This 26 cm section of tubing, referred to as the riser, has an internal volume of 0.51 cm^3. The temperature is measured at the end of this riser with a 1/32 in. Type K thermocouple but is not monitored in the riser section. Since only a portion of the riser is located in the sand, the riser is non-isothermal. It is unknown at what point in the riser reaction stops, nor is volumetric flowrate (which is a function of density which is itself a function of temperature) known. Given that the volume of the fittings (inlet cross, exit tee and 1/4 in. to 1/8 in. adapters) is 0.28 cm^3, the non-isothermal riser accounts for only 4% of the total reactor volume (reactor, fittings and riser). Since residence time of the fluid in the reactor is

calculated by dividing the reactor volume by the volumetric flowrate, the uncertainties in reactor volume and volumetric flowrate contribute to the reported error in the residence time. But, the riser volume is only a small percentage of the total reactor volume, and these uncertainties only lead to about a 2 to 3% uncertainty in the residence time.

3.1.4 Letdown System and Sample Collection

The reactor effluent enters the inner tube of a shell-and-tube heat exchanger and is immediately quenched. The inner tube of the heat exchanger is a 3 m length of 1/4 in. (6.35 mm) O.D. x 0.065 in. (1.65 mm) wall HC-276 tubing. The outer shell is a 2.4 m length of 1/2 in. (1.3 cm) O.D. x 0.035 in. (0.89 mm) wall copper tubing. The cooling water source is the building cold water supply which is pre-filtered through a 10 μm spiral-wound prefilter cartridge (VWR, p/n 26303-052).

Downstream of the heat exchanger there is a pressure transducer (Dynisco, Model 832) which measures the system pressure. The pressure read at this transducer is typically the same as that read by the pressure gauge located on the oxidant stream feed line within the accuracy of the instruments.

A spring-loaded, manual backpressure regulator (Tescom, p/n 26-3200), which is located downstream of the pressure transducer, controls system pressure. Upon passing through the backpressure regulator, the effluent is flashed to atmospheric pressure. The effluent is now two-phase, and the vapor and liquid streams are separated in a gas-liquid separator constructed of 20 cm of 1/2 in. (1.3 cm) O.D. 316SS tubing packed with 4 mm borosilicate glass beads. The gas travels up, passes through a sampling port, on to a soap-bubble flowmeter, and finally is vented to the hood. Gas samples are taken from the sampling port with a syringe, and the flowrate of the gas stream is measured using the soap-bubble flowmeter and a stopwatch. The liquid travels out the bottom of the separator and into a 1/8 in. (3.2 mm) O.D. 316SS liquid sampling line. Liquid samples are collected from this line, and the flowrate is measured using a Class A volumetric flask and a stopwatch.

3.1.5 Health and Safety

There are many potential hazards associated with the operation of this high-pressure, high-temperature reactor system. These risks include: overpressurization of the reactor system; electric

shock from the DOH system; inhalation of the sand; burns from the hot fluid, heated metal or the sand from the sandbath; and exposure to toxic chemicals. Careful analysis of each of these hazards has led to the installation of equipment and the adoption of operating procedures which provide an adequate level of safety for the operator.

Overpressurization

The risk of overpressurization of the reactor system is minimized in many ways. First, the digital HPLC pumps can shut down if they reach a user-specified maximum pressure, and they automatically shut down if the pressure exceeds the maximum pump pressure of 4600 psig (318 bar). There is a rupture disk downstream of the heat exchanger (High Pressure Equipment) set to burst at 4,500 psig (311 bar) +6%, -3%. The organic and oxygen saturators both have rupture disk on them which will burst at 1,988 psig (138 bar) +6%, -3% at 25°C to prevent their overpressurization. The entire reactor system is housed inside 3/8 in. (0.95 cm) to 1/2 in. (1.3 cm) Lexan mounted on a Unistrut frame to protect the operators should a piece of metal under pressure let go.

Electric Shock Hazard

The DOH system is electrically isolated from the upstream system by the PEEK tubing, and downstream of the negative lead there is a backup ground which will conduct the current to ground should the negative lead lose contact with the tubing. All electrically conducting sections of the DOH system are well insulated to eliminate the possibility of individuals accidentally contacting any electrically conducting metal tubing. There are three readily accessible locations to cut power to the DOH system, including the main circuit breaker.

Inhalation Hazard

The fluidized sandbath is located inside a ventilated Lexan box. The sandbath itself has an air reclamation system which recaptures expelled sand, and ventilation of the Lexan box prevents any escaped sand from entering the laboratory. Whenever it is necessary to work on or around the fluidized sandbath, dust masks are worn to prevent sand inhalation.

Burn Hazard

All heated sections of the system are located inside the Lexan shielding. Additionally, all heated metal is either in the sandbath or enclosed in insulation, so the operator cannot directly

contact hot metal. If any heated section of the reactor develops a leak, the hot fluid will be contained inside both the insulation or sandbath and the Lexan shielding.

Chemical Exposure Hazard

Exposure to the organic feed and the liquid and vapor effluent is minimized, and the proper personal protective equipment is worn when feeds and samples must be handled. The organic feed tank is kept in a hood in a plastic coated, glass vessel. In the event that the feed tank should develop a leak, the organic would be wholly contained inside this hood. The vapor-phase reactor effluent is vented directly to this same hood, and the liquid sample collection port is enclosed in a ventilated box. This active ventilation system ensures that organic vapors will not be present in the laboratory.

3.1.6 Disadvantages of the Bench-Scale SCWO System

Due to its design and internal dimensions, the main application for the bench-scale, tubular reactor system is for studying reactions of water-soluble organic compounds which do not contain heteroatoms and do not rapidly react without O_2. Without modification, the reactor system cannot be used to study the reaction kinetics of organics which are not water soluble under ambient conditions due to the design of the feed system (see Section 3.1.1). Measuring kinetic data of organics which react in supercritical water without oxygen is very difficult because initial breakdown of the organic begins in the non-isothermal preheating section (see Section 3.1.2) preventing the direct measurement of the isothermal, isobaric reaction rate in the main reactor. Heteroatom (*i.e.*, Cl, N, S or P) containing organics typically decompose in the preheater, producing acids (*i.e.*, HCl, HNO_3, H_2SO_4 or H_3PO_4) which can rapidly corrode the preheater tubing and eventually lead to stress-corrosion cracking of the preheater walls. These acids can be neutralized by the addition of base to the feed, forming salts. Practically, because of extremely low salt solubilities, precipitation can occur in the supercritical sections of the reactor, and due to the extremely small internal dimensions of the reactor (the mixing tee only has an I.D. of 0.01 in. or 0.25 mm) any precipitated salts would rapidly plug the reactor. These small internal dimensions also prevent the study of contaminated soils. Additionally, due to the high surface to volume ratio of the reactor, surface reactions may contribute to the observed reaction rates. If measured reaction rates are influenced by surface reactions, the kinetic data cannot be used reliably for the design of industrial reactors which will have much lower surface to volume ratios and, therefore, wall reaction

contribute to the overall kinetics by a much smaller degree. Lastly, this reactor is not designed for *in situ* monitoring of the reactant and reaction products.

3.1.7 New Reactor Systems

Two new reactors, a large-scale tubular flow reactor and a continuous stirred tank reactor, were designed to complement the bench-scale, tubular flow reactor. The continuous stirred tank reactor (CSTR) has an internal volume of 500 mL, and addresses many of the limitations of the bench-scale reactor. The pure organic feed is pumped cold directly into the CSTR where it is instantaneously heated by and mixed with the supercritical water. This direct feed of the organic enables the study of organics which are not water soluble and also prevents the premature reaction of the organic before reaching the reactor. Heteroatom containing wastes can be preneutralized with base since salt plugging will not be problematic given the large internal volume of the reactor. The CSTR is equipped with a spinning basket which can be used to, among other things, hold contaminated soils. Additionally, the CSTR has a much lower surface-to-volume ratio. Surface reactions, if present, will have a much smaller influence on kinetics. Details on the design of the CSTR as well as the results from initial kinetics measurements are given in Marrone (1998).

The large-scale tubular flow reactor was designed to allow *in situ* analysis of the reactant and reaction products and provide a wall-less reaction environment. The reactor is equipped with sapphire windows which give visual and spectroscopic access into a section of the reactor at supercritical conditions. There is a moveable sampling probe which allows for the measurement of temperature and for sample collection along the entire length of the reactor. The benefit of such a probe is that measurements at multiple residence times can be made in one experiment. With the bench-scale reactor, each experiment only gives information at a single residence time. Additionally, simultaneous measurements with Raman spectroscopy will allow a comparison of *in situ* measurements with the end-of-pipe measurements using the sampling probe. The large-scale reactor was designed to prevent contact of the reactants and reaction products with the reactor walls. This wall-less system will ensure that the measured kinetic rates are not affected by any heterogeneous reactions which may occur in the small-diameter, bench-scale reactor.

3.2 Reactor Operation and Data Collection

During start-up deionized water from the water feed tank is pumped through the system. With a steady flow of water, the system is pressurized and cooling water flow to the heat exchanger is established. Next, power to the sandbath and the heat tape is turned on, and the DOH preheating system is turned on a short time later. Meanwhile, the organic and hydrogen peroxide feeds are prepared (if saturators are being used feed preparation is done the previous day). When the preheaters and the sandbath reach reaction temperature, the feeds to the pumps are switch from the water feed tank to the organic and oxidant feeds. About half an hour is required to achieve steady state conditions after beginning the organic and oxidant feeds. In total approximately two and a half hours is needed before the reactor reaches steady state and data collection begins.

A typical experiment, where kinetic data is measured at a single pressure, temperature, residence time, and initial organic and oxygen concentration, lasts about one and a half hours. During this time period between three and six liquid and six gas effluent samples are collected for analysis. The gas effluent is injected immediately onto three separate gas chromatographs. Consistency amongst the samples of the gas-phase products indicates steady state conditions in the reactor. Temperatures in the preheaters, sandbath, reactor, and before the heat exchanger are logged to a computer every 10 seconds. Liquid and gas flow rates are measured as often as possible, but at a minimum each is measured whenever liquid and gas samples are collected. The pressure is read and recorded from the pressure transducer just before the back pressure regulator with every flowrate measurement. When a hydrogen peroxide feed solution is being used, samples of the solution are collected for measurement before and after the experiment. Samples of the organic feed from the organic feed tank are collected periodically during an experiment. After obtaining six consistent measurements of the gas-phase and collecting the six liquid samples, conditions can be changed or the reactor is shut down. When changing conditions, about one hour is needed to reach steady state at the new conditions. During the course of one day, data usually can be obtained at three sets of conditions.

3.2.1 Temperature Measurement

There are thirteen thermocouples located throughout the reactor system as marked in Figure 3-1. Temperatures which are regularly recorded are: the temperature of both the organic and oxidant feeds at the end of the DOH system (these are also the control thermocouples for the DOH

system); the temperature in the cross at the beginning of the reactor, that in the tee at the end of the reactor, and the temperature at the end of the riser just before the heat exchanger; and the temperature at the top and the bottom of the sandbath. The measurements from these seven thermocouples are logged every ten seconds using a software package called HOTMUX™ from DCC Corporation. Measurements from the thermocouples in the saturators are only logged when the saturators are in use. The thermocouples located inside the insulated box of the DOH preheating system allow monitoring of the fluid temperatures, but the temperatures here are not recorded. The reading from the thermocouple located in the gas-liquid separator also is not normally recorded.

3.3 Analytical Methods

During the course of one experiment, between three and six liquid and six vapor samples were collected for analysis. The gas samples were analyzed immediately by gas chromatography. The liquid samples were collected in 2 mL amber autosampler vials capped with PTFE/silicone caps and stored in a refrigerated autosampler tray maintained at 5°C. Samples of the organic feed were also collected in the 2 mL vials and stored in the tray. Analysis of the liquid effluent and feed samples was performed via gas chromatography after the gas analysis was complete.

There are four gas chromatographs (GCs) for performing the analysis of the organic feed and the liquid- and vapor-phase effluent. There are two Hewlett Packard (HP) 5890 Series II GCs. The first is equipped with a thermal conductivity detector (TCD) and a flame ionization detector (FID) and has an autosampler and an autosampler tray. The second has an electron capture detector (ECD) and an FID. There is a Hewlett Packard (HP) 6890 GC with both an FID and a TCD which also has an autosampler and autosampler tray. Lastly, there is a Perkin Elmer Sigma 1B GC with a TCD. The carrier, make-up and detector gases are all Grade 5.

3.3.1 Organic Feeds and Liquid-Phase Effluent Analysis

The FIDs on the first HP 5890 GC and on the HP 6890 GC were used to analyze the organic feeds and the liquid-phase effluent samples in the experimental work of this thesis. The autosamplers injected 0.2 to 1.0 μL of the liquid sample through Merlin Microseal duckbill septa (HP, p/n 5182-3442), specialty long-life septa for use with autosamplers. On the 5890 injection was into a splitless, single taper, glass wool packed, capillary inlet liner (HP, p/n 5062-3587). Analytes

were separated on a 30 m x 530 μm x 5 μm film thickness DB-1 column (J&W Scientific, p/n 125-1035) preceded by 5 m of a Restek Hydroguard retention column (Restek, p/n 100810), a specialty column for focusing water with aqueous samples. On the 6890 the same inlet liner and guard column was used, but the main column was a 30 m x 530 μm x 1 μm film thickness DB-WAX column (J&W Scientific, p/n 125-7032). The detailed analytical methods for the feed and liquid effluent analysis are located in Appendix 10-1.

Multiple analyses of each liquid effluent and organic feed sample were performed. The results were used to calculated average concentrations and standard deviations of the feed and liquid-phase constituents. The measured average concentrations and their associated standard deviations were used in the data and error analysis for the experiment.

3.3.2 Gas-Phase Effluent Analysis

Gas phase analysis was performed on the FID on the second HP 5890 GC, as well as on the three TCDs in the experimental work of this thesis.

Analysis of Light Gases

The TCDs on the 5890 and 6890 GCs were used for the analysis of O_2, N_2, CO, CO_2, and CH_4. Both GCs are identically configured with two packed columns connected in series through an air actuated switching valve (HP Valving Option 404) and use helium as the carrier gas. The first column is a 5 ft. x 1/8 in. 60/80 mesh Carboxen 1000 column and the second is an 8 ft. x 1/8 in. 60/80 mesh Molsieve 5A column. Gas samples of the vapor-phase effluent were taken by inserting a gas-tight teflon tipped syringe into the septa-sealed sampling port located above the gas/liquid separator and withdrawing a 200 μL sample. The sample was injected alternately into each of the two GCs such that three gas samples were analyzed on each GC. The gas sample first passes through the Carboxen column, which separates CO, CO_2 and CH_4 but does not retain O_2, N_2 or H_2. The O_2, N_2 and H_2 pass on to and are separated by the Molsieve column prior to reaching the detector. The CO, which is less retained than CO_2 and CH_4 on the Carboxen column, also passes through the Molsieve column and on to the detector. Since CO_2 irreversibly absorbs onto the Molsieve column, the switching valve reverses the flow of the carrier gas before the CO_2 and CH_4 reach the column. The CO_2 and CH_4 pass back through the Carboxen column to the detector. The elution order of the compounds is: H_2, O_2, N_2, CO, CO_2 and CH_4. The analysis program is

presented in detail in Appendix 10-1. The average and standard deviations of the gas concentrations from the gas samples were used in the data and error analysis of the experiment.

Analysis of Hydrogen and Helium

The TCD on the Perkin Elmer Sigma 1B GC was used for detection of hydrogen and helium. Even though hydrogen can be detected in large concentrations on the TCDs used for the analysis of the light gases, the sensitivity of these TCDs to hydrogen is very low because helium is used as a carrier gas. Helium, which is occasionally found in the effluent gas since it is used to provide head pressure to the organic and hydrogen peroxide feeds, cannot be detected with a helium carrier gas. The TCD on the Perkin Elmer Sigma 1B GC uses a nitrogen carrier gas which allows the detection of low levels of hydrogen and of helium. The separation of helium and hydrogen is accomplished on a 12 ft. x 1/8 in. 80/100 mesh Porapak T column in series via a switching valve with an 8 ft. x 1/8 in. 60/80 mesh Molsieve 5A (the valve is always left in its initial position during this analysis). Details of the method are given in Appendix 10-1. Gas samples were injected for analysis of helium and hydrogen concurrent with the analysis of the other light gases. The average and standard deviations of the hydrogen and helium concentrations from these six injections were used in the data and error analysis of the experiment.

Analysis of Light Hydrocarbons

Analysis of light hydrocarbons was performed on the second HP 5890 Series II GC which has both the ECD and FID. The FID only was used for the light hydrocarbon analysis. A 200 µL gas sample was injected into a glass wool packed, split/splitless capillary inlet liner (HP, p/n 19251-60540). A complete separation of all C_1-C_6 hydrocarbon gases was accomplished using a 15 m x 320 µm bonded PLOT column developed by Astec for the analysis of C_1-C_{10} hydrocarbons (Astec Gas Pro, p/n 81103). Details of the analytical procedure can be found in Appendix 10-1. This analysis takes about three times as long as does the analysis of the light gases, so only two analyses of the vapor effluent for light hydrocarbons was performed per experiment. The average and standard deviation of these samples were used in the data and error analysis of the experiment.

3.3.3 Oxidant Feed Analysis

Dissolved Oxygen Concentration

The equilibrium dissolved oxygen concentration in the oxygen saturator was determined by calculation as described in Section 3.1.1. When the oxygen saturator is in use, the pressure and temperature of the saturator are monitored periodically during the experiment. The average and standard deviations of these measurements are used in the data and error analysis for the experiment to calculate the dissolved O_2 concentration of the oxidant feed. The concentration of O_2 at the inlet of the reactor depends upon the flowrate of the organic and oxidant streams as well as on the density of the supercritical water in the reactor relative to its density in the saturator.

Hydrogen Peroxide Analysis

The concentration of the hydrogen peroxide feed solution, prepared by volumetrically diluting a 30 wt% aqueous solution of H_2O_2 with deionized water, is checked using a ceric ion titration method. With this method, the H_2O_2 solution is titrated with the strong oxidant tetravalent cerium ion in the presence of ferroin indicator. When all of the H_2O_2 is oxidized by the cerium ion, the cerium ion oxidizes the indicator causing a color change. The amount of cerium ion needed to induce this color change is linearly proportional to the H_2O_2 concentration. The titration is performed using a Hach digital titrator (p/n 16900-01) and Hach hydrogen peroxide reagents (p/n 22928-00). To perform the assay, 30 mL of deionized water, 2 mL of 19.2 N H_2SO_4, and 200 µL of the H_2O_2 solution to be tested are added to a 50 mL Erlenmeyer flask. One drop of ferroin indicator solution is added to the flask, and the flask is stirred by adding a stir bar and placing the flask on a magnetic stir plate. While stirring, the solution is titrated with 0.5 N ceric ion solution until the solution changes from its original bright orange color to pale blue. The number of digits, as read from the digital titrator, of ceric ion necessary to cause a color change is recorded and the procedure is repeated twice more.

In the experimental work of this thesis, the concentration of the H_2O_2 solution was measured, in triplicate, at the beginning and end of every oxidation experiment. The average and standard deviation of these six measurements were used in the data and error analysis for the experiment.

3.4 DATA ANALYSIS

The experimental measurements and the results of the analytical measurements were used to determine kinetic data. During the course of an experiment, measurements from the thermocouples (see Section 3.2.1 and Figure 3-1), the downstream pressure as measured by the transducer located before the back pressure regulator, and the liquid and vapor phase flowrates were recorded into an Excel spreadsheet. The six vapor samples, the organic feed samples, the liquid-phase samples, and the hydrogen peroxide feed samples were analyzed as described in Section 3.3, and the results were also recorded in the spreadsheet. The averages and standard deviations of these measurements were used to calculate the: residence time in the reactor; initial reactor concentrations of the organic and oxidant; fuel equivalence ratio; conversion of the reactant; apparent first order rate constant; and the concentrations of the intermediate and final products.

3.4.1 Calculated Parameters

Reactor Concentrations

While concentrations of the organic and the oxidant feeds, the reactant in the liquid effluent, and the liquid- and gas-phase reaction products are directly measured by GC, the concentrations of these species at the beginning and end of the reactor are needed to determine conversions and product profiles. To calculate initial reactor concentrations of the organic ($[organic]_o$) and oxygen ($[O_2]_o$), the volumetric flowrate of the individual organic and oxidant streams, the ambient concentrations of the feeds, as well as the ambient and supercritical water densities are needed. Since the measured effluent flowrate is the combined flow from both pumps, to obtain flowrates of the individual streams the pump calibration is used to calculate the flowrate of one pump, and the flowrate of the other is assumed to be the difference between these two. From the measured values of the reactor temperature and pressure, the density of the supercritical water (ρ_{SCW}) is calculated from the steam tables (Haar *et al.*, 1984), as is the density of water at the ambient temperature and pressure (ρ_{AMB}). Given ρ_{SCW}, ρ_{AMB}, the individual flowrates of the organic and oxidant streams, and the measured concentrations of the organic and oxidant feeds, $[organic]_o$ and $[O_2]_o$ can be calculated. Likewise, calculating the concentrations of the reactant and the liquid-phase products at the end of the reactor requires knowledge of ρ_{SCW}, ρ_{AMB}, the volumetric liquid-phase flowrate and the measured ambient concentrations of the reactant and liquid-phase products.

To calculate the concentration of the gas-phase products at the end of the reactor, the concentration of the individual gases in both the gas and liquid phase of the effluent must be determined. The aqueous concentrations of the gases is again calculated from Henry's law:

$$y_i\hat{\phi}_i(T,P,y_i)P = x_i H_{i,H_2O}(T,P) \tag{3-5}$$

Given ambient pressure in the gas/liquid separator, the gas-phase fugacity coefficients for all species are set equal to one. Ambient pressure Henry's law coefficients as a function of temperature are taken from the literature for O_2 (Benson *et al.*, 1979), CO (Rettich *et al.*, 1982), H_2, N_2, He, CO_2, ethylene and acetylene (Wilhelm *et al.*, 1977), and methane and ethane (Rettich *et al.*, 1981). The Henry's law coefficient for CO_2 includes a correction to account for the formation of HCO_3^- and CO_3^{2-}. The liquid-phase concentrations of these gases are generally very small compared to their gas-phase molar flowrates. The only exception is CO_2 which has an appreciable water solubility. Once the total molar flowrate of each species in the gas and liquid-phase effluent is known, the concentration of each of these species at the end of the reactor is calculated using ρ_{SCW} and ρ_{AMB}.

Residence Time

The residence time in the reactor is calculated by dividing the reactor volume by the volumetric flowrate at supercritical conditions. While the volumetric flowrate in the reactor can be accurately calculated from the measured liquid-effluent flowrate and the ambient and supercritical densities of water, the volume of the reactor *in which reaction takes place* is not known accurately due to finite mixing and quench times. As discussed in Section 3.1.3, it is unknown at what point reaction stops in the non-isothermal riser section at the end of the reactor. The issue of mixing and its effects on apparent induction times is considered in detail in Chapter 4. We do report the contributions of the random uncertainties (*e.g.*, errors in the liquid flowrate, T and P) and the systematic uncertainty in the reactor volume to the uncertainty in residence time, but we do not have an accurate estimate of the length of the mixing time. As a result, we generally do not conduct experiments at residence times under 2 seconds where the systematic uncertainty in the residence time introduced by the mixing time could be upwards of 25%.

Conversion, Carbon Balances, Fuel Equivalence Ratio and First Order Rate Constant

Once the concentration of all species are known at the beginning and end of the reactor, the key reaction parameters can be calculated. Conversion of the reactant is calculated based on the reactant concentrations at the beginning and end of the reactor. The initial fuel equivalence ratio (Φ) is defined as:

$$\Phi = \frac{([\text{organic}]/[\text{oxygen}])_{\text{initial}}}{([\text{organic}]/[\text{oxygen}])_{\text{stoichiometric}}} \tag{3-6}$$

such that $\Phi < 1$ denotes fuel-lean conditions and $\Phi > 1$ signifies fuel-rich conditions. Reaction products are typically reported as carbon fractions:

$$\text{Carbon Fraction} = \frac{\text{moles carbon in product}}{\text{moles carbon in feed}} \tag{3-7}$$

or as yields:

$$\text{Yield} = \frac{\text{moles carbon in product}}{\text{moles carbon reacted}} \tag{3-8}$$

which are convenient parameters for determining the fate of the reacted carbon. Carbon balances are calculated to determine the percent of carbon recovered in these products:

$$\text{Carbon Balance} = \frac{\text{moles of carbon in effluent}}{\text{moles of carbon in feed}} \times 100\% \tag{3-9}$$

Calculation of carbon balances is key to the judgment of the quality of the data from an experiment. Carbon balances from experiments typically exceed 90%, as nearly all of the reacted carbon is accounted for in the liquid and vapor phase products or as unreacted reactant. Carbon balances inconsistent with other experiments may indicate either the presence of undetected products or a problem with the analytical measurements or reactor performance for that experiment. Apparent first-order rate constants are also calculated for each experiment by assuming the reaction rate is first-order in the reactant and zero order in all other species:

$$-\frac{dC}{dt} = k^* C \tag{3-10}$$

Here, C is the concentration of the reactant and k^* is the apparent first-order rate constant in s^{-1}. Integrating Eqn. (3-10) from C_0 to C and t_0 to t, allows calculation of k^*.

3.4.2 Error Analysis

All calculated parameter values are reported with either 95% or 99% confidence intervals. These confidence intervals are calculated by assuming the error on all experimentally measured values is represented by a Student's *t*-distribution and propagating these errors through to the calculated quantities. This confidence interval for the experimentally-measured value of variable x is calculated by:

$$\bar{x} \pm \frac{\sigma \cdot t_{1-\mathrm{CL}}\left((n_{obs}-1)\text{ degrees of freedom}\right)}{\sqrt{n_{obs}}} \tag{3-11}$$

where $\bar{x}$ is the sample mean, σ is the sample standard deviation, and $t_{1-\mathrm{CL}}\left((n_{obs}-1)\text{ degrees of freedom}\right)$ is the value from the *t* table at the stated confidence level with a given number of measurements (n_{obs}). The error distribution on the measured parameters is propagated to the calculated quantities by assuming the errors on the measured values are independent and random and applying the differential method.

3.5 REFERENCES

Benson, B.B., D. Krause and M.A. Peterson, "The solubility and isotopic fractionation of gases in dilute aqueous solution. I. Oxygen." *J. Solution Chem.* **8**(9), 655 (1979).

Brelvi, S.W. and J.P. O'Connell, "Corresponding states correlations for liquid compressibility and partial molar volumes of gases at infinite dilution in liquids." *AIChE Journal* **18**(6), 1239 (1972).

Haar, L., J.S. Gallagher and G.S. Kell, *NBS/NRC Steam Tables*. Hemisphere Publishing Corp., New York, NY (1984).

Holgate, H.R., "Oxidation chemistry and kinetics in supercritical water: hydrogen, carbon monoxide, and glucose." Ph.D. Thesis, Department of Department of Chemical Engineering, Massachusetts Institute of Technology, Cambridge, MA (1993).

Holgate, H.R. and J.W. Tester, "Fundamental kinetics and mechanisms of hydrogen oxidation in supercritical water." *Combust. Sci. Technol.* **88**, 369 (1993).

Marrone, P.A., "Hydrolysis and oxidation of model organic compounds in sub- and supercritical water: reactor design, kinetics measurements, and modeling." Ph.D. Thesis, Department of Chemical Engineering, Massachusetts Institute of Technology, Cambridge, MA (1998).

Marrone, P.A., R.P. Lachance, J.L. DiNaro, B.D. Phenix, J.C. Meyer, J.W. Tester, W.A. Peters and K.C. Swallow, "Methylene chloride oxidation and hydrolysis in supercritical water." in *Innovations in Supercritical Fluids: Science and Technology*, K. W. Hutchenson and N. Foster, Eds., ACS Symposium Series, **608**, American Chemical Society, Washington, D.C., Chapter 13 (1995).

Peng, D.Y. and D.B. Robinson, "New two-constant equation of state." *Ind. Eng. Chem. Fundam.* **15**, 59 (1976).

Phenix, B.D., "Hydrothermal oxidation of simple organic compounds." Ph.D. Thesis, Department of Chemical Engineering, Massachusetts Institute of Technology, Cambridge, MA (1998).

Reid, R.C., J.M. Prausnitz and B.E. Poling, *The properties of gases and liquids*. McGraw Hill, New York, NY (1987).

Rettich, T.R., R. Battino and E. Wilhelm, "Solubility of gases in liquids. 15. High-precision determination of Henry coefficients for carbon monoxide in liquid water at 278 to 323 K." *Ber. Bunsenges. Phys. Chem.* **86**, 1128 (1982).

Rettich, T.R., Y.P. Handa, R. Battino and E. Wilhelm, "Solubility of gases in liquids. 13. High-precision determination of Henry's constants for methane and ethane in liquid water at 278 to 328 K." *J. Phys. Chem.* **85**, 3230 (1981).

Wilhelm, E., R. Battino and R.J. Wilcock, "Low-pressure solubility of gases in liquid water." *Chem. Rev.* **77**(2), 219 (1977).

Chapter 4.

Characterization of Mixing Times and Hydrogen Peroxide as an Alternative Oxidant

Prior to undertaking the detailed study on the oxidation of benzene in supercritical water, joint work was conducted with Brian Phenix to optimize mixing and implement the use of hydrogen peroxide as an alternative oxidant. This study was motivated by the desire to better understand the differences between kinetic data measured in our lab with those observed at Sandia National Laboratories. Below follows a summary of the investigation of mixing times and the use of hydrogen peroxide as an alternative oxidant. For a detailed report on these issues, please refer to Phenix (1998).

4.1 Effect of Mixing Times on SCWO Kinetics

4.1.1 Introduction

Previous SCWO kinetic studies of hydrogen (Holgate and Tester, 1993), carbon monoxide (Holgate and Tester, 1994) and acetic acid (Meyer *et al.*, 1995) all reported the presence of an induction period before the onset of oxidation. These induction periods were estimated to be about 1 to 3 seconds in length by assuming a first-order dependence of the reaction rate on the fuel and linearly extrapolating data plotted as $\ln(C/C_0)$ vs. τ back to the point of zero conversion. The residence time corresponding to the extrapolated zero conversion point was interpreted as a purely kinetic induction time attributable to the time necessary to establish the free-radical pool. These extrapolations were necessary since a direct measurement of induction times was not possible in the reactor system (similar to that described in Chapter 3) used by these investigators due to the uncertainty in the residence time introduced by uncertainties in the quench time, reactor volume, and flowrates. The predictions of elementary reaction mechanisms developed for combustion conditions and adapted to SCWO conditions were indeed able to confirm the presence of these induction times, although they were predicted to be shorter than those observed (Holgate and Tester, 1993; Holgate and Tester, 1994).

Much shorter induction times were measured by Rice *et al.* (1996) at Sandia National Laboratories (SNL) in a study of methanol SCWO kinetics. Through the use of *in situ* Raman spectroscopy, methanol concentrations were measured in their plug flow reactor system at residence times of 0.2 to 2.7 seconds at 246 bar over a temperature range of 440 to 500°C with an initial methanol concentration of 1.5 wt% and a fuel equivalence ratio (Φ) of 0.85. A majority of these experiments were performed with residence times of less than 1 second. By extrapolating this very short residence time data, induction times of 0.13 to 0.69 seconds were estimated. The induction times were found to decrease with temperature, consistent with the observations at MIT.

Brock *et al.* (1996) also attempted to determine the induction time for methanol SCWO in their isothermal, isobaric, tubular plug-flow reactor by the extrapolation of very short residence time data. Experiments were conducted with residence times from 0.1 to 3.65 seconds, with a majority of the experiments performed at residence times less than 1 second. Induction times from 0.09 to 0.5 seconds were reported, decreasing with increasing temperature, for methanol oxidation at 249 bar with temperatures ranging from 500 to 589°C, initial methanol concentrations from 0.02 to 0.05 wt%, and fuel equivalence ratios of 0.12 to 0.54.

The ability of Brock *et al.* to accurately measure very short residence time data and infer induction times from that data is questionable. The experimental apparatus used by Brock *et al.* is similar to our own. With no *in situ* techniques for measuring real time species concentrations, the reaction mixture must first be quenched for measurement of methanol concentrations in the liquid effluent samples by GC. When measuring very short residence time data, as was done here, the residence time probably is not known with good accuracy due to the large contribution of systematic uncertainties. For example, the time necessary to quench the reaction and any uncertainties in determining the exact point in the reactor where reaction stops could easily be on the order of these very short residence time measurements. Additionally, there is significant scatter in the lower temperature data measured by Brock *et al.* which hinders a precise estimation of the induction time. Although 95% confidence intervals were reported on the induction times ranging from ±10 to ±76% of the mean values, no discussion of the contributing factors to these confidence intervals was presented. The short residence time data measured by Rice *et al.* using an *in situ* technique and the induction times inferred from that data should be more accurate than the determinations of induction times by Brock and coworkers.

4.1.2 Early evidence of mixing times

Methanol oxidation kinetics measured at 500°C and 246 bar with an initial methanol concentration of 0.069 wt% and a Φ of 1.5 appear in Figure 4-1. These data were measured using an 8.2 m × 1/8 in. (3.18 mm) O.D. × 0.041 in. (1.04 mm) I.D. 316SS reactor fitted with the opposed flow 1/8 in. HC-276 high-pressure mixing cross (HIP, p/n 60-24HF2) at the reactor entrance denoted as "configuration 1" in Figure 4-2. Extrapolation of the data to zero conversion yielded an induction time (τ_{ind}) of around 3 seconds. This is significantly longer than the 0.13 second τ_{ind} reported by Rice *et al.* at 500°C, although it should be noted the measurement of τ_{ind} by Rice *et al.* was obtained with a significantly higher initial methanol concentration.

As a result of a sc.ed fitting, the mixing cross used in these first experiments (configuration 1) was replaced with what was thought to be an identical cross (configuration 2). New measurements at the same conditions and in the same 8.2 m reactor as in Figure 4-1 produced the new 4 to 12 second residence time data in Figure 4-3. Curiously, the new data appeared to be showing a shorter τ_{ind}. In order to access shorter residence times, a new 316SS 1/8 in. (3.18 mm) O.D. × 0.041 in. (1.04 mm) I.D. reactor was constructed with a length of only 2.5 m and used in

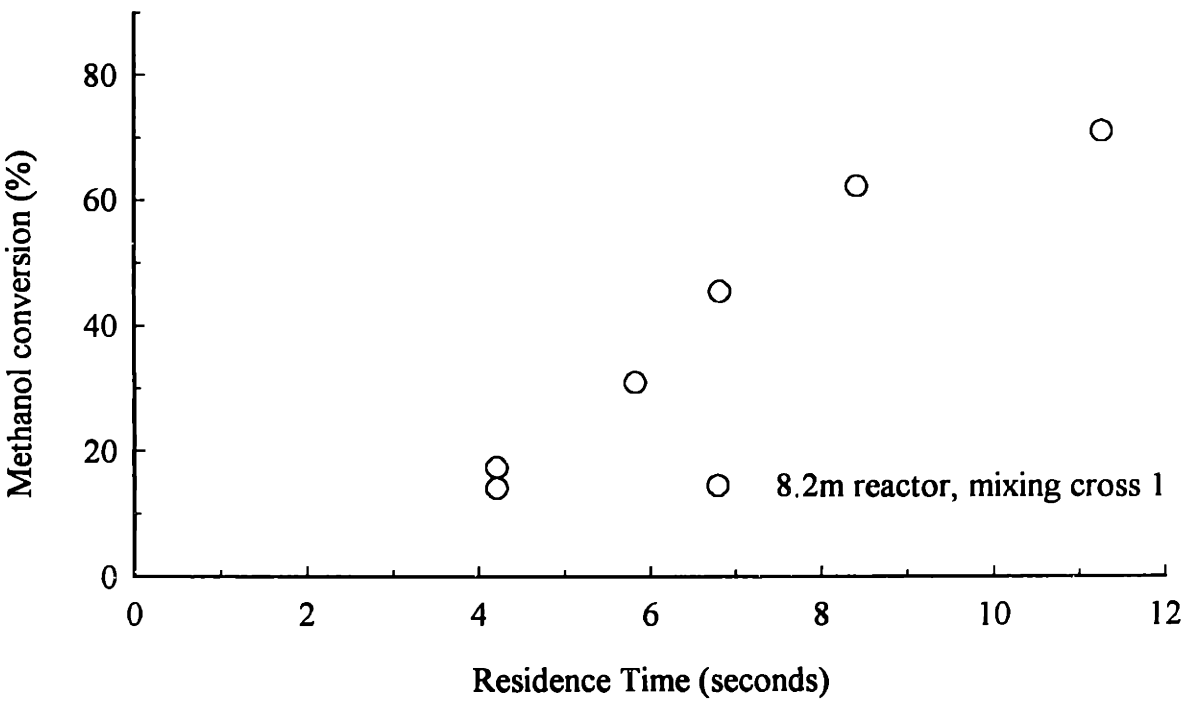

Figure 4-1 Methanol conversion as a function of time using mixing cross 1
(T=500°C, P=246 bar, $[CH_3OH]_0$=0.069 wt %, Φ=1.5)

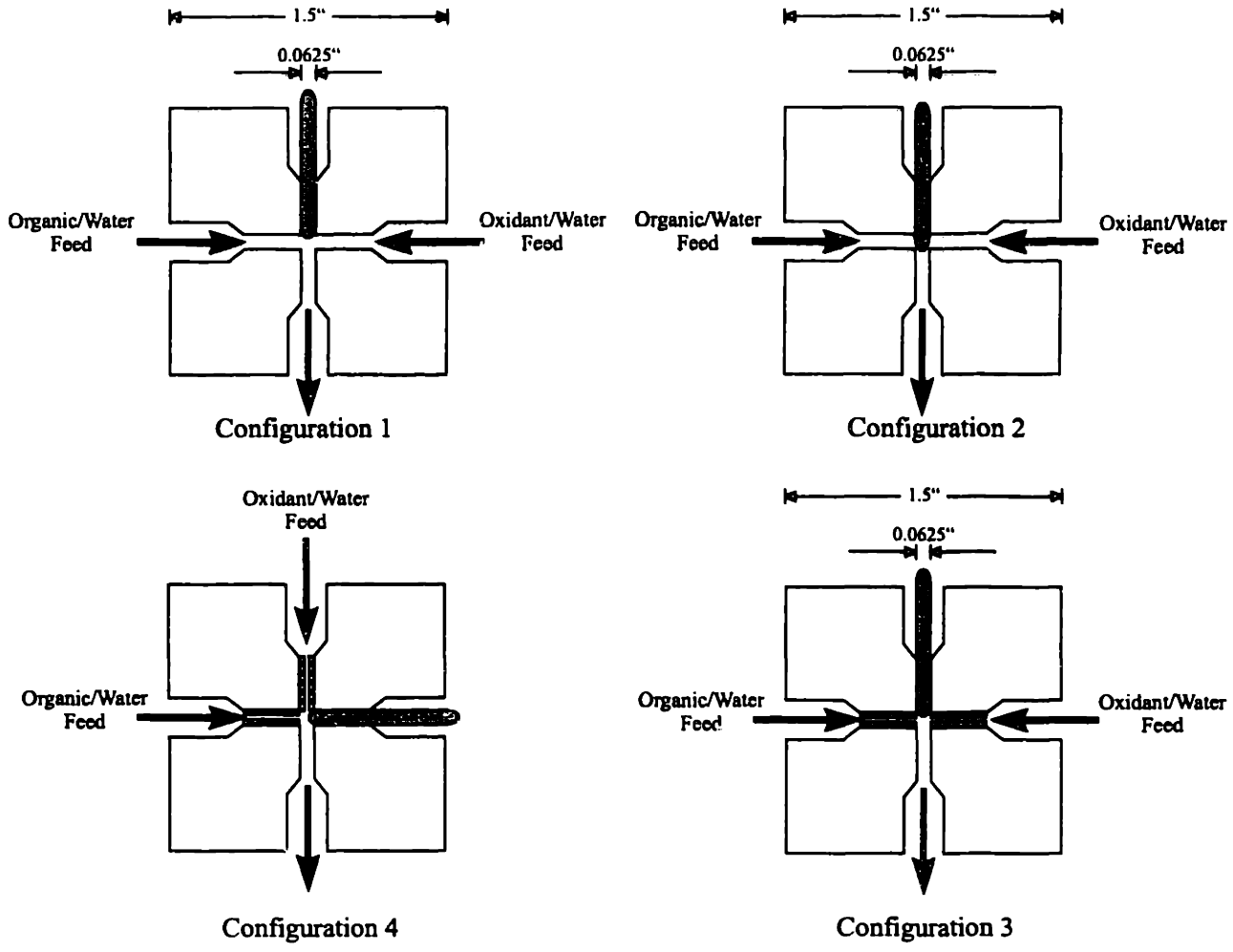

Figure 4-2 Schematics of mixing crosses used in the methanol oxidation experiments

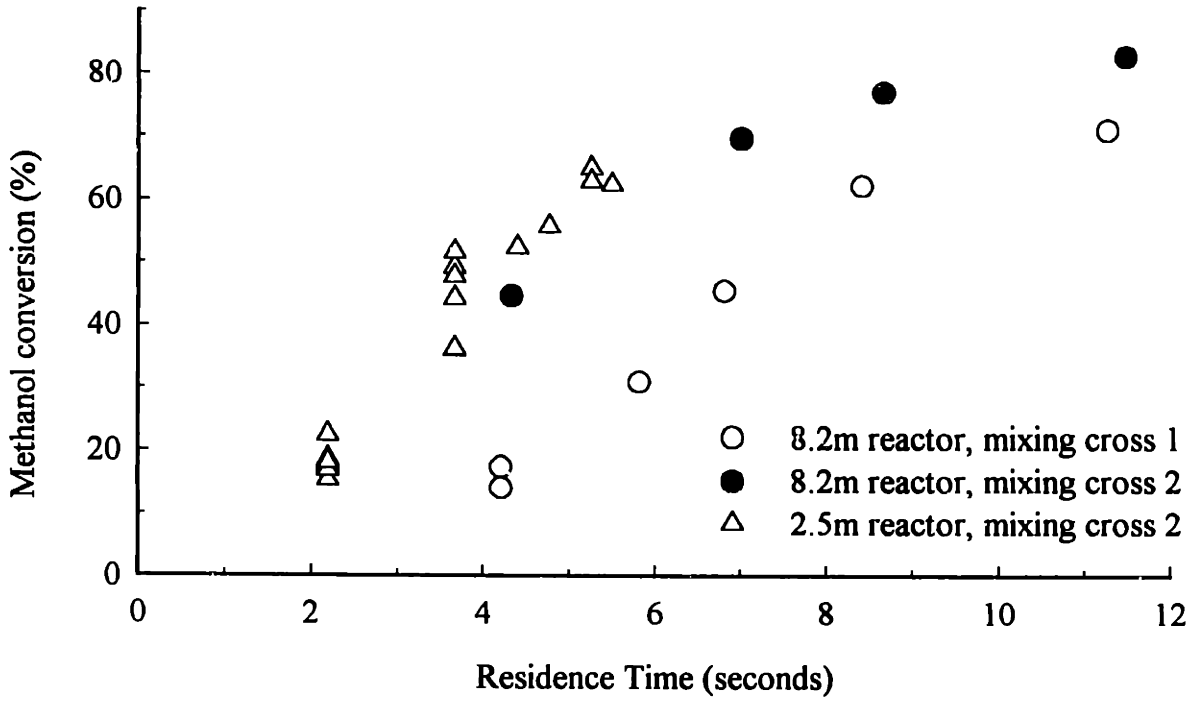

Figure 4-3 Methanol conversion as a function of time using mixing cross 2 (T=500°C, P=246 bar, $[CH_3OH]_0$=0.069 wt %, Φ=1.5)

conjunction with the same inlet cross. The residence time data between 2 and 5 seconds measured with this 2.5 m reactor (Figure 4-3) was in agreement with the data measured using the 8.2 m reactor and the new cross. Kinetic data from both the 2.5 and 8.2 m reactors with the new cross exhibited a much shorter τ_{ind} of around 0.7 seconds than the 3.2 second τ_{ind} measured in the 8.2 m reactor with the older cross (Figure 4-4).

Inspection of the two mixing crosses (which for all intents and purposes are tees since a thermocouple fully occupies one port) revealed that the 1/16 in. thermocouple extended further into the newer cross (configuration 2) than did the thermocouple in the older cross (configuration 1). In fact, the thermocouple in cross 2 extended into the opposite arm of the cross leading to the reactor. Based on this observation, it was hypothesized that the exclusion of the interior volume of the cross by the thermocouple caused higher velocities of the organic and the oxidant streams and hence enhanced the rate of mixing. If correct, some part of the observed τ_{ind} in earlier experiments at MIT was in fact due to the time required to mix the organic and oxidant streams.

4.1.3 Construction of optimized mixing crosses

In order to test this hypothesis, two new mixing crosses were constructed (configurations 3 and 4) to enhance the rate of mixing. The I.D. of the two arms through which the aqueous organic

and oxidant streams enter were reduced from 1/16 in (1.59 mm) to 0.01 in. (0.25 mm) I.D. by press-fitting short lengths of 1/16 in (1.59 mm) O.D. × 0.01 in. (0.25 mm) I.D. 316SS tubing into each arm. This volume reduction increased the ratio of the inlet stream-to-reactor flowrate from approximately 0.5 to around 24 at typical operating conditions. Additionally, the Reynolds number of the fluid in the inlet arms was increased from the 1500 to 3400 range to between 3000 to 11000. The two tees differed in that one was configured such that the organic and oxidant streams would enter the cross in opposed-flow configuration (cross 3) while in the other the streams would enter at 90° to each other (cross 4). The thermocouples were carefully situated such that their tips extended just into the center of each cross.

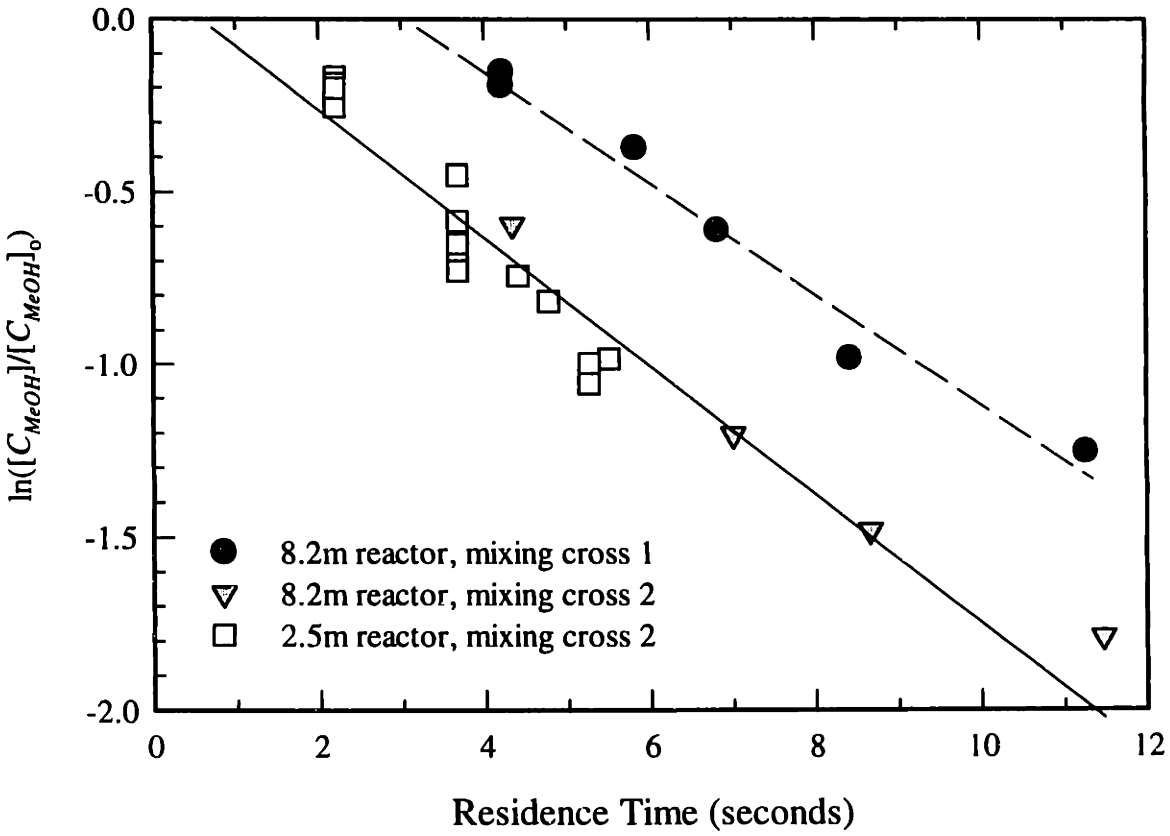

Figure 4-4 Assumed first-order plots of ln (1-X) vs. τ for the methanol data of Figure 4-3 taken using crosses 1 and 2
(T=500°C, P=246 bar, $[CH_3OH]_0$=0.069 wt %, Φ=1.5)

4.1.4 Results

The SCW methanol oxidation rate was again measured using the same 2.5 m reactor as before with these two new mixing crosses (crosses 3 and 4). Again, the methanol SCWO experiments were carried out at 500°C and 246 bar with an initial methanol concentration of 0.069 wt% and a Φ of 1.5. Identical conversion versus time profiles were measured using crosses 3 and 4 (Figure 4-5) which were also in agreement with the conversions measured using cross 2.

With these new crosses, the observed τ_{ind} decreased from 3.2 seconds with cross 1 to between 0.5 and 1 seconds as viewed in Figure 4-4 and Figure 4-5. While a significant reduction, the observed τ_{ind} is still significantly longer than the 0.13 second τ_{ind} measured at SNL at 500°C with an initial methanol concentration of 1.5 wt%. Whether a further reduction in mixing times could be achieved through additional improvements to the design of the cross remains unclear. And,

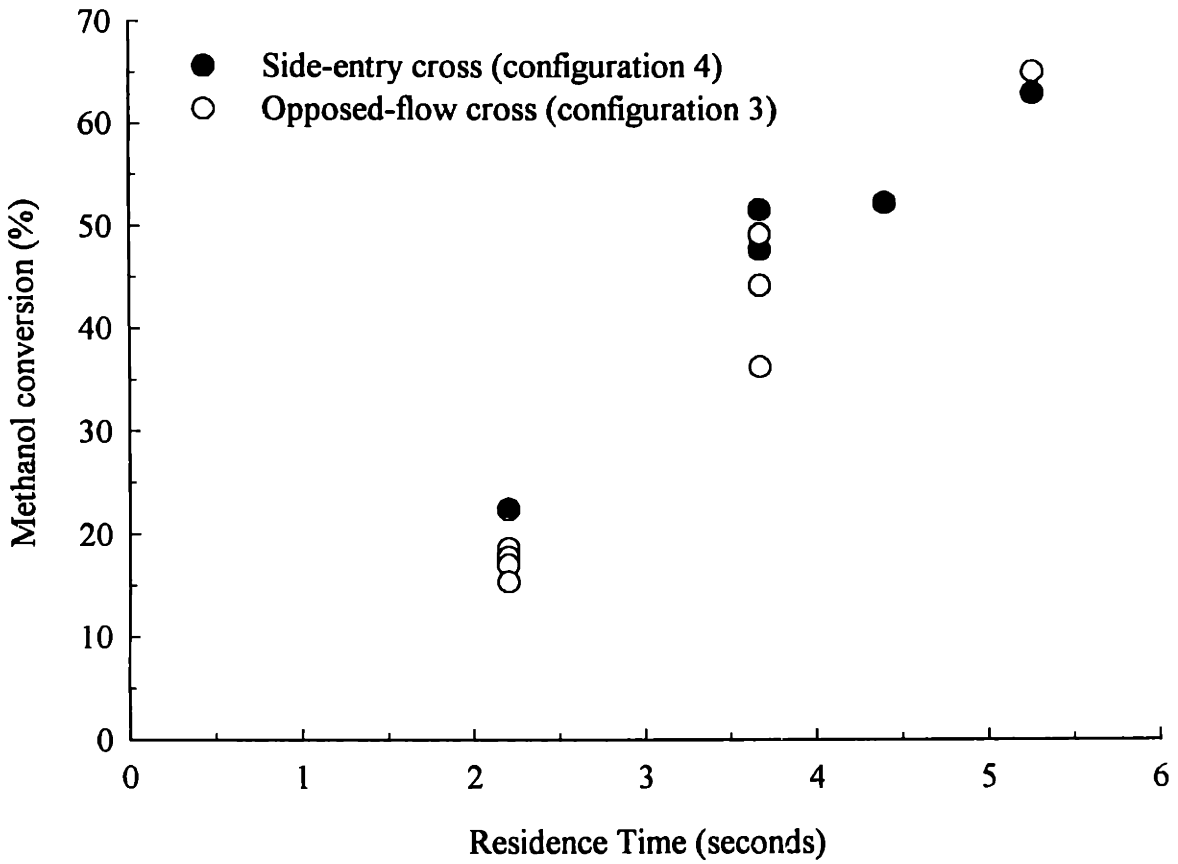

Figure 4-5 Comparison of methanol conversion measured using the opposed-flow (configuration 3) and side-entry (configuration 4) mixing crosses depicted in Figure 4-2 constructed using 0.01 in. (0.25 mm) inserts.
(T=500°C, P=246 bar, $[CH_3OH]_0$=0.069 wt %, Φ=1.5)

since the extent of the contribution of the true kinetic τ_{ind} is unknown and SCWO kinetic models are not yet sufficiently reliable to confidently predict the true τ_{ind}, the extent to which the mixing time, if at all, remains a contributor to the observed τ_{ind} cannot be established. What is known, however, is that a phenomenon originally thought to be purely kinetic in nature was shown to actually be function of the efficiency of mixing.

4.2 Hydrogen Peroxide as an Alternative Oxidant

4.2.1 Introduction

Prior to this investigation, a dissolved oxygen solution prepared using the oxygen saturator was used to provide oxygen to the reactor. Due to the limited solubility of oxygen in water, the maximum ambient aqueous oxygen concentration attainable is 3930 wppm at the 125 bar pressure rating of the oxygen saturator. In order to realize higher concentrations of oxygen in the reactor, the use of hydrogen peroxide as an alternative oxidant was explored.

The use of hydrogen peroxide as an oxidant is based on the assumption of complete decomposition of the hydrogen peroxide to oxygen and water, as described in Chapter 3. Researchers at SNL were the first to use hydrogen peroxide as the source of oxygen in an SCWO system, but its use has since been adopted by other research groups (for *e.g.*, see Brock *et al.* (1996) and Krajnc and Levec (1996)) including our own. While the assumption of complete breakdown of hydrogen peroxide to oxygen and water was not tested experimentally at Sandia, both Brock *et al.* (1996) and Krajnc and Levec (1996) did verify complete decomposition in their own reactor systems. An investigation was undertaken here to validate oxygen delivery by hydrogen peroxide in our own small-scale, tubular flow reactor by comparing methanol oxidation rates measured using hydrogen peroxide and dissolved oxygen.

A careful distinction must be made between the use of hydrogen peroxide as an oxygen source and as a primary oxidant. The use of hydrogen peroxide as a rate enhancer was explored in the oxidation of 2,4-dichlorophenol and acetic acid (Lee *et al.*, 1990). In separate experiments, hydrogen peroxide and oxygen were premixed with the organics in batch reactors. The premixed solutions were then heated to 400 to 500°C. At comparable conditions, the conversions of both compounds were higher with hydrogen peroxide than with oxygen. This finding is not surprising given the premixing of the organics with this strong oxidizer. A more recent study of the effect of

hydrogen peroxide on SCWO oxidation rates was carried out by Bourhis *et al.* (1995). In these experiments, a cold water feedstream was spiked with hydrogen peroxide at a concentration of 0.75 to 3 wt% and mixed with a pure organic waste stream. Oxidation was initiated when this mixture was combined with a SCW/air stream in a 6.2 m × 0.925 cm I.D. tubular reactor. The hydrogen peroxide concentration never exceeded 5% of the stoichiometric oxygen requirement. The extent of reaction was inferred by measuring the axial temperature rise along the outer surface of the reactor and monitoring the CO levels in the effluent. The addition of small amounts of hydrogen peroxide was found to significantly raise the temperature profile down the length of the reactor and, hence, the rate of oxidation.

The purpose here is not to exploit the rate enhancing properties of hydrogen peroxide but instead to ensure complete breakdown of hydrogen peroxide to oxygen and water in the preheater. Experiments measuring this decomposition rate in SCW at SNL led to the development of the following rate expression (Croiset *et al.*, 1997):

$$k_{overall}\left(\mathrm{s}^{-1}\right) = k_h\left(\mathrm{s}^{-1}\right) + k_w\left(\mathrm{cm}\cdot\mathrm{s}^{-1}\right) * \left(\frac{S}{V}\right)\left(\mathrm{cm}^{-1}\right) \tag{4-1}$$

where $k_{overall}$ is the overall, first-order rate constant for hydrogen peroxide decomposition, and S/V is the surface-to-volume ratio of the reactor. Hydrogen peroxide decomposition is catalyzed by metal surfaces, and hence both homogeneous, k_h, and heterogeneous, k_w, reactions contribute to the overall rate. The first-order rate constants for the homogeneous and heterogeneous reactions were developed for temperatures of 300 to 420°C and pressures from 245 to 340 bar (Croiset *et al.*, 1997):

$$k_h\left(\mathrm{s}^{-1}\right) = 10^{13.7\pm1.2}\exp\left[-180\pm16(\mathrm{kJ/mol})/RT\right] \tag{4-2}$$

$$k_w\left(\mathrm{cm}\cdot\mathrm{s}^{-1}\right) = 10^{3.3\pm0.3}\exp\left[-62.5\pm4.4(\mathrm{kJ/mol})/RT\right] \tag{4-3}$$

In order to gain a conservative estimate of the extent of reaction in our reactor system, we can assume that hydrogen peroxide decomposition only occurs in the isothermal section of preheater located in the main sandbath even though reaction will initiate in the DOH section of the preheater. Estimating the residence time in the sandbath preheater at 6 seconds (see Section 5.4.2) and given that the surface-to-volume ratio of the preheater tubing is 37 cm^{-1}, Eqn. (4-1) predicts

100% conversion of the hydrogen peroxide at temperatures above 400°C, which is a much lower temperature than is normally used in our experiments.

4.2.2 Oxygen evolution control experiments

Two control experiments were performed to measure the mass of oxygen evolved from the breakdown of hydrogen peroxide in the reactor system. An aqueous hydrogen peroxide solution was fed to the reactor system at 500°C and 246 bar. The concentration of hydrogen peroxide in the feed was determined by the method described in Section 3.3.3. Effluent flowrates of the evolved gas-phase (which was analytically confirmed to be 100% oxygen) and water streams were measured. The concentration of dissolved oxygen in the water was calculated by Henry's Law (Section 3.4.1). Based on the measured effluent concentration of oxygen in the gas and aqueous phases, the concentration of hydrogen peroxide necessary in the feed solution to produce this concentration of oxygen upon full decomposition was back-calculated and compared to the measured concentration of the hydrogen peroxide feed solution used for each experiment. The results of experiments at two different flowrates, shown in Table 4-1, reveal that the measured and back-calculated H_2O_2 concentrations are in close, but not perfect, agreement. While the measured and back-calculated H_2O_2 concentrations for the high flowrate experiment agree within their

Table 4-1. Results of oxygen evolution experiments using H_2O_2 feed solutions
(500±1°C, 246±0.4 bar)

Liquid Effluent Flowrate (mL/min)	Back-Calculated [H_2O_2] in Feed (wppm)	Measured [H_2O_2] in Feed (wppm)
3.15±0.01	3175±48	3450±225
8.22±0.02	3241±57	3450±225

uncertainties, these two measurements for the low flowrate experiment do not. Since it is difficult to determine from these experiments if a small amount of H_2O_2 remained undissociated after the preheater and because very small amounts of H_2O_2 left undissociated could affect oxidation kinetics given that H_2O_2 will dissociate to OH radicals in SCW, a second series of experiments was conducted directly comparing methanol oxidation kinetics using H_2O_2 and dissolved oxygen.

4.2.3 Comparison of oxidation kinetics using oxygen and hydrogen peroxide

A total of 36 experiments were conducted, 21 with hydrogen peroxide and 15 with dissolved oxygen, comparing the SCW oxidation rate of methanol. Experiments were conducted at 500°C and 246 bar with 1.4 to 4.0 second residence times. The initial methanol concentration was maintained at 0.069 wt% (1.9 mM) and experiments were conducted at fuel-rich conditions (Φ=1.5) in an effort to maximize the ability to discriminate between the two oxidants. In the experiments using dissolved oxygen, the oxygen saturator pressure was maintained at 42 bar. The concentration of hydrogen peroxide was prepared to deliver an equivalent concentration of oxygen upon complete dissociation.

Figure 4-6 shows the conversion of methanol as a function of residence time using dissolved oxygen and hydrogen peroxide. The data convincingly demonstrate that the rate of oxidation is equal for the two oxidants. The concentrations at supercritical conditions of CO and CO_2, the primary oxidation products, are displayed in Figure 4-7. As is evident from these graphs, essentially identical calculated concentrations of CO and CO_2 were obtained using either oxidant.

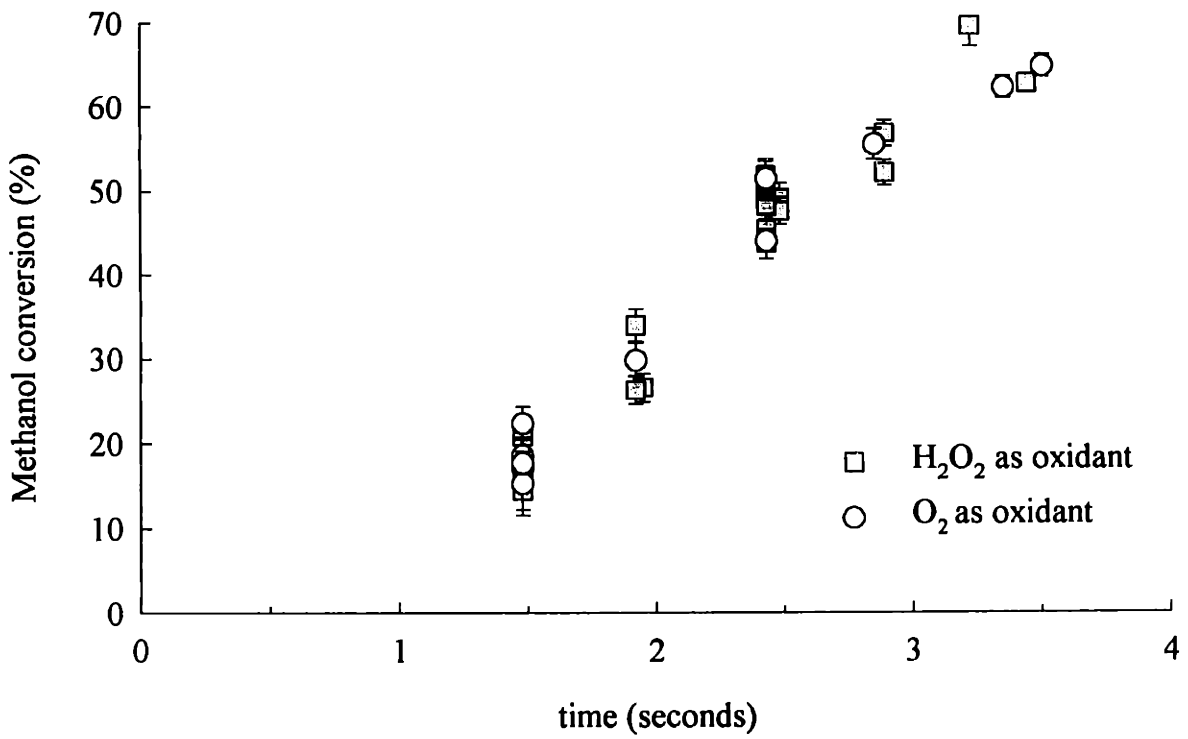

Figure 4-6 Comparison of methanol conversion as a function of time using dissolved oxygen and hydrogen peroxide as oxidants
(T=500°C, P=246 bar, $[CH_3OH]_0$=0.069 wt %, Φ=1.5)

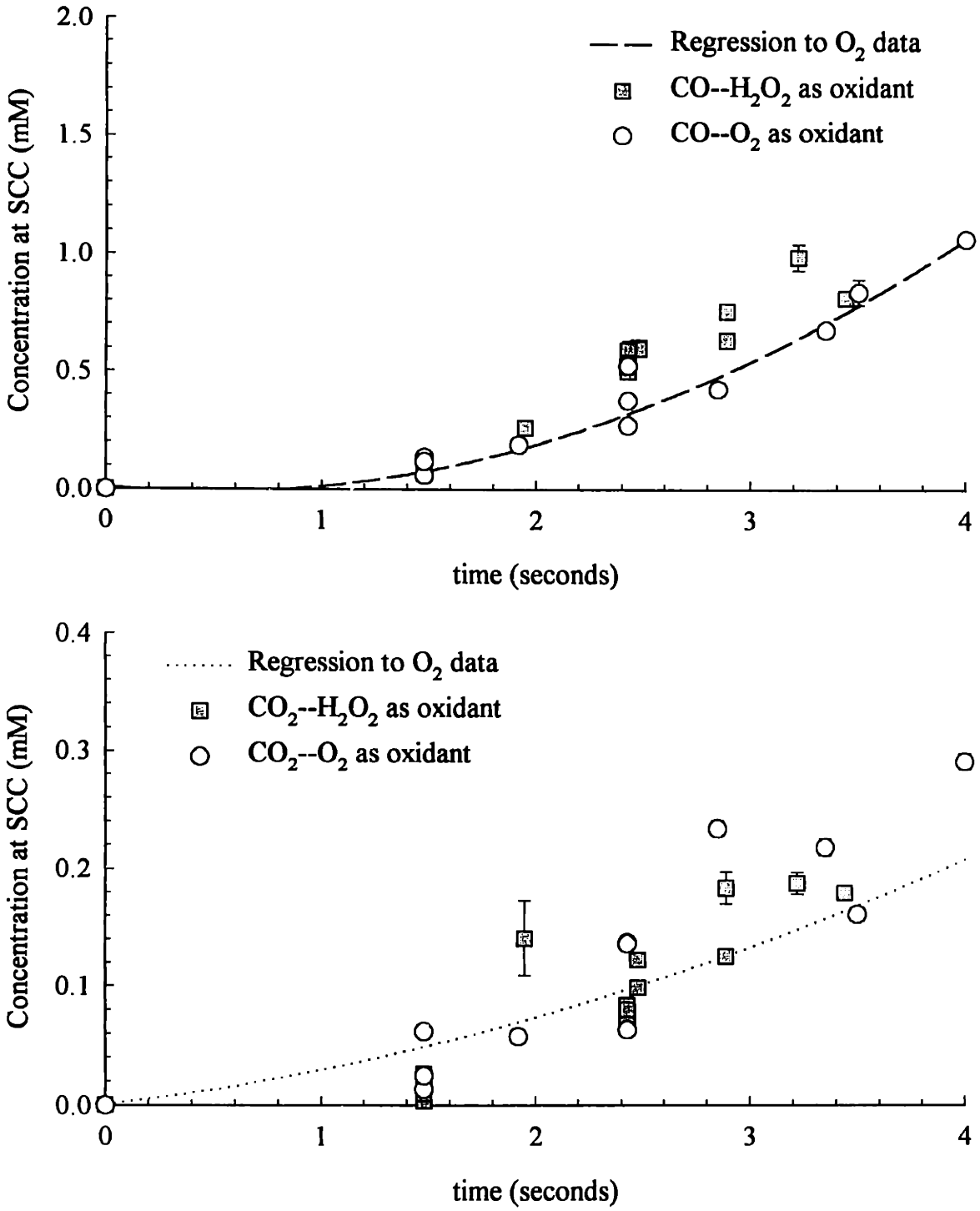

Figure 4-7 Comparison of CO and CO_2 concentrations as a function of time using both dissolved oxygen and hydrogen peroxide as oxidants
(T=500°C, P=246 bar, $[CH_3OH]_0$=0.069 wt %, Φ=1.5)

4.3 CONCLUSIONS

The apparent induction time was shown to be influenced by the geometry and flow conditions within the mixing cross. Two new mixing crosses were designed in an attempt to optimize this rate of mixing. By reducing the inner diameter of the oxidant and organic arms of the cross to increase their Reynolds numbers and the ratio of the inlet stream-to-reactor flowrates, the observed induction time was reduced from 3.2 to 0.7 seconds.

The use of an aqueous hydrogen peroxide solution was demonstrated as a viable means to generate molecular oxygen *in situ* in our laboratory-scale SCWO reactor system. The oxidation of methanol was found to proceed at the same rate using either aqueous hydrogen peroxide or dissolved oxygen. Moreover, the concentration of the oxidation products in the reactor effluent were identical using either oxidant. Of course, the results obtained here are specific to this reactor system, and similar experiments should be performed to verify complete hydrogen peroxide decomposition in reactor systems where hydrogen peroxide is used.

4.4 REFERENCES

Bourhis, A.L., K.C. Swallow, G.T. Hong and W.R. Killilea, "The use of rate enhancers in supercritical water oxidation." in *Innovations in Supercritical Fluids*, K. W. Hutchenson and N. R. Foster, Eds., ACS Symposium Series, **608**, American Chemical Society, Washington, D.C., 338 (1995).

Brock, E., Y. Oshima, P. Savage and J. Barker, "Kinetics and mechanism of methanol oxidation in supercritical water." *J. Phys. Chem.* **100**, 15834 (1996).

Croiset, E., S.F. Rice and R.G. Hanush, "Hydrogen peroxide decomposition in supercritical water." *AIChE Journal* **43**(9), 2343 (1997).

Holgate, H.R. and J.W. Tester, "Fundamental kinetics and mechanisms of hydrogen oxidation in supercritical water." *Combust. Sci. Technol.* **88**, 369 (1993).

Holgate, H.R. and J.W. Tester, "Oxidation of hydrogen and carbon monoxide in sub- and supercritical water: reaction kinetics, pathways, and water-density effects. 1. Experimental results." *J. Phys. Chem.* **98**, 800 (1994).

Krajnc, M. and J. Levec, "On the kinetics of phenol oxidation in supercritical water." *AIChE Journal* **42**(7), 1977 (1996).

Lee, D.S., E.F. Gloyna and L. Li, "Efficiency of H_2O_2 and O_2 in supercritical water oxidation of 2,4-dichlorophenol and acetic acid." *J. Supercrit. Fluids* **3**, 249 (1990).

Meyer, J.C., P.A. Marrone and J.W. Tester, "Acetic acid oxidation and hydrolysis in supercritical water." *AIChE Journal* **41**(9), 2108 (1995).

Phenix, B.D., "Hydrothermal oxidation of simple organic compounds." Ph.D. Thesis, Department of Chemical Engineering, Massachusetts Institute of Technology, Cambridge, MA (1998).

Rice, S.F., T.B. Hunter, A.C. Ryden and R.G. Hanush, "Raman spectroscopic measurement of oxidation in supercritical water. 1. Conversion of methanol to formaldehyde." *Ind. Eng. Chem. Res.* **35**(7), 2161 (1996).

Chapter 5.

Experimental Results on the Oxidation of Benzene in Supercritical Water

Benzene is a volatile, colorless, flammable liquid aromatic hydrocarbon primarily used as a chemical raw material. Uses for benzene include the synthesis of styrene, phenol, cyclohexane, aniline, maleic anhydride (polyester resins), alkyl benzenes (detergents), chlorobenzenes, and other products used in the production of drugs, dyes, insecticides and plastics. Benzene, along with other light, high octane, aromatic hydrocarbons such as toluene and xylenes, is a component of gasoline. Benzene was also once commonly used as a solvent but has been replaced by safer solvents in most applications with the recognition of benzene as a human carcinogen.

Given the widespread use of benzene, the finding that benzene constitutes a common environmental contaminant is not surprising. Benzene is a refractory chemical compound, meaning that severe conditions are necessary for its remediation due to its high thermal and chemical stability. Like many hydrocarbons benzene exhibits a poor solubility in water and will normally be found bound to soils in contaminated groundwater systems.

The research into SCWO reaction kinetics here at MIT focuses on measuring reaction kinetics of model compounds. In keeping with this goal, a study of the hydrolysis and oxidation of benzene was undertaken. In addition to being classified as a toxic waste, a known human carcinogen, and an environmental contaminant, the single aromatic ring of benzene is the building block for polyaromatic hydrocarbons (PAHs) and substituted aromatic compounds. A study of the SCWO of benzene will then contribute to the collective knowledge of reaction kinetics by providing kinetic data for benzene, itself a ubiquitous hazardous chemical, and lending insight as to the reactive behavior of a more general class of hazardous chemicals.

5.1 Literature Review

Only limited data are available for the homogeneous oxidation of benzene in supercritical water. Benzene and many other aromatic compounds were proven amenable to treatment by SCWO

(Thomason *et al.*, 1990). In these demonstrations the focus was on the measurement of destruction efficiencies and not on obtaining kinetic data. Ding *et al.* (1995a) reported limited measurements for homogenous benzene oxidation, but their research emphasized catalytic SCWO.

Since the early 1990's, researchers have amassed an extensive amount of data on the SCW reactions of substituted aromatic compounds. Savage *et al.* at the University of Michigan were major contributors of experimental data on a wide range of such compounds. Their early investigations focused on phenol SCWO in tubular flow and batch reactors from 380 to 480°C with pressures from 190 to 282 bar and stoichiometric to large excess amounts of oxygen (Thornton and Savage, 1990; Thornton *et al.*, 1991; Li *et al.*, 1992; Thornton and Savage, 1992b; Thornton and Savage, 1992a; Gopalan and Savage, 1995). In these studies, Savage's research group employs temperatures considerably below the current standards for practical industrial SCWO reactors (450-600°C). Their stated purpose for operating in this low-temperature regime is the identification of intermediates in the oxidation process which at higher temperatures might react too quickly to be detected. Their intent, of course, is to gain mechanistic insights by tracking the intermediate species. Phenol was not observed to react to a significant degree in the absence of oxygen below 420°C. Phenol conversion increased with both the amount of excess oxygen and the system pressure, but was found independent of the initial phenol concentration. The detected reaction products under oxidation conditions include 4-phenoxyphenol, 2-phenoxyphenol, dibenzofuran, 2,2'-biphenol, dibenzo-*p*-dioxin, benzenediols, *p*-benzoquinone, and glyoxylic, oxalic, formic and succinic acids along with CO and CO_2. The dimers (*i.e.*, 4-phenoxyphenol, 2-phenoxyphenol, dibenzofuran and 2,2'-biphenol) were identified as the primary oxidation products and selectivity to the dimerization products was favored at low phenol conversions. Higher phenol conversions resulted in higher selectivity to CO and CO_2. Dibenzofuran was the intermediate species most resistant to further oxidation. Interestingly, the yield of CO_2 always exceeded that of CO leading Savage and coworkers to hypothesize that pathways exist for the formation of CO_2 which do not involve CO. Gopalan and Savage (1995) proposed a reaction network where phenol first reacts to form dimers, ring-opening and other products by parallel pathways. The dimers oxidize to ring-opening and other products which further oxidize to CO and CO_2.

Savage *et al.* observed similar results for substituted phenols. A study of the oxidation of the *o*-, *m*- and *p*- isomers of phenols with —CH_3 (cresols) and —CHO (hydroxybenzaldehydes)

substituent groups (Martino *et al.*, 1995; Martino and Savage, 1997) again revealed CO_2 yields exceeding those of CO, even at the lowest reactant conversions, supporting the idea that pathways exist for the formation of CO_2 other than the direct oxidation of CO. Dimers were observed but only with low selectivities, and the combined yields of CO and CO_2 exceeded the combined yields of all other intermediates. The major primary intermediates during *o*-, *m*- and *p*-cresol oxidation were phenol and hydroxybenzaldehydes. At cresol conversions less than 50%, hydroxybenzaldehyde yields exceeded those of phenol indicating that oxidation of the $—CH_3$ substituent group is favored over elimination. Between 50 and 118% of the carbon present as cresols in the feed was recovered in the reaction products, with lower carbon balances reported for the near-critical temperatures. Phenol was the dominant intermediate in the oxidation of the hydroxybenzaldehyde isomers.

In another study, Martino and Savage (1999a; 1999b) examined the thermolysis and oxidation of the *o*-, *m*- and *p*- isomers of phenols with $—C_2H_5$ (ethylphenols), $—COCH_3$ (hydroxyacetophenones), $—NO_2$ (nitrophenols), $—OCH_3$ (methoxyphenols) and —OH (benzenediols) substituent groups at 460°C, a pressure of 253 bar and residence times ranging from 0.5 to 6.7 seconds. All of the substituted phenols did react to varying degrees in the absence of oxygen. The ortho isomers of methoxy- and nitrophenol reacted very rapidly without oxygen, and their oxidation reactions could not be investigated. During the oxidation of the remaining substituted phenols, they again observed that the main oxidation products were CO and CO_2 with the yield of CO always less than that of CO_2, even at the lowest reactant conversions. Only in the case of nitrophenol SCWO were the CO yields comparable to those of CO_2. Phenol and benzenediols were common intermediate products except in the oxidation of benzenediols where CO and CO_2 were the only observed products. Between 65 and 100% of the carbon in the feed was recovered in the reaction products.

Levec and coworkers at the University of Ljubljana in Slovenia performed complementary investigations on phenol oxidation in supercritical water to those of Savage *et al.* Although Levec's group primarily studied catalytic aqueous reactions, Krajnc and Levec (1996) examined the homogenous SCWO of phenol in their bench-scale, tubular, plug flow reactor at temperatures of 380 to 450°C, pressures from 230 to 265 bar, and 15 to 200 second residence times. In agreement with the observations of Savage *et al.*, a pyrolysis experiment at 400°C, 240 bar and 179 s residence

time showed a phenol conversion of less than 2%, and phenol conversion by oxidation increased with the oxygen-to-phenol ratio and was independent of the initial phenol concentration. Dibenzofuran, 2-phenoxyphenol, 2,2'-biphenol, 4-phenoxyphenol, dibenzofuranol, and dibenzo-1,4-dioxin were identified and quantified by GC with a mass selective detector. HPLC analysis revealed the presence of propionic, maleic, succinic, formic and acetic acid. At short residence times, most of the reacted carbon was present in the form of dimers. Analysis of the reaction products led to the proposal of a parallel, consecutive reaction scheme whereby phenol first reacts to form 2-phenoxyphenol, 4-phenoxyphenol or 2,2'-biphenol. These multiringed intermediates rearrange to form other intermediates, some of which have not been identified, before forming organic acids and finally undergoing oxidation to CO_2. Based on experiments where the oxygen-to-phenol ratio was varied, Krajnc and Levec concluded that phenol is easier to oxidize than the intermediate products formed, and that with a stoichiometric amount of oxygen it is unlikely that phenol will be completely oxidized to CO_2 with a reasonable length reactor.

In comparison with their earlier work on the catalytic liquid-phase oxidation of phenol at 150 to 210°C and 30 bar (Pintar and Levec, 1994), they stated that SCWO led to much more hazardous and harder to oxidize intermediates. In this previous study, CO_2 was observed even at very low phenol conversions (X<3%) and short residence times. Based on the observation of prompt CO_2 formation and on the observed products from an earlier study on aqueous phenol oxidation, they proposed a reaction pathway whereby the catalytic reaction of phenol with oxygen leads to the formation of benzenediols and benzoquinones which quickly react yielding CO_2 and C_4 products.

The recent examination of phenol SCWO over a transition-metal oxide catalyst led to insights on the influence of the catalyst on the reaction mechanism (Krajnc and Levec, 1997). By oxidizing phenol in their flow reactor system in the presence of a copper, zinc and cobalt oxide containing catalyst at temperatures of 400 to 440°C, pressures of 230 to 250 bar and residence times of 0.33 to 1.82 seconds, they observed higher phenol conversions at shorter residence times than they observed without catalyst. Phenol conversion increased both with initial phenol concentration and the oxygen-to-phenol ratio. Dimers, single-ring aromatics and organic acids were detected, but with very low selectivities. The oxidation intermediates present with the highest selectivities were the dimers 4-phenoxyphenol, 2-phenoxyphenol and dibenzo-1,4-dioxin and the

single-ring aromatics *p*-benzenediol and *p*-benzoquinone. Formic and acetic acid were the only organic acids present, in contrast with the multitude of organic acids detected in the homogeneous oxidation of phenol (Krajnc and Levec, 1996). Most of the reacted carbon was present as CO_2, the only gas-phase product detected.

Based on their analysis of the product spectrum, Levec's group concluded that the catalyzed and uncatalyzed SCWO of phenol are similar mechanistically. They postulated that phenol oxidation proceeds by parallel, consecutive reaction pathways, one leading to the formation of dimers (phenoxyphenols) and the other to single-ring aromatics (benzenediols, benzoquinones). The dimers are rapidly oxidized as evidenced by their decreased selectivity with increasing phenol conversion. The single-ring products appear more refractory than the dimers, but ultimately undergo ring-opening reactions to form organic acids and finally oxidation to CO_2. Higher temperatures and higher initial oxygen-to-phenol ratios favor the formation of single-ring products and their subsequent ring opening reactions yielding light organic compounds and CO_2 over dimerization. The use of a catalyst reduces the temperatures needed to achieve complete oxidation of phenol to CO_2 by reducing the activation energy of the formation of the phenoxy radical ($C6H5O\bullet$), the reactive radical formed by the abstraction of the phenolic H atom from phenol, and then aiding in the oxidation of the intermediate acids.

Rice and Steeper (1998) studied the temperature dependence of homogeneous phenol oxidation in supercritical water at fuel-lean conditions at temperatures of 504 to 585°C in their flow reactor. Their measured oxidation rates compare well to the global rate expression developed by Krajnc and Levec (1996) when extrapolated to the higher temperatures. TOC and GC analyses showed an appreciable amount of oxidizable carbon remaining in the effluent that was not phenol but instead both higher and lower molecular weight oxidation products. Rice and Steeper state that they suspect as temperature is raised the higher activation energy ring-opening reactions dominate over those that form condensation products.

Koo *et al.* (1997) investigated phenol oxidation using sealed bomb reactors from 380 to 440°C with pressures from 193 to 276 bar, 100% to 1,750% excess oxygen and residence times of 12 to 120 seconds. They observed that phenol did not react at 380°C and 223 bar without oxygen, and conversion increased with oxygen concentration, consistent with the prior investigations of phenol. Their work, in addition, provided some very interesting information on the role of water. As

did both Levec's and Savage's groups, Koo *et al.* observed that phenol conversion increased with increasing pressure. Whether the pressure or water concentration is influencing the reaction rate in an SCWO system is normally difficult to discern since increasing the pressure also increases the water concentration. To overcome this dilemma, Koo *et al.* changed the system pressure in two ways: first by increasing water concentration and then by holding water concentration constant and adding helium to increase the pressure. The results revealed that pressure itself did not affect the phenol oxidation rate. Instead, increasing water concentration led to the increase in conversion. Assuming that oxidation reactions at supercritical conditions above 400°C proceed predominantly via free radical mechanisms, water must participate in radical generating reactions in the oxidation of phenol. Increasing water concentration leads to an increase in the rates of these reactions.

The research of Abraham has concentrated on catalytic SCWO. For example, Jin *et al.* (1992) studied the catalyzed and uncatalyzed oxidation of 1,4-dichlorobenzene in a batch reactor at temperatures of 288 to 412°C. Detected products were benzene, chlorobenzene and CO_2, with no CO detected. Essentially the same reaction rates and CO_2 yields were observed with and without a V_2O_5 catalyst, with up to 60% of the carbon oxidized to CO_2. Ding *et al.* (1995a; 1995b) studied the catalyzed and uncatalyzed oxidation of phenol, benzene and 1,3-dichlorobenzene in their flow system. In all cases CO_2 was the major product, CO was not detected, and significant yields of partial oxidation products were measured. These partial oxidation products included dimers such as biphenol and biphenyl, oxidized single-ring aromatic species such as benzenediols and light oxygenated hydrocarbons such as acetic and formic acid. Of the three aromatics studied, phenol was the easiest to oxidize. Almost complete phenol conversion with a high selectivity to CO_2 was achieved without catalyst at only 390°C and 241 bar with a 13 second residence time. Addition of catalyst significantly increased the selectivity to CO_2. Statistically significant oxidation of benzene at 241 bar and a 13 second residence time did not occur until 450°C. Addition of catalyst increased the amount of conversion as well as the selectivity to CO_2. Curiously, increasing the concentration of oxygen led to a decrease in benzene conversion in the homogeneous case and with one of the catalysts. Dichlorobenzene caused a loss in catalytic activity and, as a result, was not well studied.

Other groups have also studied the oxidation of various aromatics in supercritical water. Phenol oxidation was studied by Oshima *et al.* (1998). Thammanayakatip *et al.* (1998) oxidized hydroquinone in supercritical water at 360 and 410°C and 245 bar. They observed a very rapid

initial reaction of hydroquinone to *p*-benzoquinone with only a small yield of CO_2. Due to what was attributed to be an inhibition effect of *p*-benzoquinone, conversion of hydroquinone increased very rapidly with reactor residence time until conversion of hydroquinone reached 98%. After that point, however, conversion increased only very slowly with residence time. Yang and Eckert (1988) studied the catalyzed and uncatalyzed oxidation of *p*-chlorophenol in a tubular flow reactor from 310 to 400°C with pressures from 76 to 243 bar. Very little reaction was observed in the absence of oxygen. Catalytic oxidation rates were not significantly higher than the uncatalyzed rates, but a significant surface effect was observed whereby increasing the surface-to-volume ratio enhanced the oxidation rate. They observed CO_2 to be the most significant gas-phase product followed by CO, and the primary liquid product was *p*-benzoquinone. Hydrochloric acid was also formed. A free-radical oxidation mechanism was postulated but not tested that accounted for *p*-benzoquinone formation and included *p*-benzenediol as an intermediate. Crain *et al.* (1993) studied reactions of pyridine in supercritical water in their flow reactor. Pyridine was stable in the absence of oxygen at temperatures up to 521°C. They conducted oxidation reactions from 426 to 527°C at a pressure of 276 bar with residence times ranging from 2.2 to 10.5 seconds. Conversions ranged from 3% at 426°C to 68% at 527°C with a 10 second residence time. Pyridine oxidation produced numerous products, including carboxylic acids, ammonia, CO and CO_2. In a study of the catalytic SCWO of pyridine (Aki and Abraham, 1999), CO, CO_2 and nitrous oxide were the only detected products. CO_2 was always the dominant product, and the presence of CO, which was detected in the homogenous oxidation of pyridine, depended on the catalyst.

Several similarities exist between the above investigations on the reactions of aromatic compounds in supercritical water. Carbon dioxide is the product in the highest yield in all investigations, even dominating over carbon monoxide at very low conversions of the aromatic reactant and at very short reactor residence times. The high yields of CO_2 at short residence times and temperatures too low for the oxidation of CO to CO_2, based on the previous investigation of CO SCWO kinetics (Holgate *et al.*, 1992), indicate that CO_2 is formed by a pathway other than through the direct oxidation of CO. The observation that CO_2 is always the highest yielding product suggests that once the aromaticity of the reactant is disrupted complete oxidation to CO_2 proceeds rapidly. A second similarity is the presence of benzenediols and benzoquinones. Oxidation of the aromatic compounds appears to proceed by parallel, consecutive pathways: one forming dimers and

the other forming single-ring products. Higher temperatures and higher levels of oxygen appear to favor the single-ring products (the benzoquinones and benzenediols) over the dimers.

While a great deal of research exists on the SCWO of substituted aromatic compounds, benzene has received only limited attention. Benzene was proven amenable to treatment by SCWO in the MODAR process (Thomason *et al.*, 1990), and Ding *et al.* (1995a) reported some data on the homogeneous oxidation of benzene in a study where the primary focus was on catalytic SCWO. A deeper understanding of the oxidative behavior of benzene SCWO will contribute to the advancement of the SCWO technology given that benzene is a hazardous chemical itself and a model compound for PAHs and substituted aromatic compounds. The experimental investigation that follows is a comprehensive investigation of the homogeneous oxidation kinetics of benzene in supercritical water.

5.2 Experimental Apparatus

The experimental study of the oxidation and hydrolysis of benzene in supercritical water was performed using the bench-scale, tubular, plug flow reactor system described fully in Chapter 3. A.C.S. grade benzene (minimum purity level 99.0%) was purchased from VWR Scientific (p/n, EM-BX0220) in 500 mL quantities and used as received. Due to the low solubility of benzene in ambient water, a saturated benzene/water solution was used for the benzene feed. The saturated benzene solution was prepared by filling the 5 liter plastic-coated, glass feed vessel (the organic feed tank) with about 4.5 liters of deaerated, deionized water and adding a sufficient quantity of benzene to form a 2-phase solution. The headspace was purged and pressurized with 1.7 bar of helium. The container was placed on a magnetic stirring plate, and the 2-phase benzene/water solution was stirred with a magnetic stir bar for at least 12 hours. The solution rested for another 12 hours allowing separation of all undissolved benzene from the water. The organic feed pump drew the saturated aqueous benzene feed from the bottom of the feed tank. Using this method, the benzene concentration in the feed solution was approximately at its room temperature aqueous solubility concentration of 1800 wppm. The 4.5 liter saturated solution was a sufficient volume of feed for five to six individual experiments. During the course of the experimental study, multiple bottles of pure benzene were used, and the oxidation rate was found to be independent of the lot of benzene. Hydrogen peroxide was used in the majority of the oxidation experiments as the oxygen

source. Several experiments using dissolved oxygen in place of hydrogen peroxide confirmed that both oxidants give the same benzene oxidation rate.

5.3 Analytical Procedures and Product Analysis

The benzene feed solution, liquid- and gas-phase effluent were analyzed by GC. The configurations of the GCs for performing these analyses were described in Chapter 3 and the detailed analytical procedures are presented in Appendix 10.1.

During an experiment, at least five samples of the benzene feed solution were taken for analysis. The feed samples were analyzed on either the 5890 GC by FID, the 6890 GC by FID, or on both GCs. Even though the feed solution was approximately at the solubility limit of benzene in water (1800 wppm), the measured concentration of the feed solution was always used in the experimental analysis. Samples were collected in 2 mL autosampler vials, capped with PTFE/silicone caps, stored in the 5°C refrigerated autosampler trays and analyzed along with the liquid-phase effluent samples at the end of each experiment. In early benzene hydrolysis and oxidation experiments, the vials were filled with the saturated benzene feed solution directly from the sampling line on the organic feed tank. This method of feed sample collection, however, resulted in positive errors in the benzene feed concentration and high sample-to-sample variability, both believed to be a result of attempting a direct measurement of the benzene solution at its solubility limit. In later experiments the feed solution was diluted by volumetrically measuring 25 mL of deionized water into a Class A 50 mL volumetric flask and adding 25 mL of the feed solution from the sampling line. A 2 mL sample of the diluted feed solution was then transferred to the autosampler vials. This method improved the accuracy of the concentration measurements and reduced sample-to-sample variability.

The liquid-phase effluent samples were also analyzed by FID on either or both of the GCs used in the analysis of the benzene feed samples. Six liquid-phase samples were collected directly into the sample vials from the system effluent line. The only species detected in the liquid-phase effluent by the GC analysis were phenol and unreacted benzene.

The gas-phase effluent was analyzed by GC using three thermal conductivity and one flame ionization detector as noted in Chapter 3. The detected gas-phase species were CO, CO_2, O_2, H_2, helium, methane, ethylene, acetylene, propylene and unreacted gas-phase benzene.

5.4 Experimental Results

A total of 7 hydrolysis and 107 oxidation experiments were conducted to characterize the reactivity of benzene in supercritical water. The temperature (*T*), residence time (τ), initial benzene concentration ($[C_6H_6]_o$), fuel equivalence ratio (Φ) and pressure (*P*) were varied during these experiments. Table 5-1 presents the range of conditions explored for our experiments. The data from all experiments is presented in tabular form in Appendix 10.2.

The hydrolysis experiments measured the conversion of benzene in the absence of oxygen. Due to the design of this experimental system, kinetics cannot be conveniently measured on compounds which thermally decompose or react to a significant degree with water alone. The purpose of these experiments, then, was to understand the effect of non-oxidation reactions in our studies of benzene oxidation kinetics.

Table 5-2 groups the oxidation experiments in Table 5-1 into four categories. Variable and fixed condition parameter values and residence time ranges are given in Table 5-2. Note that since some experiments belong to more than one category, the number of experiments listed under the four categories sum to more than 107.

The maximum residence time used in the experiments was based upon maintaining a Reynolds number in the turbulent regime and the minimum on the accuracy to which residence times can be determined. At 540°C, where a majority of the experiments were performed, the maximum achievable residence time is 7 seconds. At short residence times systematic errors (*e.g.*, mixing and quenching times), which are not accounted for in the error in residence times as reported in Appendix 10.2, are a larger percentage of the total error than at longer times. Mixing times, which were discussed in Chapter 4, were estimated to be on the order of 1 second. The

Table 5-1. Range of conditions explored in benzene SCW experiments

	Oxidation Experiments	Hydrolysis Experiments
T (°C)	479-587	530-625
P (bar)	138-278	246
τ (s)	3-7	6
$[C_6H_6]_o$ (mM)	0.4-1.2	0.48-1.25
Φ	0.5-2.5	-

shortest residence time at which experiments are conducted in this system is 3 seconds to ensure that the systematic error in the residence time is not larger than the residence time itself.

For consistency with all previous experiments conducted at MIT, a nominal operating pressure of 246 bar was selected. This pressure is representative of those used industrially and is far enough above the critical pressure that the physical properties of water (*e.g.*, ρ, ε, K_w) are not affected by small pressure fluctuations.

A stoichiometric level of oxygen (Φ=1) was used in the majority of the experiments where Φ is defined as:

$$\Phi = \frac{([C_6H_6]/[O_2])_{initial}}{([C_6H_6]/[O_2])_{stoichiometric}} \quad (5\text{-}1)$$

Both hydrogen peroxide and dissolved oxygen were used as the source of oxygen. As indicated in Table 5-2, Φ was varied from 0.5 (100% excess oxygen) to 2.5 (40% of oxygen demand).

The initial benzene concentration ($[C_6H_6]_o$) is the concentration at the reactor entrance. Since a saturated aqueous solution of benzene with a concentration of approximately 1800 wppm was used as the organic feed, the ratio of the organic to the oxidant stream flowrates and the fluid density (ρ=*f*(*T*,*P*)) determined $[C_6H_6]_o$. Normal operation of the DOH preheater system requires a

Table 5-2. Summary of benzene oxidation experiments

Parameter Studied (number of experiments)	Parameter Range	Fixed Conditions	Residence Time Range
1. Temperature variation (21)	479-587°C	$[C_6H_6]_o$= 0.6 mM Φ = 1.1 P = 246 bar	6 s
2. Φ variation (31 @ 540°C, 11 @ 550°C)	0.5-2.5	T = 540, 550°C $[C_6H_6]_o$= 0.6 mM P = 246 bar	3-7 s
3. $[C_6H_6]_o$ variation (3 @ 530°C, 24 @ 540°C, 11 @ 550°C)	0.4-1.2 mM	T = 530, 540, 550°C Φ = 1.0±0.1 P = 246 bar	6 s @ 530°C 3-7 s @ 540°C 3-7 s @ 550°C
4. Pressure (density) variation (22)	138-278 bar (0.03-0.09 g/mL)	T = 540°C $[C_6H_6]_o$= 0.6 mM Φ = 0.9	3-6 s

minimum ambient flowrate of each feed stream of about 1.5 mL/min. Given this flowrate restriction, at 540°C (the temperature where a majority of the experiments were performed) the maximum attainable $[C_6H_6]_o$ was around 1.2 mM and the minimum about 0.4 mM. An initial benzene concentration of 0.6 mM was selected as the basis for most experiments so that the $[C_6H_6]_o$ could be varied up and down by approximately a factor of 2 during the $[C_6H_6]_o$ variation experiments.

5.4.1 Data Collection and Error Analysis

During the course of an experiment, multiple measurements were taken of all measurable quantities for the purpose of establishing confidence intervals on the measured and calculated values. A typical experiment lasted one to two hours, during which: five to fifteen measurements of the gas- and liquid-phase flowrates were taken; the pressure was recorded at least ten times; the temperatures were recorded every ten seconds; four measurements were performed of the hydrogen peroxide feed concentration; at least five samples of the feed and six of the liquid-phase effluent were collected; and six gas-phase samples were analyzed. The feed and liquid-phase effluent samples were each subject to duplicate or triplicate GC analysis. The averages and standard deviations of these measurements were used to estimate confidence intervals on both the measured and calculated parameters.

The error bars on all measured and calculated variables are reported at the 99% confidence level. The confidence intervals on the experimentally measured quantities were calculated by assuming a Student's *t*-distribution approximates the error distribution, and the following expression was used to calculate confidence intervals:

$$\bar{x} \pm \frac{\sigma \cdot t_{1-0.99}\left((n_{obs}-1)\text{ degrees of freedom}\right)}{\sqrt{n_{obs}}} \tag{5-2}$$

where $\bar{x}$ is the average of a measured value, σ is the sample standard deviation, and $t_{1-0.99}\left((n_{obs}-1)\text{ degrees of freedom}\right)$ is the value from the *t*-table at the 99% confidence level given n_{obs} repeat measurements. Reporting errors at the 99% versus the standard 95% confidence level leads to slightly larger confidence intervals. For example, with 10 observations the *t*-value divided by $\sqrt{n_{obs}}$ increases from 0.7 to 1.0 and with 15 observations grows from 0.6 to 0.8. The errors on the measured values were assumed independent and random permitting the propagation of the confidence intervals of each measured parameter through the calculations by the differential method

to give 99% confidence intervals on the calculated values. Systematic errors, such as the absolute error in the GC calibrations and thermocouple accuracies, are not accounted for in the error analysis. Repeat experiments were performed to yield some information on the absolute variability of the kinetic data.

5.4.2 Hydrolysis

Seven hydrolysis experiments were conducted to determine the reactivity of benzene in supercritical water in the absence of oxygen at 246 bar and reactor temperature from 530 to 625°C. A discussion of the results follows and the detailed summary of the seven hydrolysis experiments appears in Appendix 10.2. The organic feed pump delivered the deaerated, saturated benzene solution to the reactor, and the oxidant feed pump fed deaerated, deionized water in place of a hydrogen peroxide or dissolved oxygen solution during the hydrolysis experiments. The residence time in the reactor was maintained at 6 seconds during all hydrolysis experiments.

Since the feed streams were preheated before entering the reactor, the benzene solution was exposed to heating for significantly longer than the 6 seconds spent in the reactor. The volume of preheater that the benzene solution passes through is approximately 13.5 mL, comparable to the 11.5 mL reactor volume. The final 5.2 m or 4.8 mL of the preheater is located in the main sandbath. Here, the benzene solution is approximately at the same temperature as the reactor. Since the ambient benzene volumetric flowrate is nominally 5 mL/min and increases by about an order of magnitude at supercritical conditions, the benzene solution spends about 6 s in this section of the preheater alone. Additionally, the benzene solution spends a minimum of 10 s in the non-isothermal DOH section of the preheater. As a result, the total time benzene is exposed to heating is more than twice the reactor residence time.

Figure 5-1 presents the resulting conversion of benzene as a function of temperature measured in the hydrolysis experiments. Here, conversion is defined as:

$$\text{Conversion} = \frac{[C_6H_6]_o - [C_6H_6]}{[C_6H_6]_o} \times 100\% \qquad (5\text{-}3)$$

where $[C_6H_6]_o$ and $[C_6H_6]$ are the benzene concentrations at the reactor inlet and exit, respectively. Again, the error bars on conversion and temperature are at the 99% confidence level and account for the random errors in each quantity. The data markers obscure the temperature error bars, but the

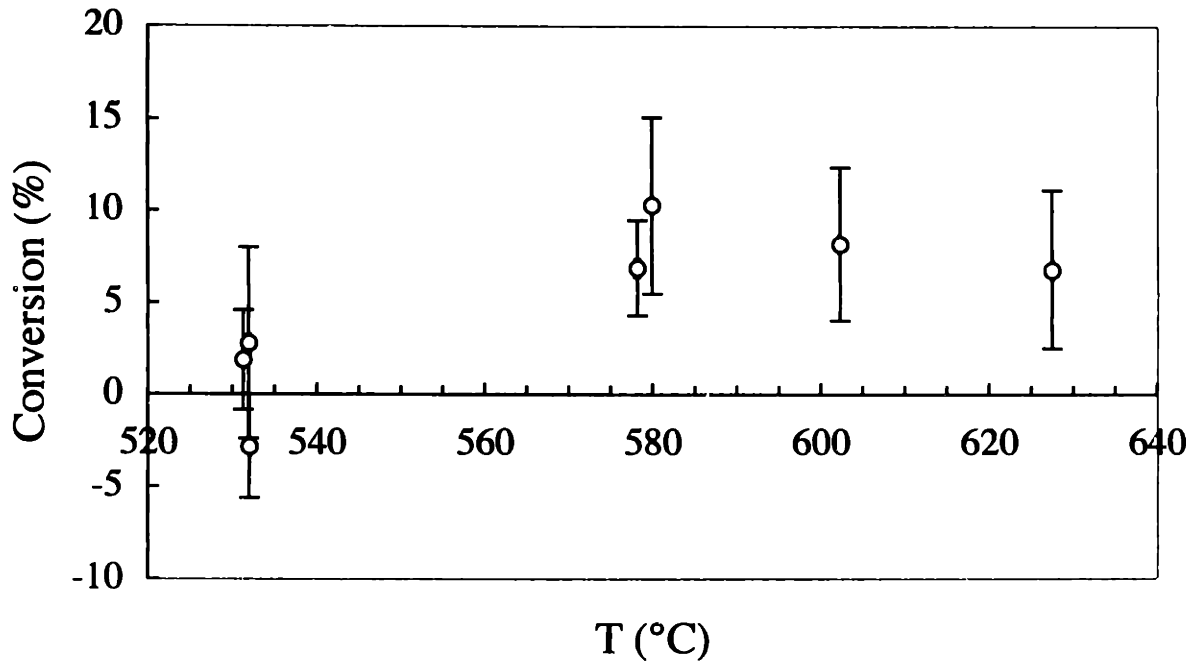

Figure 5-1 Benzene conversion in SCW in the absence of oxygen
($\tau_{reactor}$=6.2±0.6 s, P=246±2 bar, $[C_6H_6]_o$=0.48-1.25 mM)

calculated errors in all quantities are tabulated in Appendix 10.2. The three hydrolysis experiments at 530°C, which show almost no benzene conversion, were conducted after implementing the improved feed sampling technique (see Section 5.3). The hydrolysis conversion above 575°C, for reasons which will be explained below, is believed to be lower than that shown in Figure 5-1. Phenol was the only quantifiable, detected hydrolysis product. Although CO, CO_2, methane, ethane, ethylene and hydrogen were also observed, their amounts were not quantified as the gas flowrate was too low to measure (<0.06 mL/min.).

Figure 5-2 presents the corresponding carbon balances for each of the hydrolysis experiments, with carbon balance defined as:

$$\text{Carbon Balance} = \frac{\text{moles of carbon in effluent}}{\text{moles of carbon in feed}} \times 100\% \qquad (5\text{-}4)$$

At 530°C, accounting for only the unreacted benzene and the low levels of phenol in the effluent, complete closure of the carbon balances was achieved. In comparison, only 90 to 95% of the carbon was recovered in the higher temperature experiments.

The more complete carbon balance closure at 530°C is most likely a result of the improved feed sampling technique. Assuming 1) no hydrolysis products were present in the effluent which

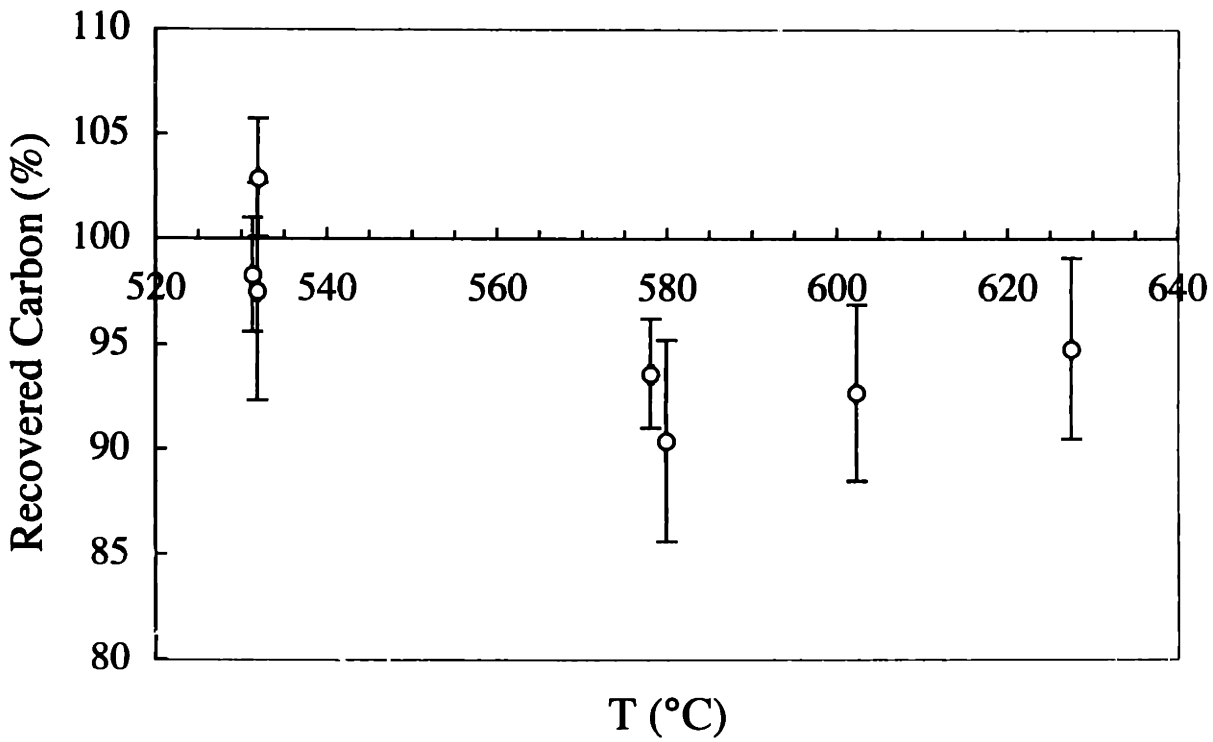

Figure 5-2 Percent of carbon in feed recovered in the effluent in the benzene hydrolysis experiments
($\tau_{reactor}$=6.2±0.6 s, P=246±2 bar, $[C_6H_6]_o$=0.48-1.25 mM)

would go undetected by the effluent analysis method presented in Appendix 10.1 and 2) no systematic errors in the effluent concentration measurements of benzene, the incomplete carbon balance closure above 575°C suggests a positive systematic error in the measured feed concentrations of benzene using the earlier feed sampling technique. If so, the actual benzene conversions above 575°C are lower than those shown in Figure 5-1.

The effluent phenol concentrations can be used to estimate the true benzene hydrolysis conversion levels as long as phenol is only hydrolysis product of significant concentration. This assumes the absence of any species which would go undetected by the effluent analysis method presented in Appendix 10.1. The calculated benzene conversion based on the effluent phenol concentrations is less than 2% at all temperatures. Given that the benzene conversion in the absence of oxygen is determined to be no greater than 10% and realistically closer to 2% at temperatures up to 625°C, and as will be shown below benzene undergoes near complete conversion by an oxidative pathway with similar reaction conditions by a temperatures of 575°C, the hydrolysis pathway will not interfere with the study of benzene oxidation kinetics.

5.4.3 Oxidation

The results from the 107 benzene oxidation experiments are described below. The detailed summary of the oxidation experiments appears in tabular form in Appendix 10.2.

Temperature Variation Experiments: The temperature variation experiments in Table 5-2 were the first set of oxidation experiments conducted. Temperature was varied from 479 to 587°C at a fixed pressure of 246 bar, residence time of 6 seconds, initial benzene concentration of 0.6 mM and with a stoichiometric level of oxygen. Benzene conversion as a function of reactor temperature appears in Figure 5-3. Benzene oxidizes only minimally at temperatures less than 520°C. Conversion increases rapidly with temperature between 520 and 565°C and is essentially complete above 565°C.

Six replicate, independent experiments at 540°C and four at 575°C verified the repeatability of measurements. Two of these replicate experiments at 540°C and two at 575°C were performed with decreased levels of preheating in the DOH section for the purpose of verifying that when exposed to the full DOH preheating load the organic and oxidant feeds reach the reactor temperature well before entering the reactor. Conversion was found independent of the amount of preheating indicating that with the normal preheating level the feeds are unquestionably at the desired temperature.

Carbon monoxide, carbon dioxide, methane and phenol are the primary products of benzene oxidation. Figure 5-4 and Figure 5-5 display the carbon fractions of these products along with that of unreacted benzene as a funtion of temperature, where carbon fraction is defined as:

$$\text{Carbon Fraction} = \frac{\text{moles of carbon in product}}{\text{moles of carbon in feed}} \tag{5-5}$$

By plotting each product on a carbon basis as defined by Eqn. (5-5), the fate of the carbon in the feed is readily apparent. The total of all product carbon fractions and that of the unreacted benzene sum to one if all of the carbon in the feed is recovered in effluent.

Carbon dioxide and carbon monoxide are the oxidation products accounting for the largest amount of reacted carbon. The oxidation of benzene yields more CO_2 than CO at all conditions, fully consistent with the SCWO of phenol and substituted phenols as discussed in Section 5.1. Even at 479°C, where the benzene conversion is very low, the CO_2 yield was 7.53×10^{-3} mol/mol

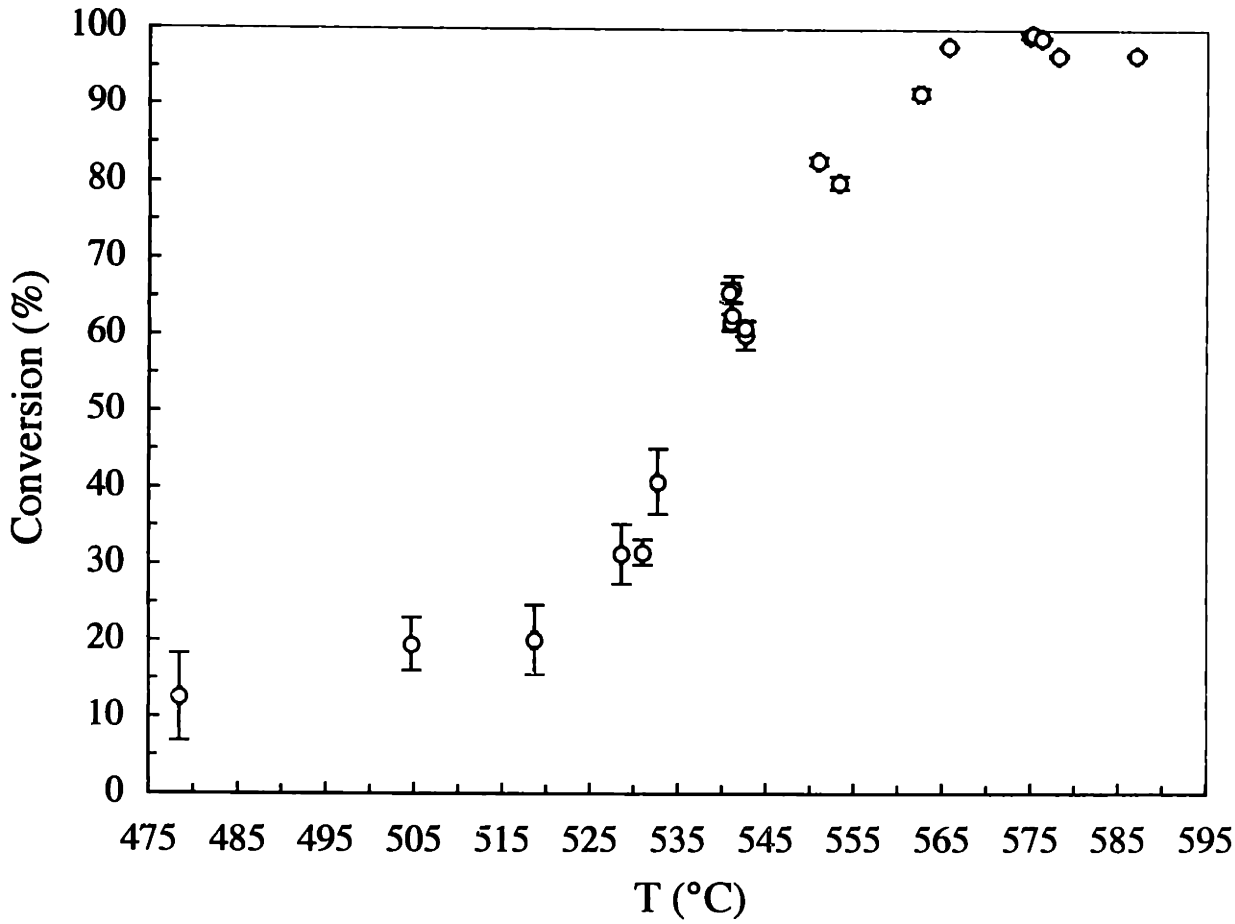

Figure 5-3 Benzene conversion as a function of temperature
(τ=6.2±0.4 s, P=246±2 bar, Φ=1.1±0.1, $[C_6H_6]_o$=0.60±0.04 mM)

compared to 4.81×10^{-3} mol/mol for CO. While the carbon fraction of CO_2 continually increases with temperature, that of CO increases only up to 540°C after which the temperature is sufficient for the oxidation of CO to CO_2. By 575°C, nearly 100% benzene conversion is achieved, with CO_2 accounting for 90% of the carbon in the feed.

Methane was the only other gas-phase, carbon containing product detected in appreciable quantities. Methane accounted for up to 5% of the carbon in the feed. The methane carbon fraction increases with increasing temperature, indicating that methane is not undergoing further oxidation at these conditions.

Several additional light gases were detected. Ethylene, acetylene and propylene were observed, although in quantities unimportant to the carbon balance. Hydrogen was only found at high temperatures under oxygen-depleted conditions and was presumably formed via a global water-gas shift pathway. Unreacted benzene was also detected in the gas-phase.

Phenol was the only detected liquid-phase product. At most, phenol accounted for 2% of the carbon. Phenol was not detected below 505°C, indicating that phenol is not formed at the lower temperatures where only minimal benzene oxidation occurs. No phenol was detected above 575°C, suggesting that phenol is oxidized at a rate comparable to its rate of formation.

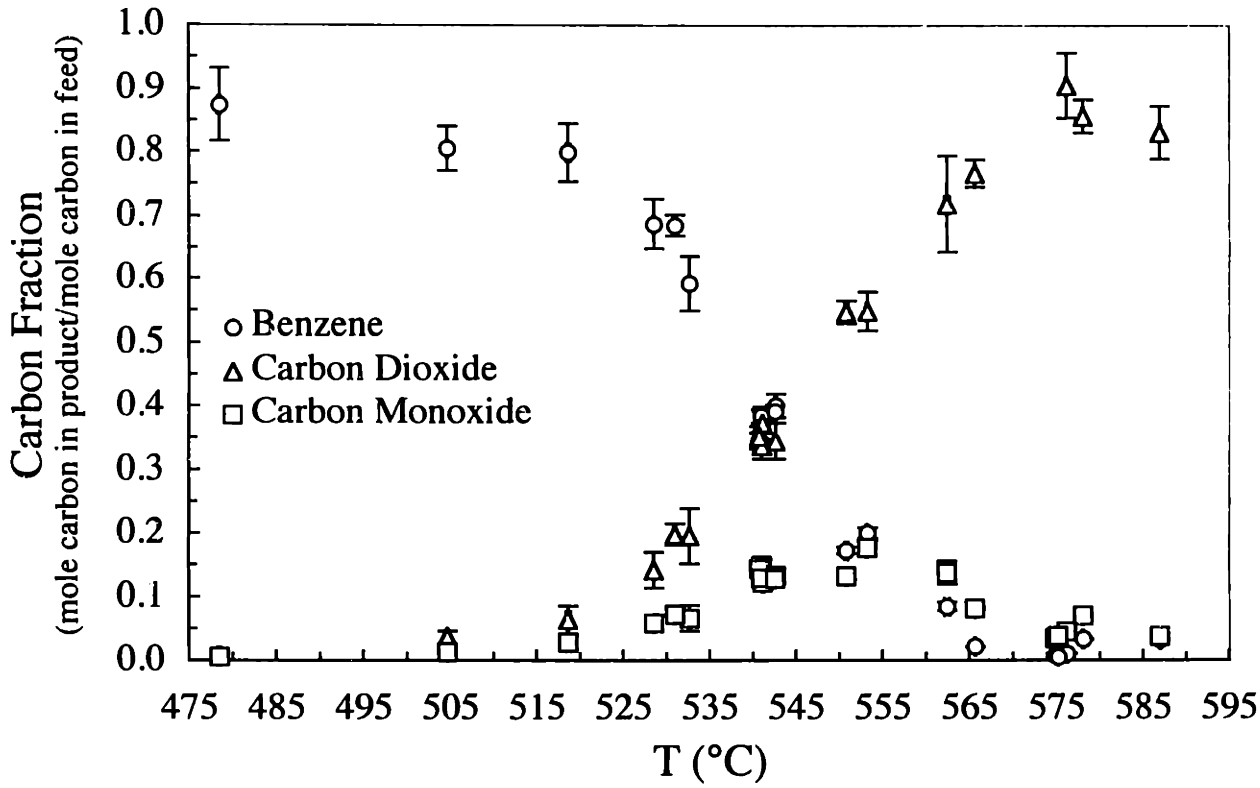

Figure 5-4 Carbon fractions of carbon dioxide, carbon monoxide and unreacted benzene as a function of temperature
(τ=6.2±0.4 s, P=246±2 bar, Φ=1.1±0.1, $[C_6H_6]_o$=0.60±0.04 mM)

Carbon balances calculated using CO, CO_2, methane, phenol, the trace light hydrocarbon gases and unreacted benzene range from 90 to 100%. Figure 5-6 shows a graph of the carbon balance as a function of temperature. Higher carbon balances are observed with higher benzene conversions as all of the reacted carbon is in the form of CO, CO_2 and methane.

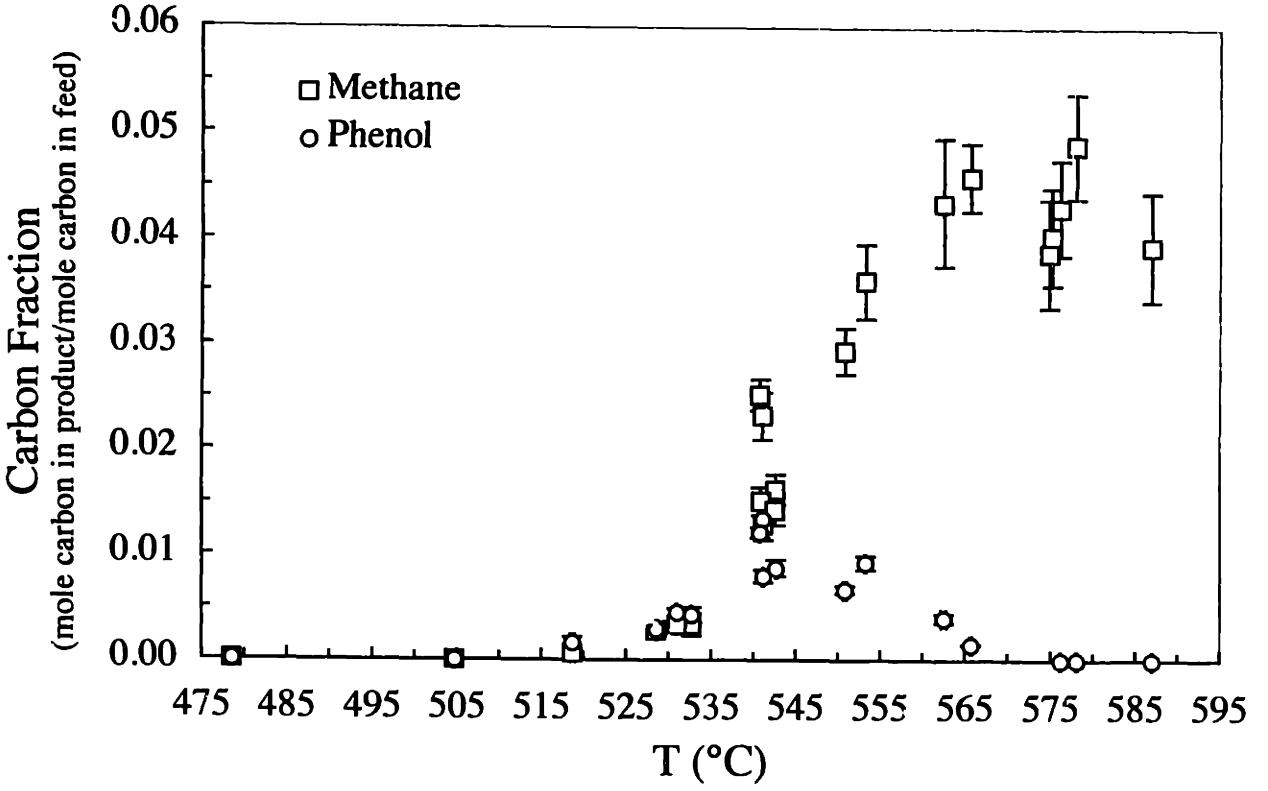

Figure 5-5 Carbon fractions of methane and phenol as a function of temperature
(τ=6.2±0.4 s, P=246±2 bar, Φ=1.1±0.1, $[C_6H_6]_o$=0.60±0.04 mM)

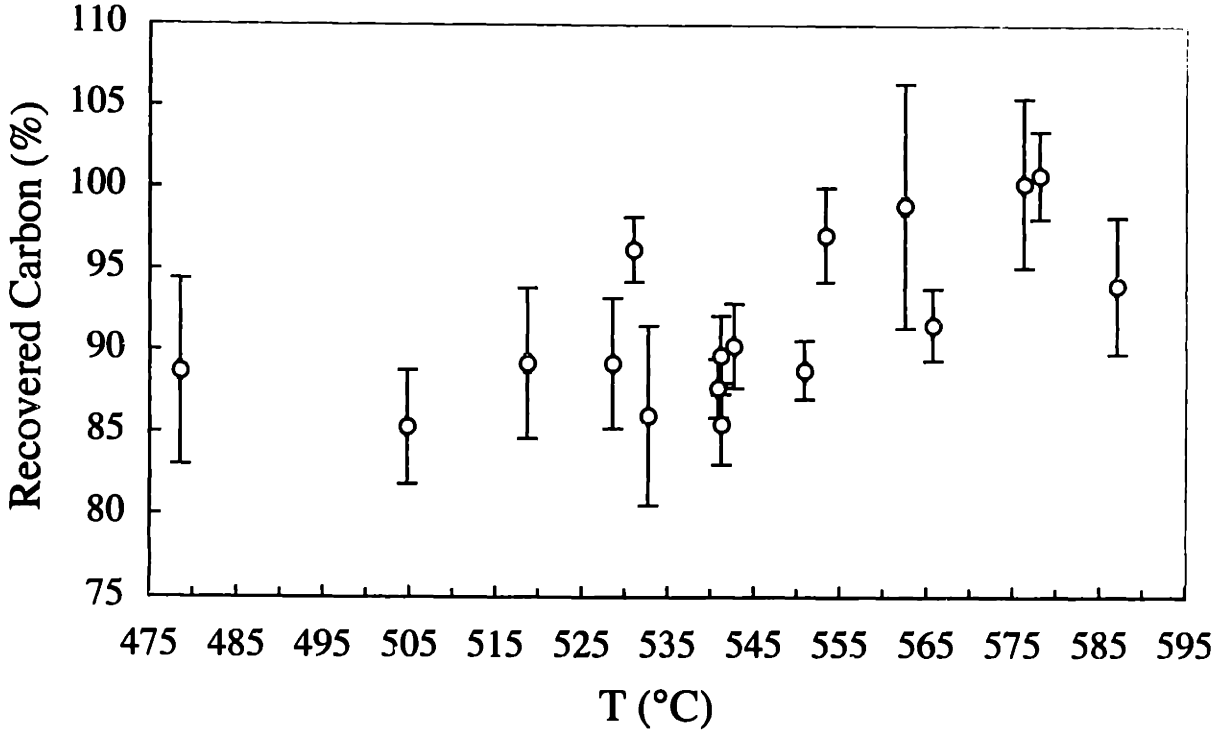

Figure 5-6 Carbon balances as a function of temperature
(τ=6.2±0.4 s, P=246±2 bar, Φ=1.1±0.1, $[C_6H_6]_o$=0.60±0.04 mM)

Fuel Equivalence Ratio Variation Experiments: Experiments to determine the effect of the oxygen-to-benzene ratio on benzene conversion were conducted at 540 and 550°C with a pressure of 246 bar and an initial benzene concentration of 0.6 mM. These temperatures were selected given the moderate levels of benzene conversion at 540 and 550°C in the temperature variation experiments.

The fuel equivalence ratio (Φ) was varied from 0.48 (100% excess oxygen) to 2.5 (40% of oxygen demand) at 540 and 550°C. Benzene conversion exhibits a pronounced dependence on Φ at both 540°C (see Figure 5-7) and 550°C (see Figure 5-8). The lines in the figures are trendlines included only for visualization purposes. The positive relationship between conversion and oxygen concentration is consistent with the experimental observations on phenol SCWO (Thornton and

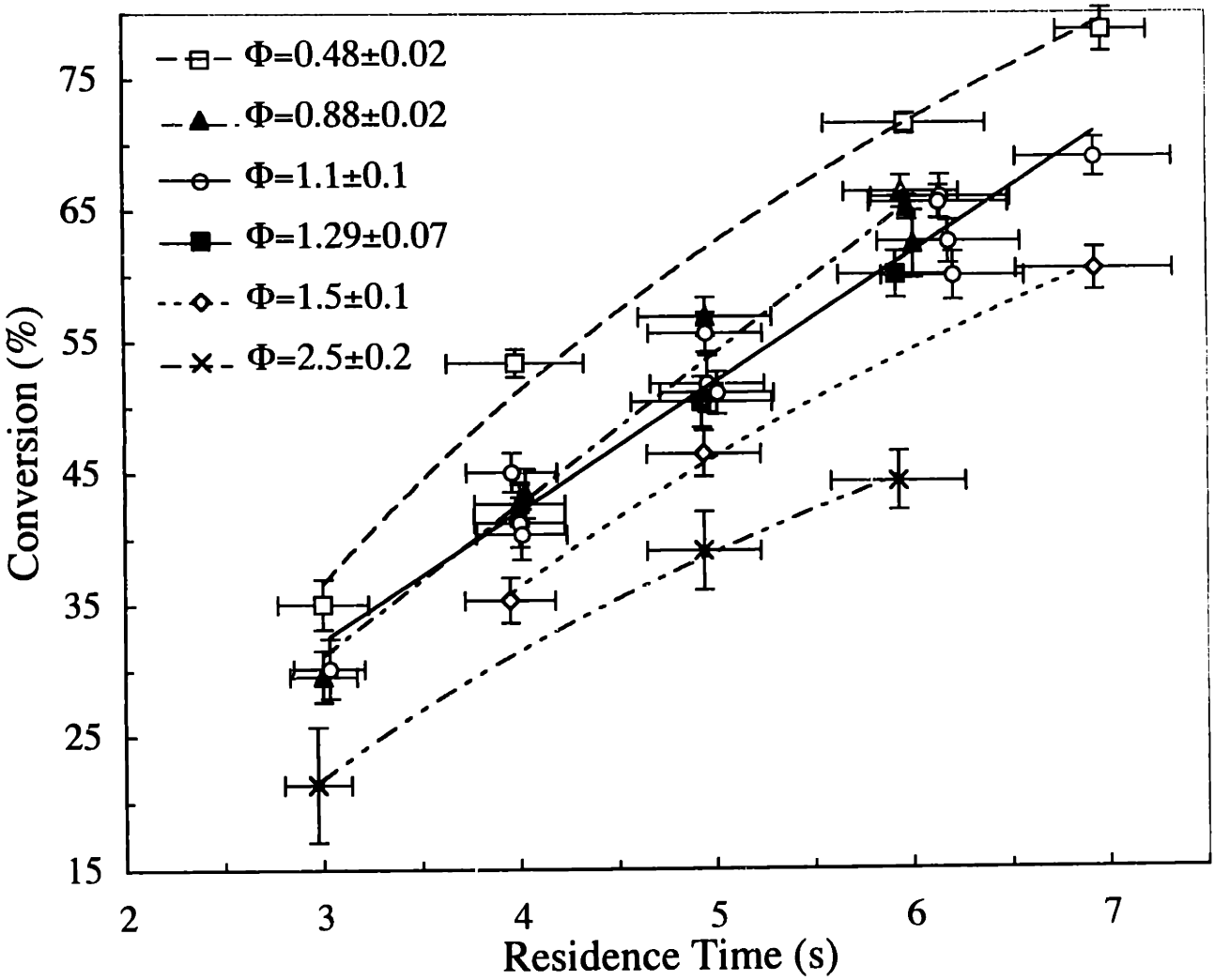

Figure 5-7 Benzene conversion as a function of residence time and Φ at 540°C
(T=540±2°C, P=246±2 bar, $[C_6H_6]_o$=0.60±0.04 mM)

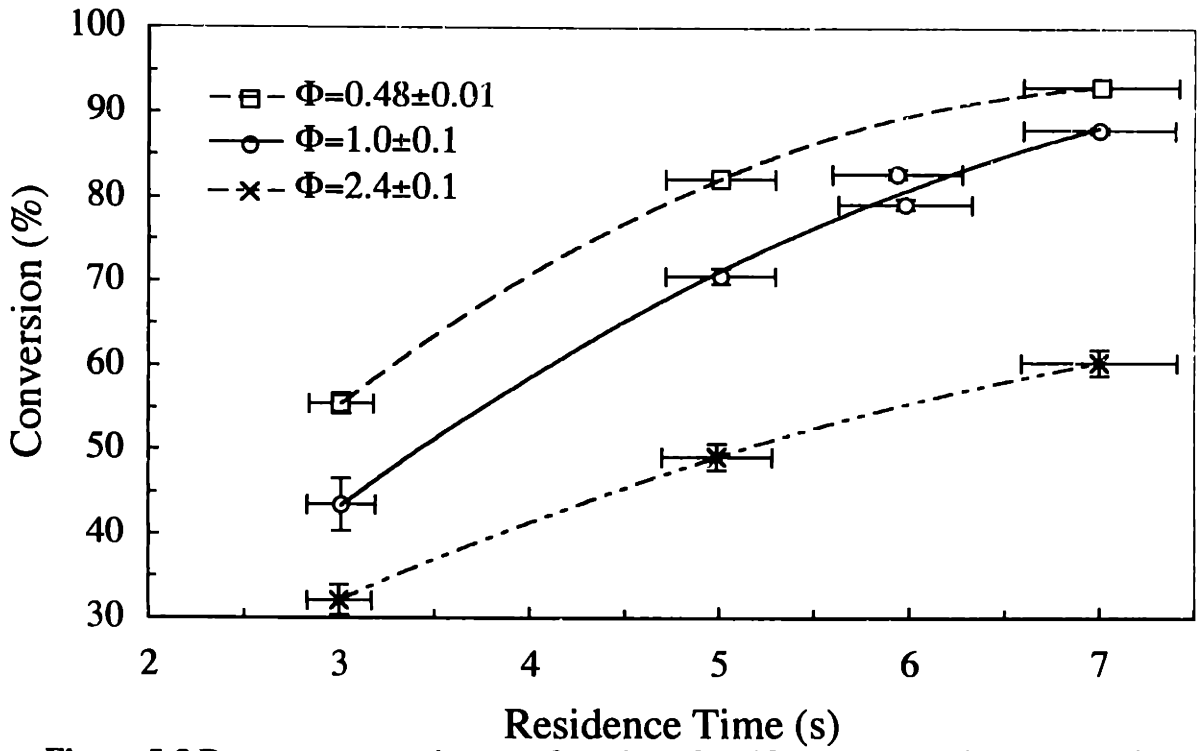

Figure 5-8 Benzene conversion as a function of residence time and Φ at 550°C
(T=550±2°C, P=246±2 bar, $[C_6H_6]_0$=0.59±0.01 mM)

Savage, 1990; Krajnc and Levec, 1996; Koo *et al.*, 1997). One should note that a dependence on oxygen concentration is not always observed for oxidation in SCW (Holgate and Tester, 1993). The fact that benzene and phenol conversions are functions of Φ signifies that oxygen participates in important radical-generating reactions in their oxidation mechanisms.

The fate of the reacted carbon also exhibits a dependence on Φ. Figure 5-9 and Figure 5-10 compare yields of CO_2 and CO at 550°C with yield defined on a reacted carbon basis:

$$\text{Yield} = \frac{\text{moles carbon in product}}{\text{moles carbon reacted}} \tag{5-6}$$

The moles of carbon reacted is based on the initial and effluent benzene concentrations. With an increasing oxygen-to-benzene ratio, not only does more benzene react, but more of the reacted carbon is in the form of CO_2. The yields of CO, phenol and methane decrease with increasing oxygen concentrations fed. Hydrogen is only observed at fuel rich conditions (Φ>1) lending support to the previous assumption that the global water-gas shift pathway is the source of hydrogen. At fuel-lean conditions the water-gas shift pathway is not competitive with the non-hydrogen producing pathway for CO to CO_2 oxidation (Holgate *et al.*, 1992), and hydrogen is not formed. Carbon balances for these experiments were consistently 85 to 95%.

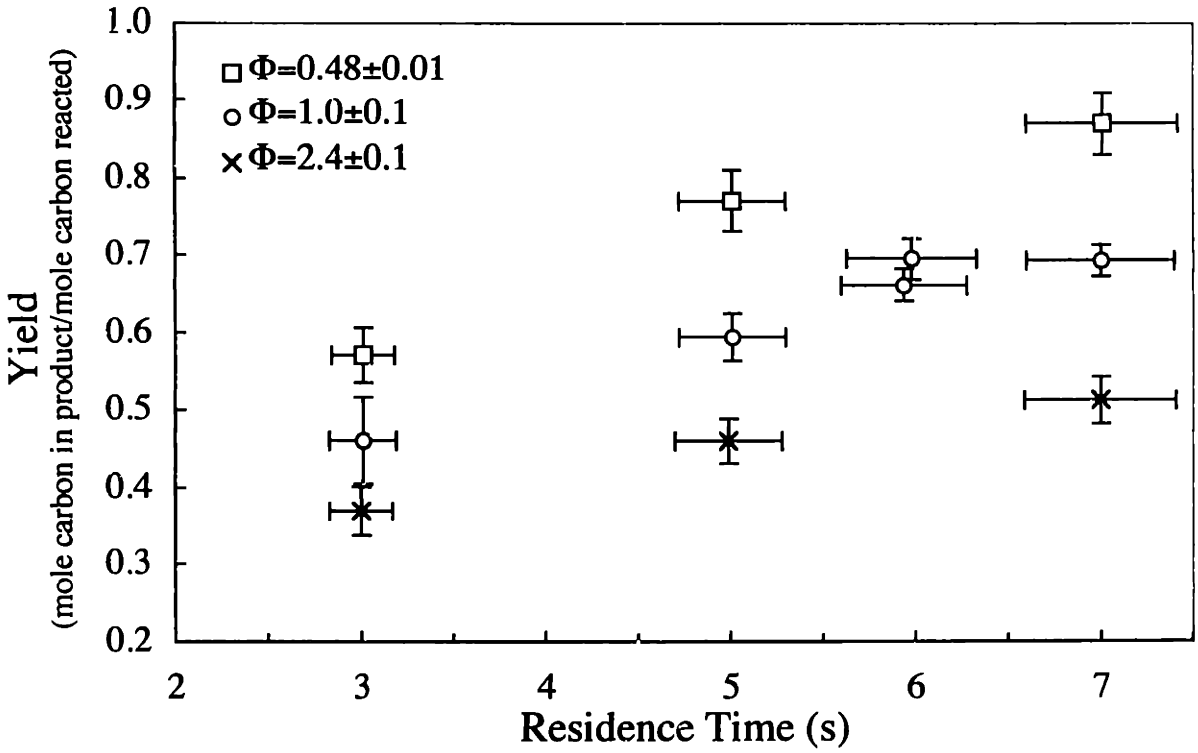

Figure 5-9 CO_2 yield as a function of residence time and Φ at 550°C
(T=550±2°C, P=246±2 bar, $[C_6H_6]_o$=0.59±0.01 mM)

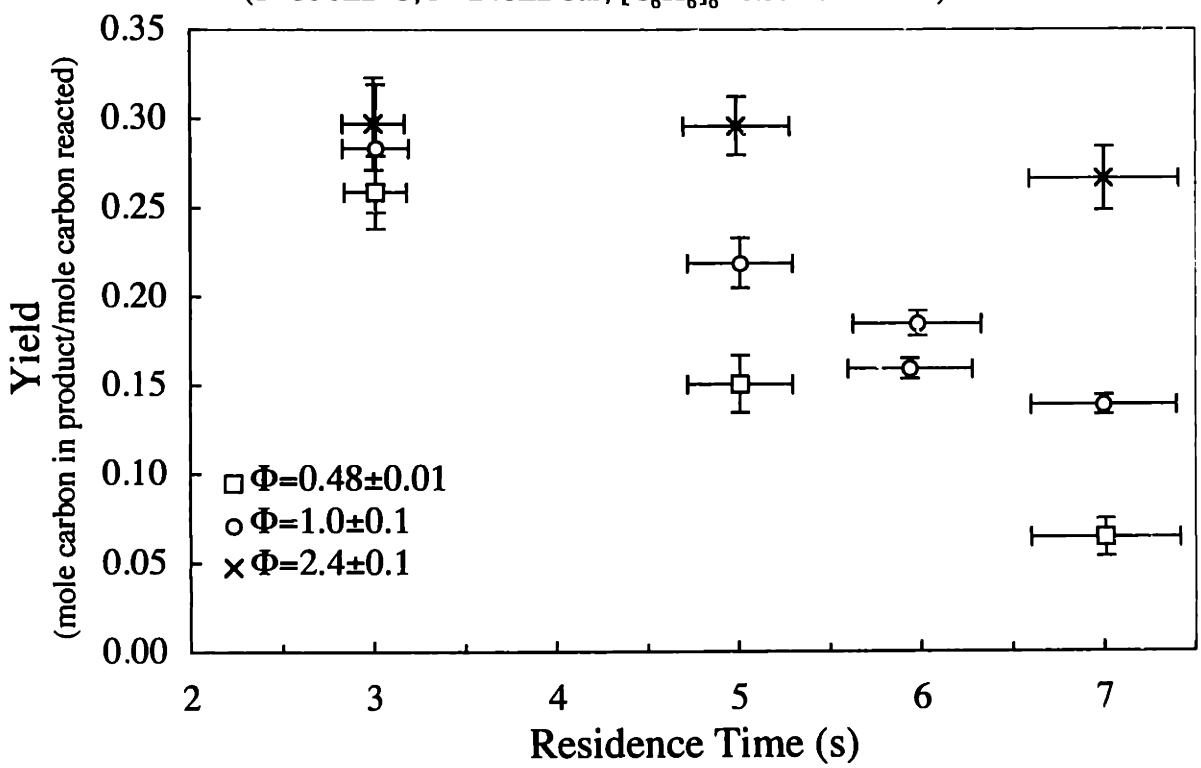

Figure 5-10 CO yield as a function of residence time and Φ at 550°C
(T=550±2°C, P=246±2 bar, $[C_6H_6]_o$=0.59±0.01 mM)

The dependence of reaction product yields on Φ is enhanced at higher benzene conversions. For example, the yields of CO_2 and CO in Figure 5-9 and Figure 5-10 are clearly more influenced by Φ at longer residence times where there is a higher conversion of benzene. Likewise, the yields of all species exhibit a lesser dependence on Φ at 540°C where benzene conversions are lower. At low benzene conversions a significant amount of oxygen is available for reaction with the intermediate species, even at low oxygen-to-benzene ratios, so the oxidation rates of the intermediate species are more affected by Φ at high conversions where oxygen levels are depleted.

Effect of Oxidant: As discussed in Section 3.1.1, upon heating hydrogen peroxide will decompose to water and oxygen. Experiments measuring this decomposition rate in SCW at Sandia National Laboratory led to the development of the following rate expression (Croiset *et al.*, 1997):

$$k_{overall}\left(\mathrm{s}^{-1}\right) = k_h\left(\mathrm{s}^{-1}\right) + k_w\left(\mathrm{cm}\cdot\mathrm{s}^{-1}\right) * \left(\frac{S}{V}\right)\left(\mathrm{cm}^{-1}\right) \tag{5-7}$$

where $k_{overall}$ is the overall, first-order rate constant for hydrogen peroxide decomposition, and *S/V* is the surface-to-volume ratio of the reactor. Hydrogen peroxide decomposition is catalyzed by metal surfaces, and hence both homogeneous, k_h, and heterogeneous, k_w, reactions contribute to the overall rate. The first-order rate constants for the homogeneous and heterogeneous reactions were developed for temperatures of 300 to 420°C and pressures from 245 to 340 bar (Croiset *et al.*, 1997):

$$k_h\left(\mathrm{s}^{-1}\right) = 10^{13.7\pm1.2}\exp\left[-180\pm16(\mathrm{kJ/mol})/RT\right] \tag{5-8}$$

$$k_w\left(\mathrm{cm}\cdot\mathrm{s}^{-1}\right) = 10^{3.3\pm0.3}\exp\left[-62.5\pm4.4(\mathrm{kJ/mol})/RT\right] \tag{5-9}$$

In order to gain a conservative estimate of the extent of reaction in our reactor system, we can assume that hydrogen peroxide decomposition only occurs in the isothermal section of preheater located in the main sandbath even though reaction will initiate in the DOH section of the preheater. Estimating the residence time in the sandbath preheater at 6 seconds (see Section 5.4.2) and given that the surface-to-volume ratio of the preheater tubing is 37 cm^{-1}, 100% conversion of the hydrogen peroxide in the temperature range of the benzene oxidation experiments (479-587°C) is predicted using Eqns. (5-7) through (5-9).

In order to confirm the prediction that hydrogen peroxide completely decomposes in the preheater, dissolved oxygen was used in several of the Φ variation experiments allowing a direct comparison of the benzene oxidation rate with either oxygen source. The results, shown in Figure 5-11, indeed reveal that there is no statistically significant difference in oxidation kinetics with choice of oxidant. The yields of CO, CO_2, phenol, and all other products, likewise, did not exhibit a statistically significant dependence on oxidant type.

Were hydrogen peroxide not to decompose completely, the likely effect would be an enhancement in the reaction rate through a decrease in the induction time. In SCW, hydrogen peroxide rapidly decomposes to the very reactive •OH radicals. The use of hydrogen peroxide as a rate enhancer was explored in the oxidation of 2,4-dichlorophenol and acetic acid (Lee *et al.*, 1990). In separate experiments, hydrogen peroxide and oxygen were premixed with the organics in batch reactors. The premixed solutions were then heated to 400 to 500°C. At comparable conditions, the conversions of both compounds were higher with hydrogen peroxide than with oxygen. This ability of hydrogen peroxide to enhance reaction rates may be of industrial interest and can be exploited by directly injecting cold hydrogen peroxide into the preheated SCW/organic/oxygen mixture.

Effect of Benzene Feed Concentration: The experiments in group 3 of Table 5-2 were designed to determine the effect of the initial benzene concentration on conversion. While maintaining a

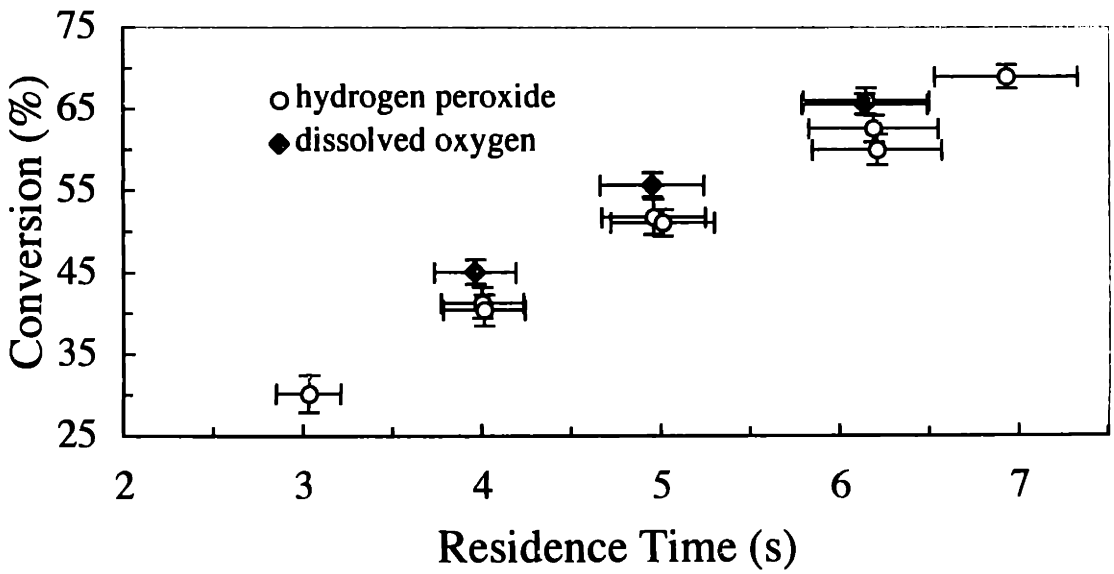

Figure 5-11 Comparison of measured benzene conversions when using hydrogen peroxide and dissolved oxygen as oxidants
(T=540±2°C, P=246±2 bar, $[C_6H_6]_o$=0.60±0.04 mM)

stoichiometric amount of oxygen and a pressure of 246 bar, experiments were performed with initial benzene concentrations of 0.4, 0.6 and 1.2 mM at 530, 540 and 550°C. As shown in Figure 5-12, at 540°C benzene conversion decreases on average 20 to 30% with a doubling of the initial benzene concentration from 0.6 to 1.2 mM. Several repeat experiments performed with $[C_6H_6]_o$=1.2 mM confirmed this inverse relationship between benzene concentration and conversion at 540°C. Complimentary experiments at 530°C at a single residence time again show decreasing conversions with increasing initial benzene concentrations (see Figure 5-13). At 550°C, however, the concentration dependence is greatly diminished and not measureable at a statistically significant level (see Figure 5-14).

The product yields, defined in Eqn. (5-6), were not found dependent on the initial benzene concentration. Figure 5-15 and Figure 5-16 show the yields at 540°C of CO and CO_2, respectively. There are no clear trends in the CO and CO_2 yields at 530, 540 or 550°C indicating that benzene forms CO and CO_2 in the same proportions. Likewise, no discernible relationship exists between the yields of phenol or methane and the initial benzene concentration at any of the three

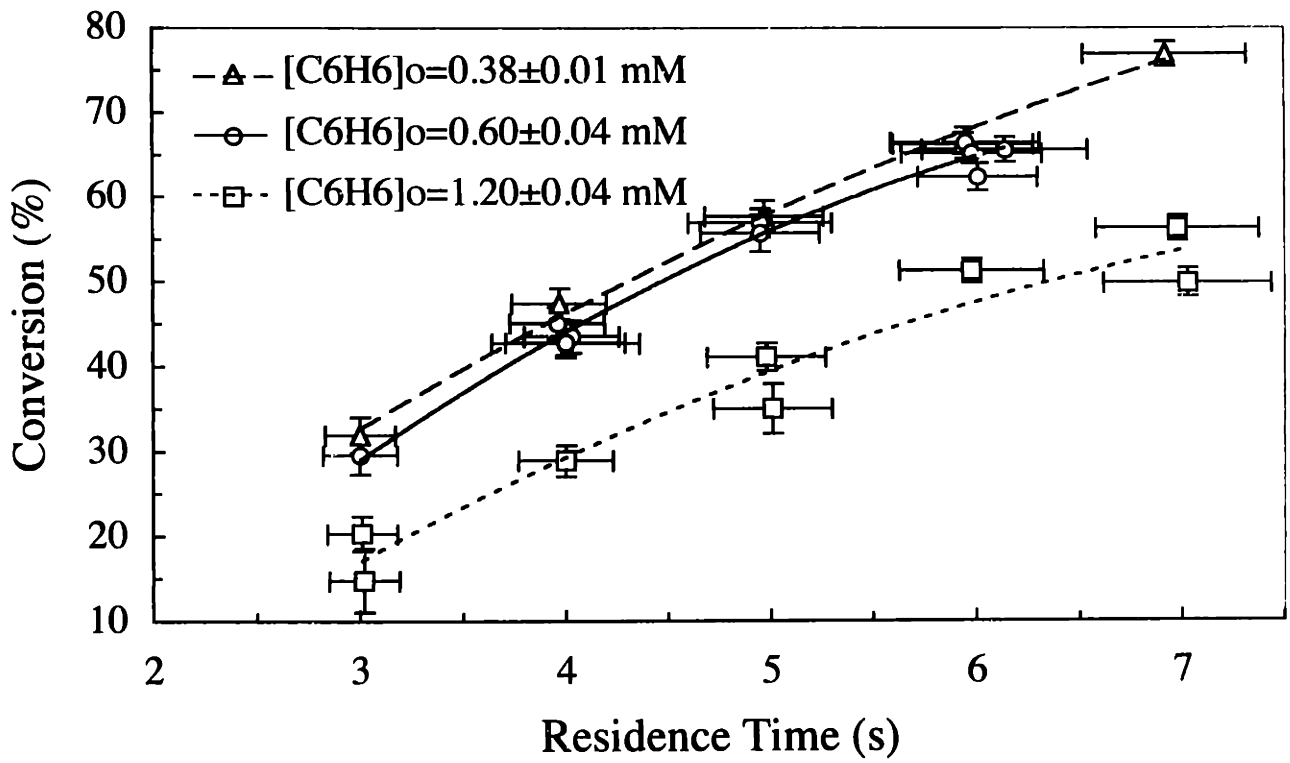

Figure 5-12 Benzene conversion as a function of residence time and $[C_6H_6]_o$ at 540°C
(T=540±2°C, P=246±2 bar, Φ=0.9±0.1)

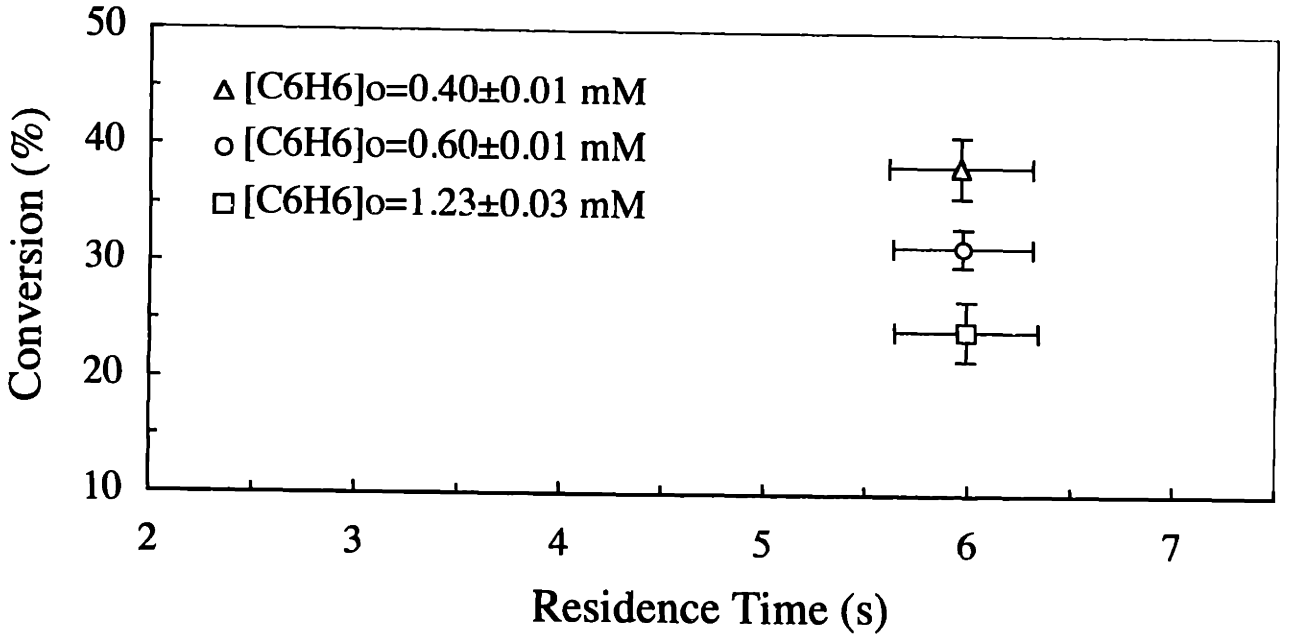

Figure 5-13 Benzene conversion as a function of $[C_6H_6]_o$ at 530°C
(T=531±2°C, P=246±2 bar, Φ=0.95±0.2)

temperatures.

Dependence of the oxidation rate on the initial feed concentration is a common observation in studies of SCW oxidation kinetics. Holgate and Tester (1993) showed that hydrogen conversion decreased with an increasing initial hydrogen concentration at 550°C with a stoichiometric amount of oxygen. Acetic acid conversion, on the other hand, increased with increasing feed concentration (Meyer *et al.*, 1995). Phenol conversion exhibited no dependence on the feed concentration (Thornton and Savage, 1992a; Krajnc and Levec, 1996).

A dependence of conversion on the feed concentration arises from the involvement of the feed in radical generating or radical quenching reactions in the overall free radical oxidation mechanism. Oxidation reactions occur by many individual elementary steps, each of which depends on temperature, possibly pressure, and the concentration of reactants. The decrease of benzene conversion with increasing benzene feed concentration suggests that benzene itself may catalyze the recombination of radicals. As an example of catalysis of radical recombination, consider the following reactions:

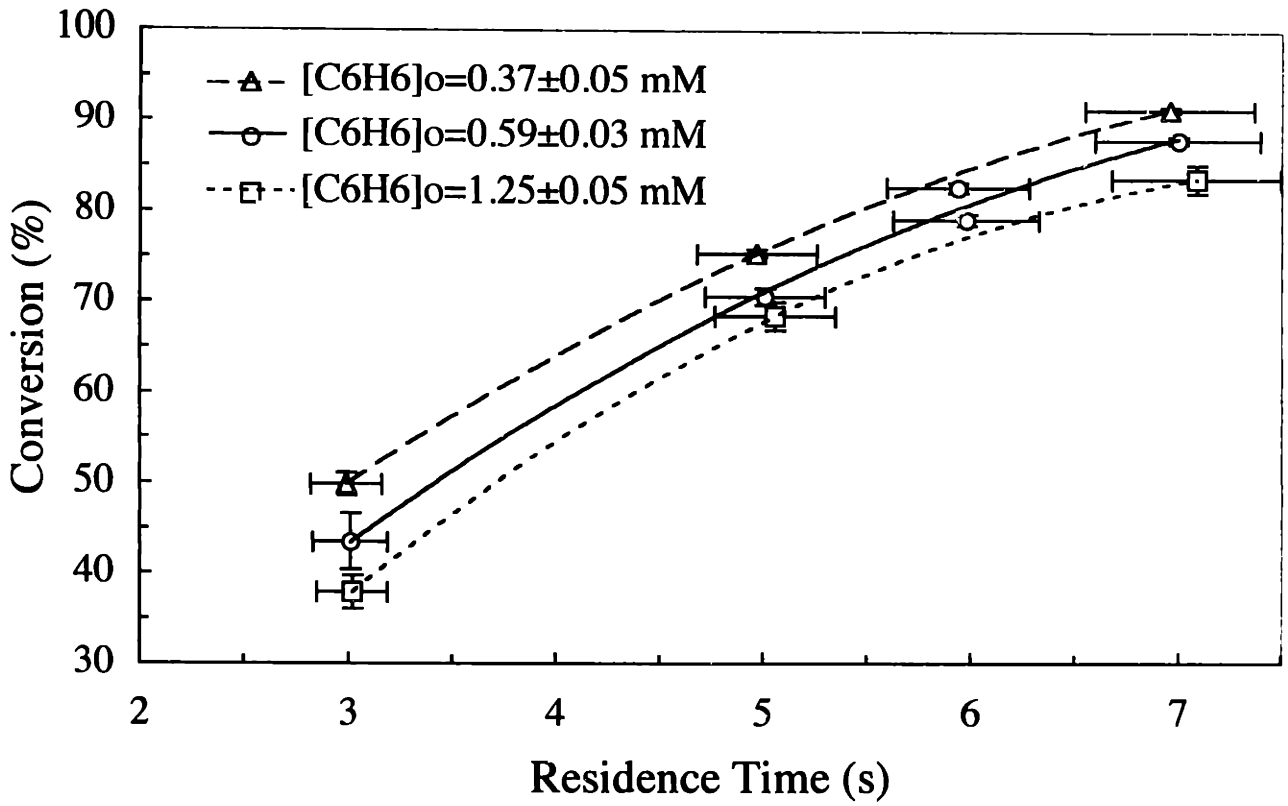

Figure 5-14 Benzene conversion as a function of residence time and $[C_6H_6]_o$ at 550°C
(T=550±2°C, P=246±2 bar, Φ=1.0±0.1)

$$XH + OH = X + H_2O \qquad R1$$
$$X + H = XH \qquad R2$$

If the net forward rates of R1 and R2 are positive, the combined effect is the recombination of radicals:

$$OH+H = H_2O \qquad R1+R2$$

For example, in a benzene combustion mechanism the following two reactions are included:

$$C_6H_6+OH = C_6H_5+H_2O \qquad R3$$
$$C_6H_5+H = C_6H_6 \qquad R4$$

Whenever the net forward rates of R3 and R4 are positive, the net effect of the two reactions is the loss of OH and H radicals.

The observation of a larger effect of the initial benzene concentration on conversion at 530 and 540°C than at 550°C lends support to the hypothesis that benzene catalyzes radical

recombination. Since the elementary reactions in the oxidation mechanism have different activation energies and hence different temperature dependencies, the significance of radical quenching effects varies with temperature.

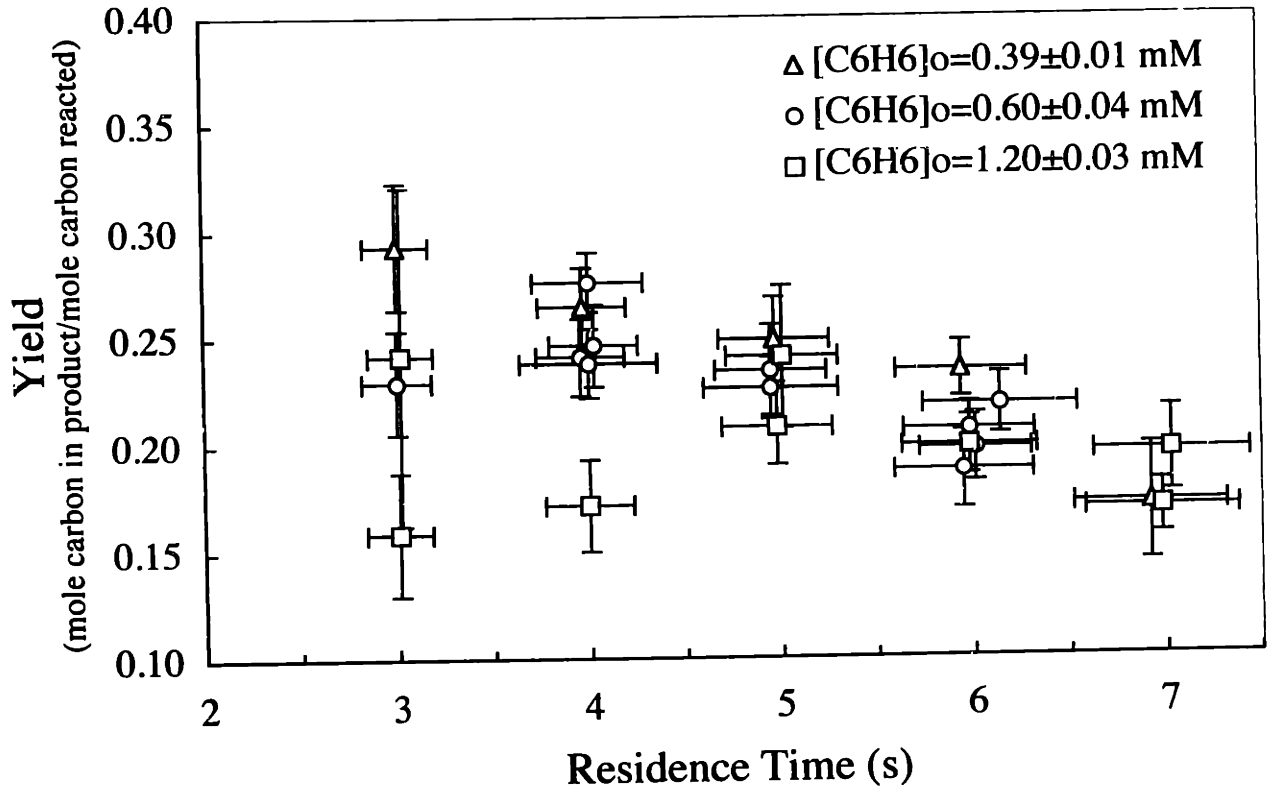

Figure 5-15 CO yield as a function of residence time and $[C_6H_6]_o$ at 540°C
(T=540±2°C, P=246±2 bar, Φ=0.9±0.1)

Effect of Fluid Pressure or Density: A final set of experiments was performed to ascertain the influence of operating pressure or fluid density on benzene conversion. Pressure was varied from 139 to 278 bar at 540°C with a stoichiometric amount of oxygen and an initial benzene concentration of 0.6 mM. The increasing pressure at 540°C produces a corresponding rise in the density from 0.041 g/mL at 139 bar to 0.091 g/mL at 278 bar. Interestingly, as shown in Figure 5-17, at subcritical pressures (P_c=221 bar) conversion is independent of pressure, while above P_c conversion clearly increases as pressure increases. A positive dependence of conversion on system pressure was also seen during phenol (Thornton and Savage, 1990; Koo *et al.*, 1997) and in hydrogen and carbon monoxide oxidation (Holgate and Tester, 1994a).

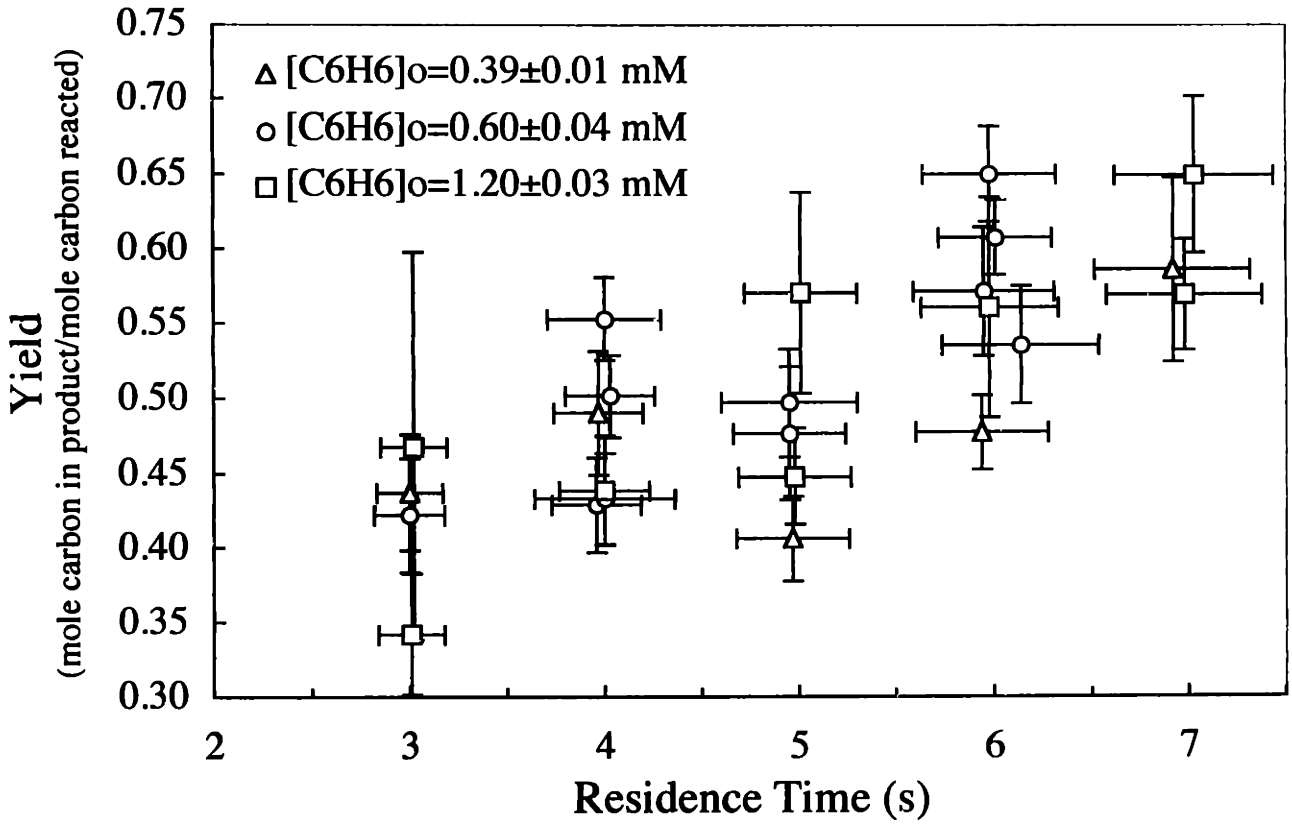

Figure 5-16 CO_2 yield as a function of residence time and $[C_6H_6]_o$ at 540°C
(T=540±2°C, P=246±2 bar, Φ=0.9±0.1)

This positive relationship between pressure and conversion may be due to the effect of pressure on the rate constants of elementary reactions. Oxidation in supercritical water proceeds by free-radical mechanisms consisting of many individual elementary reactions. The rate constants of unimolecular and recombination reactions are well-known to increase with pressure. Bimolecular chemically activated rate constants, on the other hand, decrease with pressure. The pressures in a supercritical water system are sufficiently high that most rate constants will have reached their high-pressure limit. However, the rate constants of reactions involving the recombination of small radicals (*i.e.*, molecules with one to four atoms) may still be in their fall-off regimes, and those which proceed via a chemically activated pathway may still be decreasing with pressure at SCWO pressures. As a result of the pressure dependence of the reaction rate constants, changing the total pressure has the potential for changing oxidation rates, even at the high pressures of SCWO.

In a supercritical water system, increasing pressure also increases the water density (concentration). As a result, it is not apparent which variable, pressure or water concentration, is

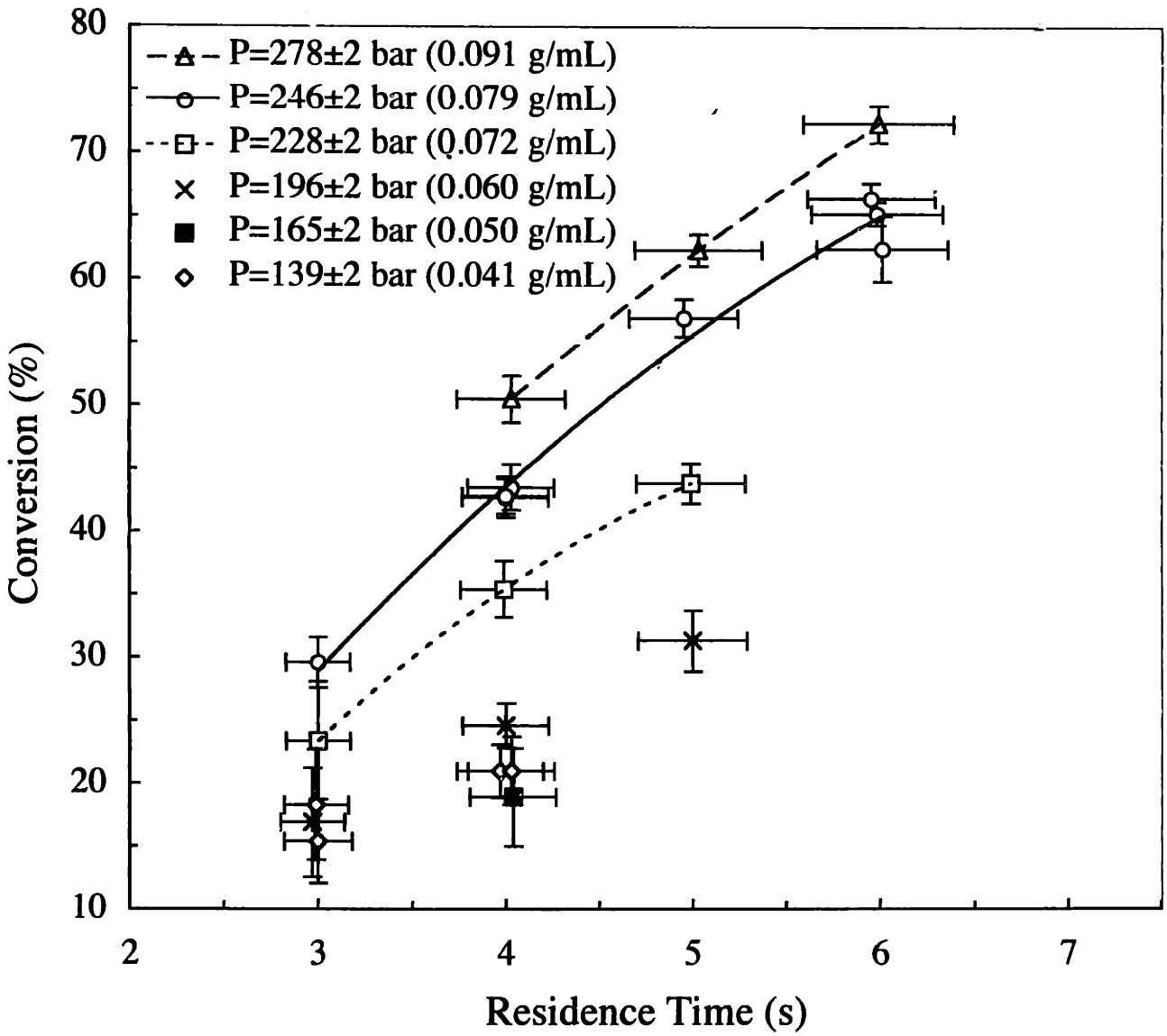

Figure 5-17 The effect of pressure and residence time on benzene conversion at 540°C
(T=540±2°C, $[C_6H_6]_o$=0.60±0.04 mM, Φ=0.9±0.1)

affecting the benzene reaction rate. Again, given that SCWO proceeds via a free-radical mechanism, if water participates directly in the oxidation as a reactant increasing water concentration will increase the rates of those reactions.

Recently, Koo *et al.* (1997) addressed this issue in the case of phenol oxidation at 400°C with 860% excess oxygen. Using a batch reactor, Koo *et al.* first measured the oxidation rate as a function of residence time at 223 bar, which corresponds to a water concentration of 6.9 M (0.124 g/mL). Next, the reactor pressure was increased to 253 bar in two ways: first by increasing the water concentration to 9.7 M (0.175 g/mL); and second by maintaining the water concentration

at 6.9 M and increasing pressure with the addition of helium. Comparison of the phenol conversion as a function of residence time from the three experiments demonstrated that the increasing water concentration, not the increasing pressure, induced the increase in the reaction rate.

Holgate theoretically explored the dependence of hydrogen and carbon monoxide oxidation rates on pressure (Holgate and Tester, 1994b). Experimentally, Holgate observed that the oxidation rates of hydrogen and carbon monoxide both increased with pressure. In order to evaluate whether the increasing pressure or water concentration was causing the corresponding increase in the oxidation rates, Holgate compared the predictions of the hydrogen and carbon monoxide elementary reaction mechanisms with his experimental data. Holgate concluded that the primary source of the model's pressure dependence was from the change in the water concentration and not due to the small changes in the rate constants of the pressure dependent reactions.

Although it is not apparent from the experimental data which variable, pressure or water concentration, is causing the increase in the benzene oxidation rate, the theoretical and experimental evidence from the SCWO of hydrogen, carbon monoxide and phenol suggest that the dependence of the benzene oxidation rate on pressure arises from the increasing water concentration. The four second residence time data from Figure 5-17 is replotted with density as the independent variable in Figure 5-18. Conversion increases with density for densities between 0.06 and 0.095 g/mL.

5.4.4 Regressed global rate expression

A global rate expression was regressed from the experimental data as a means of conveniently representing the benzene oxidation rate over the range of conditions studied. Based on the assumption that the reactor behaves as an ideal isothermal, isobaric plug-flow reactor, the reaction rate should obey the plug-flow design equation:

$$\frac{\tau}{C_{i,o}} = \int_0^{X_i} \frac{dX_i}{-R_i} \tag{5-10}$$

where τ is the residence time, $C_{i,o}$ is the initial concentration of reactant i, X_i is the measured conversion of species i and R_i is the reaction rate for species i. The form of the global rate expression that was selected to represent the oxidation of benzene is given by:

$$-R_i = -\frac{d[C_6H_6]}{dt} = A\exp(-E_a/RT)[C_6H_6]^a[O_2]^b \tag{5-11}$$

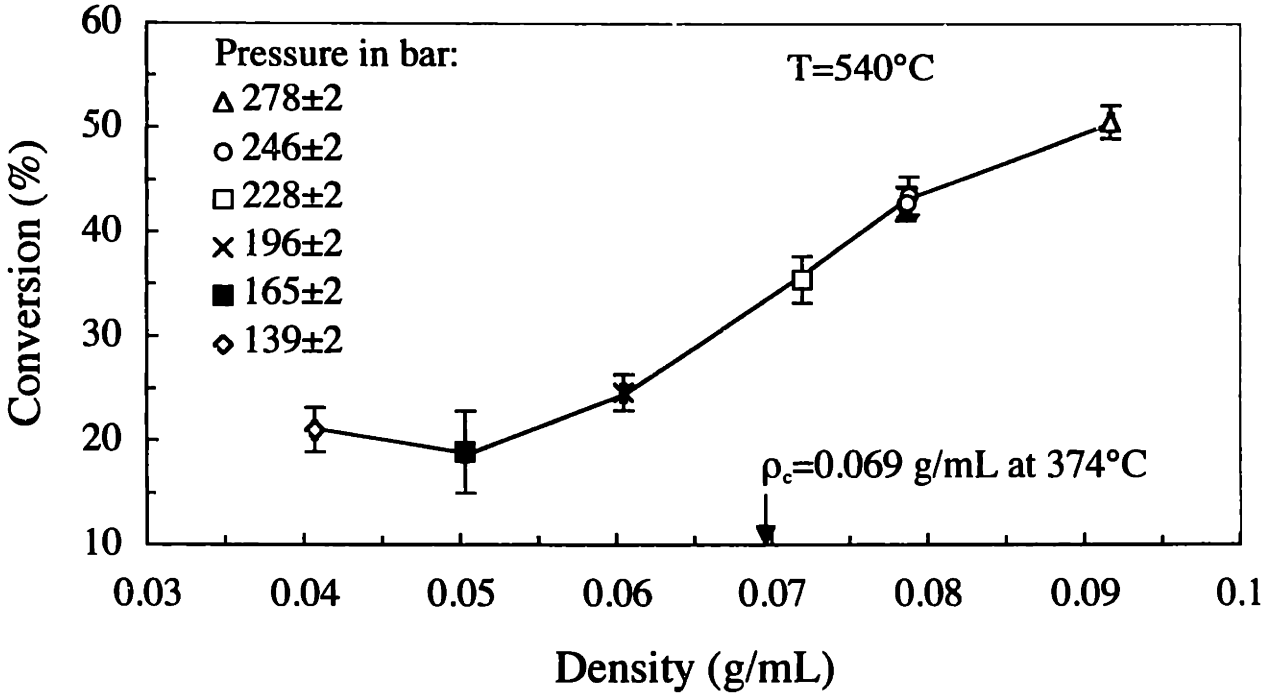

Figure 5-18 Variation of benzene conversion with density
(T=540±2°C, $[C_6H_6]_o$=0.60±0.04 mM, Φ=0.9±0.1)

and assumes the global oxidation of benzene depends only on the temperature and benzene and oxygen concentrations and that the water concentration explicity has no effect at isobaric conditions. The preexponential factor, A, activation energy, E_a, and reaction orders a and b are determined from the regression. Rewriting $[C_6H_6]$ and $[O_2]$ in terms of X and inserting Eqn. (5-11) into Eqn. (5-10) results in the following expression for an isothermal experiment:

$$k\tau[C_6H_6]_o^{a+b-1} = \int_0^X \frac{dX}{(1-X)^a(\phi - 7.5X)^b} \tag{5-12}$$

where

$$k = A\exp(-E_a/RT) \quad ; \quad \phi = [O_2]_o/[C_6H_6]_o \tag{5-13}$$

and 7.5 is the stoichiometric ratio of oxygen-to-benzene. Notably, use of the stoichiometric oxygen-to-benzene ratio in Eqn. (5-12) is based on the assumption that all reacted benzene undergoes complete oxidation to CO_2 and water. While this assumption is not completely accurate as incomplete oxidation products, mostly CO and some phenol and methane, were detected in the effluent, using the stoichiometric ratio as a correlating parameter is reasonable since CO_2 was always the highest yielding product.

A nonlinear regression of all experimental data with the exception of that from the pressure (density) variation experiments was performed in order to determine A, E_a, a and b in Eqn. (5-11). The regression routine used user-specified initial values for A, E_a, a and b and numerically integrated Eqn. (5-12) using experimental values for X, τ, $[C_6H_6]_o$ and ϕ from each experiment to solve for T (temperature). The algorithm then adjusted A, E_a, a and b until a best-fit was achieved between the predicted and experimental temperatures from all experiments. The multivariable Powell SSQMIN algorithm (Kuester and Mize, 1973) was used as the nonlinear optimization routine. Although $[C_6H_6]_o$ or τ could have been used in place of T as the dependent variable (X and ϕ could not be used because their values are required for the evaluation of the integral in Eqn. (5-12)), temperature was selected since its value is known with the highest precision in any given experiment.

The regression routine calculated the following best-fit global rate expression for benzene oxidation in supercritical water:

$$-\frac{d[C_6H_6]}{dt} = 10^{13.1\pm0.9}\exp(-2.4\pm0.1\times10^5/RT)[C_6H_6]^{0.40\pm0.06}[O_2]^{0.18\pm0.05} \qquad (5\text{-}14)$$

which can be used to calculate the benzene oxidation rate in SCW within the range of the conditions over which it was regressed. The units of the parameters are J, mol, L, s. The parameter uncertainties are calculated at the 95% confidence level using an inverted curvature matrix (Press *et al.*, 1986). The regression returned a reaction order with respect to benzene significantly less than 1 and a non-zero reaction order with respect to oxygen. In comparison, for phenol oxidation in SCW the reaction order with respect to phenol was found equal to approximately unity by three different groups of researchers who presented global rate expressions (Gopalan and Savage, 1995; Krajnc and Levec, 1996; Koo *et al.*, 1997). Since the regressed parameters are correlated and their numerical values also depend upon the regression routine used, care should be taken when directly comparing parameters, especially A and E_a, with the results from other research groups. A better test of data consistency is a one-to-one comparison of predicted to experimental conversions.

Figure 5-19 compares the predicted and experimental benzene conversion. Predicted conversion is plotted along the Y-axis and experimental conversion along the X-axis. If Eqn. (5-14) perfectly represented the data, all points would lie along the solid 45° line. As can be seen

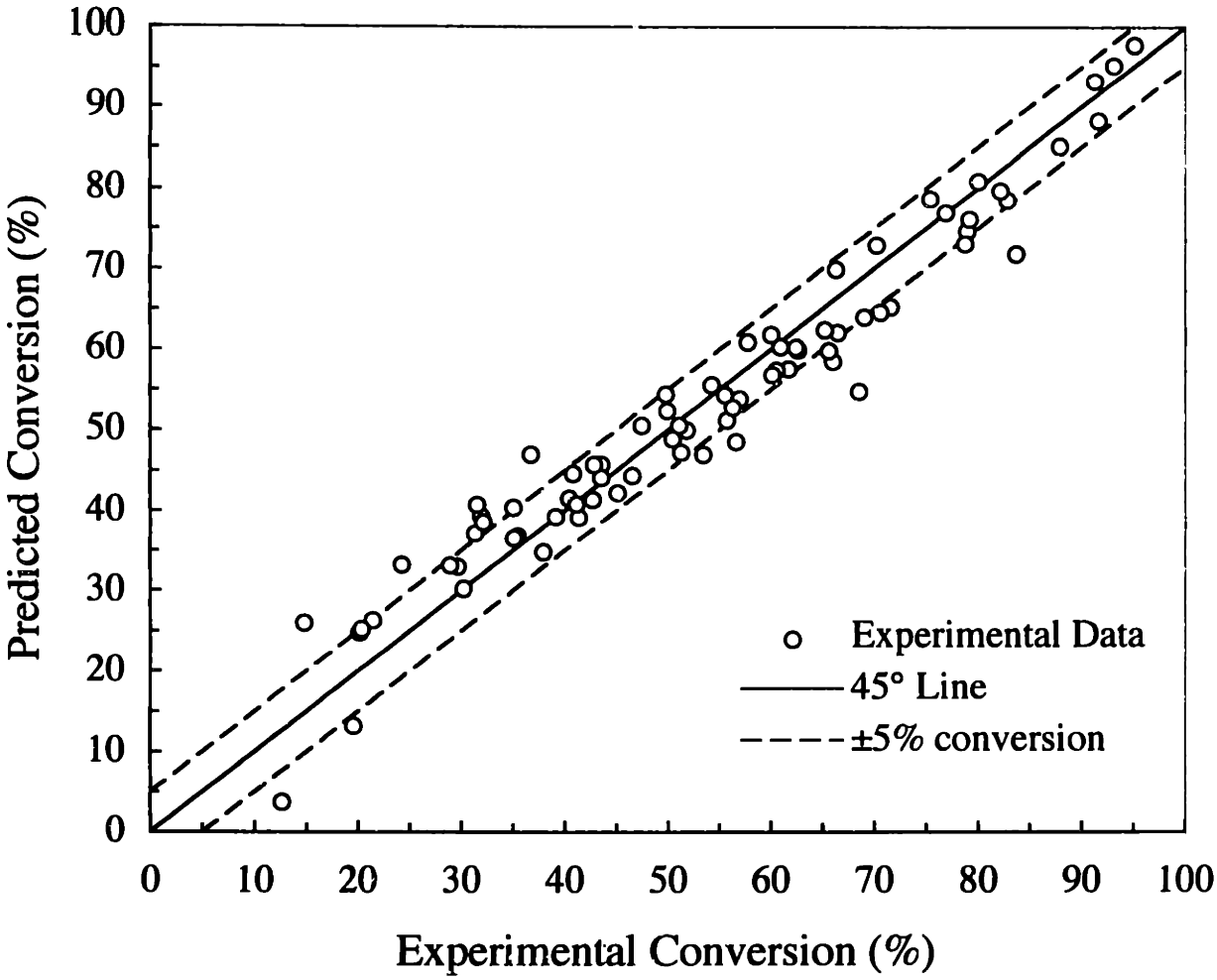

Figure 5-19 Comparison of experimental conversion with predictions of the regressed global rate expression
(T=479-587°C, τ=3-7 s, P=246 bar, $[C_6H_6]_o$=0.4-1.2 mM, Φ=0.5-2.5)

most of the data lie within ±5% conversion of the 45° line, indicating that Eqn. (5-14) well represents benzene oxidation at the studied experimental conditions (T=479-587°C, P=246 bar, $[C_6H_6]_o$=0.4-1.2 mM, Φ=0.5-2.5 and τ=3-7 s). The fact that Eqn. (5-14) predicts the experimentally measured benzene conversion to within ±5% conversion at all conditions suggests internal consistency amongst the data. The largest discrepancies between model prediction and data are at benzene conversions less than 35%. The two drastically underpredicted, low conversion points in Figure 5-19 correspond to the measurements at 478 and 505°C from Figure 5-3, and the overpredicted points at low conversions are largely short residence time data (τ=3-4 s) at various conditions. Since benzene conversion exceeded 35% in a majority of the experiments, the parameters in Eqn. (5-14) are overweighted to better represent higher-conversion data and, as a result, Eqn. (5-14) should not be expected to predict low conversion data as well as that at high

conversion. Additionally, the two low temperature data points were among the first data taken and were measured before the improved feed measurement technique was implemented (see Section 5.3). As a result the measured conversions may be higher than the actual conversions at these temperatures following the same reasoning given in Section 5.4.2 when discussing the possible errors in measured conversion in the early hydrolysis experiments. The predictions of Eqn. (5-14) may be more accurate than the measurements for these two points.

5.4.5 Formation of Higher Molecular Weight Species as Trace Reaction Products

As noted in Section 5.1, a common observation amongst researchers studying the oxidation kinetics of phenol and substituted phenols is the formation of dimers and single-ring aromatic species (see for example Thornton and Savage (1990) or Krajnc and Levec (1996)). The formation of such products is dependent on the reactor conditions and appeared more abundant at lower temperatures and with lower oxygen levels. Based on the carbon balances in the oxidation experiments of this study, at the conditions as listed in Table 5-1 and Table 5-2 benzene oxidizes to form primarily CO, CO_2, phenol and methane. In fact, at temperatures above 575°C with a stoichiometric level of oxygen benzene undergoes near complete conversion to CO_2. Any additional, undetected partial oxidation products, including organic acids, dimers and single-ring aromatic species, will only constitute a very minor fraction of the reacted carbon (<1 mol%) and their amounts will decrease at higher temperatures and longer residence times.

Five experiments were conducted for the purpose of searching for single and multi-ringed aromatic products and monitoring their occurrence as a function of temperature and the initial oxygen concentration. The experimental conditions, measured benzene conversions and calculated carbon balances based on the effluent concentrations of CO, CO_2, methane, phenol and unreacted benzene are shown in Table 5-3. These experiments were conducted before undertaking the detailed investigation of benzene oxidation kinetics summarized in Section 5.4.3 and were performed in an 8 m x 1/8 in. (3.2 mm) O.D. x 0.046 in. (1.2 mm) I.D. 316SS reactor. Otherwise, the reactor system was identical to that used for the reported benzene oxidation experiments. The measured benzene conversions and product yields are fully consistent with those observed in the 4.71 m Inconel 625 reactor but were not reported along with the other experiments in Section 5.4.3 because a slightly lower initial benzene concentration was used. The detailed summary of these five experiments appears in Appendix 10.2.

Table 5-3. Summary of experiments conducted for the detection of single- and multi-ringed aromatic products
(τ=6.0±0.1 s, P=246±2 bar, $[C_6H_6]_o$=0.50±0.02 mM)

Run No.	Temperature (°C)	Φ	Conversion (%)	Carbon Balance (%)
632	577	1.2±0.3	92.4±0.6	102±5
633	528	1.1±0.4	23±4	89±4
636	625	1.0±0.3	95.4±0.3	102±5
637	625	1.3±0.3	90.9±0.6	94±4
638	625	0.9±0.3	98.4±0.1	97±5

The aqueous effluent from each of these five experiments was collected and prepared for analysis by GC/MS by EPA Method 3510C (U.S. EPA, 1986). The 500 to 750 mL of aqueous effluent was acidified with 12 M HCl and extracted with three 40 to 50 mL aliquots of methylene chloride in a 1000 mL separatory funnel. The extract was then concentrated to approximately 10 mL. To remove the residual water, the extract was poured over anhydrous sodium sulfate. The sodium sulfate was rinsed thoroughly with methylene chloride to ensure complete passage of the extracted products. The dried extract combined with the methylene chloride used to rinse the anhydrous sodium sulfate was then concentrated to 1 mL.

The extracted, concentrated samples were analyzed for single- and multi-ringed aromatic species by GC/MS using EPA Method 8270C "Semivolatile Organic Compounds by GC/MS" (U.S. EPA, 1986). The mass spectra of the analytes were compared to library spectra in order to identify the peaks. For those products for which standards were available, retention times of the standards were compared with those of the analytes in the extracted effluent samples for verification of the species identities. Table 5-4 lists the most prevalent partial oxidation products. Those products in column one were identified both by matching mass spectra and retention times. Since standards were not available for those species in column two, they were identified by mass spectra matches only, and their identities must be considered tentative since other complex compounds could have similar spectra. For illustration, the chemical structures are drawn in Figure 5-20.

Quantification of the analytes was performed by measuring the concentration of each species in the extracted, concentrated sample and then back-calculating their concentrations in the reactor assuming no loss of analytes during sample preparation. Since the procedure for preparing samples from each experiment for analysis by GC/MS involved extraction, followed by

Table 5-4. Single- and multi-ringed aromatic partial oxidation products identified by GC/MS analysis of the concentrated effluent

Positively Identified Products[1]	Tentatively Identified Products[2]
Styrene	Benzaldehyde
Acetophenone	*p*-Benzoquinone
Biphenyl	Benzofuran
Naphthalene	2,3 Dihydro-1H-Inden-1-one
Dibenzofuran	9H-Fluoren-9-one
Anthracene	Xanthone

[1]Identified both by mass spectrum and retention time match
[2]Identified by mass spectrum match only

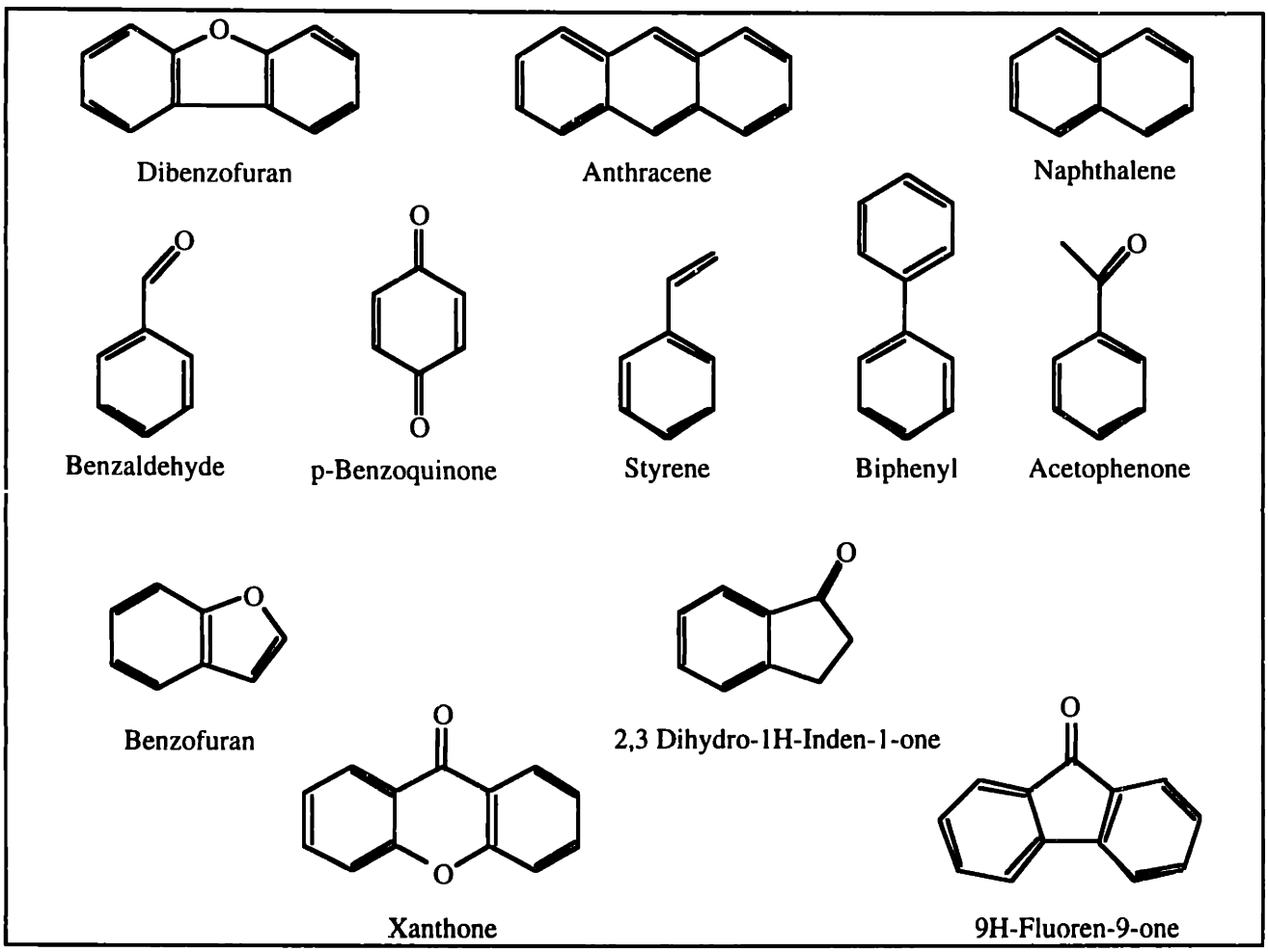

Figure 5-20 Stuctures of the single- and multi-ringed species detected in benzene SCWO

concentration, then drying and then a final concentration step, some loss of analytes is likely making accurate quantification of each species difficult. With most of the carbon fed to the reactor accountable as CO, CO_2, methane, phenol and unreacted benzene (see carbon balances in Table 5-3), accurate quantification of these trace species listed in Table 5-4 was not required. Thus, we directed our efforts to provide a rough estimate of their concentrations and their persistence. No attempt was made to account for the loss of analytes during the sample work-up. The GC/MS was calibrated for the six compounds listed in column one of Table 5-4 using purchased analytical standards. To estimate concentrations of the compounds listed in column two, the average response factor (RF) of styrene and acetophenone was used as the RF for the single-ringed aromatics, and the average RF of biphenyl, naphthalene, dibenzofuran and acetophenone used as the RF for the multi-ringed aromatics.

Given that the same procedure was followed for the work-up of the samples from the five experiments, each sample should be subject to similar experimental errors. By comparing the relative concentrations of analytes from the five experiments, these errors should partially cancel. Figure 5-21 and Figure 5-22 show the concentration of the intermediates in Table 5-4 from runs 632 (577°C, Φ=1.2), 636 (625°C, Φ=1.0) and 638 (625°C, Φ=0.9) relative to their concentrations in run 633 (528°C, Φ=1.1). The non-oxygenated species are in higher concentrations at 625°C than at 577°C with stoichiometric oxygen levels, but their concentrations decrease substantially with excess oxygen. Styrene, naphthalene and anthracene are soot precursors formed by the addition of acetylene to the benzene ring. By operating under fuel-lean conditions, it appears that soot formation can be avoided. The concentrations of all oxygenated intermediates decreased with both temperature and the oxygen concentration. Dibenzofuran and xanthone were the most difficult to oxidize. These two compounds are structurally similar as they consist of two aromatic rings joined by an O atom.

For the purpose of showing the effect of the fuel equivalence ratio alone at 625°C on the formation of the species in Table 5-4, Figure 5-23 and Figure 5-24 compare the concentrations of the intermediates in runs 637 (Φ=1.3, 75% of oxygen demand) and 638 (Φ=0.9, 10% excess oxygen) relative to their concentrations in run 636 (Φ=1.0). Both oxygenated and non-oxygenated intermediate concentrations decreased with the increasing oxygen concentration. The concentration

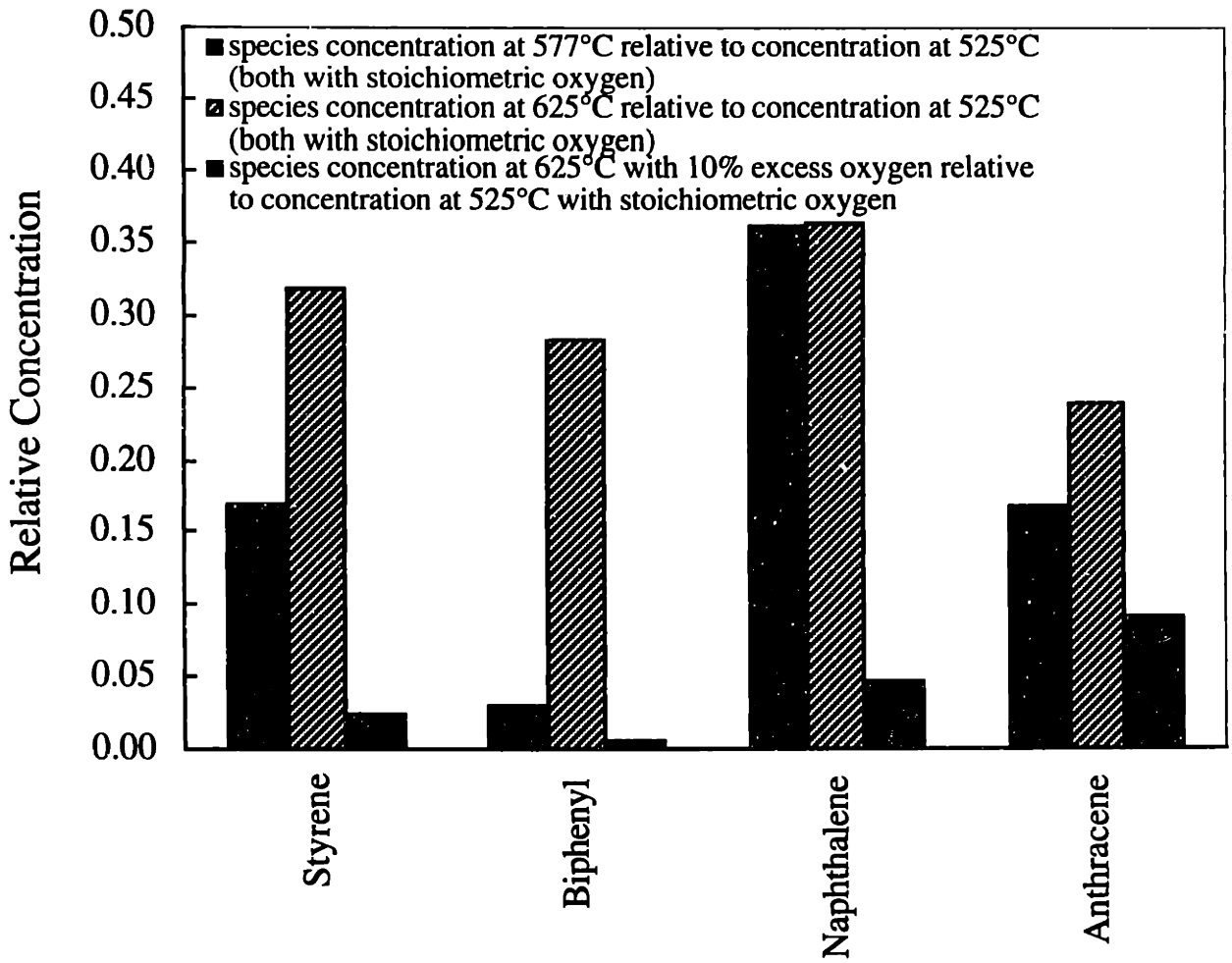

Figure 5-21 Relative concentrations of the non-oxygenated single- and multi-ringed intermediates as a function of temperature
(τ=6.0±0.1 s, P=246±2 bar, $[C_6H_6]_o$=0.50±0.02 mM)

of the soot precursors styrene, naphthalene and anthracene under fuel-rich conditions were similar to or, in the case of styrene, higher than their concentrations with stoichiometric oxygen. Styrene and naphthalene concentrations both decreased significantly under fuel-lean conditions, but that of anthracene was not as sensitive to the oxygen concentration. The absolute anthracene concentration, however, was much lower than that of either styrene or naphthalene. Since styrene is the precursor of both naphthalene and anthracene, and based on the observation that the styrene concentration decreases significantly at fuel-lean conditions, the avoidance of anthracene and soot formation should be controllable by operation at higher relative oxygen concentrations. The concentration of biphenyl, formed by the combination of two phenyl radicals (C6H5•), was lower at both fuel-rich and fuel-lean conditions relative to its concentration with stoichiometric oxygen indicating that both

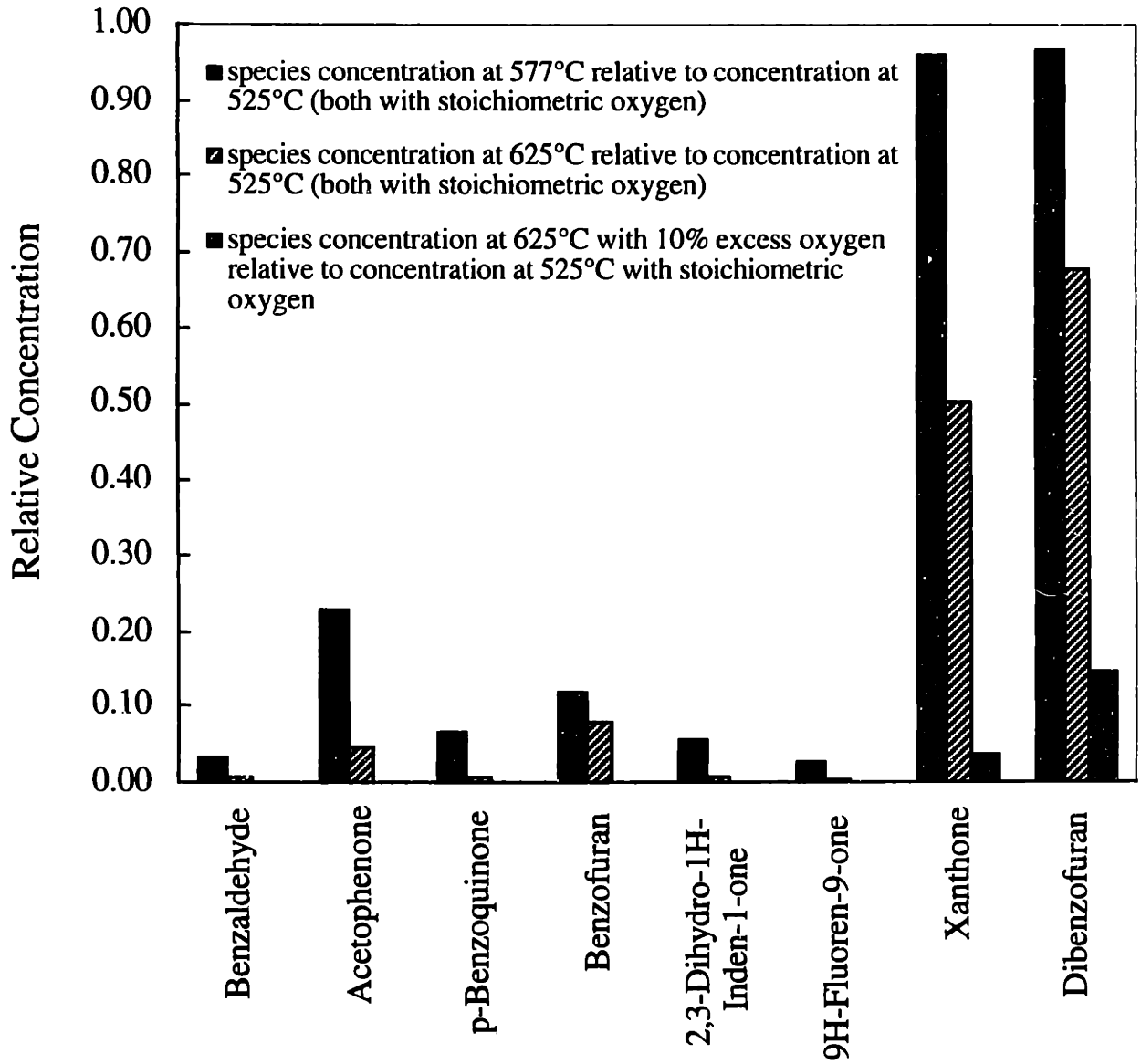

Figure 5-22 Relative concentrations of the oxygenated single- and multi-ringed intermediates as a function of temperature
(τ=6.0±0.1 s, P=246±2 bar, $[C_6H_6]_o$=0.50±0.02 mM)

the formation and oxidation of biphenyl may depend on the oxygen concentration. All oxygenated species, with the exception of xanthone and dibenzofuran, were undetectable at reaction temperatures of 625°C with excess oxygen present.

While the discussion above focused on relative concentrations, it is important to note that the absolute concentrations of all products in Table 5-4 are very low relative to the effluent concentrations of the main partial and final oxidation products. The ranges of the absolute concentrations of the single- and multi-ringed aromatic species are shown in Table 5-5. Also shown

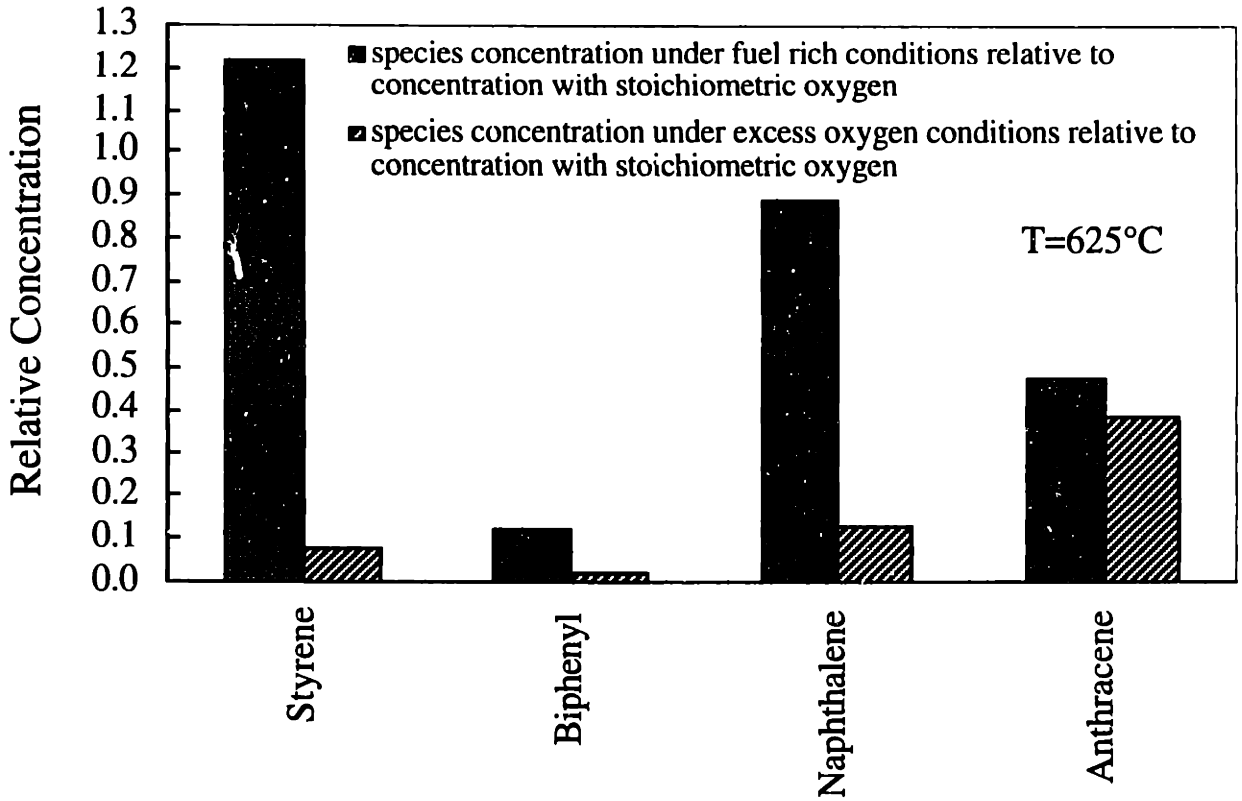

Figure 5-23 Relative concentrations of the non-oxygenated single- and multi-ringed intermediates as a function of the oxygen-to-benzene ratio at 625°C
(T=625±2°C, τ=6.0±0.1 s, P=246±2 bar, $[C_6H_6]_o$=0.50±0.02 mM)

are the total contribution of all single and multi-ringed species to the carbon balance in each experiment. Again, one should note that the species concentrations and carbon balance contributions are only approximate as some of the analytes may have been lost during sample preparation. Without accounting for sample loss, at 625°C with excess oxygen less than 0.1% of the initial carbon is present in the form of single- and multi-ringed products. Of all of the species listed in Table 5-4, dibenzofuran and biphenyl were the most persistent of the single- and multi-ringed intermediates. At 625°C with excess oxygen, dibenzofuran and biphenyl were the highest concentration intermediates of those listed in Table 5-4 and were among the highest concentration intermediates at all other conditions listed in Table 5-3.

5.5 Conclusions

A total of 7 hydrolysis and 107 oxidation experiments were conducted to characterize the reactivity of benzene in supercritical water. Since the conversion of benzene in the absence of oxygen was determined to be no greater than 10% and realistically closer to 2% at temperatures up

Table 5-5. Absolute concentrations of the single- and multi-ringed intermediates
(τ=6.0±0.1 s, P=246±2 bar, $[C_6H_6]_o$=0.50±0.02 mM)

Run no. (conditions)	Concentration range of single- and multi-ringed products (mol/mL)	Percent of initial carbon accounted for by the sum of all single- and multi-ringed products
633 (528°C, Φ=1.1)	10^{-9}-10^{-11}	0.2%
632 (577°C, Φ=1.2)	10^{-10}-10^{-12}	2.0%
636 (625°C, Φ=1.0)	10^{-10}-10^{-12}	0.3%
637 (625°C, Φ=1.3)	10^{-11}-10^{-13}	0.1%
638 (625°C, Φ=0.9)	10^{-11}-10^{-13}	0.02%

to 625°C, the hydrolysis pathway did not interfere with the study of benzene supercritical water oxidation (SCWO) kinetics. Essentially complete conversion of benzene was achieved at 575°C and 246 bar with stoichiometric oxygen, and carbon dioxide accounted for 90% of the initial carbon. Benzene conversion by SCWO increased with both increasing oxygen concentration and system pressure. While at 530 and 540°C the benzene oxidation rate decreased with increasing initial benzene concentrations, at 550°C no significant dependence of conversion on the initial concentration existed. A global rate expression was developed which well represents benzene oxidation at the studied experimental conditions.

More than 90% of the carbon in the reactor feed was recovered in the effluent products. Carbon dioxide accounted for more of the reacted carbon than any other oxidation product, including carbon monoxide, at all reactor conditions and for all levels of benzene conversion. Methane and phenol were also dominant oxidation products. Trace levels of ethylene, acetylene and propylene were detected. Single and multi-ringed aromatic products were also detected in the effluent. Their concentrations decreased significantly, many to undetectable levels, as both the temperature and oxygen concentration were increased, and at 625°C and with 10% excess oxygen less than 0.1% of the initial carbon was present in the form of single- and multi-ringed products. Dibenzofuran and biphenyl were the most persistent of the single- and multi-ringed intermediates.

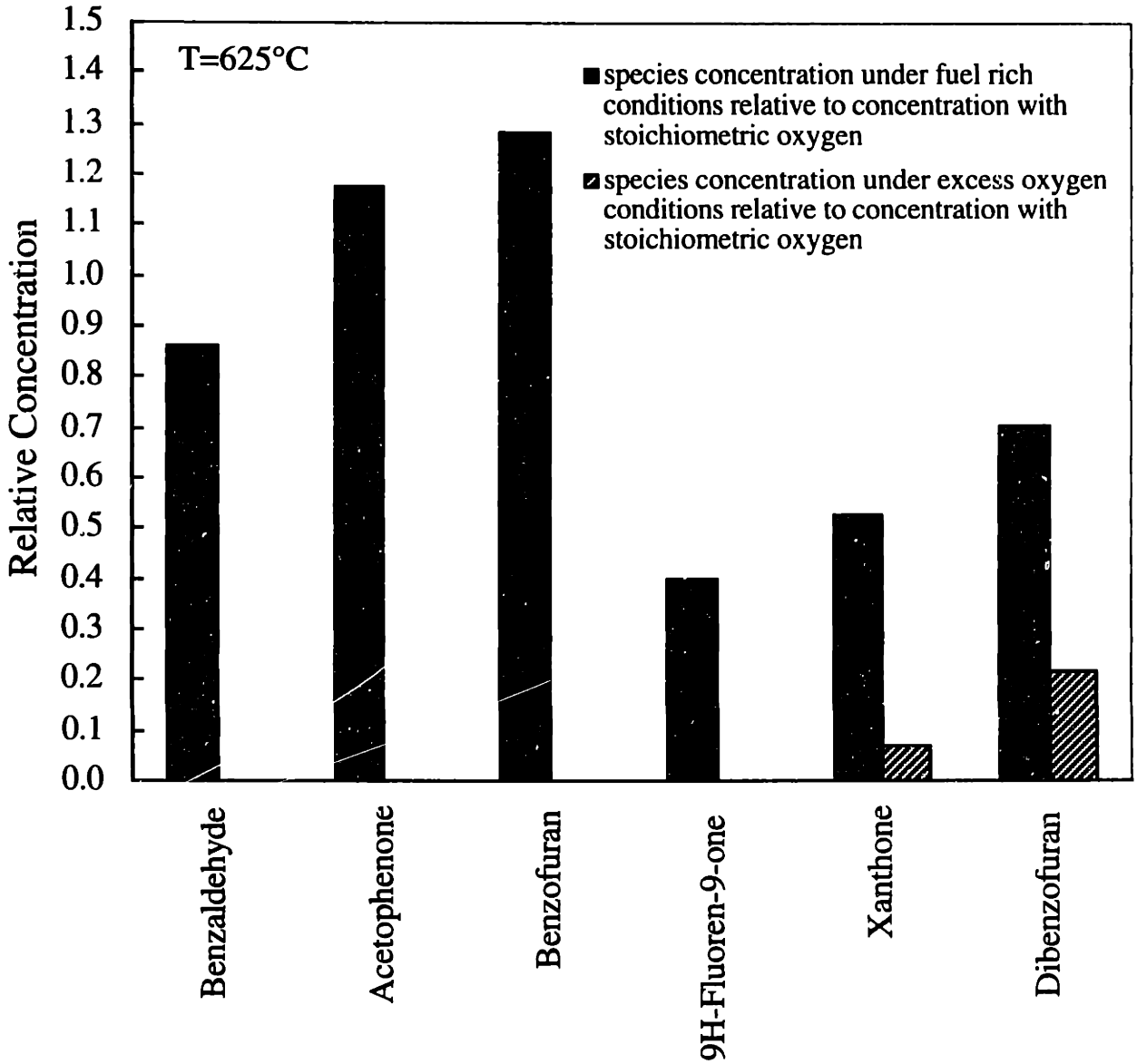

Figure 5-24 Relative concentrations of the oxygenated single- and multi-ringed intermediates as a function of the oxygen-to-benzene ratio at 625°C
(T=625±2°C, τ=6.0±0.1 s, P=246±2 bar, $[C_6H_6]_o$=0.50±0.02 mM)

5.6 REFERENCES

Aki, S. and M.A. Abraham, "Catalytic supercritical water oxidation of pyridine: comparison of catalysts." *Ind. Eng. Chem. Res.* **38**(2), 358 (1999).

Crain, N., S. Tebbal, L. Li and E.F. Gloyna, "Kinetics and reaction pathways of pyridine oxidation in supercritical water." *Ind. Eng. Chem. Res.* **32**(10), 2259 (1993).

Croiset, E., S.F. Rice and R.G. Hanush, "Hydrogen peroxide decomposition in supercritical water." *AIChE Journal* **43**(9), 2343 (1997).

Ding, Z.Y., S.N.V.K. Aki and M.A. Abraham, "Catalytic supercritical water oxidation: an approach for complete destruction of aromatic compounds." in *Innovations in Supercritical Fluids: Science and Technology*, K. W. Hutchenson and N. Foster, Eds., ACS Symposium Series, **608**, American Chemical Society, Washington, D.C., 232 (1995a).

Ding, Z.Y., S.N.V.K. Aki and M.A. Abraham, "Catalytic supercritical water oxidation: phenol conversion and product selectivity." *Environ. Sci. Technol.* **29**(11), 2748 (1995b).

Gopalan, S. and P.E. Savage, "A reaction network model for phenol oxidation in supercritical water." *AIChE Journal* **41**(8), 1864 (1995).

Holgate, H.R. and J.W. Tester, "Fundamental kinetics and mechanisms of hydrogen oxidation in supercritical water." *Combust. Sci. Technol.* **88**, 369 (1993).

Holgate, H.R. and J.W. Tester, "Oxidation of hydrogen and carbon monoxide in sub- and supercritical water: reaction kinetics, pathways, and water-density effects. 1. Experimental results." *J. Phys. Chem.* **98**, 800 (1994a).

Holgate, H.R. and J.W. Tester, "Oxidation of hydrogen and carbon monoxide in sub- and supercritical water: reaction kinetics, pathways, and water-density effects. 2. Elementary reaction modeling." *J. Phys. Chem.* **98**, 810 (1994b).

Holgate, H.R., P.A. Webley, J.W. Tester and R.K. Helling, "Carbon monoxide oxidation in supercritical water: the effects of heat transfer and the water-gas shift reaction on observed kinetics." *Energy and Fuels* **6**, 586 (1992).

Jin, L., Z.Y. Ding and M.A. Abraham, "Catalytic supercritical water oxidation of 1,4-dichlorobenzene." *Chem. Eng. Sci.* **47**(9-11), 2659 (1992).

Koo, M., W.K. Lee and C.H. Lee, "New reactor system for supercritical water oxidation and its application on phenol destruction." *Chem. Eng. Sci.* **52**(7), 1201 (1997).

Krajnc, M. and J. Levec, "On the kinetics of phenol oxidation in supercritical water." *AIChE Journal* **42**(7), 1977 (1996).

Krajnc, M. and J. Levec, "Oxidation of phenol over a transition-metal oxide catalyst in supercritical water." *Ind. Eng. Chem. Res.* **36**(9), 3439 (1997).

Kuester, J.L. and J.H. Mize, *Optimization Techniques with Fortran.* McGraw-Hill, New York (1973).

Lee, D.S., E.F. Gloyna and L. Li, "Efficiency of H_2O_2 and O_2 in supercritical water oxidation of 2,4-dichlorophenol and acetic acid." *J. Supercrit. Fluids* **3**, 249 (1990).

Li, R., T.D. Thronton and P.E. Savage, "Kinetics of CO_2 formation from the oxidation of phenols in supercritical water." *Environ. Sci. Technol.* **26**(12), 2388 (1992).

Martino, C.J. and P.E. Savage, "Supercritical water oxidation kinetics, products, and pathways for CH_3- and CHO-substituted phenols." *Ind. Eng. Chem. Res.* **36**(5), 1391 (1997).

Martino, C.J. and P.E. Savage, "Oxidation and thermolysis of methoxy-, nitro-, and hydroxy-substituted phenols in supercritical water." *Ind. Eng. Chem. Res.* **38**(1784-1791) (1999a).

Martino, C.J. and P.E. Savage, "Supercritical water oxidation kinetics and pathways for ethylphenols, hydroxyacetophenones, and other monosubstituted phenols." *Ind. Eng. Chem. Res.* **38**, 1775 (1999b).

Martino, C.J., P.E. Savage and J. Kasiborski, "Kinetics and products from *o*-cresol oxidation in supercritical water." *Ind. Eng. Chem. Res.* **34**(6), 1941 (1995).

Meyer, J.C., P.A. Marrone and J.W. Tester, "Acetic acid oxidation and hydrolysis in supercritical water." *AIChE Journal* **41**(9), 2108 (1995).

Oshima, Y., K. Hori, M. Toda, T. Chommanad and S. Koda, "Phenol oxidation kinetics in supercritical water." *J. Supercrit. Fluids* **13**, 241 (1998).

Pintar, A. and J. Levec, "Catalytic liquid-phase oxidation of phenol aqueous solutions. A kinetic investigation." *Ind. Eng. Chem. Res.* **33**, 3070 (1994).

Press, W.H., B.P. Flannery, S.A. Teukolsky and W.T. Vetterlinf, *Numerical Recipes: The Art of Scientific Computing.* Cambridge University Press, New York (1986).

Rice, S.F. and R.R. Steeper, "Oxidation rates of common organic compounds in supercritical water." *J. Hazard. Mater.* **59**(2-3), 261 (1998).

Thammanayakatip, C., Y. Oshima and S. Koda, "Inhibition effect in supercritical water oxidation of hydroquinone." *Ind. Eng. Chem. Res.* **37**(5), 2061 (1998).

Thomason, T.B., G.T. Hong, K.C. Swallow and W.R. Killilea, "The MODAR supercritical water oxidation process." in *Innovative Hazardous Waste Treatment Technology Series, Volume 1: Thermal Processes*, H. M. Freeman, Ed., Technomic Publishing, Lancaster, PA, 31 (1990).

Thornton, T.D., D.E. LaDue, III and P.E. Savage, "Phenol oxidation in supercritical water: formation of dibenzofuran, dibenzo-*p*-dioxin, and related compounds." *Environ. Sci. Technol.* **25**, 1507 (1991).

Thornton, T.D. and P.E. Savage, "Phenol oxidation in supercritical water." *J. Supercrit. Fluids* **3**, 240 (1990).

Thornton, T.D. and P.E. Savage, "Kinetics of phenol oxidation in supercritical water." *AIChE Journal* **38**(3), 321 (1992a).

Thornton, T.D. and P.E. Savage, "Phenol oxidation pathways in supercritical water." *Ind. Eng. Chem. Res.* **31**(11), 2451 (1992b).

U.S. EPA, *Test Methods for Evaluating Solid Waste, SW 846.* U.S. Environmental Protection Agency, Office of Solid Waste and Emergency Response, Washington, D.C. (1986).

Yang, H.H. and C.A. Eckert, "Homogeneous catalysis in the oxidation of *p*-chlorophenol in supercritical water." *Ind. Eng. Chem. Res.* **27**, 2009 (1988).

Chapter 6.

Uncertainty Analysis of a Supercritical Water Hydrogen Oxidation Mechanism

While global rate expressions are useful for designing reactors and predicting conversions inside the range of conditions over which they were developed, they yield little mechanistic insight as to the reactions occurring at a molecular level. In order to gain such an understanding of reactions in supercritical water, detailed elementary reaction networks applicable at supercritical water conditions have been developed in this phase of our research. A key issue in these reaction networks is the propagation of errors due to uncertainties of rate constants. Chapter 6 reports the results of a specific investigation, jointly conducted with Brian Phenix (Phenix, 1998; Phenix *et al.*, 1998), that explored the effects of uncertainties in the input parameters on the predictive capability of a free-radical, SCW hydrogen oxidation mechanism.

6.1 Introduction and Literature Review

6.1.1 Use of Detailed Kinetic Models for Predicting Oxidation Rates in SCW

The present working hypothesis maintains that oxidation in supercritical water proceeds by free-radical reactions, and that the individual elementary reactions are similar to those which take place in combustion at the temperature and pressure of SCWO systems (500-650°C, 240-260 bar). Furthermore, the water medium, which participates in reactions both as a reactant and as a third-body collider, does not interfere with reaction events through solvation effects. This hypothesis is derived from the evidence that water above its critical point closely resembles a nonpolar, dense gas (Holgate and Tester, 1993; Brock and Savage, 1995; Dagaut *et al.*, 1995; Dagaut *et al.*, 1996). At typical reaction conditions for commercial SCWO applications, densities range from 0.07 to 0.1 g/mL and the viscosity of the reaction medium is about a factor of 25 lower than at ambient conditions (Lamb *et al.*, 1981). Likewise, the static dielectric constant at 250 bar decreases from its room temperature value of 78 to a value of 1 to 2 at 500°C (Uematsu and Frank, 1980). As a

consequence the ion product of water, K_w, at 250 bar decreases with increasing temperature from its subcritical value of 10^{-14} to approximately 10^{-23} in the range of 450-600°C (Marshall and Franck, 1981) indicating that water only weakly dissociates and poorly solvates ions in its supercritical state. Since supercritical water cannot support charged species, free-radical reactions are assumed to dominate over ionic reactions.

Our hypothesis has received support by the multiple attempts to model reactions using such combustion mechanisms adapted to the SCWO reaction conditions. Previous modeling efforts have yielded kinetic mechanisms describing the oxidation of simple compounds such as hydrogen (Holgate and Tester, 1993; Paterson *et al.*, 1993; Holgate and Tester, 1994; Brock and Savage, 1995; Dagaut *et al.*, 1995; Alkam *et al.*, 1996), carbon monoxide (Holgate and Tester, 1994; Brock and Savage, 1995; Dagaut *et al.*, 1995), methane (Webley and Tester, 1991; Brock and Savage, 1995; Dagaut *et al.*, 1995; Savage *et al.*, 1998), methanol (Webley and Tester, 1989; Butler *et al.*, 1991a; Butler *et al.*, 1991b; Schmitt *et al.*, 1991; Brock and Savage, 1995; Alkam *et al.*, 1996; Dagaut *et al.*, 1996) and phenol (Gopalan and Savage, 1995). These mechanisms have been incorporated into one-dimensional, isobaric flow models with either isothermal or imposed axial temperature profiles. The resulting plug-flow reactor models have been compared, with varying degrees of success, to experimentally-measured, stable species concentration profiles.

An important, recurring question in these studies has been whether disagreements between model predictions and experimental data are a consequence of an inadequate adaptation of combustion kinetics to SCWO conditions, either as a result of the improper treatment of the pressure or temperature dependence of elementary reaction rate constants or of missing reactions, or are attributable to the uncertainties inherent in the parameters used in the model itself. In SCWO and combustion modeling, some of the potential sources of uncertainty include reaction rate constants, species thermochemistry, initial conditions, and transport properties. The uncertainties in these quantities need to be systematically and explicitly addressed in order to determine their impact on the model outputs and to establish the likely limits to the predictive performance of the model. The goal of this phase of the present study was to incorporate uncertainty into a relatively simple hydrogen oxidation mechanism and to determine the level of precision that should be expected from the model predictions.

6.1.2 Introduction to Uncertainty Analysis

The two principal elements of uncertainty analysis are sensitivity analysis and uncertainty propagation. Sensitivity analysis examines the dependence of model outputs to changes in model inputs and is routinely employed in the analysis of chemical kinetic mechanisms as a means of identifying key reaction rate parameters. Uncertainty propagation, however, is relatively rare. Its primary aim is the computation of the uncertainty in the model outputs induced by uncertainty or error in the model inputs. Uncertainty analysis also directly identifies the inputs which contribute the most to the uncertainty in the model predictions, highlighting those where a reduction in uncertainty would best improve the predictive capability of the model.

The atmospheric chemistry community has examined in some detail the role of uncertainty in coupled transport and reaction modeling. For example, gas-phase chemical mechanisms have been identified as one of the most important components in photochemical and air quality models, and it is recognized that uncertainties in these mechanisms can introduce significant uncertainties into the calculated species concentrations (Gao *et al.*, 1996). Previous uncertainty analyses in atmospheric modeling have employed Monte Carlo simulation with either simple or stratified sampling methods and have been applied to regional air quality models (Gao *et al.*, 1996), aerosol formation and growth (Raes *et al.*, 1992), and photochemical ozone models (Stolarski *et al.*, 1978; Ehhalt *et al.*, 1979; Derwent and Øystein, 1988). Alternative approximation methods have also been used to calculate the expected values and variances of response variables in atmospheric models (Atherton *et al.*, 1975).

In the Monte Carlo simulations, each uncertain model parameter is treated as a random variable and assigned a suitable probability representation. Values are drawn from the probability distribution of each random variable and the coupled transport/kinetic model is solved to yield the complete time evolution of the response variables of interest (typically species concentrations). The solution process is repeated until stable statistics are achieved for the response distributions in the model. By necessity, the number of random variables in these studies is relatively small because the computational tractability of Monte Carlo methods is heavily dependent on the number of random variables, the complexity of the model, and the sampling method used. In cases where reaction mechanisms are coupled with detailed transport models, the number of random variables typically ranges from four (Raes *et al.*, 1992) to ten (Derwent and Øystein, 1988). Larger numbers of

random variables have been incorporated into Monte Carlo simulations of reaction mechanisms, though usually at the expense of realistic transport modeling and through the use of sophisticated sampling techniques (Ehhalt *et al.*, 1979; Gao *et al.*, 1996). As an example, consider the work of Gao *et al.* (1996) who employed Latin-hypercube sampling to simulate a regional acid-deposition model with 59 uncertain rate parameters and 17 uncertain stoichiometric coefficients. Although the authors were successfully able to calculate the uncertainties in predicted species concentrations and identify the key controlling model parameters, they acknowledged that inclusion of this mechanism in a more comprehensive air quality model--taking detailed account of transport, mixing and surface removal, meteorology, and boundary and initial conditions--would require a reduction of the number of uncertain parameters in the mechanism.

6.2 Incorporation of Uncertainty into a SCW Hydrogen Oxidation Mechanism

The effects of parameter uncertainty on the predictive capabilities of detailed kinetic mechanisms was explored in the context of a supercritical water hydrogen oxidation mechanism. Hydrogen oxidation was selected because the oxidation reactions are well-studied at combustion conditions, SCW hydrogen oxidation mechanisms have been developed by several investigators, and only a relatively small number of reactions are involved in hydrogen oxidation making the task of uncertainty analysis manageable. Two methods are used for the uncertainty propagation: a new, computationally efficient means of carrying out uncertainty propagation called the Deterministic Equivalent Modeling Method (DEMM); and Monte Carlo simulations.

6.2.1 Model Development

The hydrogen oxidation mechanism of Yetter *et al.* (1991) was used with rate constants updated, where applicable, from recent literature sources (Cobos and Troe, 1985; Tsang and Hampson, 1986; Atkinson *et al.*, 1989; Baulch *et al.*, 1992). This is the same mechanism originally used by Holgate and Tester (1993) to model the supercritical water oxidation of hydrogen and appears in Table 6-1. Species thermochemical data were taken from the CHEMKIN database (Kee *et al.*, 1988), except for the standard-state heat of formation for HO_2 radical which was updated from the JANAF value of 0.5 kcal/mol to 3.0 kcal/mol (Shum and Benson, 1983; Fisher and Armentrout, 1990; DeMore *et al.*, 1992; Bauschlicher and Partridge, 1993; Leung and Lindstedt, 1995).

Table 6-1. Chemical kinetic mechanism for the high-pressure oxidation of hydrogen[a]

No.	Reaction			A^b	n	E_a/R	Ref.
1	OH + H	↔	H_2O	1.620E+14	0	75	*c*
2	H_2 + OH	↔	H_2O + H	1.024E+08	1.6	1660	*d*
3	H + O_2	↔	HO_2	1.481E+12	0.6	0	*e*
4	HO_2 + HO_2	↔	H_2O_2 + O_2	1.867E+12	0	775	*d*
5	H_2O_2 + OH	↔	H_2O + HO_2	7.829E+12	0	670	*d*
6	H_2O_2 + H	↔	HO_2 + H_2	1.686E+12	0	1890	*d*
7	H_2O_2	↔	OH + OH	3.000E+14	0	24400	*d*
8	OH + HO_2	↔	H_2O + O_2	2.891E+13	0	-250	*d*
9	H + O_2	↔	OH + O	1.990E+14	0	8460	*d*
10	O + H_2	↔	OH + H	5.126E+04	2.67	3160	*d*
11	OH + OH	↔	O + H_2O	1.504E+09	0	50	*d*
12	H_2 + M	↔	H + H + M	2.230E+14	0	48350	*f*
13	H + HO_2	↔	OH + OH	1.690E+14	0	440	*d*
14	H + HO_2	↔	H_2 + O_2	4.280E+13	0	710	*d*
15	O + HO_2	↔	OH + O_2	3.250E+13	0	0	*d*
16	H_2O_2 + H	↔	H_2O + OH	1.020E+13	0	1800	*d*
17	O + H + M	↔	OH + M	4.708E+18	-1	0	*f*
18	O + O + M	↔	O_2 + M	1.890E+13	0	-900	*f*
19	H_2O_2 + O	↔	OH + HO_2	6.620E+11	0	2000	*d*

[a]Mechanism of Yetter *et al.* (1991) adapted to high-pressure; [b]$k=AT^n exp(-E_a/RT)$ with units of cm^3, mol, s, K; [c]Cobos and Troe (1985); [d]Baulch *et al.* (1992); [e]Atkinson *et al.* (1989); [f]Tsang and Hampson (1986)

The species thermochemistry is used in conjunction with the forward rate constants to calculate reverse rate constants. By the principle of microscopic reversibility, the forward and reverse rate constants, $k_{f,j}$ and $k_{r,j}$, for each of the j reactions are related by the concentration-based equilibrium constant $K_{c,j}$:

$$k_{r,j} = k_{f,j} K_{c,j}^{-1} \tag{6-1}$$

$K_{c,j}$, in turn, is related to the fugacity- or activity-based equilibrium constant, $K_{a,j}$, by:

$$K_{c,j}^{-1} = K_{a,j}^{-1} \left[\frac{ZRT}{f_i^0} \right]^{\sum_i \upsilon_{i,j}} \prod_i \hat{\phi}_i^{\upsilon_{i,j}} \tag{6-2}$$

where Z is the mixture compressibility factor, R is the gas constant, f_i^0 is the standard state fugacity of species i, $\upsilon_{i,j}$ is the stoichiometric coefficient of species i in reaction j, and $\hat{\phi}_i$ is the mixture fugacity coefficient for species i. $K_{a,j}$ can be expressed in terms of the standard-state Gibbs-free-energy change for reaction j:

$$\ln K_{a,j} = \frac{-\Delta G_{rx,j}^0(T)}{RT} \tag{6-3}$$

Substitution of Eqn. (6-3) into Eqn. (6-2) yields the following expression for $K_{c,j}^{-1}$:

$$K_{c,j}^{-1} = \exp\left(\Delta G_{rx,j}^0(T)/RT\right) \left[\frac{ZRT}{f_i^0} \right]^{\sum_i \upsilon_{i,j}} \prod_i \hat{\phi}_i^{\upsilon_{i,j}} \tag{6-4}$$

In combustion systems, Z, f_i^0 and $\hat{\phi}_i$ are all approximately unity, thereby simplifying Eqn. (6-4) The relationship between $\Delta G_{rx,j}^0$ and the individual species thermochemical parameters is given by the integrated form of the Gibbs-Helmholtz equation (Tester and Modell, 1997):

$$\Delta G_{rx,j}^0(T) = \sum_i \nu_{i,j} \Delta H_{f,i}^0(T^0) - T \sum_i \nu_{i,j} S_i^0(T^0) - \int_{T^0}^{T} \frac{1}{T^2} \left\{ \int_{T^0}^{T} \sum_i C_{p,i}^0 dT \right\} dT \tag{6-5}$$

Eqn. (6-5) utilizes the supplied standard state heats of formation $\Delta H_{f,i}^0$, standard state entropies S_i^0, and standard state constant pressure heat capacities $C_{p,i}^0$ for each species i.

6.2.2 Adaptation of Combustion Mechanisms to SCWO Conditions

The application of combustion mechanisms to modeling SCWO reactions requires the adaptation of the mechanism to the lower temperatures and significantly higher pressures of SCWO. The most obvious modification is the proper adaptation of the elementary rate constants

for the unimolecular and recombination reactions for pressure. All pressure-dependent rate constants in Table 6-1 were set to their high-pressure limits. A second common modification is the inclusion of nonideal or real-gas effects in the calculation of the reverse rate constants (Melius *et al.*, 1990; Butler *et al.*, 1991a; Butler *et al.*, 1991b; Schmitt *et al.*, 1991; Schmitt *et al.*, 1993; Alkam *et al.*, 1996). This modification requires estimation of the mixture compressibility factor and the mixture fugacity coefficients for all species in the reaction medium and is typically carried out with a classical thermodynamic (*PVTN*) equation of state (Tester and Modell, 1997). However, an accurate thermodynamic description of the multicomponent, supercritical reaction medium requires data to specify the pure-component and interaction parameters for stable and unstable species. Given the limited mixture data available for stable species in supercritical water and the complete absence of such data for free-radical intermediates, accounting for solution-phase non-idealities via a classical equation of state introduces considerable uncertainty into the modeling process. In principle, critical parameters for unstable, free-radical intermediates and binary interaction parameters for stable and unstable species are needed. In practice, pure component radical species critical properties are estimated using group contribution methods, while binary interaction parameters are frequently set to zero because of the lack of data available for estimating them.

6.2.3 Incorporation of Uncertainty

Accepting that the adaption of combustion mechanisms directly to SCWO conditions introduces inherent and systematic uncertainties, we are interested in addressing the additional uncertainty arising from the kinetic mechanism parameters themselves, *i.e.*, the reaction rate constants and species thermochemistry. In many cases, the uncertainty in rate constants and the thermochemistry can be quite large, with many rate constant values known only to within a factor of two to three. Likewise, the values of key thermochemical parameters, are continually being updated to reflect recent experimental and computational efforts to improve their reported values.

In terms of dealing with potential real-gas effects, we chose to set the mixture compressibility factor, Z, to its pure water value (at reaction T and P) due to the dilute nature of the reaction medium. Mixture fugacity coefficients, $\hat{\phi}_i$, were set equal to unity. As will be shown in the discussion section, the real-gas correction to the model predictions through the inclusion of Z and the $\hat{\phi}_i$'s is minor compared to the parametric uncertainty present in the mechanism itself.

In this work, the forward rate constants, $k_{f,j}$'s, and species standard-state heats of formation, $\Delta H^0_{f,i}$'s, were treated as random variables and were assumed to be the sole sources of uncertainty in the kinetic mechanism. The standard-state heat capacities and entropies, initial concentrations, and all remaining model parameters and inputs were treated as deterministic ("exact") quantities. The standard-state condition for all species was taken to be that of an ideal gas at 298.15 K and 1 bar. Each forward rate constant was assigned a log-normal probability distribution, thereby limiting $k_{f,j}$ to positive values, and was parameterized by a median value, computed from the parameters in Table 6-1, and a multiplicative uncertainty factor, UF_j. The uncertainty factors were either drawn from Baulch *et al.* (1992) or estimated from other literature sources. This simple parameterization procedure was chosen because the available kinetic data for the majority of elementary reactions rarely warrant the assignment of a sophisticated, data-based probability distribution. If sufficient data were available to construct an empirically-based probability distribution, the resulting rate constant distribution could readily be incorporated into our analysis. In this work, the bounds on a given rate constant are defined in terms of its median value and uncertainty factor, where the upper bound is given by:

$$Median(k_{f,j}) \times UF_j \tag{6-6}$$

and the lower bound by:

$$Median(k_{f,j}) \div UF_j \tag{6-7}$$

The upper and lower bounds were interpreted as encompassing 95% of all possible values of $k_{f,j}$. The consequences of this interpretation and its impact on the calculated uncertainty in the model output are presented in the discussion section.

The full high-pressure, hydrogen oxidation mechanism (Table 6-1) was reduced by a sensitivity analysis before carrying out the uncertainty study. The reduced mechanism, along with the uncertainty factors (UF_j) assigned to the individual forward rate constants, appears in Table 6-2. The resulting reduced mechanism predicts species concentration profiles identical to those of the full model. With their emphasis on HO_2 and H_2O_2 chemistry, both the full and reduced mechanisms are similar to the low-temperature (850-1200K), high-pressure (1-16 bar) hydrogen oxidation mechanism recently developed by Kim (1994).

Table 6-2. Reduced high-pressure hydrogen oxidation mechanism with reported uncertainty factors

No.	Reaction			*UF*[a]
1	$OH + H$	$\leftrightarrow$	H_2O	3.16[b]
2	$H_2 + OH$	$\leftrightarrow$	$H_2O + H$	1.26[c]
3	$H + O_2$	$\leftrightarrow$	HO_2	1.58[d]
4	$HO_2 + HO_2$	$\leftrightarrow$	$H_2O_2 + O_2$	1.41[c]
5	$H_2O_2 + OH$	$\leftrightarrow$	$H_2O + HO_2$	1.58[c]
6	$H_2O_2 + H$	$\leftrightarrow$	$HO_2 + H_2$	2.00[c]
7	H_2O_2	$\leftrightarrow$	$OH + OH$	3.16[c]
8	$OH + HO_2$	$\leftrightarrow$	$H_2O + O_2$	3.16[c]

[a]*UF*=multiplicative uncertainty factor (see text for definition); [b]Estimated; [c]Baulch *et al.* (1992); [d]Atkinson *et al.* (1989).

The standard-state heats of formation, $\Delta H^0_{f,i}$, for each species i were assigned normal (Gaussian) probability distributions and were parameterized by their mean values and standard deviations. The standard deviations were estimated based on reported experimental error limits (Shum and Benson, 1983; Chase *et al.*, 1985; Kee *et al.*, 1988; Fisher and Armentrout, 1990; DeMore *et al.*, 1992; Bauschlicher and Partridge, 1993; Leung and Lindstedt, 1995) and are shown, along with their mean values, in Table 6-3. While not the only possible choice, the selection of normally-distributed $\Delta H^0_{f,i}$'s naturally leads to reverse rate constants which, like their forward counterparts, are log-normally distributed. Inspection of Eqn. (6-5) reveals that $\Delta G^0_{rx,j}$ is linearly dependent on the species standard-state heats of formation. Since $\Delta G^0_{rx,j}$ is a linear function of the independent, normally-distributed $\Delta H^0_{f,i}$'s, $\Delta G^0_{rx,j}$ is also normally distributed. By definition, the corresponding inverse equilibrium constant $K^{-1}_{c,j}$ is log-normally distributed because of its exponential dependence on $\Delta G^0_{rx,j}$. As shown by Eqn. (6-1), the reverse rate constant is a product of two independent, log-normally distributed random variables ($K^{-1}_{c,j}$ and $k_{f,j}$) and, therefore, is log-normal. Thus, the selection of normal $\Delta H^0_{f,i}$'s and log-normal $k_{f,j}$'s naturally leads to a self-consistent form of the probability representation for the reverse rate constants.

Table 6-3. Mean values (μ) and standard deviations (σ) for species standard-state[a] enthalpy of formation ΔH_f^{0}[b]

	H	O	OH	H_2O	H_2O_2	HO_2
μ	52.10	59.56	9.3	-57.80	-32.53	3.0
2σ	0.01	0.02	0.2	0.01	0.07	0.5

[a]Standard state: ideal gas at 1 bar, 298.15 K; [b]Units of kcal/mol. All values of ΔH_f^0 are from Kee *et al.* (1988) except those for HO_2 which are based on evaluation of recently reported values from Kee *et al.* (1988), Shum and Benson (1983), DeMore *et al.* (1992), Leung and Lindstedt (1995), Fisher and Armentrout (1990), Bauschlicher and Partridge (1993), and Chase *et al.* (1985).

6.3 Uncertainty Analysis

6.3.1 Uncertainty Analysis Methodology

The uncertainty analysis was carried out using two solution methodologies. The first was a straightforward Monte Carlo simulation employing pseudo-random sampling. The second was the Deterministic Equivalent Modeling Method (DEMM), a new, computationally efficient approach developed by Tatang (Tatang, 1995; Tatang *et al.*, 1997) for incorporating parametric uncertainty into complex engineering models. Using the two procedures to perform the same uncertainty analysis serves to illustrate the features of each method and to demonstrate the computational advantage of DEMM, particularly when applied to larger kinetic mechanisms. The isothermal, tubular reactor modeled in this study was assumed to be well approximated by the plug-flow idealization. As a result, the governing species conservation equations reduce to a set of coupled, nonlinear, first-order, ordinary differential equations. Both solution methods employed the deterministic stiff ODE solver LSODE (Hindmarsh, 1983) for the solution of these equations.

Figure 6-1 outlines the approach used for the Monte Carlo simulation. For each run, the log-normal distributions of the $k_{f,j}$'s and $K_{c,j}^{-1}$'s are sampled randomly, the $k_{r,j}$'s are calculated as the product of the sampled $k_{f,j}$'s and $K_{c,j}^{-1}$'s, and the resulting set of rate constants are passed to LSODE for solution of the species conservation equations. The predicted species concentrations and their associated residence times are then stored, and the sampling and solution process is repeated until the response distributions are statistically stable. At the end of the sampling/solution process, the individual response distributions at each point in time are sorted and analyzed to determine their means, medians, and upper and lower 2.5% tail regions. For the hydrogen oxidation

mechanism shown in Table 6-2 with 16 random variables, 15,000 sampling points were sufficient to achieve stable response statistics.

Even when sophisticated sampling techniques are used, Monte Carlo methods can become computationally intractable for complex models with large numbers of random variables. DEMM provides an attractive alternative approach to Monte Carlo by reducing the number of model solutions needed to establish the probability distributions of the response variables. The basic concept of the DEMM methodology is to approximate the response variables of the model as probabilistically-weighted polynomial functions of the uncertain model parameters. DEMM relies on the direct representation of parametric uncertainty via polynomial chaos expansions and utilizes orthogonal collocation to calculate the response distributions of the model outputs. For the uncertainty analysis presented in this paper, second-order polynomials were sufficient to adequately approximate the species response distributions in the model. The number of collocation points needed to calculate the response distributions is a function of the number of random variables and the number of terms used in the polynomial chaos expansions (the order of the approximation). In this case, with 16 random variables and a second order approximation, 153 collocation points, and therefore 153 calls to the LSODE solver, were needed to generate the desired response distributions. A summary of the key steps in the DEMM solution process is shown in Figure 6-2. For a detailed discussion of the DEMM methodology and examples of its application in air quality and atmospheric modeling see Tatang (Tatang, 1995; Tatang *et al.*, 1997).

Two key features of the DEMM methodology are the use of symbolic manipulation and compiler technology, and the ability to solve models with uncertainties using the same numerical algorithms employed for the corresponding deterministic problems. Like Monte Carlo, DEMM has the capability to predict the time evolution of the probability distributions of each species in the mechanism. DEMM also provides a systematic means of identifying the variables to which the model output is most sensitive, highlighting those where a reduction in uncertainty would best improve the predictive performance of the model. As will be demonstrated, DEMM also offers the advantage of a significant decrease in the computational time required to solve the model--often two to three orders of magnitude--while closely approximating the results from a full Monte Carlo simulation.

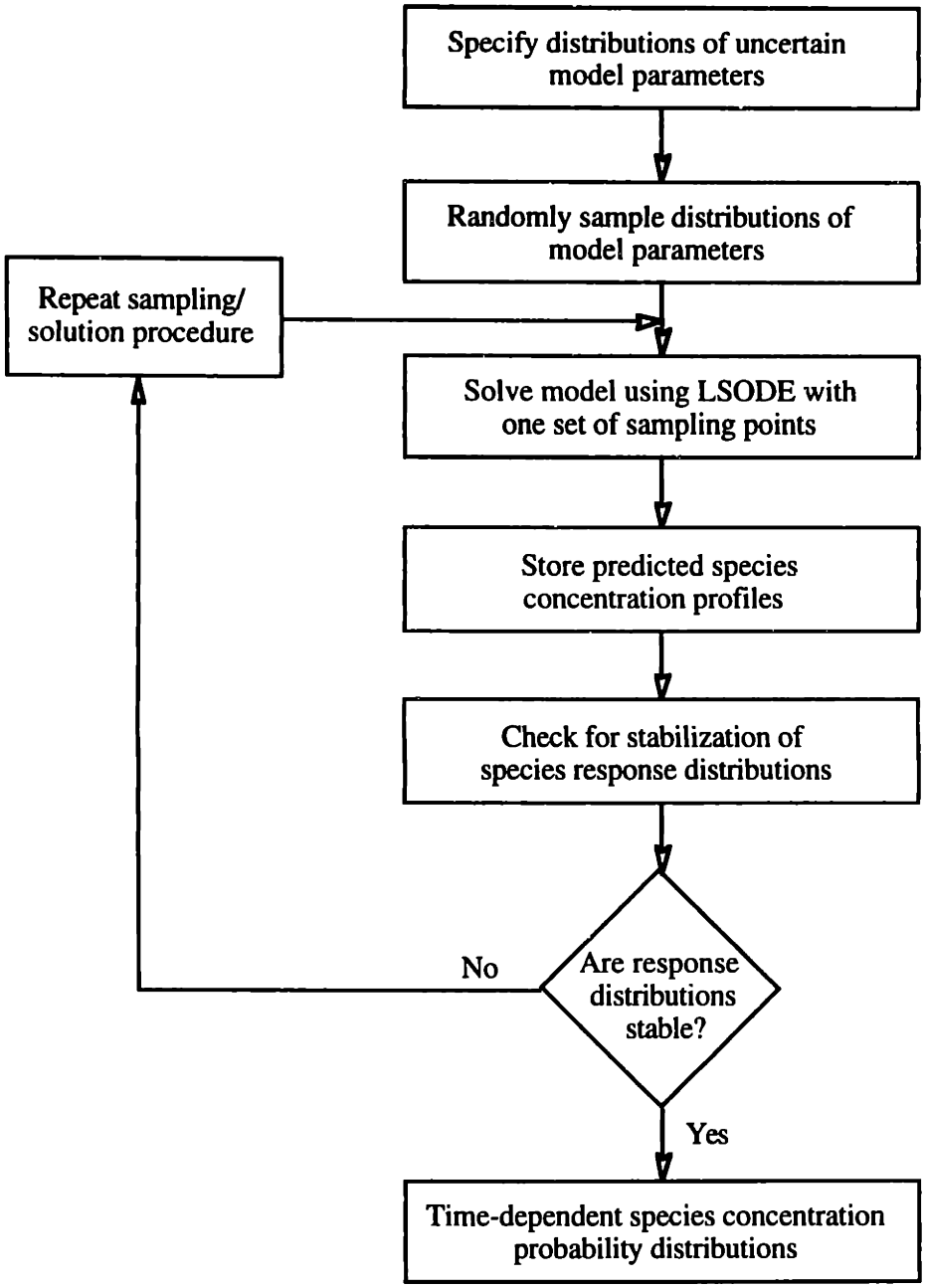

Figure 6-1 Flowsheet illustrating the steps used in the Monte Carlo simulation of the reduced hydrogen oxidation mechanism of Table 6-2

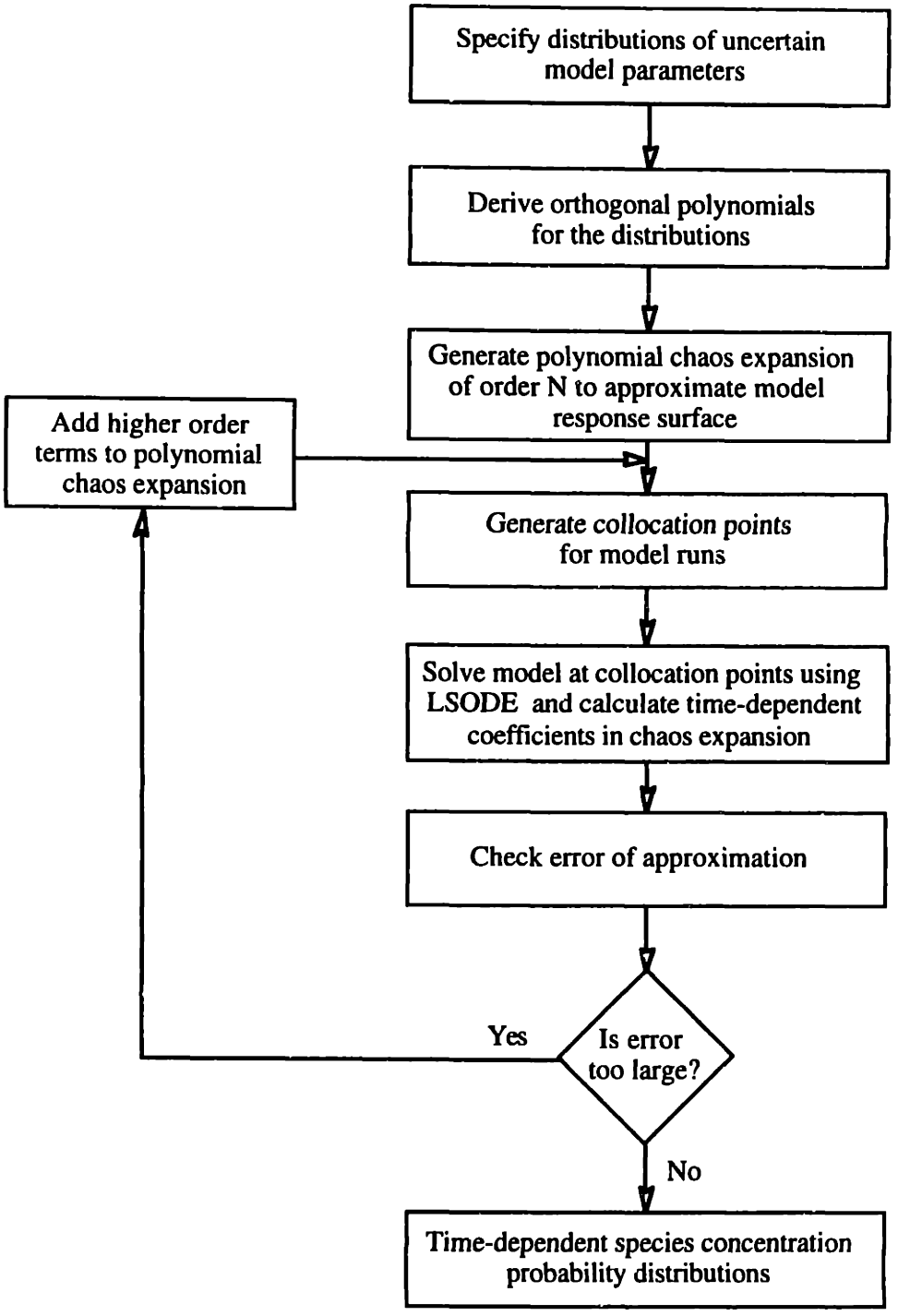

Figure 6-2 Flowsheet illustrating the steps used in the Deterministically Equivalent Modeling Method (DEMM) analysis of the reduced hydrogen oxidation mechanism of Table 6-2

6.3.2 Discussion of Results

Figure 6-3 shows the sampled distributions of two representative forward rate constants used in the Monte Carlo simulation of the H_2 oxidation mechanism. Both histograms are the result of 15,000 pseudo-random sampling points and serve to demonstrate that the sampled distributions are representative of the parameterized log-normal distributions from which they were drawn (see Table 6-2). The x-axes of the histograms display the range of sampled values for each rate constant, while the y-axis shows the percentage of the runs in which each value was used. Also indicated on each diagram are the upper and lower uncertainty bounds as defined by Eqn. (6-6) and Eqn. (6-7). As intended, 95% of the sampled values of each rate constant lie within these bounds.

Both Monte Carlo and DEMM methods were applied to the reduced hydrogen oxidation model. Both methods predict nearly identical median species concentrations and time-dependent probability distributions. Figure 6-4 displays the predicted median concentrations for the species H_2, O_2, H_2O_2, and HO_2, over a simulated ten second reaction time interval. The median concentration, or the 50% probability contour, represents the species concentration above and below which 50% of the model predictions lie. Also shown in each panel of Figure 6-4 are the MC-derived upper 97.5% and lower 2.5% probability contours of the species concentration distributions. The probability contours predicted by DEMM are virtually identical to those predicted by MC, but are not shown to simplify the figure. Ninety-five percent of the model predictions lie within the region bounded by the 97.5% and 2.5% probability contours, with 2.5% lying above and below these bounds.

Figure 6-4 shows that the uncertainty in the predicted species concentrations is not constant but varies with time. At the start of the reaction, there is no uncertainty in predicted species concentrations since the initial concentrations of all species were treated as deterministic quantities. As the reaction proceeds, the uncertainty in each species concentration increases and reaches a maximum at approximately 2 seconds. At these maxima, the uncertainties in the predicted species distributions are quite large. The upper and lower 2.5% bounds for the H_2 and O_2 concentrations vary by ±70% from their median values. More dramatically, the predicted HO_2 and H_2O_2 concentrations vary by +90% to -70% and +180% to -80% from their respective medians. Past the 2 second mark, the uncertainty in all species concentrations decreases and eventually goes to zero

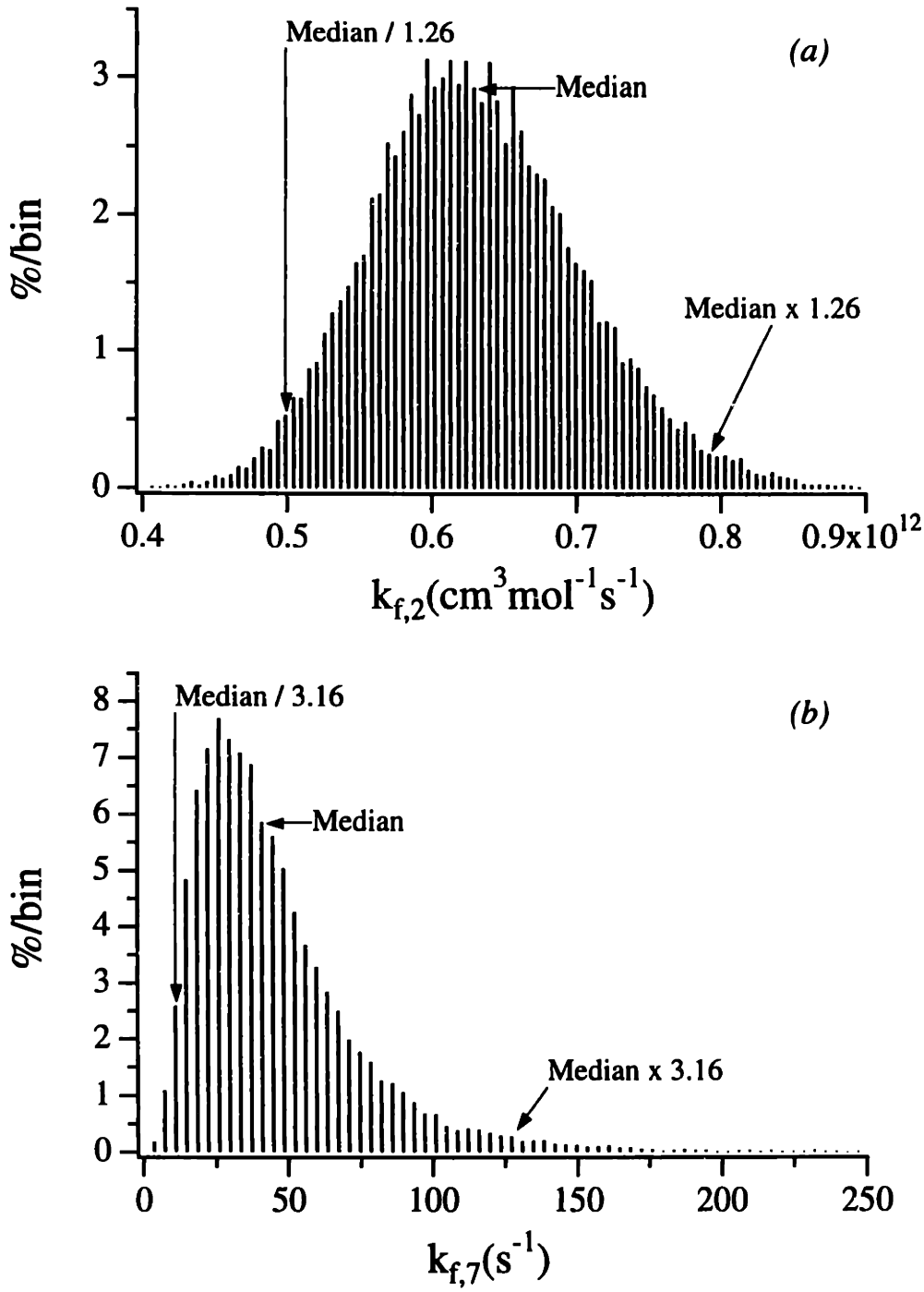

Figure 6-3 Sampled log-normal forward rate constant distributions for the reactions: $H_2+OH=H_2O+H$ (*a*); and $H_2O_2=2OH$ (*b*) based on the median values and uncertainty factors presented in Tables 6-1 and 6-2

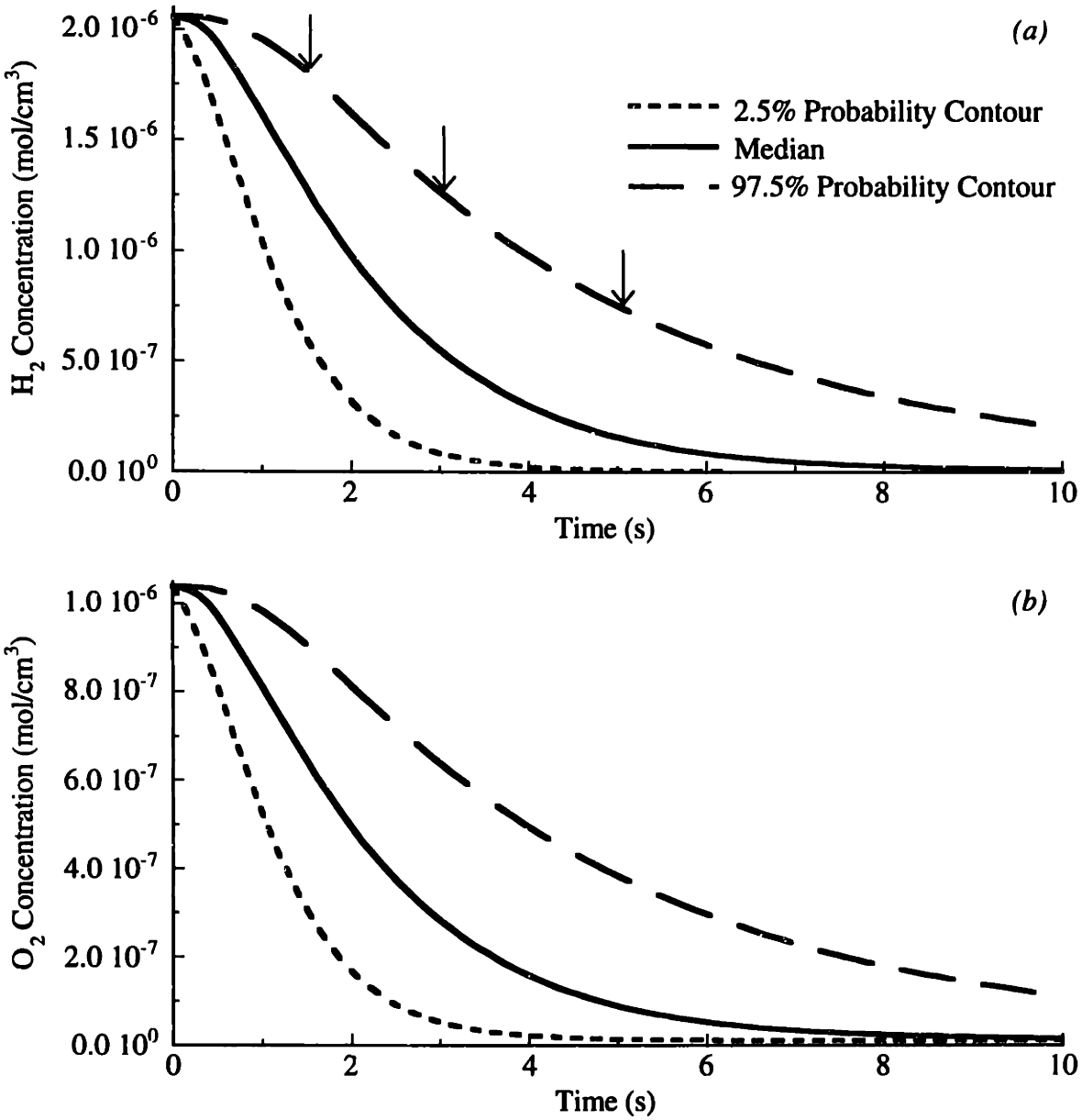

Figure 6-4 **H_2 (*a*) and O_2 (*b*) concentration probability distributions as a function of time resulting from Monte Carlo simulation of the H_2 oxidation mechanism in Table 6-2 with 15,000 pseudorandom sampling points**

(Conditions: T=823 K, P=246 bar, $[H_2]_o$=2.06x10^{-6}, $[O_2]_o$=1.04x10^{-6}, $[H_2O]_o$=4.281x10^{-3} mol/cm^3. The solid lines represent the median values of the probability distributions. The upper and lower dashed lines are the 2.5% and 97.5% probability contours, respectively, and encompass 95% of the predicted concentration values. The arrows in panel (*a*) indicate the times of the three cross-sections of the $[H_2]$ probability distribution shown in Figure 6-5.)

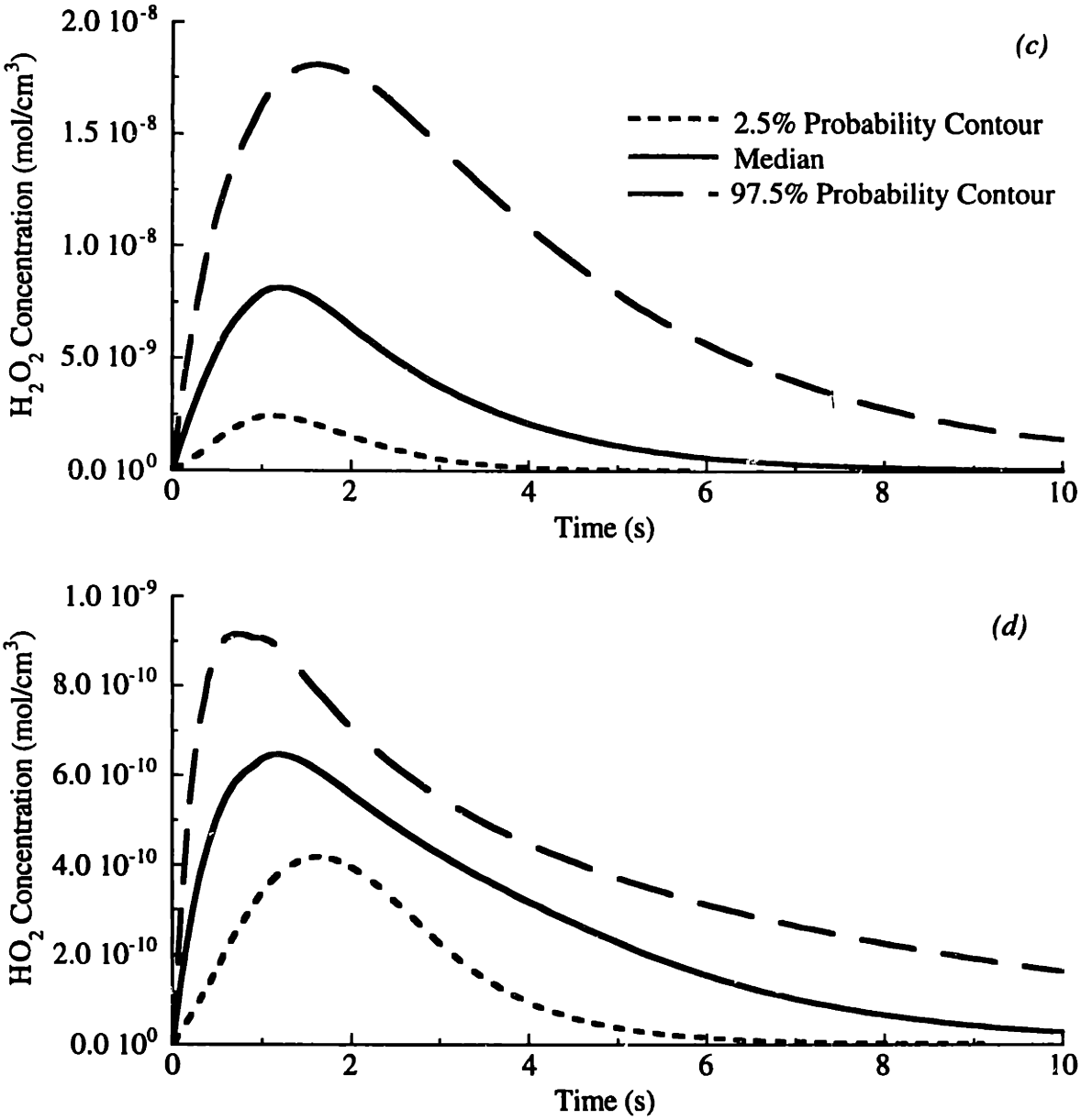

Figure 6-4 (continued) H_2O_2 (*c*) and HO_2 (*d*) concentration probability distributions as a function of time resulting from Monte Carlo simulation of the H_2 oxidation mechanism in Table 6-2 with 15,000 pseudorandom sampling points

(Conditions: T=823 K, P=246 bar, $[H_2]_o$=2.06x10^{-6}, $[O_2]_o$=1.04x10^{-6}, $[H_2O]_o$=4.281x10^{-3} mol/cm^3. The solid lines represent the median values of the probability distributions. The upper and lower dashed lines are the 2.5% and 97.5% probability contours, respectively, and encompass 95% of the predicted concentration values.)

since the model, with virtually any probable combination of rate constants, predicts the completion of the reaction at long residence times.

The shape of the concentration probability distributions can also be deduced from Figure 6-4. For example, with increasing time the $[H_2]$ probability distribution shifts from being skewed downwards to being skewed upwards. This shift is seen more clearly in Figure 6-5 which shows the $[H_2]$ probability distribution at three points in time: 1.5; 2.5; and 5.0 seconds. These times are indicated by the arrows in Figure 6-4*a*. The vertical lines are the response histograms generated by MC simulation while the solid lines represent the DEMM approximation to the response using the same set of sampling points. Both methods show that with increasing time the probability distribution shifts from being skewed to the right at 1.5 seconds, to an almost normal distribution at 2.5 seconds and finally skewed to the left at times greater than 5 seconds.

Figure 6-5 also serves to illustrate the remarkable agreement between the two methods. The agreement between MC and DEMM could be improved by increasing the order of the DEMM-polynomials beyond the second-order approximation used in this study. However, as is evident from the comparison, the use of the second-order polynomial already shows excellent agreement with the MC results and produces nearly identical median and 2.5% and 97.5% probability contour predictions as MC in a fraction of the time required to perform the MC simulation. More remarkably, for the 8 reversible reaction mechanism shown in Table 6-2, DEMM required 153 calls to the LSODE solver routine, compared with 15,000 for the Monte Carlo simulation--resulting in approximately a 100-fold reduction in the computational time required to carry out the analysis.

Figure 6-4 and Figure 6-5 also demonstrate that significant uncertainty exists in the predicted species concentrations for even the relatively simple hydrogen oxidation mechanism employed in this study. However, not all of the uncertain model parameters contribute equally to the uncertainty in the model output. For example, the model is quite sensitive to the highly uncertain value of the rate constant for H_2O_2 dissociation (Table 6-2, reaction 7). Restricting the uncertainty analysis to treat $k_{f,7}$ as the only uncertain parameter, with all other $k_{f,j}$'s and the $\Delta H^0_{f,i}$'s treated as deterministic quantities, reveals the range of the concentration predictions achievable by only varying $k_{f,7}$. Figure 6-6*a* shows the result of such an analysis and compares the range of

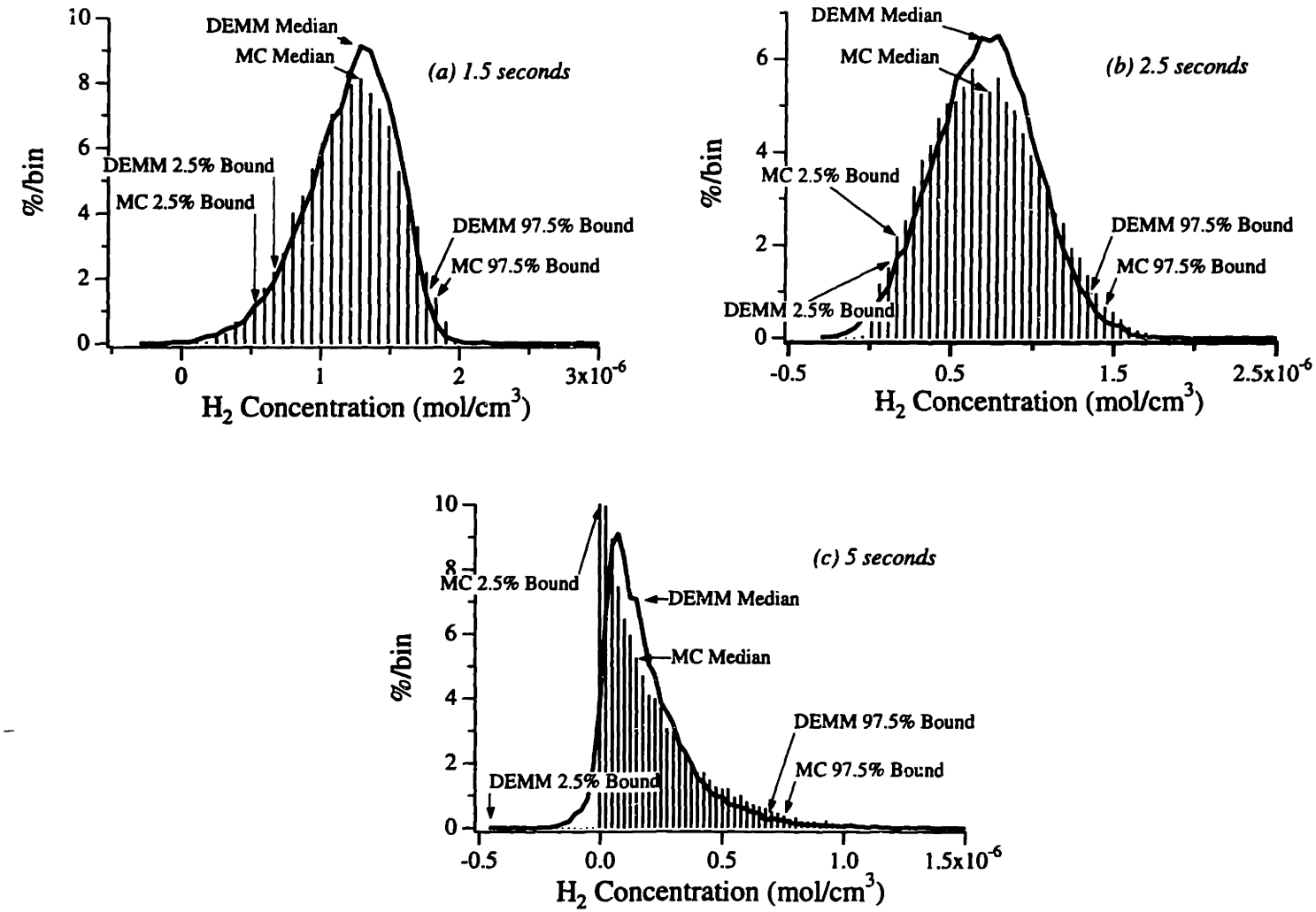

Figure 6-5 Hydrogen concentration probability distribution at the three points in time, 1.5 seconds (*a*); 2.5 seconds (*b*); and 5.0 seconds (*c*), indicated by the arrows in Figure 6-4

(Conditions: T=823 K, P=246 bar, $[H_2]_o$=2.06x10^{-6}, $[O_2]_o$=1.04x10^{-6}, $[H_2O]_o$=4.281x10^{-3} mol/cm^3. Vertical lines represent the distributions resulting from Monte Carlo simulation with 15,000 pseudo-random sampling points; solid lines are the polynomial approximations of the distributions obtained via DEMM using the same 15,000 sampling points.)

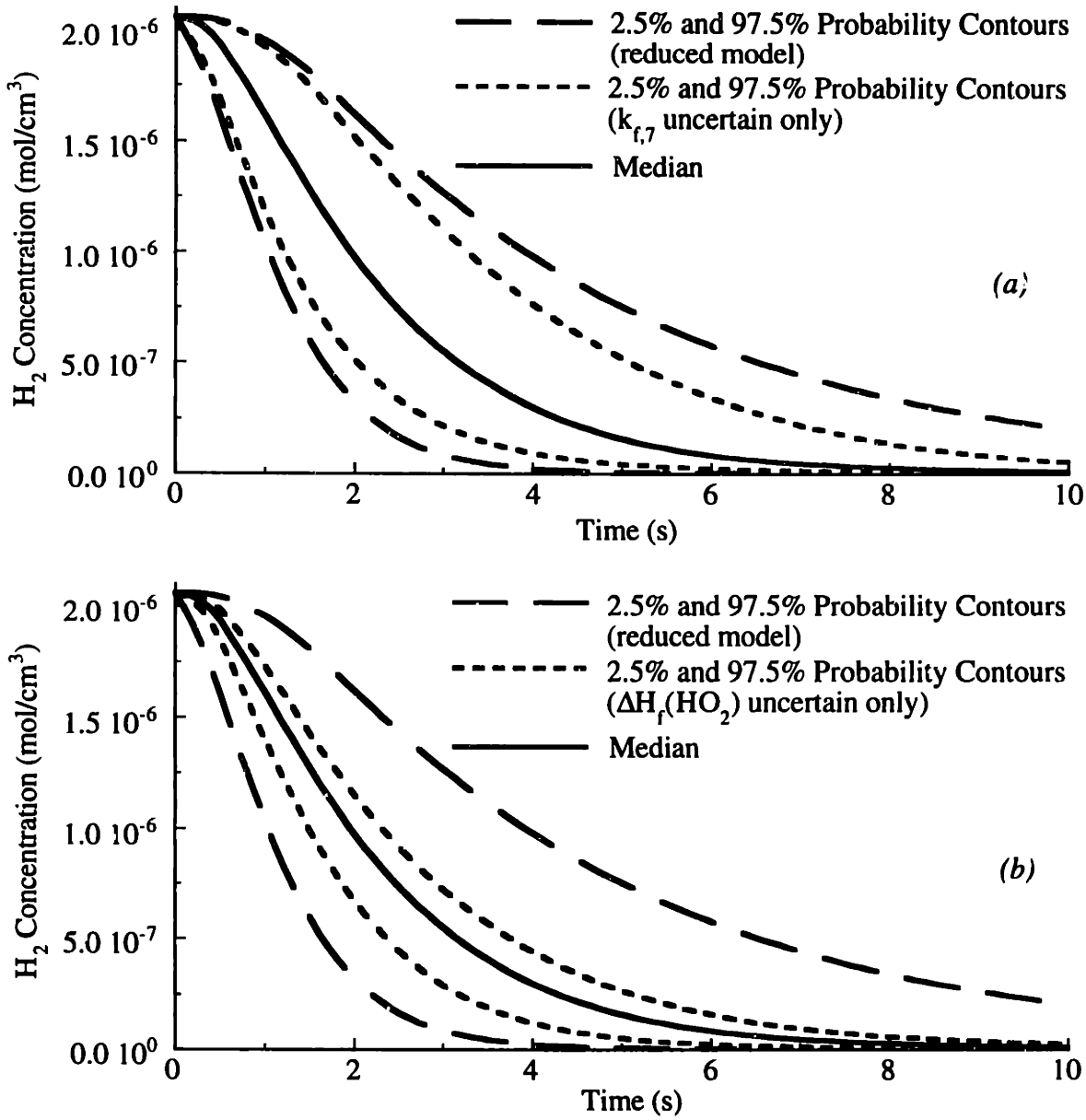

Figure 6-6 Uncertainty in the predicted H_2 concentration probability distribution resulting from: uncertainty in the k_f for the reaction H_2O_2 --> 2OH (*a*); and uncertainty in the $\Delta H_f^0(HO_2)$ (*b*), with all remaining k_{fj}'s and species ΔH_f^0's treated as deterministic quantities

(Middle solid lines are the median values of the predicted [H_2] probability distributions; regions bounded by dashed lines (97.5% and 2.5% probability contours) show the range of [H_2] predictions due to uncertainty in $k_{f,7}$ alone (*a*), and in $\Delta H_f^0(HO_2)$ alone (*b*). Also shown for comparison are the upper and lower bounds for the reduced model (Table 6-2) from Figure 6-4*a*)

predicted [H_2] concentrations due to uncertainty in $k_{f,7}$ alone (region bounded by short dashed lines) with the range resulting from the full model given in Table 6-2. The short dashed lines in Figure 6-6*a* represent the 2.5% and the 97.5% probability contours of the predicted [H_2] when $k_{f,7}$ is treated as the only uncertain parameter.

The uncertainty in the standard-state heat of formation of HO_2 radical, whose reported mean value has varied between 0.5 (Chase *et al.*, 1985) and 3.8 kcal/mol (Bauschlicher and Partridge, 1993) in recent years, also has considerable impact on the uncertainty in the predicted [H_2] concentration. The 95% probability interval shown in Figure 6-6*b* (the region bounded by the short dashed lines) results from restricting the MC simulation to treat $\Delta H_f^0(HO_2)$ as the only uncertain parameter and indicates the variability in the predicted [H_2] profile by adjusting the value of the $\Delta H_f^0(HO_2)$ alone. As shown in Table 6-3, the mean value and error estimate for the $\Delta H_f^0(HO_2)$ were taken to be 3.0±0.5 kcal/mol in this study. Both the $\Delta H_f^0(HO_2)$ and the forward rate constant for reaction (7) were identified as the key contributors to the H_2 uncertainty through examination of the magnitudes of the coefficients in the series approximation for the hydrogen response distribution. Thus, in addition to carrying out the uncertainty computation itself, the DEMM-based methodology also provides a straightforward and systematic means of identifying important random variables in the model. Given the uncertainty estimates for this simple H_2 mechanism, increasing the size of a mechanism to model more complex compounds may lead to the conclusion that the uncertainty in the model predictions will continue to grow as the number of random variables is increased. This, however, is not necessarily the case. For example, referring to Figure 6-6*a* and Figure 6-6*b*, the total model uncertainty (the region bounded by the long dashed lines) is less than the simple sum of the uncertainty contributions from $k_{f,7}$ and $\Delta H_f^0(HO_2)$ when considered alone. Since the total uncertainty is a nonlinear function of the individual uncertainty contributions, an increase in the number of random variables does not necessarily lead to an increase in the overall model uncertainty.

Identifying those model parameters with the greatest influence on the uncertainty in the predicted concentration profiles reveals which parameters need to be known more precisely in order to reduce the overall uncertainty of the model output. If the concentration predictions are highly uncertain, model refinements such as real-gas corrections may be unwarranted given the uncertainty in the rate parameters of the base mechanism. In the case studied, a large improvement to the

predictive capability of the model would result when uncertainties in the aforementioned key model parameters are reduced. To make this point more emphatically, consider the work of Alkam *et al.* (1996) who applied real-gas corrections to a mechanism similar to that given in Table 6-1. Predictions from their mechanism with and without real-gas corrections are presented in Figure 6-7 along with uncertainty estimates from the present reduced mechanism with no real-gas corrections. Real-gas corrections are seen to change the $[H_2]$ predictions by 57% at most. However, both the $[H_2]$ predictions with and without real-gas corrections are encompassed by the 95% probability interval (area bounded by solid lines) from the MC analysis. These observations indicate that the Alkam *et al.* model is not significantly different from the one in Table 6-2 given the uncertainty assigned to the $k_{f,j}$'s and $\Delta H^0_{f,i}$'s, and the incorporation of real-gas effects is overshadowed by the variability in the predicted $[H_2]$ caused by $k_{f,j}$'s and $\Delta H^0_{f,i}$'s uncertainties.

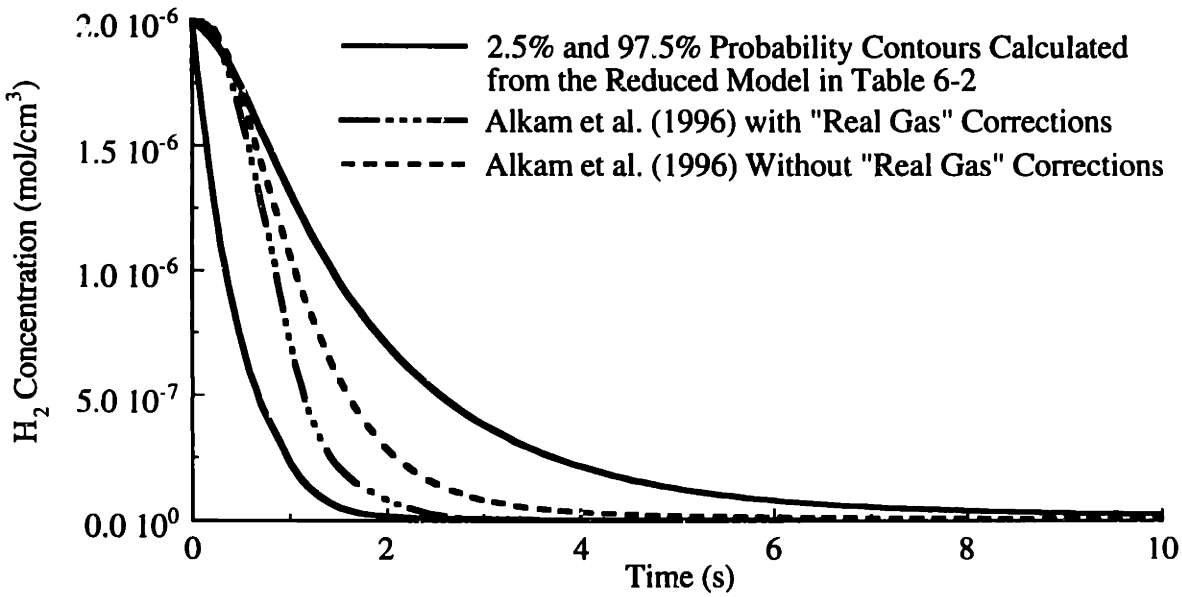

Figure 6-7 The effect of real-gas corrections on the H_2 concentration predicted by the mechanism of Alkam *et al.* (1996) compared with the $[H_2]$ probability distribution calculated from Monte Carlo simulation of the mechanism in Table 6-2

(Conditions: T=855 K, P=246 bar, $[H_2]_o$=2.06x10^{-6}, $[O_2]_o$=1.04x10^{-6}, $[H_2O]_o$=3.997x10^{-3} mol/cm^3. Upper and lower solid lines represent the 97.5% and 2.5% probability contours resulting from Monte Carlo simulation.)

6.4 CONCLUSIONS

DEMM and Monte Carlo simulation were used in an uncertainty analysis of a reduced hydrogen mechanism for oxidation in supercritical water. Both methods produced identical predictions of species concentration profiles and their time-dependent probability distributions. Further, both analyses revealed that there is considerable uncertainty in the predicted species concentration profiles arising from the reported uncertainties in the forward rate constants and species enthalpies of formation. Model predictions were found to be highly sensitive to two relatively uncertain parameters: the ΔH_f^0 of HO_2 radical and the rate constant for H_2O_2 dissociation. Thus, further improvement in the predictive capability of the model should be directed at improving the precision with which these two quantities are known. Also demonstrated in this study is the minimal impact of real-gas corrections on the predicted species profiles relative to the parametric uncertainty inherent in the mechanism itself.

For the simple eight-reaction hydrogen oxidation mechanism considered in this study, both DEMM and Monte Carlo simulation proved to be computationally tractable means of conducting parametric uncertainty analysis. However, the two methods differed substantially in the amount of computation time necessary to perform the analysis. To adequately develop the time-dependent response distributions of the model, Monte Carlo required 15,000 calls to the LSODE solver routine. By comparison, DEMM required 153 calls. This two order of magnitude reduction in the required number of model solutions makes DEMM an attractive tool for the analysis of more complex mechanisms where the computational time and memory requirements of Monte Carlo may become prohibitive. Additionally, inspection of the coefficients in the polynomial expansions employed by DEMM provides a straightforward means of identifying key uncertain model parameters which dominate the uncertainty in the predicted species concentrations.

6.5 IMPLICATIONS FOR SCWO ELEMENTARY REACTION MODELS

The hydrogen-oxygen mechanism may be the best understood subset of reactions at combustion conditions. The mechanism consists of only a small number of reactions, the reaction pathways are known with a high degree of certainty, and multiple investigators have measured a majority of the rate constants over a wide range of conditions (for e.g., see Baulch *et al.*, 1992). As shown in this study, even the predictions from this well-understood mechanism contain a

considerable amount of uncertainty resulting from uncertainty in the rate constants and in species thermochemistry. Of course, the uncertainty in the rate constants is higher at SCWO conditions as experimental measurements are not yet available for most of the rate constants at high pressures. In the present case, more precise measurements of key rate constants and thermodynamic data would lead to a reduction of model uncertainty, both at SCW and combustion conditions.

As the size and complexity of the oxidation mechanisms increase in order to model the oxidation of larger compounds, the main source of uncertainty shifts from the model parameters to a lack of understanding of the reaction mechanism itself. This holds particularly true at SCWO conditions where new reaction pathways are accessible due to the high pressure and many of the high activation barrier, thermal decomposition pathways which play important roles at combustion conditions are inaccessible at these lower temperatures. In cases where the mechanism itself is not well known, the largest reduction in overall uncertainty will come through an improved knowledge of the mechanism rather than through a reduction of uncertainty of the model parameters (*e.g.*, the rate constants or species thermochemistry).

Using elementary reaction mechanisms at T, P and Φ conditions other than for those for which they were developed can lead to a deeper understanding of the oxidation mechanism. Since different pathways become rate-controlling under different conditions, understanding both at what conditions a model succeeds and fails can highlight poorly understood pathways within the mechanism and provide a direction for future research. The following chapter discusses modeling the SCW oxidation of benzene. The starting point is a low-pressure benzene combustion mechanism available from the literature. Although benzene oxidation has been heavily studied, uncertainty of the reaction pathways exists even at atmospheric combustion conditions. While the purpose of the following study was to gain mechanistic insight of the SCWO process, the modeling effort also allowed the application of the current knowledge of benzene combustion to drastically different conditions from which this knowledge was developed. Analyzing the strengths and the shortcomings of the SCWO model lends insight into benzene oxidation in SCW and may result in an improved understanding of atmospheric benzene combustion as well.

6.6 REFERENCES

Alkam, M.K., V.M. Pai, P.B. Butler and W.J. Pitz, "Methanol and hydrogen oxidation kinetics in water at supercritical states." *Combust. Flame* **106**, 110 (1996).

Atherton, R.W., R.B. Schainker and E.R. Ducot, "On the statistical sensitivity analysis of models for chemical kinetics." *AIChE Journal* **21**(2), 441 (1975).

Atkinson, R., D.L. Baulch, R.A. Cox, R.F. Hampson, J.A. Kerr and J. Troe, "Evaluated kinetic and photochemical data for atmospheric chemistry. 3. IUPAC subcommittee on gas kinetic data evaluation for atmospheric chemistry." *J. Phys. Chem. Ref. Data* **18**(2), 881 (1989).

Baulch, D.L., C.J. Cobos, R.A. Cox, C. Esser, P. Frank, T. Just, J.A. Kerr, M.J. Pilling, J. Troe, R.W. Walker and J. Warnatz, "Evaluated kinetic data for combustion modelling." *J. Phys. Chem. Ref. Data* **21**(3), 411 (1992).

Bauschlicher, C.W. and H. Partridge, "An accurate determination of the HO_2 heat of formation." *Chem. Phys. Lett.* **208**(3,4), 241 (1993).

Brock, E.E. and P.E. Savage, "Detailed chemical kinetics model for supercritical water oxidation of C_1 compounds and H_2." *AIChE Journal* **41**(8), 1874 (1995).

Butler, P.B., N.E. Bergan, T.T. Bramlette, W.J. Pitz and C.K. Westbrook, "Oxidation of hazardous waste in supercritical water: A comparison of modeling and experimental results for methanol destruction." DE91-017097, U.S. Department of Energy Report, (1991a).

Butler, P.B., N.E. Bergan, T.T. Bramlette, C.K. Westbrook and W.J. Pitz, "Oxidation of hazardous waste in supercritical water Part I: A comparison of modeling and experimental results for methanol destruction." DE92-008565, U.S. Department of Energy Report, (1991b).

Chase, M.W., C.A. Davies, J.R. Downey, D.J. Frurip, R.A. McDonald and A.N. Syverud, *JANAF Thermochemical Tables*. American Chemical Society, American Institute for Physics, National Bureau of Standards, (1985).

Cobos, C.J. and J. Troe, "The influence of potential energy parameters on the reaction H + CH_3=CH_4." *Chem. Phys. Lett.* **113**(5), 419 (1985).

Dagaut, P., M. Cathonnet and J.-C. Boettner, "Chemical kinetic modeling of the supercritical-water oxidation of methanol." *J. Supercrit. Fluids* **9**(1), 33 (1996).

Dagaut, P., B. Daney de Marcillac, Y. Tan, M. Cathonnet and J.-C. Boettner, "Chemical kinetic modeling of the supercritical water oxidation of simple fuels: H_2, CO and CH_4." *J. Chim. Phys.* **92**(5), 1124 (1995).

DeMore, W.B., S.P. Sander, D.M. Golden, R.F. Hampson, M.J. Kurylo, C.J. Howard, A.R. Ravishankara, C.E. Kolb and M.J. Molina, "Chemical kinetics and photochemical data for use in stratospheric modeling." JPL 92-20, NASA/Jet Propulsion Laboratory, Pasadena (1992).

Derwent, R. and H. Øystein, "Application of sensitivity and uncertainty analysis techniques to a photochemical ozone model." *J. of Geophys. Res.* **93**(D3), 5185 (1988).

Ehhalt, D.H., J.S. Chang and D.M. Butler, "The probability distribution of the predicted CFM-induced ozone depletion." *J. of Geophys. Res.* **84**(C12), 7889 (1979).

Fisher, E.R. and P.B. Armentrout, "Heat of formation of HO_2. A direct determination from guided ion beam studies of $O_2^+(^2\Pi_g, v=0) + CH_4$." *J. Phys. Chem.* **94**(11), 4396 (1990).

Gao, D., W.R. Stockwell and J.B. Milford, "Global uncertainty analysis of a regional-scale gas-phase chemical mechanism." *J. of Geophys. Res.* **101**(C4), 9107 (1996).

Gopalan, S. and P.E. Savage, "Phenol oxidation in supercritical water. From global kinetics and product identities to an elementary reaction model." in *Innovations in Supercritical Fluids*, K. W. Hutchenson and N. R. Foster, Eds., ACS Symposium Series, **608**, American Chemical Society, Washington, D.C., 217 (1995).

Hindmarsh, A.C., "ODEPACK, a systematized collection of ODE solvers." in *Scientific Computing*, R. S. Stepleman, et al., Ed., North-Holland, Amsterdam, 55 (1983).

Holgate, H.R. and J.W. Tester, "Fundamental kinetics and mechanisms of hydrogen oxidation in supercritical water." *Combust. Sci. Technol.* **88**, 369 (1993).

Holgate, H.R. and J.W. Tester, "Oxidation of hydrogen and carbon monoxide in sub- and supercritical water: reaction kinetics, pathways, and water-density effects. 2. Elementary reaction modeling." *J. Phys. Chem.* **98**, 810 (1994).

Kee, R.J., J.F. Grcar, M.D. Smooke and J.A. Miller, 85-8240/UC-2, Sandia National Laboratory, (1988).

Kim, T.J., "Gas-phase kinetic studies of the hydrogen-oxygen and carbon monoxide-hydrogen-oxygen systems." Ph.D. Thesis, Department of Department of Mechanical Engineering, Princeton University, Princeton (1994).

Lamb, W.J., G.A. Hoffman and J. Jonas, "Self-diffusion in compressed supercritical water." *J. Chem. Phys.* **74**(12), 6875 (1981).

Leung, K.M. and R.P. Lindstedt, "Detailed kinetic modeling of C_1-C_3 alkene diffusion flames." *Combust. Flame* **102**(N1), 129 (1995).

Marshall, W.L. and E.U. Franck, "Ion product of water substance, 0-1000°C, 1-10,000 bars. New international formulation and its background." *J. Phys. Chem. Ref. Data* **10**(2), 295 (1981).

Melius, C.F., N.E. Bergan and J.E. Shepherd, "Effects of water on combustion kinetics at high pressure." in *Twenty-Third Symposium (International) on Combustion*, The Combustion Institute, Pittsburgh, 217 (1990).

Paterson, C., D. Breshears and B. Foy, "Steady state combustion of hydrogen and oxygen in supercritical water." *Combust. Sci. Technol.* **89**(411-423) (1993).

Phenix, B.D., "Hydrothermal oxidation of simple organic compounds." Ph.D. Thesis, Department of Chemical Engineering, Massachusetts Institute of Technology, Cambridge, MA (1998).

Phenix, B.D., J.L. DiNaro, M.A. Tatang, J.W. Tester, J.B. Howard and G.J. McRae, "Incorporation of parametric uncertainty into complex kinetic mechanisms: application to hydrogen oxidation in supercritical water." *Combust. Flame* **112**, 132 (1998).

Raes, F., A. Saltelli and R. Van Dingenen, "Modelling formation and growth of H_2SO_4-H_2O aerosols: Uncertainty analysis and experimental evaluation." *J. Aerosol Sci.* **23**(7), 759 (1992).

Savage, P.E., J.L. Yu, N. Stylski and E.E. Brock, "Kinetics and mechanism of methane oxidation in supercritical water." *J. Supercrit. Fluids* **12**(2), 141 (1998).

Schmitt, R.G., P.B. Butler and N.B. French, "Chemkin real gas: A Fortran package for analysis of thermodynamic properties and chemical kinetics in nonideal systems." UIME PBB 93-006, University of Iowa, Iowa City (1993).

Schmitt, R.G., P.B. Butler, C.K. Westbrook and W.J. Pitz, "Destruction of hazardous waste in supercritical water. Part II: A study of high pressure methanol oxidation kinetics." DE92-008559, U.S. Department of Energy Report, (1991).

Shum, L.G.S. and S.W. Benson, "Review of the heat of formation of the hydroperoxyl radical." *J. Phys. Chem.* **87**(18), 3479 (1983).

Stolarski, R.S., D.M. Butler and R.D. Rundel, "Uncertainty propagation in a stratospheric model 2. Monte Carlo analysis of imprecisions due to reaction rates." *J. of Geophys. Res.* **83**(6), 3074 (1978).

Tatang, M.A., "Direct incorporation of uncertainty into chemical and environmental engineering systems." Ph.D. Thesis, Department of Chemical Engineering, Massachusetts Institute of Technology, Cambridge, MA (1995).

Tatang, M.A., W.W. Pan, R.G. Prinn and G.J. McRae, "An efficient method for parametric uncertainty analysis of numerical geophysical models." *J. of Geophys. Res.* **102**(D18), 21925 (1997).

Tester, J.W. and M. Modell, *Thermodynamics and its Applications*. Prentice Hall, Upper Saddle River, NJ (1997).

Tsang, W. and R.F. Hampson, "Chemical kinetic data base for combustion chemistry. Part I. Methane and related compounds." *J. Phys. Chem. Ref. Data* **15**(3), 1087 (1986).

Uematsu, M. and E.U. Frank, "Static dielectric constant of water and steam." *The Journal of Physical Chemical Reference Data* **9**(4), 1291 (1980).

Webley, P.A. and J.W. Tester, "Fundamental kinetics of methanol oxidation in supercritical water." in *Supercritical Fluid Science and Technology*, K. P. Johnston and J. M. L. Penninger, Eds., ACS Symposium Series, **406**, American Chemical Society, Washington, D.C., 259 (1989).

Webley, P.A. and J.W. Tester, "Fundamental kinetics of methane oxidation in supercritical water." *Energy and Fuels* **5**, 411 (1991).

Yetter, R.A., F.L. Dryer and H. Rabitz, "A comprehensive reaction mechanism for carbon monoxide/hydrogen/oxygen kinetics." *Combust. Sci. Technol.* **79**, 97 (1991).

Chapter 7.

Development of a Supercritical Water Oxidation Elementary Reaction Model for Benzene

As discussed in Chapters 1 and 6, oxidation in SCW above 450°C is thought to proceed primarily by free-radical reactions. Attempts to model SCWO reactions using combustion mechanisms adapted to the temperature and pressure of SCWO have met with varying success, but have largely supported our hypothesis that SCWO reactions are similar to those which take place in combustion at the temperatures and pressures of SCWO systems.

In order to gain mechanistic insight of benzene oxidation in SCW, a detailed elementary reaction model of benzene oxidation was developed from the benzene combustion mechanism of Shandross (Shandross, 1996; Shandross *et al.*, 1996). Quantum Rice-Ramsperger-Kassel (QRRK) (Robinson and Holbrook, 1972) analysis was employed in the adaptation of the combustion mechanism to SCWO conditions in order to calculate the rate constants of pressure-dependent reactions. In addition, new reaction pathways were hypothesized which likely occur as a result of the high pressure. The predictions of the SCWO benzene mechanism were then compared to the experimental data first presented in Chapter 5.

7.1 Literature Review

Aromatic compounds are components of many fossil fuels and can be formed in the combustion of non-aromatics. The characteristic tendency of aromatic fuels to form soot during combustion makes understanding their destruction mechanisms essential in order to control soot formation. As a result of the importance of understanding aromatic combustion, the oxidation of benzene has been relatively well-studied both through experimental measurements of species profiles in flames and with the development of detailed kinetic mechanisms. The result of the research has been the development of several benzene oxidation mechanisms for the prediction of the experimentally-measured species profiles in laboratory benzene flames.

7.1.1 Review of experimental measurements of benzene flames

Several investigators have measured data on benzene oxidation. Bittner and Howard (1980) measured the profiles of over 52 species in their 20 torr, premixed benzene-oxygen-argon flame under fuel-rich, "near-sooting" conditions. The experimental temperature profile ranged from ambient to 1900 K (1625°C). Brezinsky (1986) presented a limited number of experimentally measured profiles for benzene oxidation in the adiabatic, atmospheric pressure, Princeton flow reactor. Using the same reactor, Lovell *et al.* (1988) later provided a more comprehensive set of concentration profiles for benzene oxidation. Burcat *et al.* (1986) reported measurements of the ignition delay time of benzene-oxygen-argon mixtures. Shandross *et al.* (Shandross *et al.*, 1996) measured the profiles for 44 species in a fuel rich, 22 torr, laminar, premixed hydrogen-oxygen-argon flame seeded with benzene. The maximum flame temperature achieved was 1940 K (1670°C). Recently, Chai and Pfefferle (1998) reported intermediate species profiles measured at both fuel-rich and fuel-lean conditions at 900 to 1300 K (625 to 1025°C) and 350 torr in a well-mixed reactor. Of interest was the detection of oxygenated intermediates such as cyclopentadienone (C_5H_4O) and benzoquinones ($C_6H_4O_2$) and the very early appearance of CO_2 leading to speculation about pathways for CO_2 formation which do not involve CO.

7.1.2 Review of benzene combustion modeling

Several models in various levels of detail have been developed to model the available experimental data. The review article by Brezinsky (1986) presented a qualitative outline of a benzene oxidation mechanism. Bittker (1991) developed a benzene oxidation mechanism, based on of the qualitative scheme outlined by Brezinsky, to compute the experimental results of Lovell *et al.* (1988) and Burcat *et al.* (1986). This mechanism successfully predicted the qualitative trends of the data and gave good quantitative agreement with several of the composition profiles and ignition delay times. Emdee *et al.* (1992) developed a mechanism to describe the oxidation of toluene to benzene near 1200 K (925°C). The model contained a 68 reaction benzene submechanism. Linstedt and Skevis (1994) developed a 395 reaction benzene oxidation mechanism with many reactions and rate constants taken from the benzene submechanism in the Emdee *et al.* model. They validated their model against the data of Bittner and Howard (1980) and found excellent agreement with the experimental profiles for benzene, carbon monoxide, carbon dioxide, oxygen and other radical and stable species but found that phenoxy (C_6H_5O), phenyl (C_6H_5) and phenol (C_6H_5OH) were all

overpredicted. Zhang and McKinnon (1995) also used the Emdee *et al.* benzene submechanism as a starting point to develop a 514 elementary reaction mechanism for benzene oxidation which they tested against the data of Bittner and Howard (1980). Most of the rate constants were taken from the literature, but some - most notably those involving cyclopentadienyl (C_5H_5) - had to be estimated. Some elementary reactions were also taken from Bittker's (1991) model. Since the Bittner and Howard (1980) data were measured at 20 torr, Zhang and McKinnon carefully accounted for the pressure dependence of the unimolecular (fall-off) and bimolecular (chemical activation) reactions using the quantum Rice-Ramsperger-Kassel, QRRK, method (Robinson and Holbrook, 1972). Their resulting pressure corrected mechanism gave good quantitative agreement for benzene and many other stable and radical intermediate species. Like the Lindstedt-Skevis mechanism, however, their model overpredicted both phenyl and phenoxy.

Using net rate analysis, Shandross (Shandross, 1996; Shandross *et al.*, 1996) evaluated the ability of the Lindstedt-Skevis (LS), Zhang-McKinnon (ZM) and Emdee-Brezinsky-Glassman (EBG) models to predict his experimental data (Shandross *et al.*, 1996). He found that the three mechanisms strongly overpredicted phenol destruction at high temperatures. Using the ZM mechanism as a basis, modifications to reactions of benzene and phenol species were made (Shandross *et al.*, 1996) including the addition of new reactions and the use of bimolecular QRRK and Rice-Ramsperger-Kassel-Marcus (RRKM) (Robinson and Holbrook, 1972) methods to account for the pressure dependence of rate constants. The modified mechanism gave improved agreement with the phenol chemistry, but the destruction rate was still overpredicted. The net rates of the other critical intermediates phenyl, phenoxy and cyclopentadiene also were not well predicted.

Most recently, Tan and Frank (1996) developed a benzene oxidation mechanism built on an earlier model for hydrocarbon combustion of methane to propane and their mixtures (Tan *et al.*, 1994). Reactions involving C_5 and C_6 were added with updated rate constants. The model relies heavily on a recent shock tube investigation of reactions between phenyl and oxygen by Frank *et al.* (1994). New reaction pathways leading to the formation of *p*-benzoquinone and its subsequent reaction were included. The addition of these pathways is supported by the recent detection of *p*-benzoquinone and other oxygenated intermediates during benzene oxidation (Chai and Pfefferle, 1998). Excellent agreement between model predictions and experimental data was obtained by Tan and Frank for benzene, carbon monoxide, carbon dioxide and other stable and radical species.

Uncertainty was still present in the reactions involving C_5 species, and, as with the other benzene mechanisms, phenyl radical was overpredicted although by a lesser amount than in previous modeling attempts.

Noting the lack of kinetic and mechanistic information on combustion reactions of C_5 species, Joseph Bozzelli's research group at the New Jersey Institute of Technology recently assembled submodels of cyclopentadiene (C_5H_6) and cyclopentadienyl (C_5H_5) reactions with H, O, OH, HO_2 and O_2 (Zhong and Bozzelli, 1997; Zhong and Bozzelli, 1998) for insertion in combustion mechanisms where these species are important. New rate constants for H abstraction pathways were presented and QRRK calculations were performed on reactions involving additions or combinations. As a test of the C_5H_5/C_5H_6 submechanism, they included the submechanism in their full model and compared their model predictions with experimental data on benzene, toluene and cyclopentadiene oxidation and on phenol pyrolysis. The best agreement was obtained with the phenol pyrolysis data, but the model well predicted the fuel, cyclopentadiene and other intermediate species profiles in the other three cases as well.

Alzueta *et al.* (1998) developed a submechanism for *p*-benzoquinone oxidation based on the measured species profiles from *p*-benzoquinone pyrolysis and oxidation at atmospheric pressure and temperatures ranging from 600 to 1500 K (325 to 1225°C) in their isothermal flow reactor. Given the experimental observation of *p*-benzoquinone in benzene flames (Chai and Pfefferle, 1998) and the inclusion of *p*-benzoquinone in the benzene oxidation mechanism of Tan and Frank (1996), there is a presumed need to include a complete *p*-benzoquinone submechanism in benzene oxidation mechanisms.

The mechanisms reviewed above successfully predict the oxidation of benzene as well as many other stable and radical intermediates. The main shortcomings of these models are their pronounced overpredictions of the key C_6 intermediates (C_6H_5, C_6H_5O and C_6H_5OH). Given that these species are the primary products of benzene oxidation, the inability of the current models to predict these profiles properly is troubling. As noted by Chai and Pfefferle (1998), the current benzene oxidation models, developed primarily for high temperatures (>1600 K or 1325°C) and at fuel-rich conditions, are not useable outside of the temperature and stoichiometric conditions at which they were adjusted, and the understanding of the detailed oxidation mechanism is particularly poor at moderate temperatures (900-1300 K or 625-1025°C) and fuel-lean conditions.

In Chapter 5, experimental results were presented on the SCWO of benzene close to this moderate temperature range (750-860 K or 480-590°C) with sub- to superstoichiometric levels of oxygen. Most experiments were conducted with a pressure of 246 bar. The concentration profiles of benzene, phenol, carbon monoxide, carbon dioxide and methane were measured as a function of reactor residence time.

In this Chapter, an elementary reaction mechanism is developed to model the experimentally measured benzene SCWO data using the latest understanding of benzene oxidation under combustion conditions. There are two reasons for the current study: 1) to gain mechanistic insight of the oxidation of benzene in supercritical water and 2) to determine if existing free-radical reaction network models of benzene oxidation at atmospheric, combustion conditions can describe oxidation in supercritical water. Since the experimental data were obtained at conditions of much lower temperatures, higher pressures (densities) and higher oxygen concentrations than current benzene oxidation models were developed for, assessing the strengths and shortcomings of the current models at these conditions may aid in the understanding of benzene oxidation at combustion conditions.

7.2 Development of a SCW Benzene Oxidation Model

The basis for the SCW benzene oxidation mechanism is the detailed kinetic mechanism of Shandross (Shandross, 1996; Shandross *et al.*, 1996). Many of the unimolecular and bimolecular, chemically activated reactions were adjusted by Shandross for the pressure of 246 bar using QRRK (Dean *et al.*, 1991) or RRKM. Details of the QRRK and RRKM calculations can be found in the thesis of Shandross (1996). Pressure dependent reactions left in the low-pressure limit by Shandross included those in the H_2/O_2 submechanism, reactions of C_2 species and the CO/CO_2 submechanism. The H_2/O_2 submechanism was replaced with the previously reported SCW hydrogen oxidation mechanism (see Chapter 6 and Phenix *et al.*, 1998) yielding a 545 reaction and 81 species "partially pressure corrected" mechanism. The mechanism is referred to as "partially pressure corrected" at this point because not all reactions were adjusted to a pressure of 246 bar.

This mechanism was reduced to 41 reactions using sensitivity analysis as implemented by SENKIN (Lutz *et al.*, 1988) and using CHEMKIN (Kee *et al.*, 1989) for the associated thermochemical calculations. The reduction was performed at 813 K (540°C) and 246 bar with

stoichiometric oxygen, at which conditions the most complete set of residence time data was measured in the present experiments. The resulting reduced model appears in Table 7-1. The rate constants shown are those used by Shandross in all cases with the exception of the reactions in the H_2/O_2 submechanism which were taken from Phenix *et al.* (1998). The reduced and full models yield identical predictions of C_6H_6, C_6H_5OH, CO, CO_2, and O_2.

The calculation of the species profiles was performed using SENKIN (Lutz *et al.*, 1988), and CHEMKIN (Kee *et al.*, 1989) was applied for all thermochemical calculations. Thermochemistry was taken from various sources and is presented in Appendix 10.3. Figure 7-1 compares the predictions of the reduced model in Table 7-1 with the residence time data measured at 813 K (540°C) and 246 bar with stoichiometric oxygen. The model predicts an extremely rapid initial reaction of benzene and drastically overpredicts the phenol concentration.

In order to improve the agreement between the model and the experimental data, the reactions and rate constants in the reduced mechanism of Table 7-1 were evaluated and updated where necessary. Table 7-2 serves to highlight changes in rate constants of the reactions in the original reduced model (Table 7-1) but does not include the reactions added to the mechanism. The final reduced model, with updated rate constants and new reaction pathways, is shown in Table 7-3. The full mechanism is presented in Appendix 10.3. A discussion of all modifications made to the model in Table 7-1 follows.

7.2.1 Analysis of Individual Rate Constants

Given that the residence time data in the present experiments was measured at a pressure of 246 bar, the most obvious modification necessary to the mechanism of Table 7-1 for prediction of SCWO data is proper treatment of the pressure dependence of the elementary reaction rate constants. Unimolecular reactions are well recognized to be linearly proportional to pressure in the low-pressure limit and to have a pressure-independent rate constant (k_∞) at their high pressure limit. At intermediate pressures in what is known as the "fall-off" region, these rate constants exhibit a non-linear pressure dependence. The pressures at which the transition from the low-pressure limit to the fall-off region to the high-pressure limit occur are reaction-specific.

Table 7-1. Partially pressure-corrected benzene oxidation mechanism of Shandross reduced from 545 to 41 reactions at 813 K (540°C) and 246 bar with Φ=1.0

No.	Reaction	A (cm^3-mol-s)	n	E_a (cal/mol)	Reference
1.	$H + O_2 \Leftrightarrow HO_2$	1.481×10^{12}	0.6	0.	a
2.	$HO_2 + HO_2 \Leftrightarrow H_2O_2 + O_2$	2.22×10^{12}	0.	-1690.	b
3.	$H_2O_2 + OH \Leftrightarrow H_2O + HO_2$	7.829×10^{12}	0.	1331.4	c
4.	$H_2O_2 \Leftrightarrow OH + OH$	3.000×10^{14}	0.	48485.1	c
5.	$OH + HO_2 \Leftrightarrow H_2O + O_2$	2.891×10^{13}	0.	-496.8	c
6.	$H + O_2 \Leftrightarrow OH + O$	1.990×10^{14}	0.	16810.8	c
7.	$OH + OH \Leftrightarrow O + H_2O$	1.504×10^{9}	1.14	99.4	c
8.	$O + HO_2 \Leftrightarrow OH + O_2$	3.250×10^{13}	0.	0.	c
9.	$H + C_6H_5O \Leftrightarrow C_6H_5OH$	2.50×10^{14}	0.	0.	d
10.	$OH + C_6H_6 \Leftrightarrow C_6H_5OH + H$	1.34×10^{13}	0.	10592.	d
11.	$OH + C_6H_6 \Leftrightarrow C_6H_5 + H_2O$	2.11×10^{13}	0.	4571.	n
12.	$O + C_6H_6 \Leftrightarrow C_6H_5O + H$	2.40×10^{13}	0.	4668.	e
13.	$OH + C_6H_5OH \Leftrightarrow H_2O + C_6H_5O$	1.39×10^{8}	1.43	-962.	f
14.	$C_6H_5 + O_2 \Leftrightarrow C_6H_5O + O$	1.91×10^{37}	-6.78	22070.	g
15.	$C_7H_8 + OH \Leftrightarrow C_7H_7 + H_2O$	1.26×10^{13}	0.	2583.	h
16.	$C_5H_5 + C_2H_2 \Leftrightarrow C_7H_7$	3.72×10^{11}	0.	8300.	i, k_∞
17.	$C_6H_5OH + O \Leftrightarrow C_6H_5O + OH$	2.81×10^{13}	0.	7352.	h
18.	$C_6H_5OH + HO_2 \Leftrightarrow C_6H_5O + H_2O_2$	3.00×10^{13}	0.	15000.	j
19.	$C_6H_5OH + CH_2CHCHCH \Leftrightarrow C_4H_6 + C_6H_5O$	6.00×10^{12}	0.	0.	h
20.	$C_6H_5OH + CH_2CHCCH_2 \Leftrightarrow C_4H_6 + C_6H_5O$	6.00×10^{12}	0.	0.	h
21.	$C_6H_5OH + C_6H_5 \Leftrightarrow C_6H_6 + C_6H_5O$	4.91×10^{12}	0.	4400.	h
22.	$C_6H_5O + C_5H_6 \Leftrightarrow C_5H_5 + C_6H_5OH$	3.16×10^{11}	0.	8000.	h
23.	$C_5H_5 + CO \Leftrightarrow C_6H_5O$	2.14×10^{8}	0.	19649.	i, k_∞
24.	$C_6H_5 + O_2 \Leftrightarrow 2CO + C_2H_2 + C_2H_3$	7.50×10^{13}	0.	15002.	o
25.	$C_5H_6 + O_2 \Leftrightarrow C_5H_5 + HO_2$	2.00×10^{13}	0.	25000.	h
26.	$C_5H_6 + O_2 \Leftrightarrow C_5H_5O + OH$	1.00×10^{13}	0.	20712.	j
27.	$C_5H_6 + CH_2CHCCH_2 \Leftrightarrow C_5H_5 + C_4H_6$	6.00×10^{12}	0.	0.	h
28.	$CH_2CHCHCH + CO \Leftrightarrow C_5H_5O$	2.40×10^{-3}	2.66	30100.	i, k_∞
29.	$C_5H_5 + OH \Leftrightarrow C_5H_4OH + H$	3.00×10^{13}	0.	0.	h
30.	$C_5H_5 + O \Leftrightarrow CH_2CHCHCH + CO$	1.00×10^{14}	0.	0.	h
31.	$C_5H_5 + HO_2 \Leftrightarrow C_5H_5O + OH$	3.00×10^{14}	0.	0.	h
32.	$C_5H_5 + O \Leftrightarrow C_5H_5O$	1.00×10^{13}	0.	0.	j
33.	$C_5H_4O + H \Leftrightarrow C_5H_4OH$	4.03×10^{12}	0.44	4860.	i, k_∞
34.	$CH_2CHCCH_2 + O_2 \Leftrightarrow C_4H_4 + HO_2$	1.20×10^{11}	0.	0.	h
35.	$C_4H_4 + OH \Leftrightarrow H_2CCCCH + H_2O$	7.50×10^{6}	2.0	5000.	k
36.	$C_2H_3 + O_2 \Leftrightarrow CH_2O + HCO$	4.00×10^{12}	0.	-250.	k
37.	$C_2H_3 + M \Leftrightarrow C_2H_2 + H + M$ H_2O/16.0/ H_2/2.6/ CO/1.9/ CO_2/3.8/ CH_4/16.0/[q]	3.00×10^{15}	0.	32006.	p

38.	$CH_2O + OH \Leftrightarrow HCO + H_2O$	3.43×10^{15}	1.18	-447.	k
39.	$HCO + M \Leftrightarrow H + CO + M$	2.50×10^{14}	0.	16802.	k
40.	$CO + O + M \Leftrightarrow CO_2 + M$	2.19×10^{13}	0.	-4540.	l
	H_2/3.333/ H_2O/16.0/ CO_2/5.067/ CO/2.533/[q]				
41.	$CO + OH \Leftrightarrow CO_2 + H$	3.09×10^{11}	0.	735.	m

a: (Atkinson *et al.*, 1989), b: (Hippler *et al.*, 1990) fit to single exponential for temperatures around 800 K, c: (Baulch *et al.*, 1992), d: (He *et al.*, 1988), e: (Ko *et al.*, 1991), f: (Shandross *et al.*, 1996), g: (Shandross, 1996) QRRK calculation, h: (Emdee *et al.*, 1992), i: (Zhang and McKinnon, 1995), j: (Bittker, 1991), k: (Miller and Melius, 1992), l: (Shandross, 1996), m: (Dixon-Lewis, 1972), n: (Madronich and Felder, 1985), o: (McLain *et al.*, 1979), p: (Warnatz, 1984), q: Efficiencies for several bath gases (M) are given. The rate constant is multiplied by this efficiency. For the present case, M=H_2O and $k_{f,37}$ and $k_{f,41}$ are multiplied by 16 in the calculations.

The reverse of the unimolecular reactions, that is radical recombination reactions, at first would seem to have the same pressure dependence by the principle of microscopic reversibility. Although this is true when only one pathway for reaction is possible, when additional products can be formed by chemically activated pathways a very complex pressure and temperature dependence can result from the competition between the stabilization and the decomposition and/or isomerization pathways (Dean, 1985; Dean *et al.*, 1991). For such reactions, experimentally measured rate constants cannot be extrapolated directly to other temperatures and pressures. The computer programs CHEMACT (Dean *et al.*, 1991) and CHEMDIS (Ing, 1995; Chang *et al.*, c.1999) implement the bimolecular QRRK analysis of Dean (1985) and allow the estimation of the pressure and temperature dependence of the rate constants of reactions which proceed through the formation of a chemically activated complex. Westmoreland *et al.* (1986) provide an excellent overview of the governing bimolecular and unimolecular QRRK equations and several comparisons of predicted and experimentally measured rate constants.

Bimolecular QRRK analysis was performed using CHEMACT and CHEMDIS to predict rate constants at 246 bar and 813 K (540°C) for the pressure dependent rate constants in Table 7-1. The rate constants predicted by CHEMACT or CHEMDIS are given in both Table 7-2 and Table 7-3 and are noted with the reference "QRRK" in Table 7-3. A discussion of the QRRK analysis of the individual rate constants and other modifications to the mechanism in Table 7-1 follows. Details of all bimolecular QRRK analyses using either CHEMACT or CHEMDIS can be found in Appendix 10.3.

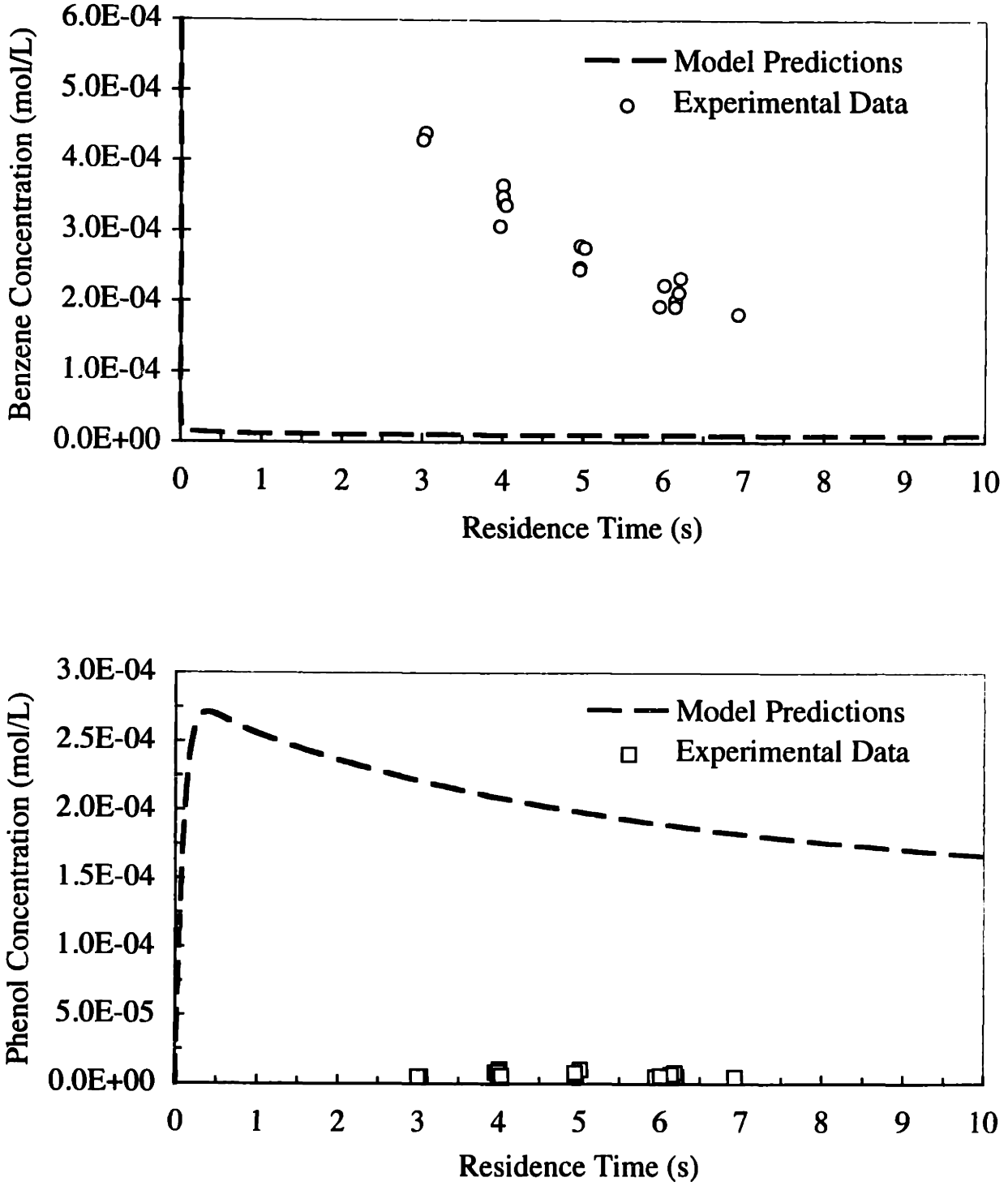

Figure 7-1 Comparison of experimental data and the predicted benzene and phenol concentrations from the mechanism in Table 7-1
(T=813 K, P=246 bar, Φ=1.0, $[C_6H_6]_0=0.6\times10^{-3}$ mol/L)

Table 7-2. Reduced benzene oxidation mechanism from Table 7-1 with updated rate constants where noted

(if "unchanged" follows the reference for a rate constant, the rate constant used is identical to that in Table 7-1)

No.	Reaction	A (cm^3-mol-s)	n	E_a (cal/mol)	Reference
1.	$H + O_2 \Leftrightarrow HO_2$	2.07×10^{18}	-1.69	890.	see text
2.	$HO_2 + HO_2 \Leftrightarrow H_2O_2 + O_2$	2.22×10^{11}	0.	-1629.	b (unchanged)
3.	$H_2O_2 + OH \Leftrightarrow H_2O + HO_2$	7.829×10^{12}	0.	1331.4	c (unchanged)
4.	$OH + OH \Leftrightarrow H_2O_2$	2.96×10^{28}	-5.26	2980.	see text
5.	$OH + HO_2 \Leftrightarrow H_2O + O_2$	1.91×10^{16}	-1.0	0.	q
6.	$H + O_2 \Leftrightarrow OH + O$	2.10×10^{15}	-0.3	20200.	see text
7.	$OH + OH \Leftrightarrow O + H_2O$	1.50×10^{9}	1.14	99.4	c (unchanged)
8.	$O + HO_2 \Leftrightarrow OH + O_2$	3.250×10^{13}	0.	0.	c (unchanged)
9.	$H + C_6H_5O \Leftrightarrow C_6H_5OH$	2.50×10^{14}	0.	0.	d (unchanged)
10.	$OH + C_6H_6 \Leftrightarrow C_6H_5OH + H$	1.34×10^{13}	0.	10592.	d (unchanged)
11.	$OH + C_6H_6 \Leftrightarrow C_6H_5 + H_2O$	1.63×10^{8}	1.42	1454.	c
12.	$O + C_6H_6 \Leftrightarrow C_6H_5O + H$	2.40×10^{13}	0.	4668.	e (unchanged)
13.	$OH + C_6H_5OH \Leftrightarrow H_2O + C_6H_5O$	1.39×10^{8}	1.43	-962.	f (unchanged)
14.	$C_6H_5 + O_2 \Leftrightarrow C_6H_5O + O$	2.57×10^{-29}	-0.15	-159.	see text
15.	$C_7H_8 + OH \Leftrightarrow C_7H_7 + H_2O$	1.26×10^{13}	0.	2583.	h (unchanged)
16.	$C_5H_5 + C_2H_2 \Leftrightarrow C_7H_7$	3.72×10^{11}	0.	8300.	i (unchanged)
17.	$C_6H_5OH + O \Leftrightarrow C_6H_5O + OH$	1.28×10^{13}	0.	2891.	r, s
18.	$C_6H_5OH + HO_2 \Leftrightarrow C_6H_5O + H_2O_2$	3.00×10^{13}	0.	15000.	j (unchanged)
19.	$C_6H_5OH + CH_2CHCHCH \Leftrightarrow C_4H_6 + C_6H_5O$	6.00×10^{12}	0.	0.	h (unchanged)
20.	$C_6H_5OH + CH_2CHCCH_2 \Leftrightarrow C_4H_6 + C_6H_5O$	6.00×10^{12}	0.	0.	h (unchanged)
21.	$C_6H_5OH + C_6H_5 \Leftrightarrow C_6H_6 + C_6H_5O$	4.91×10^{12}	0.	4400.	h (unchanged)
22.	$C_6H_5O + C_5H_6 \Leftrightarrow C_5H_5 + C_6H_5OH$	3.16×10^{11}	0.	8000.	h (unchanged)
23.	$C_6H_5O \Leftrightarrow C_5H_5 + CO$	7.40×10^{11}	0.	43853.	t
24.	$C_6H_5 + O_2 \Leftrightarrow 2CO + C_2H_2 + C_2H_3$	-	-	-	removed
25.	$C_5H_6 + O_2 \Leftrightarrow C_5H_5 + HO_2$	2.00×10^{13}	0.	25000.	u
26.	$C_5H_6 + O_2 \Leftrightarrow C_5H_5O + OH$	-	-	-	removed
27.	$C_5H_6 + CH_2CHCCH_2 \Leftrightarrow C_5H_5 + C_4H_6$	6.00×10^{12}	0.	0.	h (unchanged)
28.	$C_5H_5O \Leftrightarrow CH_2CHCHCH + CO$	7.4×10^{11}	0.	43900.	v
29.	$C_5H_5 + OH \Leftrightarrow C_5H_4OH + H$	3.63×10^{-48}	18.2	-3853.	w, see text
30.	$C_5H_5 + O \Leftrightarrow CH_2CHCHCH + CO$	1.45×10^{1}	3.76	2213.	w, see text
31.	$C_5H_5 + HO_2 \Leftrightarrow C_5H_5O + OH$	6.19×10^{-31}	13.8	-4130.	w, see text
32.	$C_5H_5 + O \Leftrightarrow C_5H_5O$	5.17×10^{30}	-5.96	3445.	w, see text
33.	$C_5H_4OH \Leftrightarrow C_5H_4O + H$	2.10×10^{13}	0.0	48000.	h
34.	$CH_2CHCCH_2 + O_2 \Leftrightarrow C_4H_4 + HO_2$	1.20×10^{11}	0.	0.	h (unchanged)
35.	$C_4H_4 + OH \Leftrightarrow H_2CCCCH + H_2O$	7.50×10^{6}	2.0	5000.	k (unchanged)
36.	$C_2H_3 + O_2 \Leftrightarrow CH_2O + HCO$	4.00×10^{12}	0.	-250.	k (unchanged)
37.	$C_2H_2 + H \Leftrightarrow C_2H_3$	7.85×10^{14}	-0.22	1770.	see text
38.	$CH_2O + OH \Leftrightarrow HCO + H_2O$	3.43×10^{15}	1.18	-447.	k (unchanged)

39.	$HCO + M \Leftrightarrow H + CO + M$	2.50×10^{14}	0.	16802.	k (unchanged)
40.	$CO + O \Leftrightarrow CO_2$	1.8×10^{10}	0.	2438.	x, y (see text)
41.	$CO + OH \Leftrightarrow CO_2 + H$	3.09×10^{11}	0.	735.	m (unchanged)

a: (Atkinson *et al.*, 1989), b: (Hippler *et al.*, 1990) fit to single exponential for temperatures around 800 K, c: (Baulch *et al.*, 1992), d: (He *et al.*, 1988), e: (Ko *et al.*, 1991), f: (Shandross *et al.*, 1996), g: (Shandross, 1996) QRRK calculation, h: (Emdee *et al.*, 1992), i: (Zhang and McKinnon, 1995), j: (Bittker, 1991), k: (Miller and Melius, 1992), l: (Shandross, 1996), m: (Dixon-Lewis, 1972), n: (Madronich and Felder, 1985), o: (McLain *et al.*, 1979), p: (Warnatz, 1984), q: (Kim *et al.*, 1994), r: (Baulch *et al.*, 1994), s: (Tan and Frank, 1996), t: (Frank *et al.*, 1994), u: (Zhong and Bozzelli, 1997), v: (Alzueta *et al.*, 1998), w: (Zhong and Bozzelli, 1998), x: (Troe, 1974), y: (Westmoreland *et al.*, 1986).

7.2.1 (*cont.*) Analysis of Individual Rate Constants

$H + O_2 \leftrightarrow HO_2^* \leftrightarrow OH + O$ The addition/elimination reaction between H and O_2 is one of the most important chain-branching steps at combustion conditions. The addition/elimination pathway proceeds through the formation of the activated intermediate HO_2^* which can be stabilized to HO_2 or dissociate yielding OH and O. The amount of HO_2 which is stabilized versus the amount which dissociates depends on pressure and temperature. The stabilization product is favored at higher pressures.

Due to the importance of this reaction in combustion, the rate constants have been measured extensively at combustion conditions (see Baulch *et al.*, 1992), but measurements of this and other rate constants at pressures exceeding a few bar are rare. In order to gain a better understanding of the pressure dependence of this important reaction, Cobos *et al.* (1985) studied the recombination reaction leading to HO_2 at 298 K (25°C) with pressures between 1 and 200 bar. By extrapolating the fall-off curves, an estimate of the high-pressure rate constant for recombination was obtained.

With the measured high-pressure rate constant for the reaction of H and O_2 to HO_2 (Cobos *et al.*, 1985), Westmoreland *et al.* (1986) performed a bimolecular QRRK analysis of this reaction using CHEMACT. The rates of both the stabilization and dissociation pathways were successfully predicted over wide ranges of temperature and pressure.

A bimolecular QRRK analysis similar to that of Westmoreland *et al.* was conducted using CHEMACT to predict the rates of the two pathways at 246 bar from 300 to 1000 K (25 to 725°C). The analysis was performed using rate constants from Cobos *et al.* (1985) and Baulch *et al.* (1992). The results showed that at 246 bar and 813 K (540°C) the reaction between H and O_2

Table 7-3. Final reduced elementary reaction mechanism for benzene oxidation in SCW used in this study

(Mechanism developed for a pressure of 245 bar and temperatures around 813 K (540°C); if "unchanged" follows the reference for a rate constant, the rate constant used is identical to that in Table 7-1)

No.	Reaction	A (cm^3-mol-s)	n	E_a (cal/mol)	Reference
	H_2/O_2 reactions				
1.	$H + O_2 \Leftrightarrow HO_2$	2.07×10^{18}	-1.69	890.	QRRK
2.	$HO_2 + HO_2 \Leftrightarrow H_2O_2 + O_2$	2.22×10^{11}	0.	-1629.	b (unchanged)
3.	$H_2O_2 + OH \Leftrightarrow H_2O + HO_2$	7.83×10^{12}	0.	1331.4	c (unchanged)
4.	$OH + OH \Leftrightarrow H_2O_2$	2.96×10^{28}	-5.26	2980.	QRRK
5.	$OH + HO_2 \Leftrightarrow H_2O + O_2$	1.91×10^{16}	-1.0	0.	q
6.	$H + O_2 \Leftrightarrow OH + O$	2.10×10^{15}	-0.3	20200.	QRRK
7.	$OH + OH \Leftrightarrow O + H_2O$	1.50×10^{9}	1.14	99.4	c (unchanged)
8.	$O + HO_2 \Leftrightarrow OH + O_2$	3.25×10^{13}	0.	0.	c (unchanged)
	C_7H_7 reactions				
9.	$C_5H_5 + C_2H_2 \Leftrightarrow C_7H_7$	3.72×10^{11}	0.	8300.	i (unchanged)
10.	$C_7H_8 + OH \Leftrightarrow C_7H_7 + H_2O$	1.26×10^{13}	0.	2583.	h (unchanged)
	C_6H_6 reactions				
11.	$OH + C_6H_6 \Leftrightarrow C_6H_5OH + H$	1.34×10^{13}	0.	10592.	d (unchanged)
12.	$OH + C_6H_6 \Leftrightarrow C_6H_5 + H_2O$	1.63×10^{8}	1.42	1454.	c
13.	$O + C_6H_6 \Leftrightarrow C_6H_5O + H$	2.40×10^{13}	0.	4668.	e (unchanged)
	C_6H_5OH reactions				
14.	$H + C_6H_5O \Leftrightarrow C_6H_5OH$	2.50×10^{14}	0.	0.	d (unchanged)
15.	$OH + C_6H_5OH \Leftrightarrow H_2O + C_6H_5O$	1.39×10^{8}	1.43	-962.	f (unchanged)
16.	$C_6H_5OH + O \Leftrightarrow C_6H_5O + OH$	1.28×10^{13}	0.	2891.	r, s
17.	$C_6H_5OH + HO_2 \Leftrightarrow C_6H_5O + H_2O_2$	3.00×10^{13}	0.	15000.	j (unchanged)
18.	$C_6H_5OH + CH_2CHCHCH \Leftrightarrow C_4H_6 + C_6H_5O$	6.00×10^{12}	0.	0.	h (unchanged)
19.	$C_6H_5OH + CH_2CHCCH_2 \Leftrightarrow C_4H_6 + C_6H_5O$	6.00×10^{12}	0.	0.	h (unchanged)
20.	$C_6H_5OH + C_6H_5 \Leftrightarrow C_6H_6 + C_6H_5O$	4.91×10^{12}	0.	4400.	h (unchanged)
	C_6H_5O reactions				
21.	$C_6H_5O + C_5H_6 \Leftrightarrow C_5H_5 + C_6H_5OH$	3.16×10^{11}	0.	8000.	h (unchanged)
22.	$C_6H_5O \Leftrightarrow C_5H_5 + CO$	7.40×10^{11}	0.	43853.	t
23.	$C_6H_5O+O \Leftrightarrow C_6H_4O_2 + H$	3.00×10^{13}	0.	0.	s
	C_6H_5 reactions				
24.	$C_6H_5 + O \Leftrightarrow C_5H_5 + CO$	9.00×10^{13}	0.	0.	t
25.	$C_6H_5 + O_2 \Leftrightarrow C_6H_5O + O$	2.57×10^{-29}	12.73	-5699.	QRRK
26.	$C_6H_5 + O_2 \Leftrightarrow C_6H_5OO$	1.85×10^{13}	-0.15	-159.	QRRK
	C_6H_5OO reactions				

27.	$C_6H_5OO \Leftrightarrow C_6H_5O + O$	4.27×10^{15}	-0.7	33027.	QRRK
28.	$C_6H_5OO+H \Leftrightarrow C_6H_5OOH$	2.50×10^{14}	0.	0.	est. (see text)
29.	$C_6H_5O + OH \Leftrightarrow C_6H_5OOH$	1.00×10^{12}	0.	0.	est. (see text)
30.	$C_6H_5OO + C_6H_5OH \Leftrightarrow C_6H_5OOH + C_6H_5O$	$1.00\times10^{11.5}$	0.	6961.	est. (see text)
31.	$C_6H_5OO + HO_2 \Leftrightarrow C_6H_5OOH + O_2$	1.87×10^{12}	0.	1540.	est. (see text)
32.	$C_6H_5O + HO_2 \Leftrightarrow C_6H_5OO + OH$	1.50×10^{14}	0.	23650.	est. (see text)
33.	$C_6H_5OO \Leftrightarrow C_6H_4O_2 + H$	4.00×10^{8}	0.	0.	z
34.	$C_6H_5OO \Leftrightarrow C_5H_5 + CO_2$	1.60×10^{8}	0.	0.	z
	$C_6H_4O_2$ reactions				
35.	$C_6H_4O_2 \Leftrightarrow C_5H_4O + CO$	3.70×10^{11}	0.	59000.	v
36.	$C_6H_4O_2 \Leftrightarrow C_5H_4 + CO_2$	3.50×10^{12}	0.	67000.	v
37.	$C_6H_4O_2 + H \Leftrightarrow C_5H_5O + CO$	2.50×10^{13}	0.	4700.	v
38.	$C_6H_4O_2 + H \Rightarrow C_6H_3O_2 + H_2$	2.00×10^{12}	0.	8100.	v
39.	$C_6H_4O_2 + OH \Rightarrow C_6H_3O_2 + H_2O$	1.00×10^{6}	2.0	4000.	v
40.	$C_6H_4O_2 + O \Rightarrow C_6H_3O_3 + H$	1.50×10^{13}	0.	4530.	v
41.	$C_6H_4O_2 + O \Rightarrow C_6H_3O_2 + OH$	1.40×10^{13}	0.	14700.	v
					v
	$C_6H_3O_2$ reactions				
42.	$C_6H_3O_2 + H \Rightarrow 2C_2H_2 + 2CO$	1.00×10^{14}	0.	0.	v
43.	$C_6H_3O_2 + O \Rightarrow C_2H_2 + HCCO + 2CO$	1.00×10^{14}	0.	0.	v
44.	$C_6H_3O_3 \Rightarrow C_2H_2 + HCCO + 2CO$	1.00×10^{12}	0.	50000.	v
	C_5H_5O reactions				
45.	$C_5H_5O \Leftrightarrow CH_2CHCHCH + CO$	7.50×10^{11}	0.	43900.	v
	C_5H_4O reactions				
46.	$C_5H_4O \Leftrightarrow C_4H_4 + CO$	1.00×10^{12}	0.	0.	s
47.	$C_5H_4O + O \Rightarrow C_4H_4 + CO_2$	1.00×10^{13}	0.	2000.	v
48.	$C_5H_4O + H \Leftrightarrow CH_2CHCCH_2 + CO$	2.50×10^{13}	0.	4700.	v
49.	$C_5H_4O \Leftrightarrow 2C_2H_2 + CO$	1.00×10^{15}	0.	78000.	v
50.	$C_5H_4OH \Leftrightarrow C_5H_4O + H$	2.13×10^{13}	0.	48000.	h
	C_5H_4 reactions				
51.	$C_5H_4+H \Leftrightarrow C_5H_3+H_2$	1.00×10^{6}	2.5	5000.	v
52.	$C_5H_4+O \Leftrightarrow C_5H_3+OH$	1.00×10^{6}	2.5	3000.	v
53.	$C_5H_4+OH \Leftrightarrow C_5H_3+H_2O$	1.00×10^{7}	2.0	0.	v
	C_5H_3 reactions				
54.	$C_5H_3+O_2 \Leftrightarrow C_2H_2+HCCO+CO$	1.00×10^{12}	0.	0.	v
	C_5H_6 reactions				
55.	$C_5H_6+H \Leftrightarrow C_2H_2+ C_3H_5$	7.14×10^{-34}	15.1	14617.	QRRK
56.	$C_5H_6+H \Leftrightarrow C_5H_5+H_2$	1.20×10^{5}	2.5	1492.	u
57.	$C_5H_6+O \Leftrightarrow C_5H_5O1\_2+H$	1.00×10^{15}	-0.6	3669.	QRRK

58.	$C_5H_6+O \Leftrightarrow C_5H_5+OH$	4.77×10^{4}	2.7	1106.	u
59.	$C_5H_6+OH \Leftrightarrow C=CC.C=COH$	4.40×10^{10}	0.82	2914.	QRRK
60.	$C_5H_6+OH \Leftrightarrow C_5H_5+H_2O$	3.10×10^{6}	2.0	0.	u
61.	$C_5H_6+O_2 \Leftrightarrow C_5H_5+HO_2$	4.00×10^{13}	0.	37150.	u
62.	$C_5H_6+HO_2 \Leftrightarrow C_5H_5+H_2O_2$	1.10×10^{4}	2.6	12900.	u
63.	$C_5H_6+HCO \Leftrightarrow C_5H_5+CH_2O$	1.10×10^{8}	1.9	16000.	u
64.	$C_5H_6+CH_3 \Leftrightarrow C_5H_5+CH_4$	0.18×10^{0}	4.0	0.	u
65.	$C_5H_6+C_2H_3 \Leftrightarrow C_5H_5+C_2H_4$	0.12×10^{0}	4.0	0.	u
66.	$C_5H_6+C_3H_5 \Leftrightarrow C_5H_5+C_3H_6$	0.20×10^{0}	4.0	0.	u
67.	$C_5H_6+CH_2CHCHCH \Leftrightarrow C_5H_5+C_4H_6$	0.12×10^{0}	4.0	0.	u
68.	$C_5H_6+C_6H_5 \Leftrightarrow C_5H_5+C_6H_6$	0.10×10^{0}	4.0	0.	u
69.	$C_5H_6 + CH_2CHCCH_2 \Leftrightarrow C_5H_5 + C_4H_6$	6.00×10^{12}	0.	0.	h (unchanged)
	C_5H_5 reactions				
70.	$C_5H_5+H \Leftrightarrow C_5H_6$	3.20×10^{14}	0.0	0.	w (k_∞)
71.	$C_5H_5+O \Leftrightarrow C_5H_5O$	5.20×10^{30}	-5.96	3445.	QRRK
72.	$C_5H_5+O \Leftrightarrow C_5H_4O+H$	4.25×10^{15}	-0.56	1230.	QRRK
73.	$C_5H_5+O \Leftrightarrow CH_2CHCHCH+CO$	1.45×10^{1}	3.76	2213.	QRRK
74.	$C_5H_5+OH \Leftrightarrow C_5H_4OH+H$	3.63×10^{-48}	18.18	-3853.	QRRK
75.	$C_5H_5+HO_2 \Leftrightarrow C_5H_5O+OH$	6.19×10^{-31}	13.81	-4130.	QRRK
76.	$C_5H_5+HO_2 \Leftrightarrow C_5H_4O+H_2O$	9.46×10^{-32}	13.13	-4803.	QRRK
77.	$C_5H_5+O_2 \Leftrightarrow COC=CKET+H$	4.35×10^{7}	1.08	16737	QRRK
78.	$C_5H_5+O_2 \Leftrightarrow C=CC=C=O+HCO$	1.31×10^{-3}	4.41	16472.	QRRK
	C_4 reactions				
79.	$CH_2CHCCH_2 + O_2 \Leftrightarrow C_4H_4 + HO_2$	1.20×10^{11}	0.	0.	h (unchanged)
80.	$C_4H_4 + OH \Leftrightarrow H_2CCCCH + H_2O$	7.50×10^{6}	2.0	5000.	k (unchanged)
	C_2 reactions				
81.	$C_2H_3 + O_2 \Leftrightarrow CH_2O + HCO$	4.00×10^{12}	0.	-250.	k (unchanged)
82.	$C_2H_2 + H \Leftrightarrow C_2H_3$	7.85×10^{14}	-0.22	1770.	QRRK
	C_1 reactions				
83.	$CH_2O + OH \Leftrightarrow HCO + H_2O$	3.43×10^{15}	1.18	-447.	k (unchanged)
84.	$HCO + M \Leftrightarrow H + CO + M$	2.50×10^{14}	0.	16802.	k (unchanged)
85.	$CO + O \Leftrightarrow CO_2$	1.80×10^{10}	0.	2438.	x, y (k_∞)
86.	$CO + OH \Leftrightarrow CO_2 + H$	3.09×10^{11}	0.	735.	m (unchanged)

a: (Atkinson *et al.*, 1989), b: (Hippler *et al.*, 1990) fit to single exponential for temperatures around 800 K, c: (Baulch *et al.*, 1992), d: (He *et al.*, 1988), e: (Ko *et al.*, 1991), f: (Shandross *et al.*, 1996), g: (Shandross, 1996) QRRK calculation, h: (Emdee *et al.*, 1992), i: (Zhang and McKinnon, 1995), j: (Bittker, 1991), k: (Miller and Melius, 1992), l: (Shandross, 1996), m: (Dixon-Lewis, 1972), n: (Madronich and Felder, 1985), o: (McLain *et al.*, 1979), p: (Warnatz, 1984), q: (Kim *et al.*, 1994), r: (Baulch *et al.*, 1994), s: (Tan and Frank, 1996), t: (Frank *et al.*, 1994), u: (Zhong and Bozzelli, 1997), v: (Alzueta *et al.*, 1998), w: (Zhong and Bozzelli, 1998), x: (Troe, 1974), y: (Westmoreland *et al.*, 1986), z: treated as adjustable parameters.

primarily forms the stabilization product HO_2 with a rate close to the high-pressure limit reported by Cobos *et al.* (1985). The predicted rate constants for both pathways are given in Table 7-2 and Table 7-3. The analysis was also performed at temperatures and pressures where experimental measurements of the rate constants of the two pathways were available as a means of evaluating the quality of the predictions. Excellent agreement was obtained between the predicted and experimentally-measured rate constants for both the recombination reaction in the high- (Cobos *et al.*, 1985) and low-pressure limit (Baulch *et al.*, 1992) and the addition/elimination pathway in the low-pressure limit (Baulch *et al.*, 1992).

$OH + OH \leftrightarrow H_2O_2$ The dissociation of H_2O_2 has been recognized as an important source of OH radicals in SCWO detailed kinetic mechanisms (Phenix *et al.*, 1998). This recombination reaction competes with the reaction $OH + OH \leftrightarrow H_2O + O$, but evidence suggests these two reactions are completely independent (Forster *et al.*, 1995). Experimental measurements of the recombination rate constant at pressures approaching those of SCWO processes have recently become available (Forster *et al.*, 1995; Fulle *et al.*, 1996). In these studies, the recombination of OH was studied at temperatures between 200 and 700 K (-73 to 425°C) and at pressures up to 140 bar using a helium bath gas. Values of k_∞ were given at 210, 298, 406, 510, 614 and 694 K based on extrapolation of the measured fall-off curves. We fit this data with a modified Arrhenius fit to obtain an estimate of k_∞ for OH recombination:

$$k_\infty\left(\frac{\text{cm}^3}{\text{mol s}}\right) = 1.99\times10^{27}T^{-4.85}\exp(-2.76\,(\text{kcal/mol})/RT) \qquad (7\text{-}1)$$

At 298 K (25°C), this high-pressure rate constant is about a factor of 2 lower than the recommended k_∞ of Baulch *et al.* (1992).

CHEMACT was used to predict a rate constant for OH recombination at 246 bar and 300 to 1000 K (25 and 725°C) using the high-pressure rate constant in Eqn. (7-1). The predicted rate constant agreed well with the recently measured values at all temperatures and pressures (Forster *et al.*, 1995; Fulle *et al.*, 1996) as well as with a measurement by Zellner *et al.* (1988) at 298 K (25°C). The predicted rate constant for OH recombination to H_2O_2 at 246 bar and for temperatures between 300 and 1000 K (25 and 725°C) is shown in Table 7-2 and Table 7-3.

$OH + HO_2 \leftrightarrow H_2O + O_2$ The rate constant for this reaction was updated to the value used in a moist CO oxidation mechanism developed for pressures from 1 to 9.7 bar and temperatures of 960 to 1200 K (690 to 925°C) (Kim *et al.*, 1994). The rate constant was based on fitting the low temperature data of Keyser (1988) which is the value recommended by Baulch *et al.* (1994) and the high temperature measurements of Hippler and Troe (1992). The rate constants given in Table 7-2 and Table 7-3 reflect this modification.

The rate constant for the preceding reaction as well as those for $HO_2 + HO_2 \leftrightarrow H_2O_2 + O_2$ and $H_2O_2 + OH \leftrightarrow HO_2 + H_2O$ all exhibit a non-Arrhenius temperature behavior suggestive of the formation of a chemically-activated intermediate (Hippler *et al.*, 1990; Hippler and Troe, 1992; Hippler *et al.*, 1995). At present, these intermediates have not been experimentally observed and their formation is merely hypothesized. If this hypothesis proves correct, the rate constants of these three reactions will exhibit a pressure dependence. At present, a pressure dependence has only been observed in the case of the HO_2 self-reaction, but the rate constants of these reactions have only been explored at pressures below a few bars. Given that the values of these rate constants in Table 7-2 and Table 7-3 are based on low-pressure measurements, their use in the SCW benzene oxidation mechanism is a possible source of error.

$C_2H_3 \leftrightarrow C_2H_2 + H$ This reaction remains in its low pressure limit in the reduced mechanism in Table 7-1. The rate constant shown in Table 7-2 and Table 7-3 was calculated using CHEMACT at 246 bar for temperatures between 300 and 1000 K (25 and 725°C). The high pressure value of Warnatz (1984) was used in the calculation. The resulting predicted rate constant is close to its high-pressure limit at 246 bar.

$CO + O \leftrightarrow CO_2$ This reaction is also in its low pressure limit in the reduced mechanism in Table 7-1. This rate constant was previously analyzed using bimolecular QRRK by Westmoreland *et al.* (1986) using a value for k_∞ reported by Troe (1974). Good agreement was obtained between predictions and experimental measurements of the rate constant. Analysis of this reaction by CHEMACT at 246 bar with temperatures from 300 to 1000 K (25 to 725°C) showed the rate constant to be in its high pressure limit. The high-pressure limit value of Troe (1974) is given in Table 7-2 and Table 7-3.

$C_6H_5 + O_2 \leftrightarrow$ products The products of the reaction between phenyl and oxygen and the rate of their formation remains and issue of continuing study. In the Bittker, LS and EBG mechanisms, the products of this reaction were set equal to phenoxy (C_6H_5O) and O, and the rate constant was assumed independent of pressure. The ZM mechanism likewise included the pathway to C_6H_5O and O formation, but also included a semi-global pathway:

$$C_6H_5 + O_2 \leftrightarrow 2CO + C_2H_2 + C_2H_3$$

Frank *et al.* (1994) studied the reaction of phenyl with O_2 between 900 and 1800 K and 1.3 to 2.5 bar. Two channels for the reaction were suggested: the first led to the production of C_6H_5O and O; and the second to the formation of *p*-benzoquinone ($C_6H_4O_2$) and H. The second pathway was necessary to explain their observation of fast initial H production and is supported by the experimental observation of $C_6H_4O_2$ in benzene flames (Chai and Pfefferle, 1998). Rate constants were measured for these two overall pathways at their conditions.

At about the same time, Yu and Lin (1994) were performing a direct study on the reaction between C_6H_5 and O_2 at lower temperatures (297-500 K or 25-225°C) and pressures (20 to 80 torr). As discussed by Yu and Lin, the overall reactions leading to C_6H_5O and O or $C_6H_4O_2$ and H formation proceed first through the formation of an energized C_6H_5OO radical. The energized radical can either undergo stabilization to C_6H_5OO or dissociation with the rate for each pathway depending on both temperature and pressure. By monitoring formation of the C_6H_5OO radical, Yu and Lin calculated a rate constant for the reaction between C_6H_5 and O_2. At the temperatures and pressures of their study, the rate constant was found to be pressure independent and the sole reaction product was stabilized C_6H_5OO. Using the rate constants for the addition/elimination pathways of Frank *et al.* (1994), Yu and Lin performed an RRKM calculation to determine the relative contribution of the three pathways to the overall rate as a function of temperature for pressures between 20 and 80 torr. Below 1000 K (775°C), the addition/stabilization pathway leading to the formation of C_6H_5OO was found to dominate.

Shandross performed his own QRRK calculation for the overall pathway to C_6H_5O and O for his conditions. The rate constant listed in Table 7-1 is that calculated for his 22 torr flame. Shandross did not include the pathway to $C_6H_4O_2$ formation, but did include the semi-global pathway used in the ZM model (Reaction 24 in Table 7-1).

Tan and Frank (1996) included both addition/elimination pathways leading to C_6H_5O and $C_6H_4O_2$ in their mechanism. They stated their opposition to the semi-global pathway used in the ZM and Shandross mechanisms. The rate constants for the two pathways were taken from Frank *et al.* (1994), but they set the rate constant for C_6H_5O and O production to half of their measured value presumably to improve model-data agreement.

Since the reaction of C_6H_5 and O_2 proceeds through the formation of C_6H_5OO, the rates for the addition/elimination pathways measured by Frank *et al.* or calculated by Shandross are not applicable at the lower temperatures and much higher pressures of SCWO. CHEMDIS was used to calculate the rates of the stabilization and addition/elimination pathway to C_6H_5O and O formation. The rate constant measurement of Yu and Lin (1994) was used as the high-pressure rate constant for C_6H_5OO formation. To estimate the high-pressure rate constant for dissociation of the energized C_6H_5OO radical ($C_6H_5OO^*$) to C_6H_5O and O required for the bimolecular QRRK analysis, the rate constant for the reverse reaction was assumed to proceed with a preexponential factor for diffusion controlled reactions ($A=10^{12}$ cm^3 mol^{-1} s^{-1}) and no energy barrier ($E_a=0$). The dissociation rate was then calculated from microscopic reversibility. A comparison between the predicted value of the rate constant for the addition/elimination pathway with the measured value by Frank *et al.* (1994) at 2.3 bar and from 1000 to 1200 K (725 to 925°C) is given in Table 7-4. Agreement between the predicted and experimental rate constants is within 10 to 20%, indicating that the estimated value of k_∞ for $C_6H_5OO^*$ dissociation to C_6H_5O and O may not be a source of significant error.

Table 7-4. Comparison of predicted and experimental rate constants at 2.3 bar for the overall reaction $C_6H_5+O_2 \Leftrightarrow C_6H_5O+O$

T (K)	Measured by Frank *et al.*	Predicted by QRRK
1000	1.2×10^{12}	1.6×10^{12}
1100	1.6×10^{12}	2.0×10^{12}
1200	2.0×10^{12}	2.2×10^{12}

At 813 K (540°C) and 246 bar, the stabilization rate is calculated to be faster than the rate for addition/elimination to C_6H_5O and O by two orders of magnitude. With C_6H_5OO being the main reaction product, other possible reactions of C_6H_5OO were estimated. These additional reactions are given in Table 7-5 and included in the SCW benzene oxidation mechanism (Table 7-3). The chemical structures of selected C_5 and C_6 species are given in Figure 7-2 for reference.

Table 7-5. Additional postulated reactions involving C_6H_5OO included in the present SCW benzene oxidation mechanism

Reaction	A (cm^3-mol-s)	n	E_a (cal/mol)
1. $C_6H_5OO+H \Leftrightarrow C_6H_5OOH$	2.5×10^{14}	0	0
2. $C_6H_5O + OH \Leftrightarrow C_6H_5OOH$	1.0×10^{12}	0	0
3. $C_6H_5OO + C_6H_5OH \Leftrightarrow C_6H_5OOH + C_6H_5O$	$1.0\times10^{11.5}$	0	6961
4. $C_6H_5OO + HO_2 \Leftrightarrow C_6H_5OOH + O_2$	1.87×10^{12}	0	1540
5. $C_6H_5O + HO_2 \Leftrightarrow C_6H_5OO + OH$	1.50×10^{14}	0	2365

k_1 Estimated from $C_6H_5O+H \Leftrightarrow C_6H_5OH$ (He *et al.*, 1988).

k_2 Rate constant assumed to have a preexponential factor for diffusion controlled reactions ($A=10^{12}$ cm^3 mol^{-1} s^{-1}) and no energy barrier ($E_a=0$).

k_3 Estimated from the reaction of poly(peroxystyrl)peroxyl radical with phenol using the measurement of $k_3=10^7$ cm^3 mol^{-1} s^{-1} at 65°C (Howard and Ingold, 1963) and assumed $A=10^{11.5}$ to infer E_a.

k_4 Estimated from $HO_2+HO_2 \Leftrightarrow H_2O_2+O_2$ (Baulch *et al.*, 1992).

k_5 Estimated from $CO+ HO_2 \Leftrightarrow CO_2+OH$ (Tan *et al.*, 1994).

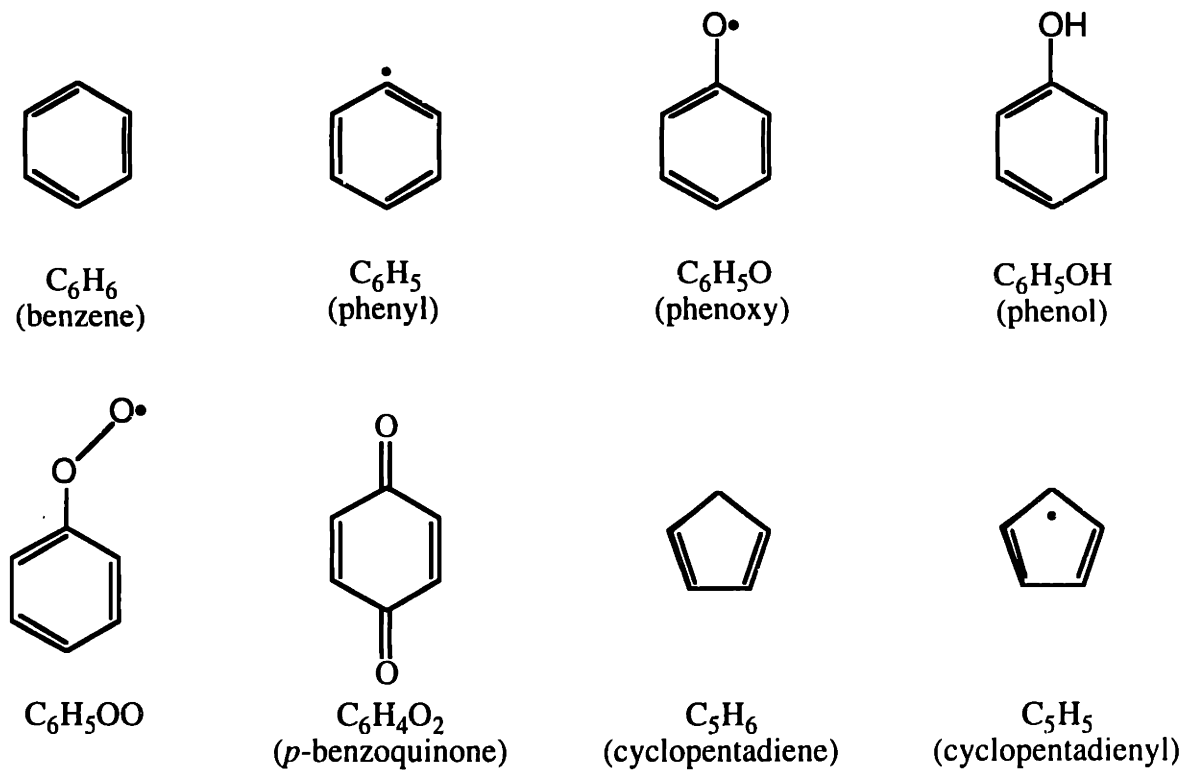

Figure 7-2 Chemical stuctures of selected C_5 and C_6 species

In addition to the reactions of C_6H_5OO given in Table 7-5, also included in the model were reactions for the dissociation of the stabilized intermediate C_6H_5OO. The rate constant for C_6H_5OO dissociation to C_6H_5O and O was calculated in the QRRK analysis and is given in Table 7-3. With no rate constants available for the dissociation pathway of C_6H_5OO leading to $C_6H_4O_2$ and H, and with an estimate of the rate constant not being straightforward since the reaction is thought to proceed through the creation of an O—O bridge across the C_6 ring (Yu and Lin, 1994), this rate constant was treated as an adjustable parameter in the present model. Another dissociation pathway of C_6H_5OO, which was proposed by Carpenter (1993), leads to the formation of C_5H_5 and CO_2. Inclusion of this pathway was also tested in the present model, again by treating the rate constant as an adjustable parameter. The effects of the inclusion of these two additional dissociation pathways and the values of their rate constants in Table 7-3 will be discussed in detail in the analysis of the final mechanism. The semi-global reaction between C_6H_5 and O_2 (reaction 24 in Table 7-1) was removed from the mechanism as the reaction between C_6H_5 and O_2 is already accounted for in the mechanism in Table 7-3. The removal of this semi-global reaction is supported by both Tan and Frank (1996) and Shandross (1996).

<u>*p*-Benzoquinone ($C_6H_4O_2$) Submechanism.</u> Included in the SCW benzene oxidation mechanism in Table 7-3 are two pathways leading to the formation of $C_6H_4O_2$. The first:

$$C_6H_5O + O \leftrightarrow C_6H_4O_2 + H \qquad \text{(R23 in Table 7-3)}$$

was proposed by Frank *et al.* (1994) and used in the Tan and Frank benzene oxidation mechanism (1996). The second pathway:

$$C_6H_5OO \leftrightarrow C_6H_4O_2 + H \qquad \text{(R33 in Table 7-3)}$$

is speculated to occur in the present work. The effect of the inclusion of this reaction will be discussed later. Tan and Frank (1996) assumed $C_6H_4O_2$ decomposed to C_5H_4O and CO, and C_5H_4O to C_4H_4 and CO at their conditions. Here, we include the recently developed submechanism for *p*-benzoquinone oxidation (Alzueta *et al.*, 1998) to account for further reactions of $C_6H_4O_2$. The specific reactions included from the $C_6H_4O_2$ submechanism appear in Table 7-6 and Table 7-3.

Table 7-6. Reactions used in the present SCW benzene oxidation model from the *p*-benzoquinone mechanism of Alzueta *et al.* (1998)

Reaction		A (cm^3-mol-s)	n	E_a (cal/mol)
1.	$C_6H_4O_2 \Leftrightarrow C_5H_4O+CO$	3.7×10^{11}	0	59000
2.	$C_6H_4O_2 \Leftrightarrow C_5H_4+CO_2$	3.5×10^{12}	0	67000
3.	$C_6H_4O_2+H \Leftrightarrow C_5H_5O+CO$	2.5×10^{13}	0	4700
4.	$C_6H_4O_2+H \Rightarrow C_6H_3O_2+H_2$	2.0×10^{12}	0	8100
5.	$C_6H_4O_2+OH \Rightarrow C_6H_3O_2+H_2O$	1.0×10^{6}	2.0	4000
6.	$C_6H_4O_2+O \Rightarrow C_6H_3O_3+H$	1.5×10^{13}	0	4530
7.	$C_6H_4O_2+O \Rightarrow C_6H_3O_2+OH$	1.4×10^{13}	0	14700
8.	$C_6H_3O_2+H \Rightarrow C_2H_2+C_2H_2+CO+CO$	1.0×10^{14}	0	0
9.	$C_6H_3O_2+O \Rightarrow C_2H_2+HCCO+CO+CO$	1.0×10^{14}	0	0
10.	$C_6H_3O_3 \Rightarrow C_2H_2+HCCO+CO+CO$	1.0×10^{12}	0	50000
11.	$C_5H_5O \Leftrightarrow CH_2CHCHCH+CO$	7.5×10^{11}	0	43900
12.[a]	$C_5H_4O \Leftrightarrow C_4H_4+CO$	1.0×10^{12}	0	0
13.	$C_5H_4O \Leftrightarrow C_2H_2+C_2H_2+CO$	1.0×10^{15}	0	78000
14.	$C_5H_4O+O \Rightarrow C_4H_4+CO_2$	1.0×10^{13}	0	2000
15.	$C_5H_4O+H \Leftrightarrow CH_2CHCCH_2+CO$	2.5×10^{13}	0	4700
16.	$C_5H_4+H \Leftrightarrow C_5H_3+H_2$	1.0×10^{6}	2.5	5000
17.	$C_5H_4+O \Leftrightarrow C_5H_3+OH$	1.0×10^{6}	2.5	3000
18.	$C_5H_4+OH \Leftrightarrow C_5H_3+H_2O$	1.0×10^{7}	2.0	0
19.	$C_5H_3+O_2 \Leftrightarrow C_2H_2+HCCO+CO$	1.0×10^{12}	0	0

[a]This reaction was taken from Tan and Frank (1996)

Cyclopentadiene and Cylcopentadienyl Reactions. The reactions and associated rate constants of the reactions involving C_5H_5 and C_5H_6 in the Shandross mechanism, some of which are included in the reduced mechanism of Table 7-1, were taken from the EBG mechanism (Emdee *et al.*, 1992). Emdee *et al.* estimated the abstraction of H from C_5H_6 by HO_2, OH, H and O from the analogous reactions with formaldehyde and based the C_5H_5 submechanism on the outline presented by Brezinsky (1986).

As discussed in Section 7.1.2, Zhong and Bozzelli (1997; 1998) recently published a submechanism for reactions of C_5H_5 and C_5H_6 with H, O, OH, HO_2 and O_2 for insertion in combustion mechanisms where these species are important. Using the thermodynamic data, high-pressure rate constants, vibrational frequencies and Lennard-Jones parameters presented in these papers, we repeated their QRRK calculations using CHEMDIS to predict rate constants for the addition and combination reactions of C_5H_5 and C_5H_6 at 246 bar from 300 to 1000 K (25 to 775°C). The reactions between C_5H_5 and C_5H_6 with O_2 and the radical species with the highest rate

constants at 540°C (813 K) are included in the SCW benzene oxidation mechanism (Table 7-3) and also shown in Table 7-7. Reaction 26 in Table 7-1 was removed as that pathway was not included by Zhong and Bozzelli (1997). The rates of the H abstraction reactions of C_5H_6 by H, O, OH, HO_2 and O_2 given by Zhong and Bozzelli (1997) are generally faster than the predicted rates of the addition/elimination pathways. Reactions 1, 3 and 5 in Table 7-7 constitute the only non-abstraction reactions of C_5H_6. Resonantly stabilized C_5H_5, instead, reacts exclusively via combination or addition/elimination pathways.

Table 7-7. The dominating reactions of the C_5H_6/C_5H_5 submechanism of Zhong and Bozzelli (1997; 1998) with rate constants calculated at 246 bar and for 300 to 1000 K.

Reaction		A (cm^3-mol-s)	n	E_a (cal/mol)	Ref.
1.	$C_5H_6+H \Leftrightarrow C_2H_2+C_3H_5$	7.14×10^{-34}	15.1	14617	a
2.	$C_5H_6+H \Leftrightarrow C_5H_5+H_2$	1.2×10^{5}	2.5	1492	b
3[d].	$C_5H_6+O \Leftrightarrow C_5H_5O1\_2+H$	1.0×10^{15}	-0.6	3669	a
4.	$C_5H_6+O \Leftrightarrow C_5H_5+OH$	4.77×10^{4}	2.7	1106	b
5[d].	$C_5H_6+OH \Leftrightarrow C=CC.C=COH$	4.4×10^{10}	0.82	2914	a
6.	$C_5H_6+OH \Leftrightarrow C_5H_5+H_2O$	3.1×10^{6}	2.0	0	b
7.	$C_5H_6+O_2 \Leftrightarrow C_5H_5+HO_2$	4.0×10^{13}	0	37150	b
8.	$C_5H_6+HO_2 \Leftrightarrow C_5H_5+H_2O_2$	1.1×10^{4}	2.6	12900	b
9.	$C_5H_6+HCO \Leftrightarrow C_5H_5+CH_2O$	1.1×10^{8}	1.9	16000	b
10.	$C_5H_6+CH_3 \Leftrightarrow C_5H_5+CH_4$	0.18×10^{0}	4.0	0	b
11.	$C_5H_6+C_2H_3 \Leftrightarrow C_5H_5+C_2H_4$	0.12×10^{0}	4.0	0	b
12.	$C_5H_6+C_3H_5 \Leftrightarrow C_5H_5+C_3H_6$	0.2×10^{0}	4.0	0	b
13.	$C_5H_6+CH_2CHCHCH \Leftrightarrow C_5H_5+C_4H_6$	0.12×10^{0}	4.0	0	b
14.	$C_5H_6+C_6H_5 \Leftrightarrow C_5H_5+C_6H_6$	0.1×10^{0}	4.0	0	b
15.	$C_5H_5+H \Leftrightarrow C_5H_6$	3.2×10^{14}	0	0	c
16.	$C_5H_5+O \Leftrightarrow C_5H_5O$	5.2×10^{30}	-5.96	3445	a
17.	$C_5H_5+O \Leftrightarrow C_5H_4O+H$	4.25×10^{15}	-0.56	1230	a
18.	$C_5H_5+O \Leftrightarrow CH_2CHCHCH+CO$	1.45×0^{1}	3.76	2213	a
19.	$C_5H_5+OH \Leftrightarrow C_5H_4OH+H$	3.63×0^{-48}	18.18	-3853	a
20.	$C_5H_5+HO_2 \Leftrightarrow C_5H_5O+OH$	6.19×0^{-31}	13.81	-4130	a
21.	$C_5H_5+HO_2 \Leftrightarrow C_5H_4O+H_2O$	9.46×0^{-32}	13.13	-4803	a
22[d].	$C_5H_5+O_2 \Leftrightarrow COC=CKET+H$	4.35×0^{7}	1.08	16737	a
23[d].	$C_5H_5+O_2 \Leftrightarrow C=CC=C=O+HCO$	1.31×0^{-3}	4.41	16472	a

a The QRRK calculated rate constant computed by CHEMDIS using the parameters in Zhong and Bozzelli (1997; 1998) as input.
b Abstraction reaction using the rate constants of Zhong and Bozzelli (1997).
c k_∞ (Zhong and Bozzelli, 1998).
d Chemical formulas of products taken from Zhong and Bozzelli (1997; 1998). See reference sources for chemical structures.

Several additional rate constants in Table 7-1 underwent minor modifications. The rate constant for reaction 11, the abstraction of H from C_6H_6 by OH, was updated to the recommended value of Baulch *et al.* (1992) which is not significantly different from the value used by Shandross (Madronich and Felder, 1985). The abstraction of the phenolic H from phenol by O (reaction 17) was updated to the value recommended by Baulch *et al.* (1994) and used by Tan and Frank (1996). At 813 K (540°C) this rate constant is an order of magnitude larger than that used by Shandross (Emdee *et al.*, 1992), but changing the value did not affect the predicted benzene profile and only had a small effect on the phenol profile. The thermal decomposition of phenoxy (reaction 23) was updated from the value used in the ZM model to reflect the recently reported value of Frank *et al.* (1994). Again, this change did not affect the benzene profile but did impact that of phenol. Reaction 33, as reported in Table 7-1, is written in the reverse direction as reported in the original source (Emdee *et al.*, 1992) with the rate constant calculated by microscopic reversibility. In Table 7-2 this reaction is written in the direction for which the rate constant was originally estimated (Emdee *et al.*, 1992) to avoid errors which would result from updates to the species thermochemistry. This change did not affect the benzene, phenol, CO or CO_2 profiles.

The final reduced elementary reaction mechanism for benzene oxidation in SCW used in this study appears in Table 7-3 and incorporates all changes previously discussed. The full mechanism can be found in Appendix 10.3. Note that the sources of the rate constants are given, and those marked with the reference "QRRK" were calculated at a pressure of 246 bar and for temperatures between 300 and 1000 K (25 and 775°C) using CHEMDIS. A discussion of the effects of these changes on the predicted species concentration profiles follows.

7.3 Comparison of Model Predictions to Benzene SCWO Data

The effects of the updates to individual rate constants and the addition of new reaction pathways presented in Section 7.2.1 on the model predictions are discussed below. The changes made to the mechanism in Table 7-1 to produce the SCW benzene oxidation model in Table 7-3 are grouped into eight "Modifications." Each "Modification" refers either to a single or many individual updates to rate constants and the addition or elimination of specific reactions. Several changes were grouped into a single "Modification" when the individual revisions did not invoke an appreciable change in the predicted benzene concentration. Each subsequent "Modification" includes the changes incorporated into all prior "Modifications" in addition to the changes specific

to that "Modification." The alterations which make up each "Modification" are discussed in the subsections that follow and summarized in the figure captions. All reaction numbers are in reference to those in Table 7-3.

7.3.1 The effects of early modifications to the reduced mechanism on concentration predictions

Figure 7-3 and Figure 7-4 display the outcome of the first four "Modifications" on the predicted benzene and phenol concentration profiles. The predictions of the reduced mechanism of Table 7-1 are also shown for reference. The first modification (Modification 1) consists of: the use of the QRRK calculated rate constants for the reactions between H and O_2 (R1 and R6), the

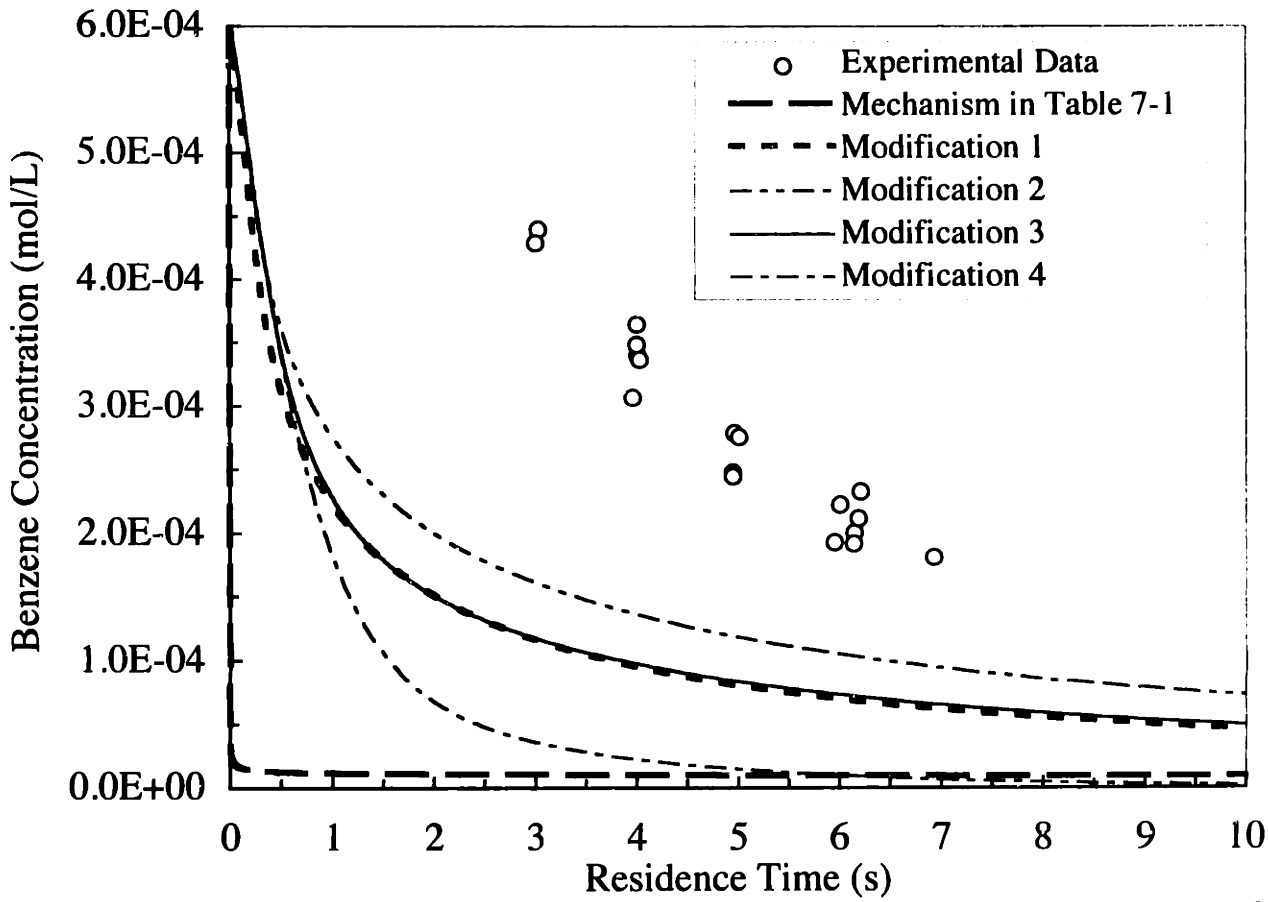

Figure 7-3 Effect of modifications to the benzene oxidation mechanism in Table 7-1 on the predicted benzene concentration
(T=813 K, P=246 bar, Φ=1.0, $[C_6H_6]_0=0.6\times10^{-3}$ mol/L); Modification 1: uses the QRRK predicted rate constants as calculated by CHEMACT or CHEMDIS for R1, R4, R6, R25-R27, R82 and R85 and incorporates the reactions of C_6H_5OO (R28-R32). Modification 2: removal of R24 fromTable 7-1 and update the rate constants of R5 and R12. Modification 3: update rate constants of R16 and R22. Modification 4: insertion of the C_6H_5/C_5H_6 submechanism (R55-R68, R70-R78).

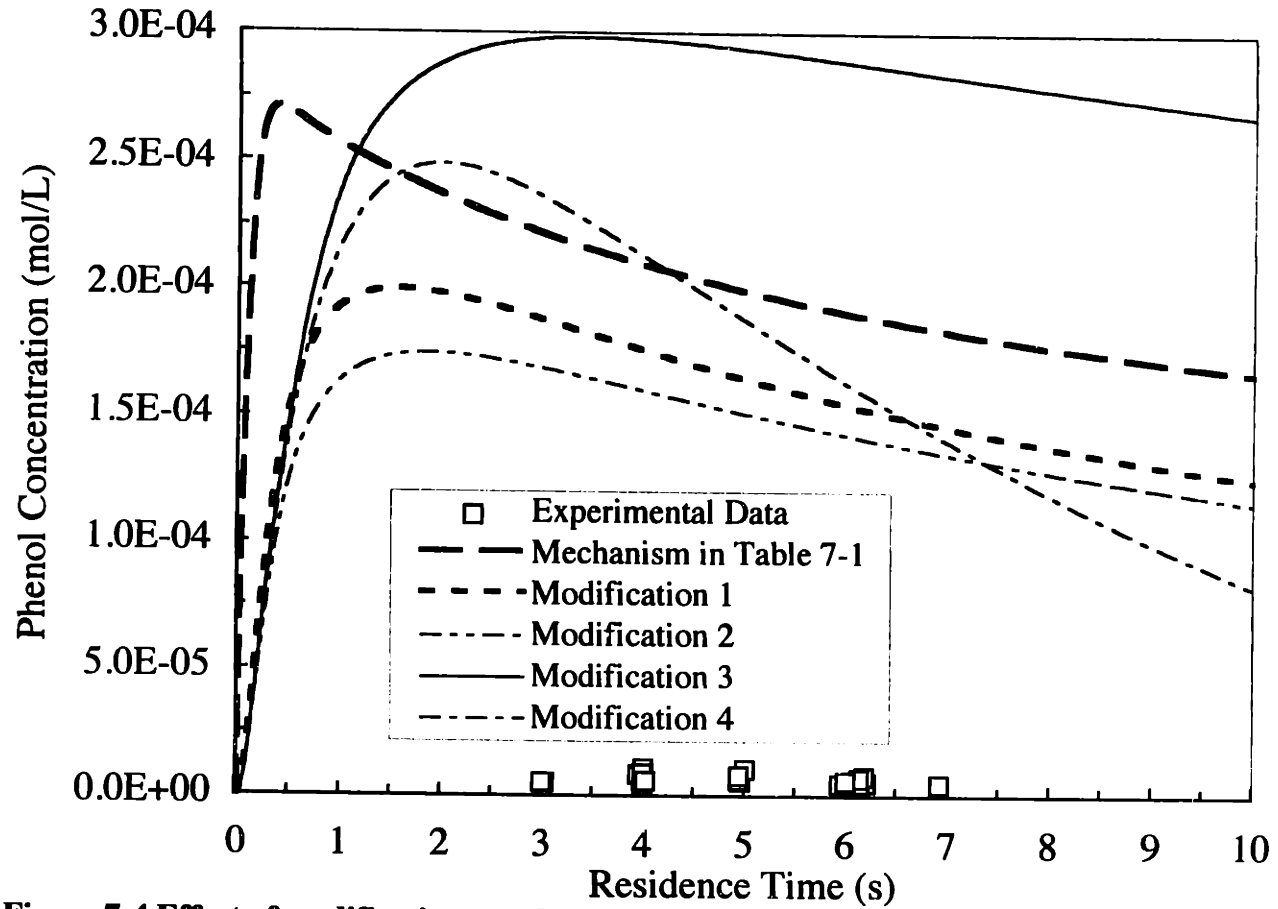

Figure 7-4 Effect of modifications to the benzene oxidation mechanism in Table 7-1 on the predicted phenol concentration
(T=813 K, P=246 bar, Φ=1.0, $[C_6H_6]_0=0.6\times10^{-3}$ mol/L); Modification 1: uses the QRRK predicted rate constants as calculated by CHEMACT or CHEMDIS for R1, R4, R6, R25-R27, R82 and R85 and incorporates the reactions of C_6H_5OO (R28-R32). Modification 2: removal of R24 fromTable 7-1 and update the rate constants of R5 and R12. Modification 3: update rate constants of R16 and R22. Modification 4: insertion of the C_5H_5/C_5H_6 submechanism (R55-R68, R70-R78).

recombination of OH to H_2O_2 (R4), the reactions between phenyl and O_2 (R25 and R26), the dissociation of C_6H_5OO to C_6H_5O and O (R27), the combination of H and C_2H_2 (R82) and the combination of O and CO (R85); and the incorporation of the reactions involving C_6H_5OO (R28 - R32) with the exception of the two speculated dissociation reactions of C_6H_5OO (R33 and R34). These changes had the effect of slowing the benzene oxidation rate and delaying the formation of phenol. Most of the abatement in the reaction rate was a consequence of the inclusion of the C_6H_5OO reactions (R28-R32). These reactions provide the C_6H_5OO radical with alternate pathways to thermal decomposition to C_6H_5O and O (R27). The fact that the usage of rate constants predicted by CHEMACT and CHEMDIS for R1, R4, R6, R25-R27, R82 and R85 did not significantly alter the predictions of the mechanism without including R28-R32 does not

necessarily indicate insensitivity of the mechanism shown in Table 7-3 to their rate constants since the model's sensitivity to individual rate constants changes when the values of other rate constants change or reactions are added or removed.

Modifications 2 through 4 did not give rise to a notable change in the shape of the benzene concentration profile and only altered the extent of the reaction. Phenol concentration is still overpredicted (Figure 7-4) by about two orders of magnitude. Modification 2 consists of the removal of the semi-global pathway of the reaction between C_6H_5 and O_2 to C_2H_2, C_2H_3 and CO (R24 in Table 7-1), the use of the rate constant of Kim *et al.* (1994) for the reaction between OH and HO_2 forming H_2O and O_2 (R5) and updating the rate constant for the abstraction of H from C_6H_6 by OH yielding C_6H_5 and H_2O (R12). Of these, the removal of the semi-global pathway has the largest influence on the model predictions. Modification 3 comprises updating the rate constants of the abstraction of the phenolic H from C_6H_5OH by O atom producing C_6H_5O and OH (R16) and for the thermal dissociation of C_6H_5O to C_5H_5 and CO (R22). Modification 4 constitutes the insertion of the C_5H_5/C_5H_6 submechanism (R55-R68 and R70-R78) first presented in Table 7-6.

Figure 7-5 shows the effects of the final set of modifications performed to produce the mechanism in Table 7-3 on the predicted benzene concentration. "Modification 4" from Figure 7-3 is also shown in Figure 7-5 to aid in the comparison of the two graphs. The prediction labeled "Modification 5" is a consequence of: adding the addition/elimination reaction between C_6H_5 and O to produce C_5H_5 and CO (R24) (Frank *et al.*, 1994) and revising the rate constant for C_5H_4OH thermal decomposition to C_5H_4O and H to $k_{f,50}=2.13\times10^{13}\exp(-48000/RT)$ (R50), both of which did not alter the predicted benzene concentration; introducing the reaction between C_6H_5O and O to produce $C_6H_4O_2$ and H (R23) which was first used in the Tan and Frank benzene mechanism (1996); and inserting the $C_6H_4O_2$ submechanism of Alzueta *et al.* (1998) (R35-R45, R47-R49, R51-R54) to account for the further reactions of $C_6H_4O_2$.

7.3.2 Inclusion of additional dissociation pathways for C_6H_5OO

Based on recent experimental and/or theoretical evidence for the formation of $C_6H_4O_2$ and H as well as C_5H_5 and CO_2 from the reaction between C_6H_5 and O_2, the inclusion of dissociation reactions of the stabilized C_6H_5OO adduct leading to these products were tested in the present mechanism. Frank *et al.* (1994) measured a rate constant for the overall reaction between C_6H_5 and O_2 leading to $C_6H_4O_2$ and H which was incorporated into the benzene oxidation mechanism of Tan

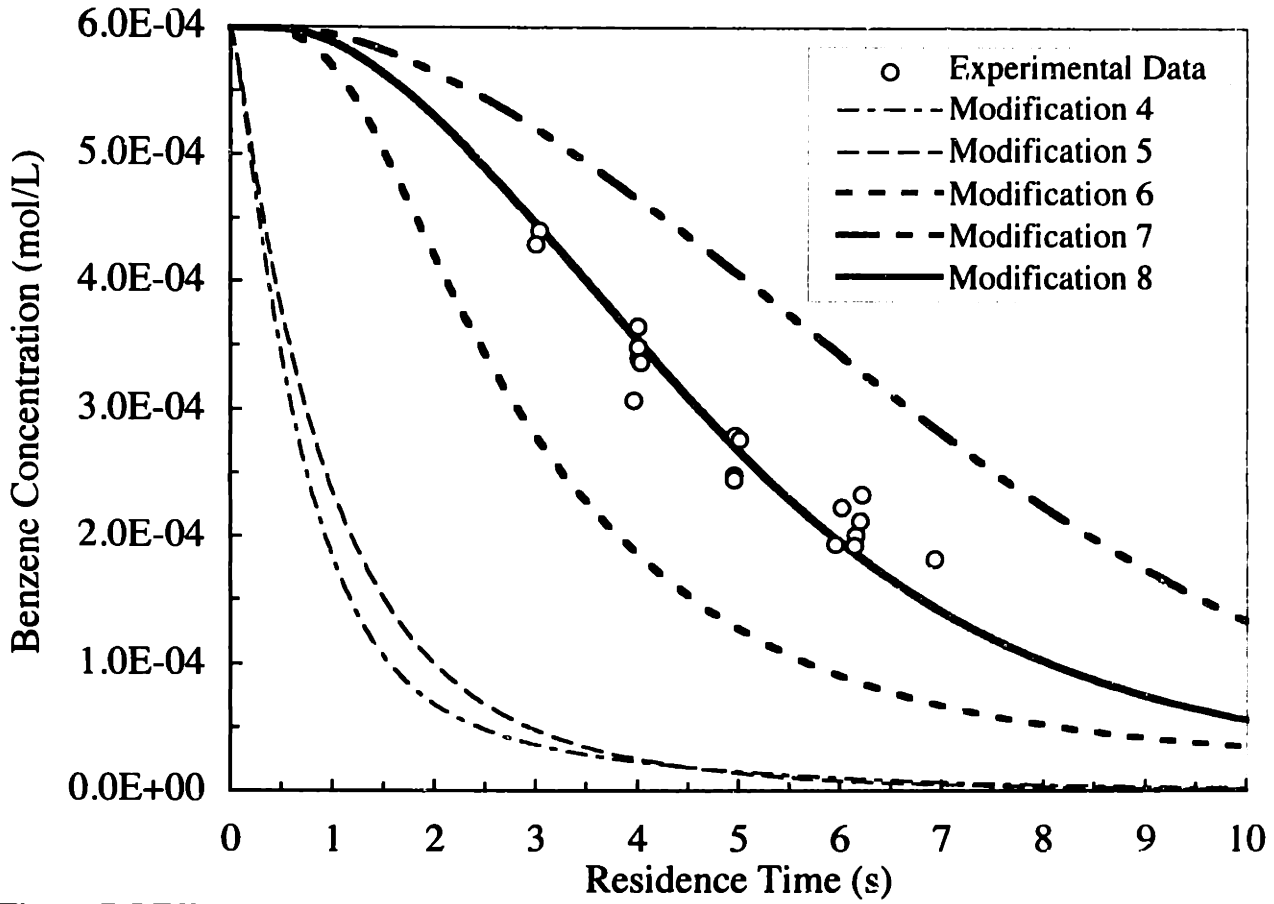

Figure 7-5 Effect of modifications to the benzene oxidation mechanism in Table 7-1 on the predicted benzene concentration
(T=813 K, P=246 bar, Φ=1.0, $[C_6H_6]_0=0.6\times10^{-3}$ mol/L); Modification 4: insertion of the C_5H_5/C_5H_6 submechanism (R55-R68, R70-R78). Modification 5: insertion of R23, R24, update rate constant of R50 and include $C_6H_4O_2$ submechanism (R35-R45, R47-R49, R51-R54). Modification 6: include $C_6H_5OO\Leftrightarrow C_6H_4O_2+H$ (R33) with $k_{f,33}=4.0\times10^8$. Modification 7: include $C_6H_5OO\Leftrightarrow C_6H_4O_2+H$ (R33) with $k_{f,33}=4.0\times10^8$ and $C_6H_5OO\Leftrightarrow C_5H_5+CO_2$ (R34) with $k_{f,34}=4.0\times10^8$. Modification 8: include $C_6H_5OO\Leftrightarrow C_6H_4O_2+H$ (R33) with $k_{f,33}=4.0\times10^8$ and $C_6H_5OO\Leftrightarrow C_5H_5+CO_2$ (R34) with $k_{f,34}=1.6\times10^8$.

and Frank (1996). As discussed in Section 7.2, the reaction between C_6H_5 and O_2 predominantly leads to the formation of the C_6H_5OO adduct at 246 bar and 813 K (540°C). Included in the mechanism of Table 7-3 are the rate constants predicted by CHEMDIS for: the addition/elimination reaction between C_6H_5 and O_2 leading to C_6H_5O and O (R25); the stabilization pathway (R26) to C_6H_5OO; and the thermal dissociation of stabilized C_6H_5OO to C_6H_5O and O (R27). As a test, the thermal dissociation of C_6H_5OO to $C_6H_4O_2$ and H (R33) and its reverse reaction with the rate constant calculated by microscopic reversibility were included in the oxidation mechanism in place of the addition/elimination reaction used by Tan and Frank (1996). As there are no measured rate

constants for the dissociation pathway to $C_6H_4O_2$ and H, the forward rate constant for this reaction was chosen to provide a best fit to the experimental data and will be discussed shortly.

Inclusion of R33 improves the agreement between the data and the predicted benzene and phenol concentration profiles. Figure 7-5 reveals that including R33 ("Modification 6") primarily increases the induction time but also somewhat moderates the rate of reaction of benzene. The induction time can be varied from 0 to a maximum of approximately 1 second by changing the rate constant of R33. The benzene concentration profile "Modification 6" represents the slowest benzene oxidation rate that can be achieved through adjustment of R33 alone. As seen in Figure 7-6 the predicted phenol concentration is in agreement with the experimental measurements with the inclusion of R33 in the mechanism. With all reactions which lead to phenol formation involving C_6H_5O with the exception of R11, and given that R11 is not competitive with R12 at these conditions as is discussed shortly, the fact that the experimental and predicted phenol concentrations are in agreement would indicate that the C_6H_5O concentration is now properly predicted if the C_6H_5O/C_6H_5OH chemistry is correctly represented in the model. The role of R33 is to provide another alternate to R27 for C_6H_5OO consumption, thereby preventing excess C_6H_5O formation.

Figure 7-7 shows the CO and CO_2 concentration predictions after incorporation of R33. Both CO and CO_2 are underpredicted by the model by up to two orders of magnitude. More importantly, the model predicts that the CO_2 concentration remains below that of CO while the data clearly show that the CO_2 concentration always exceeds that of CO for all measured residence times.

As mentioned in Section 7.2, Carpenter (1993) suggested the reaction of C_6H_5 and O_2 could lead to the formation of C_5H_5 and CO_2. This reaction has not been incorporated into any previous benzene oxidation mechanisms. Support for this and similar reactions which would lead to the early formation of CO_2 comes through experimental observations of very early CO_2 appearance in phenol, substituted phenols and benzene SCWO and in benzene combustion. Chai and Pfefferle (1998) measured unexpectedly high amounts of CO_2 at low benzene conversions during their study of benzene combustion between 900 and 1300 K. They postulated that the CO_2 was produced by other routes than through the reaction between OH and CO. Savage *et al.* observed CO_2 yields that always exceeded those of CO in their SCWO studies of phenol (Gopalan and Savage, 1995) and

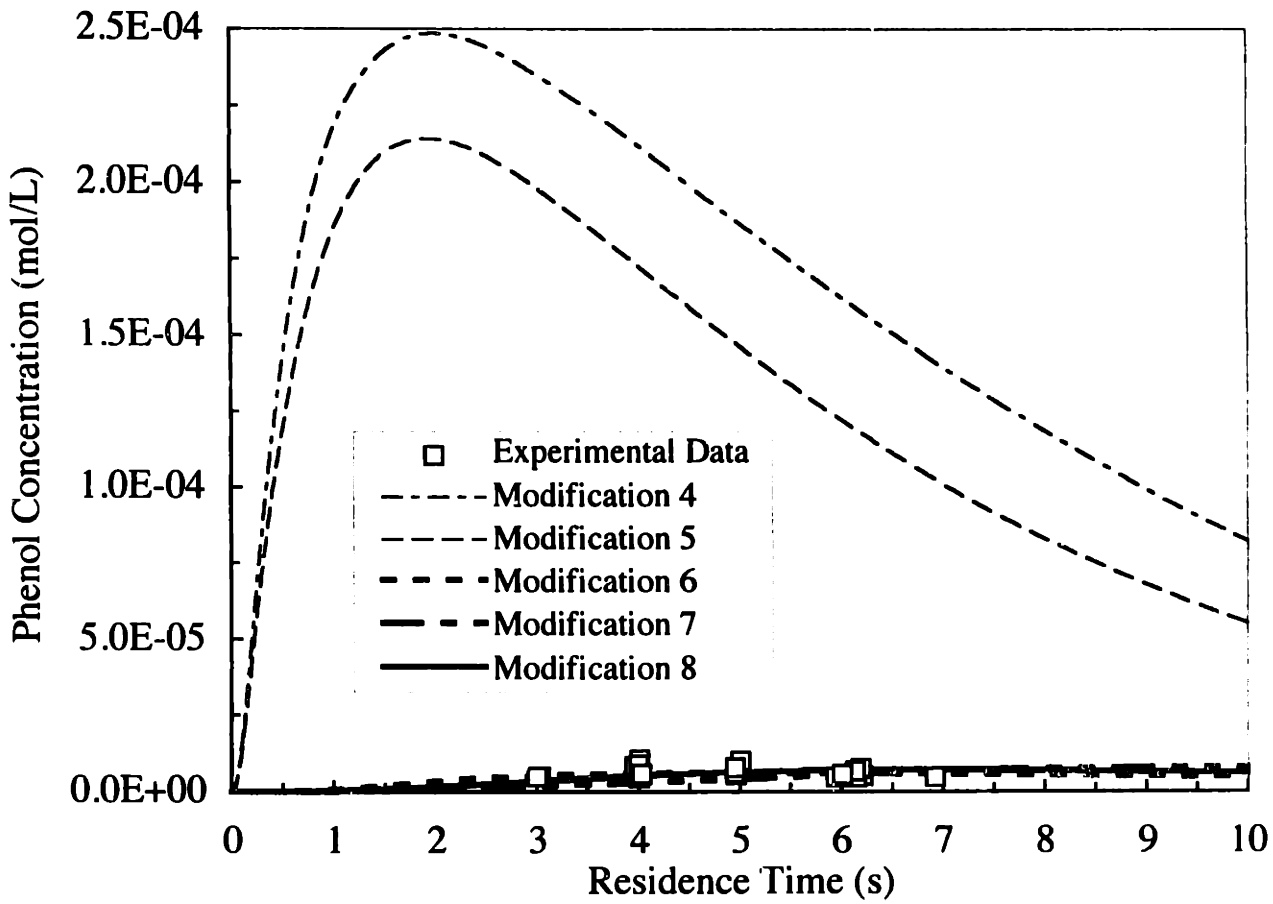

Figure 7-6 Effect of modifications to the benzene oxidation mechanism in Table 7-1 on the predicted phenol concentration
(T=813 K, P=246 bar, Φ=1.0, $[C_6H_6]_0=0.6\times10^{-3}$ mol/L); Modification 4: insertion of the C_5H_5/C_5H_6 submechanism (R55-R68, R70-R78). Modification 5: insertion of R23, R24, update rate constant of R50 and include $C_6H_4O_2$ submechanism (R35-R45, R47-R49, R51-R54). Modification 6: include $C_6H_5OO\Leftrightarrow C_6H_4O_2+H$ (R33) with $k_{f,33}=4.0\times10^8$. Modification 7: include $C_6H_5OO\Leftrightarrow C_6H_4O_2+H$ (R33) with $k_{f,33}=4.0\times10^8$ and $C_6H_5OO\Leftrightarrow C_5H_5+CO_2$ (R34) with $k_{f,34}=4.0\times10^8$. Modification 8: include $C_6H_5OO\Leftrightarrow C_6H_4O_2+H$ (R33) with $k_{f,33}=4.0\times10^8$ and $C_6H_5OO\Leftrightarrow C_5H_5+CO_2$ (R34) with $k_{f,34}=1.6\times10^8$.

substituted phenols (Martino *et al.*, 1995; Martino and Savage, 1997; Martino and Savage, 1999a; Martino and Savage, 1999b), and they too speculated about pathways for CO_2 formation which do not involve CO. In an independent study Krajnc and Levec (1996) also reported CO_2 yields which always exceeded those of CO during phenol SCWO, even at the lowest phenol conversions. The present experimental measurements on benzene SCWO (see Chapter 5) also show the early appearance of CO_2 and a CO_2 yield that always exceeds that of CO for measured residence times from 3 to 7 seconds.

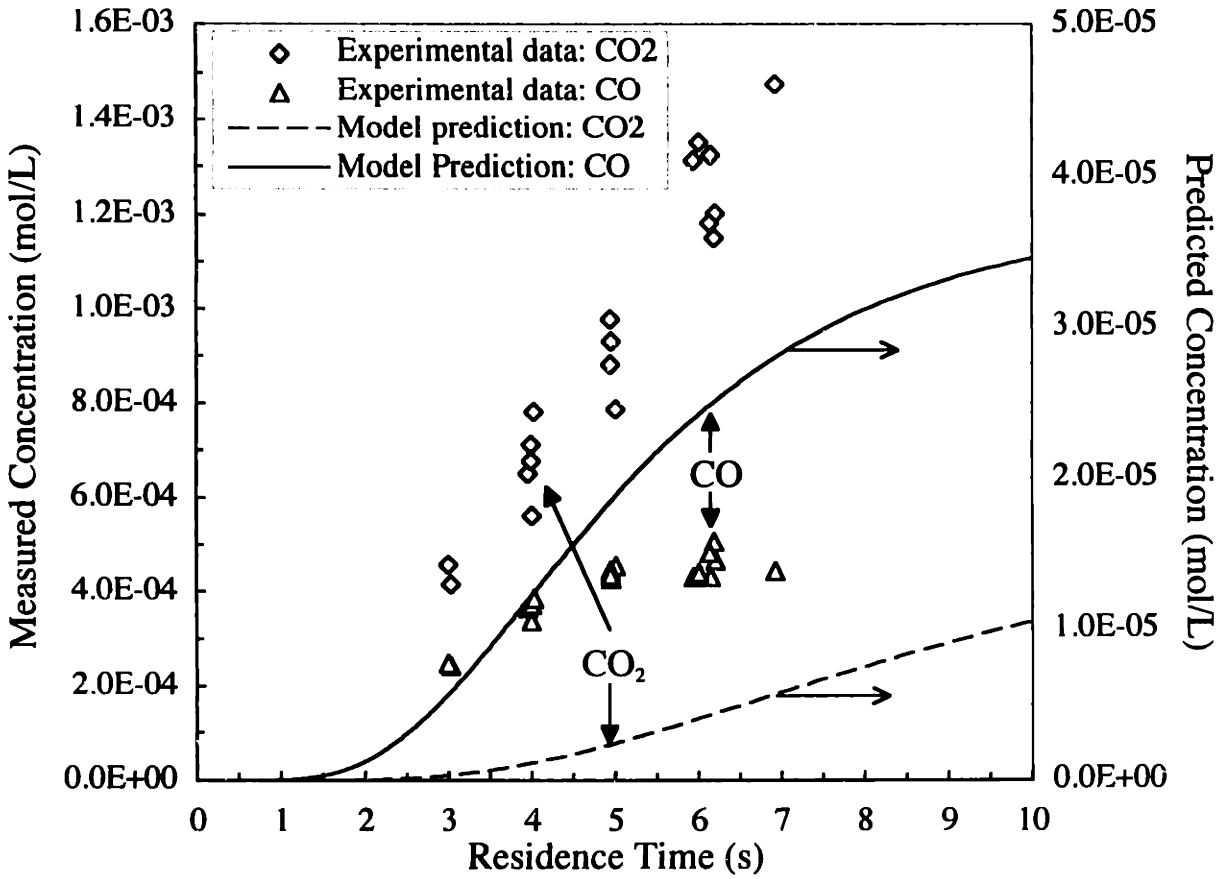

Figure 7-7 Comparison of predicted (right axis) and experimental (left axis) CO and CO_2 concentrations

Predictions after insertion of $C_6H_5OO \Leftrightarrow C_6H_4O_2+H$ (R33) with $k_{f,33}=4\times10^8$ s^{-1} (Modification 6); (T=813 K, P=246 bar, Φ=1.0, $[C_6H_6]_0=0.6\times10^{-3}$ mol/L)

Based on the observation that the model predicts CO_2 concentrations below those of CO and the evidence supporting pathways leading to CO_2 formation that do not involve CO, the dissociation reaction of C_6H_5OO to CO_2 and C_5H_5 (R34) was tested in the mechanism. The rate constants of R33 and R34 were adjusted until a good fit was achieved between the model and data.

Both the length of the induction time and the shape of the predicted benzene concentration profile agree very well with the experimental data with the inclusion of R33 and R34, as seen in Figure 7-5 ("Modification 8"). The absolute values of the rate constants were found not to cause significant differences in the model predictions as long as the rate constant of R34 was 40% of that of R33. If k_f for R34 is larger than 40% of k_f for R33, the model predicts too slow a reaction rate of benzene ("Modification 7") and vice versa. The predicted phenol concentration is not strongly dependent upon the inclusion of R34. While the model still strongly underpredicts the concentrations of CO and CO_2, as seen in Figure 7-8, it does properly predict the concentration of

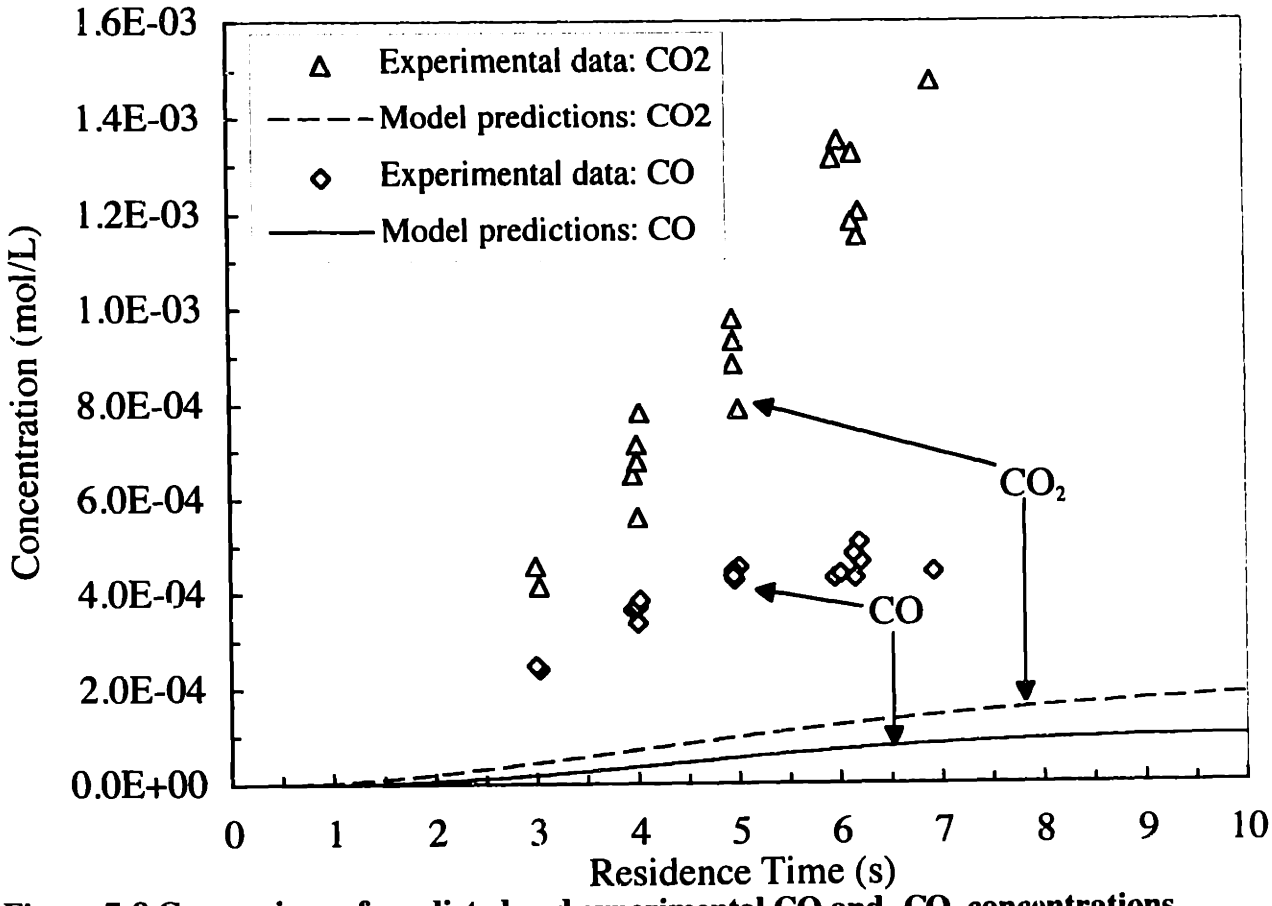

Figure 7-8 Comparison of predicted and experimental CO and CO_2 concentrations
Predictions after insertion of $C_6H_5OO \Leftrightarrow C_6H_4O_2+H$ (R33) with $k_{f,33}=4\times10^{8}$ s^{-1} and $C_6H_5OO \Leftrightarrow C_5H_5+CO_2$ (R34) with $k_{f,34}=1.6\times10^{8}$ s^{-1} (Modification 8); (T=813 K, P=246 bar, Φ=1.0, $[C_6H_6]_0=0.6\times10^{-3}$ mol/L)

CO_2 to exceed that of CO for all residence times. The very poor estimation of CO and CO_2 is due to the lack of adequate reactions in the mechanism to described to complete oxidation of all intermediates to CO and CO_2.

7.3.3 Comparison of the Model Predictions to Benzene SCWO Data at Other Conditions

The solid line in Figure 7-5 ("Modification 8") represents the best possible fit of the model to the experimental benzene concentration profile at 540°C (813 K), 246 bar and with stoichiometric oxygen using the mechanism in Table 7-3 with the rate constants for the dissociation of C_6H_5OO to $C_6H_4O_2$ and H (R33) and to C_5H_5 and CO_2 (R34) treated as adjustable parameters. As a test of the robustness of the mechanism, the model predictions were compared to experimental benzene SCWO data measured at varying reactor conditions. No further adjustments were made to the mechanism to improve model-data agreement in performing this comparison. The rate constants

of R33 and R34 were treated as temperature independent and maintained at their values given in Table 7-3.

Temperature Variations: Figure 7-9 shows a comparison of the model predictions to experimental benzene conversion data measured as a function of temperature at 246 bar with stoichiometric oxygen and a residence time of 6.2 seconds. The model and data are in excellent agreement across the entire temperature range where measurements were taken.

Fuel Equivalence Ratio Variations: The benzene oxidation rate in SCW was seen to exhibit a pronounced dependence on Φ at both 540 and 550°C. In Figure 7-10 the predicted benzene concentration profiles are compared to the experimental data measured at 540°C and 246 bar as a function of residence time with fuel equivalence ratios of 0.5 (100% excess oxygen), 1.0 (stoichiometric oxygen) and 2.5 (40% of oxygen demand). The experimental and predicted residence times profiles at Φ=1.0 are those from Figure 7-5. The model qualitatively captures the trend of benzene conversion increasing with the increasing oxygen concentration and quantitatively

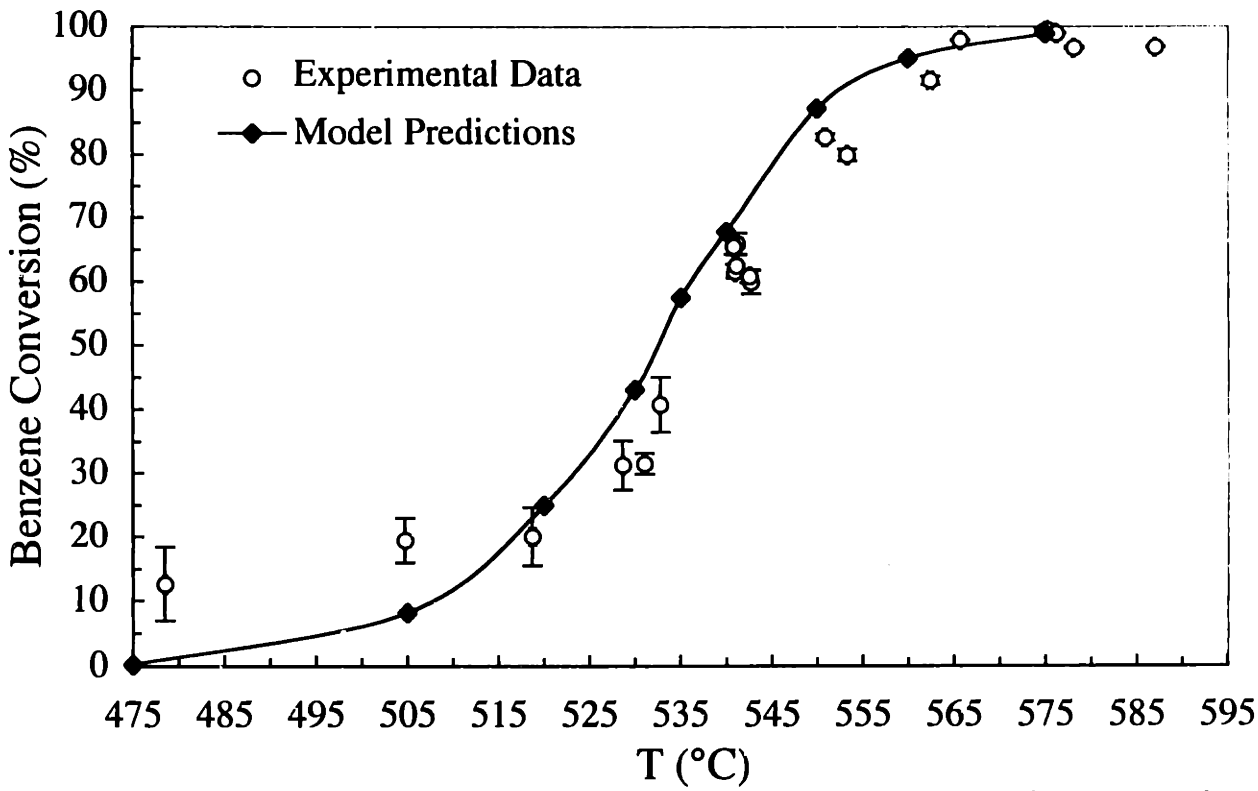

Figure 7-9 Comparison of predicted and measured benzene conversions at various temperatures
(τ=6.2 s, *P*=246 bar, Φ=1.0, $[C_6H_6]_0=0.6\times10^{-3}$ mol/L)

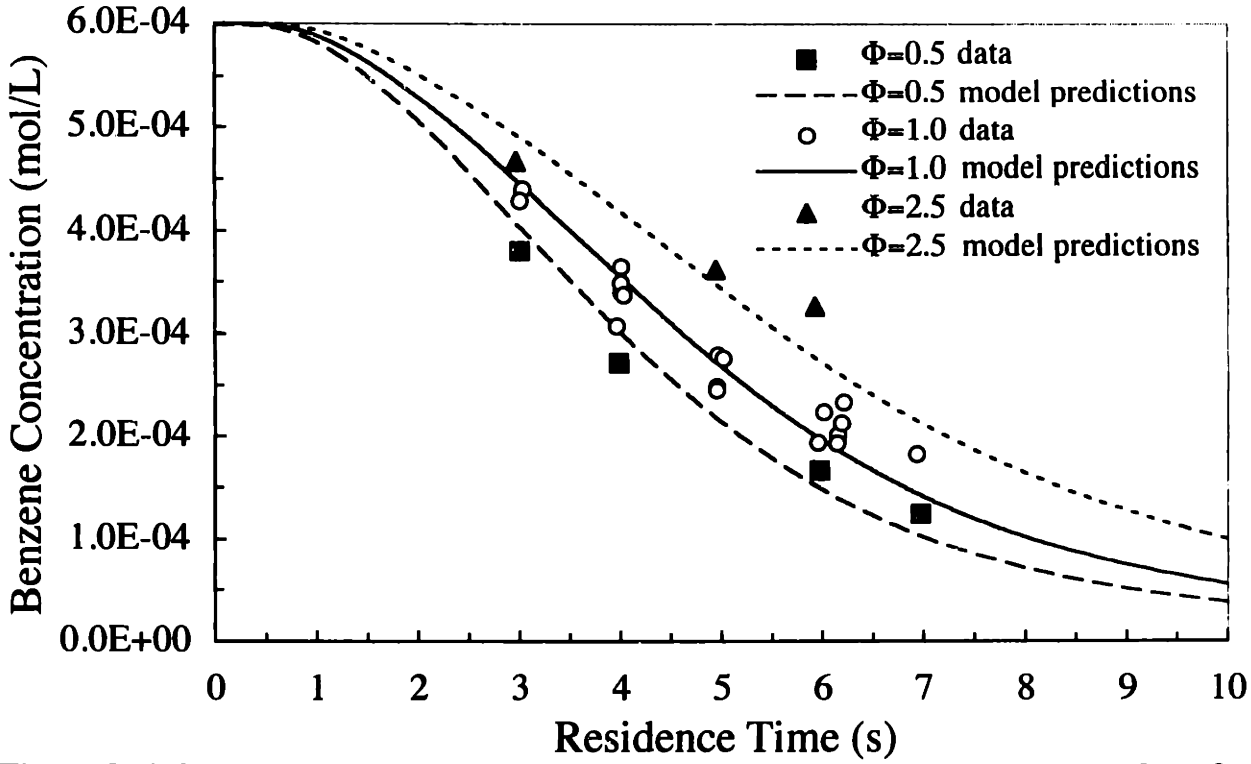

Figure 7-10 Comparison of predicted and measured benzene concentrations at three fuel equivalence ratios
(T=813 K (540°C), P=246 bar, $[C_6H_6]_0=0.6\times10^{-3}$ mol/L)

is in excellent agreement with the data measured at fuel-lean conditions. The experimental data for the fuel-rich conditions appear to exhibit a more moderate oxidation rate than the model predicts.

Benzene Concentration Variations: The conversion of benzene was found to decrease with increasing initial benzene concentration at 813 K (540°C), 246 bar and stoichiometric oxygen. Figure 7-11 compares the predicted and experimental conversions with initial benzene concentrations of 0.4, 0.6 and 1.2 mM. The predicted benzene conversion profile and experimental data with $[C_6H_6]_0$=0.6 mM are those from Figure 7-5. The model does qualitatively reproduce the trend of decreasing conversion with increasing initial benzene concentration, but the quantitative agreement, especially with that of the 1.2 mM data, is poor.

Pressure (Density) Variations: As a final test, the model predictions are compared to the experimental data measured as a function of residence time at reactor pressures ranging from 139 to 278 bar at stoichiometric oxygen and 813 K (540°C). As discussed in Chapter 5, in a supercritical water system increasing pressure also increases the water density (concentration). While benzene conversion was seen to increase with increasing pressure at 813 K (540°C), it cannot be discerned

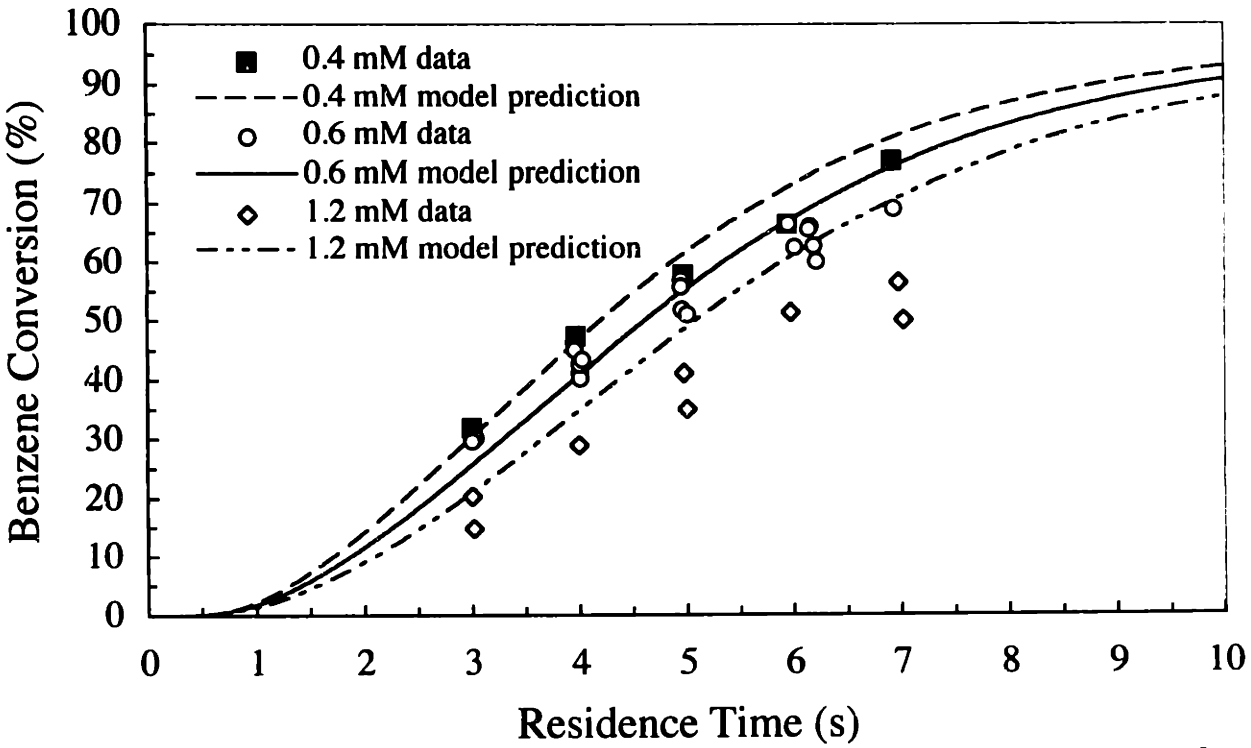

Figure 7-11 Comparison of predicted and measured benzene conversions at three different initial benzene concentrations
(T=540°C (813 K), P=246 bar, Φ=1.0)

which variable, pressure or water concentration, is affecting the benzene reaction rate. However, the experimental and theoretical evidence in the SCWO of other compounds (Holgate and Tester, 1994; Koo *et al.*, 1997) suggest that the dependence of oxidation rate on pressure arises from the increasing water concentration and not the effect of pressure on the rate constants. Benzene oxidation under SCW conditions might be assumed to behave similarly. Figure 7-12 shows the result of the changing water concentration on the predictions of benzene conversion at four pressures: 139, 228, 246 and 278 bar (ρ_{water}=0.041, 0.072, 0.079 and 0.091 g/mL, respectively). The predicted benzene conversion profile and experimental data at 246 bar are those from Figure 7-5. The model both qualitatively captures the experimentally observed trend of benzene conversion by SCWO increasing with the increasing water concentration (or increasing pressure) and gives excellent quantitative agreement at the four water concentrations (pressures) shown. The predictions at a pressure of 228 bar (ρ_{water}=0.072 g/mL) are in poorest agreement with the data.

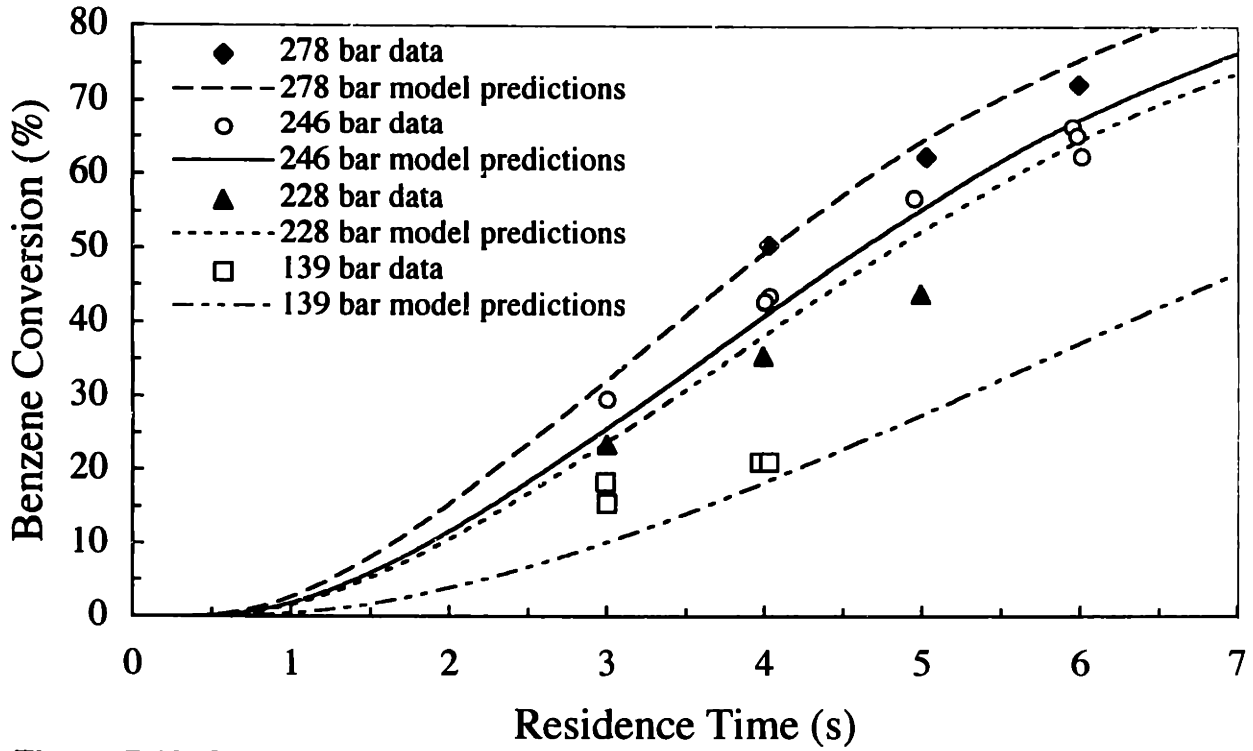

Figure 7-12 Comparison of predicted and measured benzene conversions at four reactor pressures
([H_2O] at P=139 bar, 228, 246 and 278 bar is 0.041, 0.072, 0.079 and 0.091 g/mL, respectively; T=813 K (540°C), $[C_6H_6]_0=0.6\times10^{-3}$ mol/L,Φ=1.0)

7.4 Discussion of the Model

The reaction mechanism developed for benzene oxidation in SCW in this study (see Table 7-3) successfully explains the qualitative trends in the benzene SCWO data. Additionally, good quantitative agreement is achieved between the predicted and measured benzene concentrations under many conditions, and the phenol concentration is well predicted. While the model poorly predicts the concentrations of CO and CO_2, the model properly predicts the CO_2 concentration to exceed that of CO for all residence times. The important modifications necessary to adapt the benzene combustion mechanism to the lower temperatures and higher pressures of SCWO were: the adaptation of the unimolecular and bimolecular recombination reactions for pressure (R1, R4, R6, R82 and R85); the inclusion of a pressure-corrected C_5H_5/C_5H_6 submechanism (R55-R68, R70-R78); using the reaction pathways and rate constants predicted by CHEMDIS for the reaction between C_6H_5 and O_2 (R25-R27) leading mainly to the stabilized C_6H_5OO adduct; the insertion of bimolecular reactions involving C_6H_5OO (R28-R32); and the addition of the thermal dissociation reactions of C_6H_5OO to $C_6H_4O_2$ and H (R33) and C_5H_5 and CO_2 (R34).

The rate constants given here for R33 and R34 were not based on theory or on specific measurements and were chosen only to provide a fit to the data. Moreover, a simple estimation of their rate constants is not possible because R33 and R34 are not elementary reactions. Several isomerization reactions are necessary to form the products of these reactions from the C_6H_5OO isomer shown in Figure 7-2. Therefore, the improved agreement between the predicted and experimental data upon their inclusion in the mechanism has a semi-empirical component. The rate constants used here for R33 and R34 are specific to this mechanism and any attempt to use them in other models should be pursued with much caution. The effects of their inclusion in the mechanism are discussed below.

7.4.1 Reaction Path Analysis

The net rates of formation or destruction of key species by the individual reactions in the SCW benzene oxidation mechanism in Table 7-3 were calculated to determine the controlling reactions at 813 K (540°C) and 246 bar with stoichiometric oxygen. For example, the net rate of reaction of benzene via R12 would be calculated as:

$$Net\ Rate(C_6H_6)=-k_{f,12}[C_6H_6][OH]+k_{r,12}[C_6H_5][H_2O] \quad (7\text{-}2)$$

By comparing the net rates of all reactions involving a single species, the primary destruction and formation pathways were determined.

Benzene was found to react almost exclusively by R11 and R12:

$$C_6H_6+OH \Leftrightarrow C_6H_5OH+H \quad (R11)$$

$$C_6H_6+OH \Leftrightarrow C_6H_5+H_2O \quad (R12)$$

with R12 accounting for over 97% of the oxidation rate of benzene at 813 K (540°C) and 246 bar. Phenol formed by R11 is destroyed by R18 and reformed by R21:

$$C_6H_5OH+CH_2CHCHCH \Leftrightarrow C_6H_5O+C_4H_6 \quad (R18)$$

$$C_6H_5O+C_5H_6 \Leftrightarrow C_6H_5OH+C_5H_5 \quad (R21)$$

Phenol is formed and destroyed by these two reactions at the same rate as is C_6H_5O. Given that R18 and R21 are the dominant reaction pathways from both C_6H_5O and C_6H_5OH, these compounds are not key intermediates in this benzene oxidation mechanism. The destruction of phenyl radical (C_6H_5) formed by R12 is completely accounted for by R26:

$$C_6H_5+O_2 \Leftrightarrow C_6H_5OO \quad (R26)$$

With the inclusion of the two proposed thermal decomposition pathways for C_6H_5OO:

$$C_6H_5OO \Leftrightarrow C_6H_4O_2+H \quad \text{(R33)}$$

$$C_6H_5OO \Leftrightarrow C_5H_5+CO_2 \quad \text{(R34)}$$

R33 accounts for approximately 70% of the destruction rate of C_6H_5OO and R34 for the remaining 30%. *p*-Benzoquinone formed by R33 undergoes oxidation as described by the mechanism of Alzueta *et al.* (1998) while C_5H_5 formed by R34 reacts primarily by R75:

$$C_5H_5+HO_2 \Leftrightarrow C_5H_5O+OH \quad \text{(R75)}$$

C_5H_5O then undergoes ring opening reactions leading eventually to CO and CO_2.

Since the oxidation of benzene proceeds mainly by the H-abstraction channel (R12), the induction time is determined by the amount of time required to generate the initial OH radical pool and the subsequent rate of benzene reaction by the rate of formation of OH. In the present mechanism, initiation is by -R5:

$$H_2O+O_2 \Leftrightarrow OH+HO_2 \quad \text{(-R5)}$$

and R75 is the primary production channel for OH radicals.

Without the inclusion of R33 and R34 in the mechanism, the destruction of C_6H_5OO is dominated by R27:

$$C_6H_5OO \Leftrightarrow C_6H_5O+O \quad \text{(R27)}$$

With the formation of O by R27, excess OH is generated directly by -R7:

$$O+H_2O \Leftrightarrow OH+OH \quad \text{(-R7)}$$

and indirectly by the following series of reactions:

$$C_6H_6+O \Leftrightarrow C_6H_5O+H \quad \text{(R13)}$$

$$H+O_2 \Leftrightarrow HO_2 \quad \text{(R1)}$$

$$HO_2+HO_2 \Leftrightarrow H_2O_2+O_2 \quad \text{(R2)}$$

$$H_2O_2 \Leftrightarrow OH+OH \quad \text{(-R4)}$$

causing R12 to proceed much too quickly and eliminating the induction time.

Including R33 slows down the reaction by eliminating the direct path for OH formation from R7. Since R33 generates an H radical, OH formation proceeds through R1, R2 and R4 as shown above, and inclusion of R33 alone cannot decrease the rate of benzene oxidation sufficiently to bring the model into agreement with the data.

In order to bring the model into good agreement with the data, the radical-terminating reaction R34 was included in the mechanism. While any reaction which serves as a radical sink

would have the same effect as R34, including CO_2 generating pathways is necessary to account for the experimental observation that yields of CO_2 always exceed those of CO.

The concentrations of CO and CO_2 remain severely underpredicted by the present mechanism due to the lack of the proper chemistry to account for the further oxidation of intermediate species. A large fraction of carbon remains as $C_6H_4O_2$ as the $C_6H_4O_2$ mechanism does not predict further oxidation of $C_6H_4O_2$ at a sufficient rate at the temperatures used in this mechanism. Either reactions forming $C_6H_4O_2$ should not be included in the present mechanism or new reactions and/or revised rate constants must be included to account for the oxidation of $C_6H_4O_2$. Other species present in significant concentrations are $C_6H_3O_2$, C_5H_5O, C_4H_4, H_2CCCH.

7.5 SUMMARY AND CONCLUSIONS

A supercritical water (SCW) benzene oxidation mechanism was developed using the latest understanding of benzene oxidation at combustion conditions as well as recently available submechanisms describing the oxidation of key intermediate species in benzene oxidation. The important modifications necessary to adapt the benzene combustion mechanism to the lower temperatures and higher pressures of SCWO were: 1) the adaptation of the following unimolecular and bimolecular recombination reactions for pressure:

$$H+O_2 \Leftrightarrow HO_2 \quad (R1)$$

$$OH+OH \Leftrightarrow H_2O_2 \quad (R4)$$

$$H+O_2 \Leftrightarrow OH+O \quad (R6)$$

$$C_2H_2+H \Leftrightarrow C_2H_3 \quad (R82)$$

$$CO+O \Leftrightarrow CO_2 \quad (R85)$$

2) the inclusion of a pressure-corrected C_5H_5/C_5H_6 submechanism; 3) using the reaction pathways and rate constants predicted by CHEMDIS for:

$$C_6H_5+O_2 \Leftrightarrow C_6H_5O+O \quad (R25)$$

$$C_6H_5+O_2 \Leftrightarrow C_6H_5OO \quad (R26)$$

$$C_6H_5OO \Leftrightarrow C_6H_5O+O \quad (R27)$$

4) the insertion of bimolecular reactions involving C_6H_5OO; and 5) the addition of the thermal dissociation reactions of C_6H_5OO:

$$C_6H_5OO \Leftrightarrow C_6H_4O_2+H \quad (R33)$$

$$C_6H_5OO \Leftrightarrow C_5H_5+CO_2 \quad (R34)$$

By adjusting the rate constants of R33 and R34, the model was fit to the benzene concentration profile measured in the benzene supercritical water oxidation (SCWO) experiments at 540°C and 246 bar with stoichiometric oxygen. Using the resulting mechanism both the benzene and phenol concentration profiles were accurately predicted. Carbon monoxide and carbon dioxide were both severely underpredicted, but the model did correctly predict the concentration of CO_2 to exceed that of CO at all residence times. The disagreement between the predicted and experimentally measured CO and CO_2 concentrations is due to inadequate chemistry for the further oxidation of the intermediate species formed to CO and CO_2. A comparison of the model predictions to benzene supercritical water oxidation (SCWO) data measured at conditions other than those to which the model was fit revealed that the model qualitatively explains the trends of the data and gives good quantitative agreement at many conditions. For example, the model predicts the measured benzene conversion to better than ±10% conversion at temperatures between 515 and 590°C at 246 bar with stoichiometric oxygen and at pressures from 139 to 278 bar at 540°C with stoichiometric oxygen.

The most important difference between this benzene SCWO mechanism and those previously developed for combustion conditions is the inclusion of reactions involving C_6H_5OO predicted to be formed from the reaction between C_6H_5 and O_2. Mechanisms developed for combustion conditions have set the products of this reaction equal to C_6H_5O and O and/or C_2H_2, C_2H_3 and CO through a semi-global pathway. Of the reactions included to account for the destruction of C_6H_5OO, the two thermal decomposition pathways to $C_6H_4O_2$ and H (R33) and C_5H_5 and CO_2 (R34) were most important. Without their inclusion, the predicted oxidation rate of benzene was too fast and the concentration of CO was incorrectly predicted to exceed that of CO_2. Although the rate constants for these two reactions were treated as adjustable parameters and should not be used in mechanisms developed for different conditions, the inclusion of these pathways is justified given the experimental observation of $C_6H_4O_2$ at similar conditions and the apparent need for reactions which will form CO_2 early in the oxidation process and do not involve CO. The good agreement achieved between the model predictions and the experimental SCWO data may be fortuitous, but the fact that the model both qualitatively and quantitatively reproduced the experimental data is encouraging given that the data was gathered at very different T, P (ρ) and Φ conditions than the original benzene combustion mechanism was developed for.

7.6 REFERENCES

Alzueta, M.U., M. Oliva and P. Glarborg, "Parabenzoquinone pyrolysis and oxidation in a flow reactor." *Int. J. Chem. Kin.* **30**, 683 (1998).

Atkinson, R., D.L. Baulch, R.A. Cox, R.F. Hampson, J.A. Kerr and J. Troe, "Evaluated kinetic and photochemical data for atmospheric chemistry. 3. IUPAC subcommittee on gas kinetic data evaluation for atmospheric chemistry." *J. Phys. Chem. Ref. Data* **18**(2), 881 (1989).

Baulch, D.L., C.J. Cobos, R.A. Cox, C. Esser, P. Frank, T. Just, J.A. Kerr, M.J. Pilling, J. Troe, R.W. Walker and J. Warnatz, "Evaluated kinetic data for combustion modelling." *J. Phys. Chem. Ref. Data* **21**(3), 411 (1992).

Baulch, D.L., C.J. Cobos, R.A. Cox, P. Frank, G. Hayman, T. Just, J.A. Kerr, T. Murrells, M.J. Pilling, J. Troe, R.W. Walker and J. Warnatz, "Evaluated kinetic data for combustion modelling: Supplement I." *J. Phys. Chem. Ref. Data* **23**(6), 847 (1994).

Bittker, D.A., "Detailed mechanism for oxidation of benzene." *Combust. Sci. Technol.* **79**, 49 (1991).

Bittner, J.D. and J.B. Howard, "Composition profiles and reaction mechanisms in a near-sooting premixed benzene/oxygen/argon flame." in *Eighteenth Symposium (International) on Combustion*, The Combustion Institute, Pittsburgh, 1105 (1980).

Brezinsky, K., "The high-temperature oxidation of aromatic hydrocarbons." *Prog. Energy Combust. Sci.* **12**, 1 (1986).

Burcat, A., C. Snyder and T. Brabbs, "Ignition delay times of benzene and toluene with oxygen in argon mixtures." TM-87312, NASA, (1986).

Carpenter, B.K., "Computational prediction of new mechanisms for the reactions of vinyl and phenyl radicals with molecular oxygen." *J. Am. Chem. Soc.* **115**, 9806 (1993).

Chai, Y. and L.D. Pfefferle, "An experimental study of benzene oxidation at fuel-lean and stoichiometric equivalence ratio conditions." *Fuel* **77**(4), 313 (1998).

Chang, A.Y., J.W. Bozzelli and A.M. Dean, "N frequency quantum Rice-Ramsperger-Kassel theory for complex chemical activation and unimolecular dissociation reactions: comparison with RRKM on the $C_2H_3+O_2$ system." *to be submitted for publication in J. Phys. Chem.* (c.1999).

Cobos, C.J., H. Hippler and J. Troe, "High-pressure falloff curves and specific rate constants for the reactions $H + O_2 = HO_2 = HO + O$." *J. Phys. Chem.* **89**, 342 (1985).

Dean, A.M., "Predictions of pressure and temperature effects upon radical addition and recombination reactions." *J. Phys. Chem.* **89**, 4600 (1985).

Dean, A.M., J.W. Bozzelli and E.R. Ritter, "CHEMACT: A computer code to estimate rate constants for chemically-activated reactions." *Combust. Sci. Technol.* **80**, 63 (1991).

Dixon-Lewis, G., "Flames structure and flame reaction kinetics VII. Reactions of traces of heavy water, deuterium and carbon dioxide added to rich hydrogen + nitrogen + oxygen flames." *Proc. Roy. Soc. London A* **330**, 219 (1972).

Emdee, J.L., K. Brezinsky and I. Glassman, "A kinetic model for the oxidation of toluene near 1200 K." *J. Phys. Chem.* **96**, 2151 (1992).

Forster, R., M. Frost, D. Fulle, H.F. Hamann, H. Hippler, A. Schlepegrell and J. Troe, "High pressure range of the addition of HO to HO, NO, NO_2, and CO. I. Saturated laser induced fluorescence measurements at 298 K." *J. Chem. Phys.* **103**(8), 2949 (1995).

Frank, P., J. Herzler, T. Just and C. Wahl, "High-temperature reactions of phenyl oxidation." in *Twenty-Fifth Symposium (International) on Combustion*, The Combustion Institute, Pittsburgh, (1994).

Fulle, D., H.F. Hamann, H. Hippler and J. Troe, "High-pressure range of the addition of HO to HO. III. Saturated laser-induced fluorescence measurements between 200 and 700 K." *J. Chem. Phys.* **105**(3), 1001 (1996).

Gopalan, S. and P.E. Savage, "Phenol oxidation in supercritical water. From global kinetics and product identities to an elementary reaction model." in *Innovations in Supercritical Fluids*, K. W. Hutchenson and N. R. Foster, Eds., ACS Symposium Series, **608**, American Chemical Society, Washington, D.C., 217 (1995).

He, Y.Z., W.G. Mallard and W. Tsang, "Kinetics of hydrogen and hydroxyl radical attack on phenol at high temperatures." *J. Phys. Chem.* **92**, 2196 (1988).

Hippler, H., H. Neunaber and J. Troe, "Shock wave studies of the reactions $HO+H_2O_2 \rightarrow H_2O+HO_2$ and $HO+HO_2 \rightarrow H_2O+O_2$ between 930 and 1680 K." *J. Chem. Phys.* **103**(9), 3510 (1995).

Hippler, H. and J. Troe, "Rate constants of the reaction $HO+H_2O_2 \rightarrow HO_2+H_2O$ at $T \geq 1000$ K." *Chem. Phys. Lett.* **192**(4), 333 (1992).

Hippler, H., J. Troe and J. Willner, "Shock wave study of the reaction $HO_2+HO_2 \rightarrow H_2O_2+O_2$: confirmation of a rate constant minimum near 700 K." *J. Chem. Phys.* **93**(3), 1755 (1990).

Holgate, H.R. and J.W. Tester, "Oxidation of hydrogen and carbon monoxide in sub- and supercritical water: reaction kinetics, pathways, and water-density effects. 2. Elementary reaction modeling." *J. Phys. Chem.* **98**, 810 (1994).

Howard, J.A. and K.U. Ingold, *Can. J. Chem.* **41**, 1744 (1963).

Ing, W.-C., "Reaction Kinetics of Methanol and MTBE: Oxidation and Pyrolysis." Ph.D. Thesis, Department of Chemical Engineering, New Jersey Institute of Technology, Newark, NJ (1995).

Kee, R.J., F.M. Rupley and J.A. Miller, "CHEMKIN II: A Fortran chemical kinetics package for the analysis of gas-phase chemical kinetics." SAND89-8009, Sandia National Laboratory, Livermore, CA (1989).

Keyser, L.F., "Kinetics of the reaction of OH + HO_2 → H_2O + O_2 from 254 to 382 K." *J. Phys. Chem.* **92**(5), 1193 (1988).

Kim, T.J., R.A. Yetter and F.L. Dryer, "New results on moist CO oxidation: high pressure, high temperature experiments and comprehensive kinetic modeling." in *Twenty-Fifth Symposium (International) on Combustion*, The Combustion Institute, Pittsburgh, 759 (1994).

Ko, T., G.Y. Adusei and A. Fontijn, "Kinetics of the $O(^3P)$+C_6H_6 reaction over a wide temperature range." *J. Phys. Chem.* **95**, 8745 (1991).

Koo, M., W.K. Lee and C.H. Lee, "New reactor system for supercritical water oxidation and its application on phenol destruction." *Chem. Eng. Sci.* **52**(7), 1201 (1997).

Krajnc, M. and J. Levec, "On the kinetics of phenol oxidation in supercritical water." *AIChE Journal* **42**(7), 1977 (1996).

Lindstedt, R.P. and G. Skevis, "Detailed kinetic modeling of premixed benzene flames." *Combust. Flame* **99**, 551 (1994).

Lovell, A.B., K. Brezinsky and I. Glassman, "Benzene oxidation perturbed by NO_2 addition." in *Twenty-Second Symposium (International) on Combustion*, The Combustion Institute, Pittsburgh, 1063 (1988).

Lutz, A.E., R.J. Kee and J.A. Miller, "SENKIN: A Fortran program for predicting homogeneous gas phase chemical kinetics with sensitivity analysis." SAND87-8248, Sandia National Laboratories, Livermore, CA (1988).

Madronich, S. and W. Felder, "Kinetics and mechanism of the reaction of OH with C_6H_6 over 790-1410 K." *J. Phys. Chem.* **89**(16), 3556 (1985).

Martino, C.J. and P.E. Savage, "Supercritical water oxidation kinetics, products, and pathways for CH_3- and CHO-substituted phenols." *Ind. Eng. Chem. Res.* **36**(5), 1391 (1997).

Martino, C.J. and P.E. Savage, "Oxidation and thermolysis of methoxy-, nitro-, and hydroxy-substituted phenols in supercritical water." *Ind. Eng. Chem. Res.* **38**(1784-1791) (1999a).

Martino, C.J. and P.E. Savage, "Supercritical water oxidation kinetics and pathways for ethylphenols, hydroxyacetophenones, and other monosubstituted phenols." *Ind. Eng. Chem. Res.* **38**, 1775 (1999b).

Martino, C.J., P.E. Savage and J. Kasiborski, "Kinetics and products from *o*-cresol oxidation in supercritical water." *Ind. Eng. Chem. Res.* **34**(6), 1941 (1995).

McLain, A.G., C.J. Jachimowski and C.H. Wilson, "Chemical kinetic modeling of benzene and toluene oxidation behind shock waves." TP-1472, NASA, (1979).

Miller, J.A. and C.F. Melius, "Kinetic and thermodynamic issues in the formation of aromatic compounds in flames of aliphatic fules." *Combust. Flame* **91**, 21 (1992).

Phenix, B.D., J.L. DiNaro, M.A. Tatang, J.W. Tester, J.B. Howard and G.J. McRae, "Incorporation of parametric uncertainty into complex kinetic mechanisms: application to hydrogen oxidation in supercritical water." *Combust. Flame* **112**, 132 (1998).

Robinson, P.J. and K.A. Holbrook, *Unimolecular Reactions*. Wiley-Interscience, London (1972).

Shandross, R.A., "Experimental and theoretical study of hydrogen and benzene destruction chemistries." Ph.D. Thesis, Department of Chemical Engineering, Massachusetts Institute of Technology, Cambridge, MA (1996).

Shandross, R.A., J.P. Longwell and J.B. Howard, "Destruction of benzene in high-temperature flames: chemistry of benzene and phenol." in *Twenty-Sixth Symposium (International) on Combustion*, The Combustion Institute, Pittsburgh, 711 (1996).

Tan, Y., P. Dagaut, M. Cathonnet and J.-C. Boettner, "Acetylene oxidation in a JSR from 1 to 10 atm and comprehensive kinetic modeling." *Combust. Sci. Technol.* **102**, 21 (1994).

Tan, Y. and P. Frank, "A detailed comprehensive kinetic model for benzene oxidation using the recent kinetic results." in *Twenty-Sixth Symposium (International) on Combustion*, The Combustion Institute, Pittsburgh, 677 (1996).

Troe, J., "Thermal dissociation and recombination of polyatomic molecules." in *Fifteenth Symposium (International) on Combustion*, The Combustion Institute, Pittsburgh, 667 (1974).

Warnatz, J., "Rate coefficients in the C/H/O system." in *Combustion Chemistry*, W. C. Gardiner, Ed., Springer-Verlag, New York, 197 (1984).

Westmoreland, P.R., J.B. Howard, J.P. Longwell and A.M. Dean, "Prediction of rate constants for combustion and pyrolysis reactions by bimolecular QRRK." *AIChE Journal* **32**(12), 1971 (1986).

Yu, T. and M.C. Lin, "Kinetics of the $C_6H_5 + O_2$ reaction at low temperatures." *J. Am. Chem. Soc.* **116**, 9571 (1994).

Zellner, R., F. Ewig, R. Paschke and G. Wagner, "Pressure and temperature-dependence of the gas-phase recombination of hydroxyl radicals." *J. Phys. Chem.* **92**(14), 4184 (1988).

Zhang, H.-Y. and J.T. McKinnon, "Elementary reaction modeling of high-temperature benzene combustion." *Combust. Sci. Technol.* **107**, 261 (1995).

Zhong, X. and J.W. Bozzelli, "Thermochemical and kinetic analysis on the addition reactions of H, O, OH, and HO_2 with 1,3 cyclopentadiene." *Int. J. Chem. Kin.* **29**, 893 (1997).

Zhong, X. and J.W. Bozzelli, "Thermochemical and kinetic analysis of the H, OH, HO_2, O, and O_2 association reactions with cyclopentadienyl radical." *J. Phys. Chem.* **102**, 3537 (1998).

Chapter 8.

Summary and Conclusions

The research presented in this thesis addresses both the general goal of characterizing the mechanisms and kinetics of reactions of model organic chemicals in supercritical water and the specific objective of determining the oxidative behavior of benzene, a model aromatic compound and hazardous chemical, in supercritical water. In preparation for the experimental study on the supercritical water oxidation (SCWO) of benzene, an investigation to identify the effects of mixing and oxidant choice on laboratory-scale SCWO kinetic data was undertaken. The oxidation and hydrolysis reactions of benzene in SCW were then thoroughly investigated using the laboratory-scale, plug-flow reactor system. Prior to the development of an elementary reaction mechanism (ERM) for benzene SCWO, the effects of uncertainty in the input parameters of these ERMs on their predictive capabilities was explored for hydrogen oxidation in supercritical water. Lastly, an ERM for the supercritical water oxidation of benzene was developed to provide mechanistic insights regarding key reaction pathways. The following summarizes these objectives and the conclusions reached in each investigation:

1. Characterization of Mixing Times and Oxidant Choice. This aspect of the research was conducted collaboratively with Brian Phenix using methanol as a model compound. The apparent induction time was influenced by the geometry and flow conditions within the mixing section, or cross, at the reactor entrance indicating that the observed induction time, once thought to be a purely kinetic phenomena, was at least partly a result of the time required to mix the organic and oxidant reactor feeds. Two new mixing crosses were designed in an attempt to optimize the mixing rate within the cross. By reducing the inner diameter of the oxidant and organic arms of the cross to increase their Reynolds numbers and the ratio of the inlet streams-to-reactor flowrates, the observed induction time was reduced from 3.2 to 0.7 seconds.

The use of hydrogen peroxide as an alternative source of oxygen was evaluated as a means of achieving higher concentrations of oxygen in the reactor than could be reached using the oxygen saturator system. The use of an aqueous hydrogen peroxide solution was demonstrated as a viable method for generating molecular oxygen *in situ* in our laboratory-scale SCWO reactor system. The oxidation of methanol proceeded at the same rate using either aqueous hydrogen peroxide or dissolved oxygen. Moreover, the concentration of the oxidation products in the reactor effluent were identical using either oxidant.

2. Parameter Uncertainties in Mechanism Predictions of Hydrogen Oxidation in Supercritical Water. DEMM and Monte Carlo simulation were used to assess the level of uncertainty in the predictions of a reduced supercritical water hydrogen oxidation mechanism. Both methods produced identical predictions of species concentration profiles and their time-dependent probability distributions. Further, both analyses revealed that there is considerable uncertainty in the predicted species concentration profiles arising from the reported uncertainties in the forward rate constants and species enthalpies of formation. For example, at the point of maximum uncertainty the predicted concentrations of hydrogen and oxygen deviated by ±70% of their median values at the upper 97.5% and lower 2.5% probability contours. Model predictions were found to be highly sensitive to two relatively uncertain parameters: the ΔH_f^0 of HO_2 radical and the rate constant for H_2O_2 dissociation. Also demonstrated in this study was the minimal impact of real-gas corrections on the predicted species profiles relative to the parametric uncertainty inherent in the mechanism itself.

While both DEMM and Monte Carlo simulation proved to be computationally tractable means of conducting parametric uncertainty analysis, the two methods differed substantially in the amount of computation time necessary to perform the analysis. To adequately develop the time-dependent response distributions of the model, Monte Carlo required 15,000 calls to the LSODE solver routine while DEMM required only 153. This two order of magnitude reduction in the required number of model solutions makes DEMM an attractive tool for the analysis of more complex mechanisms where the computational time and memory requirements of Monte Carlo may become prohibitive.

The hydrogen-oxygen mechanism may be the best understood subset of reactions at combustion conditions. The mechanism consists of only a small number of reactions, the reaction

pathways are known with a high degree of certainty, and multiple investigators have measured a majority of the rate constants over a wide range of conditions. In the present case, more precise measurements of key rate constants and thermodynamic data would lead to a reduction of model uncertainty. As the size and complexity of the oxidation mechanisms increase in order to model the oxidation of larger compounds, the main source of uncertainty shifts from the model parameters to a lack of understanding of the reaction mechanism itself. In cases where the mechanism itself is not well known, the largest reduction in overall uncertainty will come through an improved knowledge of the mechanism rather than through a reduction of uncertainty in the model parameters.

3. Experimental Measurements of the Oxidation of Benzene in Supercritical Water. A detailed investigation was completed on the oxidation and hydrolysis of benzene in supercritical water. A total of 7 hydrolysis and 107 oxidation experiments were conducted at temperatures ranging from 479 to 587°C, pressures from 139 to 278 bar, fuel equivalence ratios of 2.5 (40% of oxygen demand) to 0.5 (100% excess oxygen), residence times from 3 to 7 seconds and initial benzene concentrations of 0.4 to 1.2 mM. The conversion of benzene in the absence of oxygen was determined to be no greater than 10% and realistically closer to 2% at temperatures up to 625°C, and, as a result, the hydrolysis pathway did not interfere with the study of benzene SCWO kinetics. Essentially complete conversion of benzene was achieved at 575°C and 246 bar with a stoichiometric amount of oxygen, and carbon dioxide accounted for 90% of the initial carbon. Benzene conversion by SCWO increased with both increasing oxygen concentration and system pressure. While at 530 and 540°C the benzene oxidation rate decreased with increasing initial benzene concentrations, at 550°C no significant dependence of conversion on the initial concentration existed. A global rate expression regressed from the experimental data predicts the experimentally observed benzene conversion to within ±5% conversion at most conditions. The predicted rate expression is 0.18±0.05 order in oxygen and 0.40±0.06 order in benzene with an Arrhenius activation energy of 240±10 kJ/mol and a preexponential factor of $10^{13.1\pm0.9}$ $mol^{0.42}L^{-0.42}s^{-1}$.

More than 90% of the carbon in the reactor feed was recovered in the effluent products. Carbon dioxide accounted for more of the reacted carbon than any other oxidation product, including carbon monoxide, at all reactor conditions and for all levels of benzene conversion. Methane and phenol were also dominant oxidation products. Trace levels of ethylene, acetylene and

propylene were detected. Single and multi-ringed aromatic products were also detected in the effluent. Their concentrations decreased significantly, many to undetectable levels, as both the temperature and oxygen concentration were increased. At 625°C and with 10% excess oxygen, less than 0.1% of the initial carbon was present in the form of single- and multi-ringed products. Dibenzofuran and biphenyl were the most persistent of the single- and multi-ringed intermediates.

4. Development of a Supercritical Water Benzene Oxidation Mechanism. A supercritical water (SCW) benzene oxidation mechanism was developed. The model was based on an available low-pressure, benzene combustion mechanism and submechanisms describing the oxidation of key intermediate species in benzene oxidation. To adapt the benzene combustion mechanism to the lower temperatures and higher pressures of SCWO, new reaction pathways were added and quantum Rice-Ramsperger-Kassel theory was used to calculate the rate constants and reaction products for pressure dependent reactions. The important modifications made to generate the present SCW benzene oxidation mechanism were: adapting the unimolecular and bimolecular recombination reactions for pressure; including a pressure-corrected C_5H_5/C_5H_6 submechanism; using the reaction pathways and rate constants predicted by CHEMDIS for the reaction between C_6H_5 and O_2 leading mainly to the stabilized C_6H_5OO adduct; inserting bimolecular reactions involving C_6H_5OO; and adding the thermal dissociation reactions of C_6H_5OO to 1) $C_6H_4O_2$ and H and 2) C_5H_5 and CO_2. By adjusting these two thermal dissociation rate constants, the model was fit to the benzene concentration profile measured in the present experiments at 540°C and 246 bar with stoichiometric oxygen. At these conditions, the resulting mechanism accurately reproduced the experimentally measured benzene and phenol concentration. Carbon monoxide and carbon dioxide were both severely underpredicted, but the model did correctly predict the concentration of CO_2 to exceed that of CO at all residence times. The disagreement between the predicted and experimentally measured CO and CO_2 concentrations is due to inadequate chemistry for the further oxidation of the intermediate species formed to CO and CO_2. Comparison of the model predictions to benzene SCWO data measured at conditions other than those to which the model was fit reveals that the model qualitatively explains the trends of the data and gives good quantitative agreement at many conditions. For example, the model predicts the measured benzene conversion to better than ±10% conversion at temperatures between 515 and 590°C at 246 bar with stoichiometric oxygen and at pressures from 139 to 278 bar at 540°C with stoichiometric oxygen.

The most important difference between this benzene SCWO mechanism and those previously developed for combustion conditions is the inclusion of reactions involving C_6H_5OO predicted to be formed from the reaction between C_6H_5 and O_2. Mechanisms developed for combustion conditions have set the products of this reaction equal to C_6H_5O and O and/or C_2H_2, C_2H_3 and CO through a semi-global pathway. Of the reactions included to account for the destruction of C_6H_5OO, the two thermal decomposition pathways to 1) $C_6H_4O_2$ and H and 2) C_5H_5 and CO_2 were most important. Without their inclusion, the predicted oxidation rate of benzene was too fast and the concentration of CO was incorrectly predicted to exceed that of CO_2. Although the rate constants for these two reactions were treated as adjustable parameters, the inclusion of these pathways is justified given the experimental observation of $C_6H_4O_2$ in benzene flames at similar temperatures and oxygen concentrations and the apparent need for reactions which form CO_2 directly, *i.e.*, without involving CO, early in the oxidation process. The good agreement achieved between the model predictions and the experimental SCWO data has a semi-empirical component due to the inclusion of the two adjustable parameters, but the fact that the model both qualitatively and quantitatively reproduces the experimental data is encouraging given that the data were gathered at very different temperatures, pressures and oxygen concentrations than those for which the original benzene combustion mechanism was developed.

Chapter 9.

Recommendations

In this thesis the results of an experimental and theoretical investigation of the oxidation of benzene in supercritical water (SCW) were presented. The supercritical water oxidation (SCWO) rate of benzene was measured at temperatures between 479 and 587°C, pressures from 139 to 278 bar, residence times from 3 to 7 seconds, fuel equivalence ratios of 2.5 (40% of oxygen demand) to 0.5 (100% excess oxygen) and initial benzene concentrations of 0.4 to 1.2 mM. All experiments were performed using a tubular, isothermal, isobaric, plug-flow reactor system. Experiments were also performed with methanol to characterize the effects of mixing times and oxidant choice on the SCW oxidation rate. An elementary reaction mechanism (ERM) for benzene oxidation in SCW was developed, and the effect of parameter uncertainties on ERM predictions was explored in the case of hydrogen SCWO. The following are recommendations of areas which would benefit from further consideration based on observations or unresolved issues from this thesis work:

1. Characterize the Observed Dependence of Pressure (Density) on SCWO Kinetics. Elevating the pressure increased the level of benzene conversion during the SCW benzene oxidation experiments. A similar dependence on pressure has been observed in the SCWO of phenol, carbon monoxide and hydrogen. Since in an SCWO system, an increase in the system pressure is brought about by increasing the water concentration (density), one cannot unequivocally discern whether the increasing pressure or water concentration is affecting reaction rates. Recent experimental evidence in the oxidation of phenol and theoretical evidence for benzene (presented here) and hydrogen suggest that the source of the pressure dependence is wholly due to the increasing water concentration. To positively determine which variable the benzene oxidation rate depends on (pressure, water concentration or partly on each), experiments should be conducted whereby

pressure is varied independently of water concentration. This could be accomplished by increasing pressure by the addition of an inert gas, such as helium or argon, and comparing the benzene conversion with those presented here where water concentration was increased to achieve higher pressures.

2. Exploration of Mixing Times in the Plug-Flow Reactor System Through the Use of Initiators. Both the methanol and the benzene SCWO experiments were conducted in our tubular, plug-flow reactor system. At the beginning of the reactor, the preheated, aqueous organic and oxidant feeds are combined in a mixing cross. The apparent induction time of methanol depended upon the geometry and flow conditions within this cross. What was not resolved, however, was if the 0.5 to 1 second induction time remaining after redesigning the mixing cross was a true kinetic induction time or was still partly due to the time needed to mix the organic and oxidant feeds. The use of initiators in place of the oxygen feed stream would allow such a determination.

In the case of benzene oxidation, the induction time is thought to be a function of the rate at which OH radicals are generated as, based on the mechanistic study, over 98% of the rate of benzene oxidation at 540°C and 246 bar with stoichiometric oxygen is accounted for by the abstraction of H from benzene by OH. Therefore, oxygen is not necessary for benzene oxidation as long as a source of OH or an equivalent radical, such as Cl, is provided.

In place of the aqueous oxygen feed, Cl radicals in SCW could be fed to the mixing cross. By heating an aqueous solution of a chlorinated hydrocarbon, such as dichlorobenzene or methylene chloride, thermal dissociation of the organic would generate Cl radicals in the reactor preheator. The oxidation rate of benzene with this pregenerated source of Cl radicals should proceed without a kinetic induction time. Any observed induction time, then, will be due to the time necessary to mix the benzene and radical feed streams.

3. Conduct Benzene SCWO Experiments in the New CSTR. Benzene oxidation experiments should be performed in the new continuous stirred tank reactor (CSTR). Due to the possible influence of catalytic or radical terminating reactions with the reactor walls on laboratory-scale kinetic data, the scalability of such data for use in predicting oxidation rates in industrial reactors with their much smaller surface-to-volume ratios should be validated. Experiments conducted in our new CSTR would be a step towards this validation in that kinetics would be less affected by wall

reactions given the much smaller surface-to-volume ratio in the CSTR than in the tubular, plug-flow reactor system used here for the measurement of benzene SCWO kinetic data.

4. Explore Initiation Reactions in SCW. The benzene elementary reaction mechanism (ERM) developed here predicts that over 98% of the oxidation rate of benzene is accounted for by the abstraction of H from benzene by OH radical. The rate of generation of OH radical, then, controls both the benzene reaction rate and the length of the kinetic induction time. Experimentally, an induction time was observed which varied with reaction conditions but generally was on the order of 1 second, an unknown portion of which is attributable to the physical time needed to mix the organic and oxidant feeds. If, as the model predicts, the induction time is also partly due to the time necessary to establish a sufficient rate of OH radical generation, then the addition of an initiator to provide a rapid source of OH will enhance the benzene oxidation rate.

Cold hydrogen peroxide (H_2O_2) could serve as such an initiator, as H_2O_2 will dissociate into two OH radicals in SCW. Experiments could be performed using our new CSTR system whereby cold H_2O_2 is injected directly into a SCW/benzene/oxygen mixture. By comparing the oxidation rate of benzene with and without the injection of the H_2O_2, the effect of providing a source of OH radicals on both the initiation and on the overall oxidation rate could be determined.

Chapter 10.

Appendices

10.1 Detailed Analytical Methods

10.1.1 Liquid-Phase Effluent and Feed Analysis

HP 5890 Series II Gas Chromatograph - Analysis of Benzene and Phenol

Column Type and Configuration	
column:	30 m x 530 µm x 5 µm film thickness DB-1 (J&W Scientific, p/n 125-1035) preceded by 5 m of Restek Hydroguard column (Restek, p/n 100810)
carrier gas:	Helium
column flowrate:	5 mL/min @ 70°C
column head pressure:	3.3 psig
Injection Type and Configuration	
Injector:	HP GC Injector
Injection Type:	Splitless
Injection Volume:	0.2 µL
Syringe Size:	10.0 µL
Nanoliter Adapter:	Yes
Sample Washes:	2
Sample Pumps:	3
Post Injection Solvent Washes:	2 (with water)
Viscosity Delay:	2 seconds
Plunger Speed:	Fast
Inlet Liner:	Single taper, glass wool packed, capillary inlet liner (HP, p/n 5062-3587)
Inlet Septa:	Merlin Microseal duckbill (HP, p/n 5182-3442)
Inlet Oven and Detector Temperatures	
Inlet:	200°C
Detector:	200°C
Initial Oven Temperature:	80°C
Initial Time:	2.0 min.
Ramp:	40.0°C/min.
Final Oven Temperature:	160°C
Hold:	4.5 min.

HP 5890 Series II Gas Chromatograph - Analysis of Benzene and Phenol, cont.

Purge Valve Settings	
Initial Value:	Off
On Time:	1.0 min.
Purge Flow:	3.3 mL/min.
Detector Information	
Type:	FID
H_2 Flow:	30 mL/min.
Air Flow:	300 mL/min.
Auxiliary Gas:	N_2
Auxiliary Gas Flow:	37 mL/min.
Data Acquisition Rate:	20.0 Hz.
Retention Times	
Benzene:	4.3 min.
Phenol:	7.9 min.

HP 6890 Gas Chromatograph - Analysis of Benzene and Phenol

Column Type and Configuration	
column:	30 m x 530 µm x 1 µm film thickness DB-WAX (J&W Scientific, p/n 125-7032) preceded by 5 m of Restek Hydroguard column (Restek, p/n 100810)
carrier gas:	Helium
column flowrate:	4.2 mL/min @ 80°C
column head pressure:	3.7 psig
Injection Type and Configuration	
Injector:	HP GC Injector
Injection Type:	Splitless
Injection Volume:	0.5 µL
Syringe Size:	5.0 µL
Nanoliter Adapter:	No
Sample Washes:	2
Sample Pumps:	3
Post Injection Solvent Washes:	2 (with water)
Viscosity Delay:	2 seconds
Plunger Speed:	Fast
Inlet Liner:	Single taper, glass wool packed, capillary inlet liner (HP, p/n 5062-3587)
Inlet Septa:	Merlin Microseal duckbill (HP, p/n 5182-3442)
Inlet Oven and Detector Temperatures	
Inlet:	200°C
Detector:	200°C
Initial Oven Temperature:	80°C
Initial Time:	2.0 min.
Ramp:	40.0°C/min.
Final Oven Temperature:	200°C
Hold:	4.5 min.
Purge Valve Settings	
Initial Value:	Off
On Time:	1.0 min.
Purge Flow:	3.0 mL/min.
Detector Information	
Type:	FID
H_2 Flow:	40 mL/min.
Air Flow:	450 mL/min.
Auxiliary Gas:	N_2
Auxiliary Gas Flow:	45 mL/min.
Data Acquisition Rate:	20.0 Hz.
Retention Times	
Benzene:	3.0 min.
Phenol:	8.7 min.

10.1.2 Gas-Phase Effluent Analysis

HP 5890 Series II Gas Chromatograph - Analysis of Light Gases

Column Type and Configuration	
column:	5 ft. x 1/8 in. 60/80 mesh Carboxen 1000 column in series with an 8 ft. x 1/8 in. 60/80 mesh Molsieve 5A column
carrier gas:	Helium
column flowrate:	28.5 mL/min @ 80°C
column head pressure:	50 psig (with switching valve in Off position)
Injection Type and Configuration	
Injection Type:	Manual, Splitless
Injection Volume:	200 µL
Syringe Size:	250 µL
Inlet Type:	Packed
Inlet Septa:	SGE Auto-Sep 11 mm septa (p/n 041872)
Inlet Oven and Detector Temperatures	
Inlet:	110°C
Detector:	110°C
Initial Oven Temperature:	80°C
Initial Time:	4.0 min.
Ramp:	40.0°C/min.
Final Oven Temperature:	110°C
Hold:	8.0 min.
Valves	
Valve Type:	10-port switching valve
Initial Value:	Off (carrier flows first through Carboxen column then through MolSieve column)
On Time:	7.9 min. (reverse flow direction)
Detector Information	
Type:	TCD
Reference Gas:	He
Reference Gas Flow:	36.0 mL/min.
Makeup Flow:	Off
Data Acquisition Rate:	10.0 Hz.
Retention Times	
O_2:	3.3 min.
N_2:	4.5 min.
CO:	6.3 min.
CO_2:	9.3 min.
CH_4:	11.5 min.

HP 6890 Gas Chromatograph - Analysis of Light Gases

Column Type and Configuration	
column:	5 ft. x 1/8 in. 60/80 mesh Carboxen 1000 column in series with an 8 ft. x 1/8 in. 60/80 mesh Molsieve 5A column
carrier gas:	Helium
column flowrate:	20.9 mL/min @ 80°C
Injection Type and Configuration	
Injection Type:	Manual, Splitless
Injection Volume:	200 µL
Syringe Size:	250 µL
Inlet Type:	Packed
Inlet Septa:	SGE Auto-Sep 11 mm septa (p/n 041872)
Inlet Oven and Detector Temperatures	
Inlet:	110°C
Detector:	150°C
Initial Oven Temperature:	80°C
Initial Time:	4.0 min.
Ramp:	40.0°C/min.
Final Oven Temperature:	110°C
Hold:	8.25 min.
Valves	
Valve Type:	10-port switching valve
Initial Value:	On (carrier flows first through Carboxen column then through MolSieve column)
Off Time:	7.98 min. (reverse flow direction)
Detector Information	
Type:	TCD
Reference Gas:	He
Reference Gas Flow:	48.0 mL/min.
Makeup flow:	2.0 mL/min.
Data Acquisition Rate:	20.0 Hz.
Retention Times	
O_2:	3.5 min.
N_2:	4.5 min.
CO:	6.3 min.
CO_2:	9.6 min.
CH_4:	12.0 min.

HP 5890 Series II Gas Chromatograph - Analysis of Light Hydrocarbon Gases

Column Type and Configuration	
column:	15 m x 320 µm Astec GasPro bonded PLOT column (p/n 81103)
carrier gas:	Helium
column flowrate:	2 mL/min @ 70°C
column head pressure:	10.0 psig
Injection Type and Configuration	
Injection Type:	Manual, Spiit
Injection Volume:	200 µL
Syringe Size:	250 µL
Split Ratio:	15:1
Inlet Liner:	split/splitless, glass wool packed, capillary inlet liner (HP, p/n 19251-60540)
Inlet Septa:	Supelco Thermogreen LB-2 11mm septa (p/n 20654)
Inlet Oven and Detector Temperatures	
Inlet:	200°C
Detector:	200°C
Initial Oven Temperature:	50°C
Initial Time:	1.0 min.
Ramp:	8.0°C/min.
Final Oven Temperature:	160°C
Hold:	12.3 min.
Detector Information	
Type:	FID
H_2 Flow:	30 mL/min.
Air Flow:	300 mL/min.
Auxiliary Gas:	N_2
Auxiliary Gas Flow:	38.0 mL/min.
Data Acquisition Rate:	20.0 Hz.
Retention Times	
methane:	1.6 min.
ethane:	2.1 min.
ethylene:	2.5 min.
acetylene:	3.5 min.
propylene:	6.1 min.
benzene:	23.5 min.

Perkin Elmer Sigma 1B Gas Chromatograph - Analysis of Hydrogen and Helium

Column Type and Configuration	
column:	12 ft. x 1/8 in. 80/100 mesh Porapak T column in series with an 8 ft. x 1/8 in. 60/80 mesh Molsieve 5A column
carrier gas:	Nitrogen
column flowrate:	40.0 mL/min
column head pressure:	65 psig (with switching valve in Off position)
Injection Type and Configuration	
Injection Type:	Manual, Splitless
Injection Volume:	200 µL
Syringe Size:	250 µL
Inlet Type:	Packed
Inlet Septa:	Supelco Thermogreen LB-2 11mm septa (p/n 20654)
Inlet Oven and Detector Temperatures	
Inlet:	60°C
Detector:	120°C
Initial Oven Temperature:	70°C
Initial Time:	7.0 min.
Ramp:	0.0°C/min.
Final Oven Temperature:	70°C
Hold:	0.0 min.
Valves	
Valve Type:	Switching valve
Position:	valve position remains unchanged - carrier flows first through Porapak T column then through MolSieve column
Detector Information	
Type:	TCD
Reference Gas:	N_2
Ref. Gas Cylinder Pressure:	70 psig
Makeup Flow:	Off
Retention Times	
He:	2.6 min.
H_2:	2.7 min.

10.2 Experimental Benzene SCWO Data

Summary tables of the data from the benzene supercritical water oxidation experiments are presented here. Table 10.2.1 summarizes the data from the hydrolysis experiments. Table 10.2.2 summarizes all oxidation data from experiments performed at 246 bar, and Table 10.2.3 summarizes the data from the pressure variation experiments. Tables 10.2.4 through 10.2.9 group the data from 10.2.1 into categories denoting which experimental variable was varied. Table 10.2.10 summarizes the data from the oxidation experiments performed for the purposes of detecting single- and multi-ringed aromatic species.

Table 10.2.1. Summary of all experimental benzene SCW hydrolysis data measured at *P*=246±2 bar

Run No.	*T* (°C)	τ (s)	$[C_6H_6]_0$ 10^{-7} mol/mL	Conversion (%)	$[C_6H_5OH]$ 10^{-9} mol/mL	Carbon Balance (%)
698	627.5±0.1	6.3±0.4	6.1±0.1	7±4	4±4	95±4
699	579.9±0.1	6.4±0.4	6.0±0.1	10±5	4±2	90±5
700	602.3±0.1	6.4±0.4	6.0±0.2	8±4	4±3	93±4
701	578.1±0.3	6.3±0.4	5.9±0.2	7±3	3±2	94±3
794	532.0±0.1	6.0±0.4	5.9±0.2	-3±3	2±2	103±3
796	531.9±0.2	6.0±0.4	5.9±0.3	3±5	2±5	98±5
797	531.3±0.1	6.0±0.4	5.8±0.2	2±3	1±3	98±3

Table 10.2.2. Summary of all experimental benzene SCWO data measured at P=246±2 bar

Run No.	T (°C)	Φ	τ (s)	$[C_5H_6]_0$ 10^{-7} mol/mL	Conversion (%)	ln k'	$[C_6H_5OH]$ 10^{-9} mol/mL	[CO] 10^{-7} mol/mL	$[CO_2]$ 10^{-6} mol/mL	$[CH_4]$ 10^{-8} mol/mL	Carbon Balance (%)
702	578.1±0.1	1.15±0.04	6.2±0.4	6.1±0.1	97±0	-0.6±0.1	0	2.5±0.1	3.1±0.1	17.8±1.8	101±3
703	578.4±0.1	1.13±0.04	5.2±0.3	6.0±0.1	97±0	-0.4±0.1	0	3.5±0.1	2.9±0.1	17.4±1.8	99±2
704	504.7±0.1	1.26±0.13	6.2±0.4	6.0±0.2	20±4	-3.4±0.2	0	0.4±0.1	0.13±0.04	0.010±0.006	85±4
705	528.6±0.1	1.20±0.04	6.2±0.4	5.9±0.2	31±4	-2.8±0.2	1.7±0.4	2.1±0.4	0.5±0.1	1.0±0.2	89±4
706	553.3±0.1	1.19±0.08	6.2±0.4	5.9±0.2	80±1	-1.4±0.1	5.5±0.4	6.2±0.5	2.0±0.1	12.8±1.3	97±3
707	532.7±0.1	1.09±0.09	6.2±0.4	5.9±0.3	41±4	-2.5±0.2	2.5±0.4	2.3±0.7	0.7±0.2	1.2±0.4	86±6
708	542.7±0.1	1.17±0.12	6.2±0.4	5.8±0.2	60±2	-1.9±0.1	5.1±0.5	4.6±0.5	1.2±0.1	5.7±0.5	90±3
709	587.0±0.1	1.27±0.08	6.3±0.4	6.1±0.3	97±0	-0.6±0.1	0	1.4±0.2	3.1±0.2	14.4±2.0	94±4
710	562.5±0.3	1.21±0.11	6.2±0.4	5.8±0.4	92±1	-0.9±0.1	2.3±0.3	4.8±0.7	2.5±0.3	15.2±2.4	99±8
711	518.7±0.3	1.25±0.08	6.2±0.4	6.1±0.3	20±5	-3.3±0.3	1.0±0.4	1.0±0.4	0.23±.08	0.2±0.1	89±5
712	478.5±0.2	1.23±0.13	6.2±0.4	6.2±0.4	13±6	-3.8±0.5	0	0.2±0.1	0.03±0.02	0	89±6
713	543.7±0.2	1.70±0.10	6.2±0.4	6.3±0.2	54±2	-2.1±0.1	6.0±0.5	4.7±0.4	1.15±0.09	5.6±0.6	91±2
714	541.0±0.1	1.14±0.02	6.3±0.4	6.4±0.1	62±1	-1.9±0.1	6.7±0.3	4.9±0.2	1.25±0.05	5.8±0.5	88±1
715	542.6±0.1	1.14±0.02	6.2±0.4	6.4±0.1	61±1	-1.9±0.1	6.7±0.3	4.9±0.3	1.27±0.06	5.4±0.5	88±2
716	574.9±0.0	1.09±0.08	6.2±0.4	5.5±0.2	99±0	-0.2±0.1	0	1.1±0.1	3.0±0.2	12.8±1.8	99±4
717	575.2±0.0	1.09±0.08	6.2±0.4	5.5±0.2	100±0	-0.2±0.1	0	1.2±0.1	3.0±0.2	13.2±1.6	100±4
718	576.2±0.1	1.10±0.08	6.2±0.4	5.5±0.2	99±0	-0.3±0.1	0	1.5±0.1	3.0±0.2	14.2±1.6	100±5
719	500.2±0.0	1.11±0.10	6.2±0.4	7.1±0.2	35±3	-2.7±0.1	0	2.6±0.4	0.9±0.1	1.0±1.1	93±3
720	500.3±0.0	1.16±0.04	6.2±0.4	7.0±0.2	12±5	-3.9±0.5	0	0.5±0.3	0.1±0.1	0	93±5
721	541.2±0.1	1.15±0.22	6.2±0.4	5.9±0.2	66±2	-1.7±0.1	4.7±0.4	4.3±0.4	1.3±0.1	4.6±0.6	86±3
722	540.9±0.2	1.20±0.06	6.2±0.4	9.9±0.4	57±2	-2.0±0.1	9.5±1.0	6.8±0.6	1.8±0.2	5.1±1.8	87±2
723	540.8±0.1	1.08±0.16	6.2±0.4	2.9±0.4	70±7	-1.6±0.2	2.7±0.9	2.7±0.9	0.7±0.2	4.3±1.3	88±10
724	541.2±0.1	1.15±0.11	6.9±0.4	5.9±0.2	69±1	-1.8±0.1	4.7±0.4	4.4±0.4	1.5±0.1	5.6±0.8	88±3
725	541.1±0.1	1.13±0.11	5.0±0.3	5.8±0.2	52±2	-1.9±0.1	5.7±0.6	4.3±0.5	0.9±0.1	3.9±0.7	89±3
726	540.3±0.1	1.20±0.06	4.0±0.2	6.2±0.1	41±2	-2.0±0.1	4.6±0.4	3.4±0.3	0.71±0.06	2.1±0.7	88±2
727	540.1±0.1	1.22±0.06	3.0±0.2	6.3±0.2	30±2	-2.1±0.1	5.0±0.7	2.4±0.3	0.42±0.05	0.9±0.8	88±2
728	540.4±0.1	1.50±0.09	6.9±0.4	6.1±0.2	61±2	-2.0±0.1	5.6±0.4	4.5±0.4	1.24±0.08	5.5±0.6	88±2
729	540.9±0.1	1.55±0.09	4.9±0.3	6.5±0.1	47±2	-2.1±0.1	5.7±0.4	3.8±0.3	0.82±0.06	2.8±0.5	86±2
730	540.4±0.1	1.50±0.08	4.0±0.2	6.3±0.1	35±2	-2.2±0.1	4.5±0.4	3.0±0.3	0.56±0.05	2.0±0.7	89±2
731	540.7±0.1	2.53±0.15	5.9±0.3	5.9±0.2	44±2	-2.3±0.1	6.0±0.6	3.8±0.4	0.71±0.07	5.2±0.7	90±2
732	540.7±0.1	2.45±0.16	4.9±0.3	5.9±0.2	39±3	-2.3±0.1	6.1±0.9	3.3±0.5	0.59±0.08	3.9±0.6	89±3

Table 10.2.2 (*continued*) Summary of all experimental benzene SCWO data measured at *P*=246±2 bar

Run No.	*T* (°C)	Φ	τ (s)	$[C_6H_6]_0$ 10^{-7} mol/mL	Conversion (%)	ln *k*'	$[C_6H_5OH]$ 10^{-9} mol/mL	[CO] 10^{-7} mol/mL	$[CO_2]$ 10^{-6} mol/mL	$[CH_4]$ 10^{-8} mol/mL	Carbon Balance (%)
733	539.9±0.2	2.29±0.16	3.0±0.2	5.9±0.3	21±4	-2.5±0.2	4.3±1.4	1.8±0.6	0.29±0.09	1.2±0.5	93±4
734	541.1±0.1	1.10±0.05	6.2±0.4	5.7±0.1	63±2	-1.8±0.1	7.6±0.5	5.1±0.4	1.15±0.08	7.9±0.8	90±2
735	540.7±0.2	1.08±0.05	5.0±0.3	5.6±0.1	51±2	-2.0±0.1	10.1±0.7	4.5±0.3	0.79±0.05	5.6±0.5	89±2
736	540.5±0.1	1.10±0.04	4.0±0.2	5.7±0.1	40±2	-2.1±0.1	10.5±0.9	3.7±0.3	0.56±0.05	3.7±0.7	90±2
737	541.7±0.1	0.87±0.04	6.0±0.3	5.8±0.1	66±1	-1.7±0.1	4.7±0.3	4.3±0.3	1.31±0.08	5.7±0.4	87±2
738	541.7±0.1	0.87±0.05	5.0±0.3	5.8±0.1	57±1	-1.8±0.1	6.2±0.5	4.4±0.3	0.98±0.06	5.4±0.8	87±2
739	541.4±0.3	1.30±0.07	4.9±0.3	5.7±0.1	50±2	-2.0±0.1	8.2±0.6	4.1±0.3	0.73±0.06	5.0±0.5	86±2
740	541.7±0.3	1.28±0.07	5.9±0.3	5.7±0.1	60±3	-1.9±0.1	7.7±0.8	4.6±0.5	0.96±0.09	6.6±0.7	84±3
741	540.8±0.1	1.06±0.03	6.1±0.4	5.6±0.1	66±1	-1.8±0.1	6.8±0.3	4.8±0.2	1.18±0.06	8.5±0.5	88±2
742	540.9±0.1	1.04±0.03	5.0±0.3	5.5±0.1	56±1	-1.8±0.1	7.8±0.4	4.3±0.3	0.88±0.05	6.0±0.5	87±2
743	540.8±0.1	1.05±0.03	4.0±0.2	5.6±0.1	45±1	-1.9±0.1	8.2±0.5	3.7±0.3	0.65±0.04	4.4±0.8	88±2
744	566.0±0.1	0.95±0.02	6.9±0.4	5.6±0.1	99±0	-0.3±0.1	0	1.3±0.2	2.75±0.08	14.2±1.5	90±2
745	565.7±0.1	0.96±0.02	5.9±0.3	5.6±0.1	98±0	-0.4±0.1	0.85±0.05	2.7±0.1	2.59±0.08	15.5±1.1	92±2
746	566.0±0.1	0.96±0.02	5.0±0.3	5.6±0.1	95±0	-0.5±0.1	2.15±0.06	4.2±0.1	2.33±0.07	16.0±0.9	92±2
747	566.2±0.2	1.01±0.02	4.0±0.2	6.2±0.1	92±1	-0.5±0.1	3.2±0.2	5.0±0.3	2.05±0.09	14.4±1.0	82±2
748	565.7±0.2	1.02±0.02	3.0±0.2	6.2±0.1	79±1	-0.7±0.1	8.7±0.4	6.5±0.3	1.46±0.06	12.8±0.8	83±1
749	540.7±0.1	0.90±0.02	3.0±0.2	6.1±0.1	30±2	-2.1±0.1	5.0±0.6	2.5±0.3	0.46±0.06	1.7±0.3	91±2
750	540.0±0.1	0.89±0.02	4.0±0.2	6.1±0.1	43±2	-2.0±0.1	8.7±0.8	3.7±0.3	0.68±0.05	3.7±0.3	89±2
751	540.0±0.1	0.48±0.02	7.0±0.4	5.8±0.2	79±1	-1.5±0.1	2.2±0.1	3.2±0.4	1.9±0.1	4.4±1.0	86±3
752	540.0±0.2	0.48±0.02	6.0±0.4	5.8±0.2	72±1	-1.6±0.1	3.0±0.2	4.0±0.4	1.6±0.1	5.4±1.6	88±2
753	540.0±0.1	0.48±0.02	4.0±0.2	5.8±0.2	53±2	-1.7±0.1	7.0±0.8	4.0±0.5	0.91±0.08	3.7±0.8	86±3
754	540.0±0.1	0.48±0.02	3.0±0.2	5.9±0.2	35±2	-1.9±0.1	7.4±0.9	2.7±0.4	0.52±0.06	1.4±0.2	89±3
755	541.1±0.2	0.95±0.04	7.0±0.4	12.2±0.3	56±1	-2.1±0.1	12.6±0.8	7.0±0.6	2.3±0.2	5.1±3.0	87±2
756	541.5±0.3	0.95±0.04	6.0±0.4	12.2±0.3	51±1	-2.1±0.1	13.9±1.1	7.5±0.6	2.1±0.3	6.0±2.2	90±4
757	541.7±0.2	0.95±0.04	5.0±0.3	12.2±0.3	41±2	-2.2±0.1	20.4±1.8	6.3±0.6	1.3±0.1	4.1±0.5	88±2
758	540.9±0.2	0.91±0.05	4.0±0.2	12.0±0.2	29±2	-2.5±0.1	6.4±0.7	3.6±0.5	0.9±0.1	0.8±0.1	89±2
759	540.8±0.2	0.94±0.06	3.0±0.2	12.1±0.2	20±2	-2.6±0.1	5.8±1.0	2.3±0.5	0.50±0.08	0.40±0.06	90±2
760	541.1±0.1	0.83±0.04	6.9±0.4	3.9±0.1	77±1	-1.6±0.1	2.5±0.4	3.1±0.5	1.0±0.1	6.1±0.9	85±5
761	541.3±0.1	0.83±0.04	5.9±0.3	3.9±0.1	66±1	-1.7±0.1	5.9±0.4	3.6±0.2	0.74±0.05	6.4±0.6	85±2
762	541.2±0.1	0.83±0.05	5.0±0.3	3.9±0.1	58±2	-1.8±0.1	7.3±0.7	3.4±0.3	0.55±0.05	5.0±0.6	84±2
763	541.0±0.1	0.88±0.03	4.0±0.2	3.8±0.1	47±2	-1.8±0.1	3.9±0.3	2.9±0.2	0.53±0.05	3.5±0.3	91±3

Table 10.2.2 (*continued*) Summary of all experimental benzene SCWO data measured at *P*=246±2 bar

Run No.	*T* (°C)	Φ	τ (s)	$[C_6H_6]_0$ 10^{-7} mol/mL	Conversion (%)	ln *k'*	$[C_6H_5OH]$ 10^{-9} mol/mL	[CO] 10^{-7} mol/mL	$[CO_2]$ 10^{-6} mol/mL	$[CH_4]$ 10^{-8} mol/mL	Carbon Balance (%)
764	540.7±0.2	0.88±0.04	3.0±0.2	3.9±0.1	32±2	-2.1±0.1	5.0±0.6	2.2±0.3	0.32±0.04	2.2±0.3	94±2
765	550.9±0.2	1.00±0.02	5.9±0.3	5.8±0.1	83±1	-1.2±0.1	3.9±0.2	4.6±0.2	1.92±0.07	10.3±0.8	89±2
766	550.6±0.1	1.00±0.02	7.0±0.4	5.9±0.1	88±0	-1.2±0.1	3.1±0.1	4.3±0.2	2.16±0.07	12.5±1.0	89±2
767	550.5±0.1	0.98±0.06	7.1±0.4	12.1±0.6	84±1	-1.4±0.1	8.9±0.8	8.1±0.7	4.5±0.3	16.5±1.8	92±4
768	550.5±0.1	1.04±0.05	5.1±0.3	12.7±0.4	69±1	-1.5±0.1	17.7±1.4	10.4±0.7	3.0±0.2	13.4±1.2	88±2
769	550.3±0.1	1.09±0.09	3.0±0.2	12.9±0.2	38±1	-1.9±0.1	25.5±1.8	5.9±0.5	1.05±0.08	4.0±0.9	86±2
770	550.2±0.1	1.05±0.04	6.0±0.4	6.0±0.1	79±1	-1.3±0.1	4.5±0.2	5.2±0.2	1.98±0.09	10.5±0.7	94±2
771	549.2±0.2	1.09±0.04	5.0±0.3	6.2±0.1	71±1	-1.4±0.1	6.4±0.4	5.8±0.4	1.57±0.09	9.7±0.9	91±2
772	550.6±0.0	1.10±0.07	3.0±0.2	6.2±0.3	44±3	-1.7±0.1	10.0±1.5	4.6±0.7	0.8±0.1	4.9±1.0	92±4
773	550.7±0.1	0.99±0.08	7.0±0.4	3.7±0.1	91±0	-1.1±0.1	1.29±0.06	2.5±0.2	1.50±0.07	8.3±0.9	91±3
774	550.5±0.1	0.99±0.08	5.0±0.3	3.7±0.1	75±1	-1.3±0.1	3.1±0.2	3.7±0.2	1.02±0.05	7.3±0.6	93±2
775	550.2±0.0	0.99±0.08	3.0±0.2	3.7±0.1	50±2	-1.5±0.1	5.1±0.5	3.2±0.3	0.52±0.04	4.2±0.3	91±2
776	550.4±0.1	0.48±0.01	7.0±0.4	5.9±0.1	93±0	-1.0±0.1	0.69±0.08	2.1±0.4	2.9±0.1	7.0±0.9	96±4
777	550.7±0.1	0.48±0.01	5.0±0.3	5.9±0.1	82±0	-1.1±0.1	3.3±0.3	4.4±0.5	2.2±0.1	8.5±2.0	96±4
778	550.7±0.1	0.48±0.01	3.0±0.2	5.9±0.1	56±1	-1.3±0.1	10.1±0.9	5.1±0.4	1.13±0.08	5.2±0.9	94±2
779	550.2±0.2	2.38±0.10	7.0±0.4	5.8±0.2	60±2	-2.0±0.1	7.5±0.5	5.6±0.4	1.08±0.08	11.9±1.8	92±2
780	550.7±0.1	2.37±0.09	5.0±0.3	5.8±0.1	49±2	-2.0±0.1	10.3±0.7	5.1±0.3	0.78±0.06	8.3±0.9	93±2
781	550.9±0.1	2.38±0.09	3.0±0.2	5.8±0.1	32±2	-2.1±0.1	11.0±1.2	3.3±0.4	0.41±0.04	4.1±0.6	93±2
782	540.2±0.1	0.90±0.02	7.0±0.4	12.0±0.3	50±2	-2.3±0.1	11.2±1.3	7.1±0.8	2.3±0.2	4.7±1.0	94±3
783	540.8±0.1	0.90±0.03	5.0±0.3	12.0±0.3	35±3	-2.5±0.1	11.0±1.9	6.1±1.0	1.4±0.2	3.6±1.4	95±3
784	541.1±0.1	0.90±0.03	3.0±0.2	12.0±0.3	15±4	-2.9±0.3	8.0±3.1	2.6±1.1	0.5±0.2	0.6±0.2	97±4
788	541.0±0.1	0.89±0.04	6.0±0.4	5.9±0.2	62±3	-1.8±0.1	5.5±0.6	4.4±0.4	1.3±0.1	4.5±2.1	90±3
789	541.4±0.1	0.90±0.04	4.0±0.2	6.0±0.2	44±2	-2.0±0.1	5.8±0.96	3.8±0.4	0.78±0.07	3.3±1.0	91±2
792	541.6±0.1	0.85±0.04	6.0±0.4	5.8±0.1	65±1	-1.7±0.1	4.8±0.4	4.7±0.2	1.46±0.07	6.1±0.5	93±2
793	541.9±0.1	0.85±0.04	4.0±0.2	5.8±0.1	43±1	-2.0±0.1	6.8±0.8	4.1±0.3	0.82±0.05	3.9±0.5	95±2
795	532.2±0.1	0.93±0.03	6.0±0.4	12.3±0.3	24±3	-3.1±0.1	2.9±0.5	3.0±0.6	0.9±0.2	0.56±4.0	93±3
798	531.0±0.1	0.96±0.03	6.0±0.3	6.1±0.1	32±2	-2.8±0.1	2.8±0.2	2.6±0.3	0.72±0.06	1.2±0.1	96±2
799	530.9±0.0	0.96±0.10	6.0±0.4	4.0±0.1	38±3	-2.5±0.1	2.3±0.3	2.3±0.3	0.55±0.07	2.1±0.5	95±3

Table 10.2.3 Benzene SCWO pressure variation data measured at T=540°C, $[C_6H_6]_0$=0.6 mM, Φ=0.9

Run No.	T (°C)	P (bar)	Φ	τ (s)	$[C_6H_6]_0$ 10^{-7} mol/mL	Conversion (%)	ln k'	$[C_6H_5OH]$ 10^{-9} mol/mL	[CO] 10^{-7} mol/mL	$[CO_2]$ 10^{-6} mol/mL	$[CH_4]$ 10^{-8} mol/mL	Carbon Balance (%)
737	541.7±0.1	244.2±0.5	0.87±0.04	6.0±0.3	5.8±0.1	66±1	-1.7±0.1	4.7±0.3	4.3±0.3	1.31±0.03	5.7±0.4	87±2
738	541.7±0.1	244.6±0.5	0.87±0.05	5.0±0.3	5.8±0.1	57±1	-1.8±0.1	6.2±0.5	4.4±0.3	0.98±0.06	5.4±0.8	87±2
749	540.7±0.1	244.9±0.3	0.90±0.02	3.0±0.2	6.1±0.1	30±2	-2.1±0.1	5.0±0.6	2.5±0.3	0.46±0.06	1.7±0.3	91±2
750	540.0±0.1	245.3±0.3	0.89±0.02	4.0±0.2	6.1±0.1	43±2	-2.0±0.1	8.7±0.8	3.7±0.3	0.68±0.05	3.7±0.3	89±2
785	541.2±0.1	277.2±0.5	0.90±0.04	6.0±0.4	6.0±0.1	72±1	-1.5±0.1	6.2±0.2	4.7±0.2	1.67±0.08	9.0±1.9	91±2
786	541.2±0.1	278.0±0.6	0.91±0.04	5.0±0.3	6.0±0.1	62±1	-1.6±0.1	8.5±0.4	5.0±0.3	1.30±0.07	7.4±0.5	91±2
787	540.9±0.1	278.4±0.4	0.91±0.04	4.0±0.2	6.0±0.1	51±2	-1.8±0.1	12.1±0.7	4.5±0.4	0.90±0.07	5.2±0.8	90±2
788	541.0±0.1	245.8±0.5	0.89±0.04	6.0±0.4	5.9±0.2	62±3	-1.8±0.1	5.5±0.6	4.4±0.4	1.3±0.1	4.5±2.1	90±3
789	541.4±0.1	246.5±0.5	0.90±0.04	4.0±0.2	6.0±0.2	44±2	-2.0±0.1	5.8±0.96	3.8±0.4	0.78±0.07	3.3±1.0	91±2
790	539.4±0.2	138.6±0.4	0.86±0.03	4.0±0.2	5.8±0.1	21±2	-2.8±0.1	0.32±0.05	0.9±0.2	0.36±0.06	0.07±0.01	92±2
791	536.9±0.5	138.4±0.3	0.87±0.04	3.0±0.2	5.8±0.1	15±3	-2.9±0.2	0	0.7±0.3	0.24±0.08	0.04±0.4	94±3
792	541.6±0.1	245.9±0.4	0.85±0.04	6.0±0.4	5.8±0.1	65±1	-1.7±0.1	4.8±0.4	4.7±0.2	1.46±0.07	6.1±0.5	93±2
793	541.9±0.1	246.3±0.4	0.85±0.04	4.0±0.2	5.8±0.1	43±1	-2.0±0.1	6.8±0.8	4.1±0.3	0.82±0.05	3.9±0.5	95±2
800	541.9±0.0	140.5±0.5	0.94±0.02	4.0±0.2	6.1±0.1	21±3	-2.8±0.2	0.33±0.06	1.0±0.3	0.43±0.08	0.08±0.02	94±3
801	541.7±0.0	167.9±0.6	0.98±0.09	4.0±0.2	6.2±0.1	19±4	-3.0±0.2	0.7±0.2	1.2±0.4	0.4±0.1	0.17±0.05	96±4
802	541.7±0.0	197.5±0.5	0.95±0.02	4.0±0.2	6.1±0.1	25±2	-2.7±0.1	1.6±0.2	2.0±0.3	0.50±0.06	0.7±0.1	95±2
803	541.6±0.1	197.8±0.5	0.94±0.02	5.0±0.3	6.1±0.1	31±2	-2.6±0.1	2.0±0.2	2.3±0.3	0.69±0.08	0.7±0.1	94±3
804	541.5±0.1	228.6±0.5	0.80±0.33	5.0±0.3	6.1±0.1	44±2	-2.2±0.1	4.3±0.3	3.9±0.3	0.95±0.06	3.0±0.2	95±2
805	541.3±0.1	228.6±0.5	0.91±0.02	4.0±0.2	6.1±0.1	35±2	-2.2±0.1	5.5±0.7	3.4±0.4	0.67±0.07	2.5±0.2	94±2
806	541.3±0.0	138.6±0.5	0.92±0.03	3.0±0.2	6.0±0.2	18±4	-2.7±0.3	0	0.8±0.3	0.3±0.1	0.03±0.01	92±4
807	540.9±0.0	195.8±0.4	0.93±0.07	3.0±0.2	6.0±0.2	17±4	-2.8±0.3	1.1±0.4	1.3±0.5	0.3±0.1	0.3±0.1	95±4
808	540.6±0.0	227.9±0.5	0.91±0.07	3.0±0.2	6.0±0.2	23±5	-2.4±0.2	4.2±1.4	2.0±0.6	0.4±0.1	1.0±0.3	93±5

Table 10.2.4 Benzene SCWO temperature variation data measured at P=246 bar, $[C_6H_6]_0$=0.6 mM, Φ=1.1±0.1

Run No.	T (°C)	Φ	τ (s)	$[C_6H_6]_0$ 10^{-7} mol/mL	Conversion (%)	ln k'	$[C_6H_5OH]$ 10^{-9} mol/mL	[CO] 10^{-7} mol/mL	$[CO_2]$ 10^{-6} mol/mL	$[CH_4]$ 10^{-8} mol/mL	Carbon Balance (%)
702	578.1±0.1	1.15±0.04	6.2±0.4	6.1±0.1	97±0	-0.6±0.1	0	2.5±0.1	3.1±0.1	17.8±1.8	101±3
704	504.7±0.1	1.26±0.13	6.2±0.4	6.0±0.2	20±4	-3.4±0.2	0	0.4±0.1	0.13±0.04	0.010±0.006	85±4
705	528.6±0.1	1.20±0.04	6.2±0.4	5.9±0.2	31±4	-2.8±0.2	1.7±0.4	2.1±0.4	0.5±0.1	1.0±0.2	89±4
706	553.3±0.1	1.19±0.08	6.2±0.4	5.9±0.2	80±1	-1.4±0.1	5.5±0.4	6.2±0.5	2.0±0.1	12.8±1.3	97±3
707	532.7±0.1	1.09±0.09	6.2±0.4	5.9±0.3	41±4	-2.5±0.2	2.5±0.4	2.3±0.7	0.7±0.2	1.2±0.4	86±6
708	542.7±0.1	1.17±0.12	6.2±0.4	5.8±0.2	60±2	-1.9±0.1	5.1±0.5	4.6±0.5	1.2±0.1	5.7±0.5	90±3
709	587.0±0.1	1.27±0.08	6.3±0.4	6.1±0.3	97±0	-0.6±0.1	0	1.4±0.2	3.1±0.2	14.4±2.0	94±4
710	562.5±0.3	1.21±0.11	6.2±0.4	5.8±0.4	92±1	-0.9±0.1	2.3±0.3	4.8±0.7	2.5±0.3	15.2±2.4	99±8
711	518.7±0.3	1.25±0.08	6.2±0.4	6.1±0.3	20±5	-3.3±0.3	1.0±0.4	1.0±0.4	0.23±.08	0.2±0.1	89±5
712	478.5±0.2	1.23±0.13	6.2±0.4	6.2±0.4	13±6	-3.8±0.5	0	0.2±0.1	0.03±0.02	0	89±6
714	541.0±0.1	1.14±0.02	6.3±0.4	6.4±0.1	62±1	-1.9±0.1	6.7±0.3	4.9±0.2	1.25±0.05	5.8±0.5	88±1
715	542.6±0.1	1.14±0.02	6.2±0.4	6.4±0.1	61±1	-1.9±0.1	6.7±0.3	4.9±0.3	1.27±0.06	5.4±0.5	88±2
716	574.9±0.0	1.09±0.08	6.2±0.4	5.5±0.2	99±0	-0.2±0.1	0	1.1±0.1	3.0±0.2	12.8±1.8	99±4
717	575.2±0.0	1.09±0.08	6.2±0.4	5.5±0.2	100±0	-0.2±0.1	0	1.2±0.1	3.0±0.2	13.2±1.6	100±4
718	576.2±0.1	1.10±0.08	6.2±0.4	5.5±0.2	99±0	-0.3±0.1	0	1.5±0.1	3.0±0.2	14.2±1.6	100±5
721	541.2±0.1	1.15±0.22	6.2±0.4	5.9±0.2	66±2	-1.7±0.1	4.7±0.4	4.3±0.4	1.3±0.1	4.6±0.6	86±3
734	541.1±0.1	1.10±0.05	6.2±0.4	5.7±0.1	63±2	-1.8±0.1	7.6±0.5	5.1±0.4	1.15±0.08	7.9±0.8	90±2
741	540.8±0.1	1.06±0.03	6.1±0.4	5.6±0.1	66±1	-1.8±0.1	6.8±0.3	4.8±0.2	1.18±0.06	8.5±0.5	88±2
745	565.7±0.1	0.96±0.02	5.9±0.3	5.6±0.1	98±0	-0.4±0.1	0.85±0.05	2.7±0.1	2.59±0.08	15.5±1.1	92±2
765	550.9±0.2	1.00±0.02	5.9±0.3	5.8±0.1	83±1	-1.2±0.1	3.9±0.2	4.6±0.2	1.92±0.07	10.3±0.8	89±2
798	531.0±0.1	0.96±0.03	6.0±0.3	6.1±0.1	32±2	-2.8±0.1	2.8±0.2	2.6±0.3	0.72±0.06	1.2±0.1	96±2

Table 10.2.5 Benzene SCWO Φ variation data measured at T=530°C, P=246 bar, $[C_6H_6]_0$=0.6 mM

Run No.	T (°C)	Φ	τ (s)	$[C_6H_6]_0$ 10^{-7} mol/mL	Conversion (%)	ln k'	$[C_6H_5OH]$ 10^{-9} mol/mL	[CO] 10^{-7} mol/mL	$[CO_2]$ 10^{-6} mol/mL	$[CH_4]$ 10^{-8} mol/mL	Carbon Balance (%)
795	532.2±0.1	0.93±0.03	6.0±0.4	12.3±0.3	24±3	-3.1±0.1	2.9±0.5	3.0±0.6	0.9±0.2	0.56±4.0	93±3
798	531.0±0.1	0.96±0.03	6.0±0.3	6.1±0.1	32±2	-2.8±0.1	2.8±0.2	2.6±0.3	0.72±0.06	1.2±0.1	96±2
799	530.9±0.0	0.96±0.10	6.0±0.4	4.0±0.1	38±3	-2.5±0.1	2.3±0.3	2.3±0.3	0.55±0.07	2.1±0.5	95±3

Table 10.2.6 Benzene SCWO Φ variation data measured at T=540°C, P=246 bar, $[C_6H_6]_0$=0.6 mM

Run No.	T (°C)	Φ	τ (s)	$[C_6H_6]_0$ 10^{-7} mol/mL	Conversion (%)	ln k'	$[C_6H_5OH]$ 10^{-9} mol/mL	[CO] 10^{-7} mol/mL	$[CO_2]$ 10^{-6} mol/mL	$[CH_4]$ 10^{-8} mol/mL	Carbon Balance (%)
708	542.7±0.1	1.17±0.12	6.2±0.4	5.8±0.2	60±2	-1.9±0.1	5.1±0.5	4.6±0.5	1.2±0.1	5.7±0.5	90±3
713	543.7±0.2	1.70±0.10	6.2±0.4	6.3±0.2	54±2	-2.1±0.1	6.0±0.5	4.7±0.4	1.15±0.09	5.6±0.6	91±2
714	541.0±0.1	1.14±0.02	6.3±0.4	6.4±0.1	62±1	-1.9±0.1	6.7±0.[illegible]	4.9±0.2	1.25±0.05	5.8±0.5	88±1
715	542.6±0.1	1.14±0.02	6.2±0.4	6.4±0.1	61±1	-1.9±0.1	6.7±0.[illegible]	4.9±0.3	1.27±0.06	5.4±0.5	88±2
721	541.2±0.1	1.15±0.22	6.2±0.4	5.9±0.2	66±2	-1.7±0.1	4.7±0.4	4.3±0.4	1.3±0.1	4.6±0.6	86±3
724	541.2±0.1	1.15±0.11	6.9±0.4	5.9±0.2	69±1	-1.8±0.1	4.7±0.4	4.4±0.4	1.5±0.1	5.6±0.8	88±3
725	541.1±0.1	1.13±0.11	5.0±0.3	5.8±0.2	52±2	-1.9±0.1	5.7±0.6	4.3±0.5	0.9±0.1	3.9±0.7	89±3
726	540.3±0.1	1.20±0.06	4.0±0.2	6.2±0.1	41±2	-2.0±0.1	4.6±0.4	3.4±0.3	0.71±0.06	2.1±0.7	88±2
727	540.1±0.1	1.22±0.06	3.0±0.2	6.3±0.2	30±2	-2.1±0.1	5.0±0.7	2.4±0.3	0.42±0.05	0.9±0.8	88±2
728	540.4±0.1	1.50±0.09	6.9±0.4	6.1±0.2	61±2	-2.0±0.1	5.6±0.4	4.5±0.4	1.24±0.08	5.5±0.6	88±2
729	540.9±0.1	1.55±0.09	4.9±0.3	6.5±0.1	47±2	-2.1±0.1	5.7±0.4	3.8±0.3	0.82±0.06	2.8±0.5	86±2
730	540.4±0.1	1.50±0.08	4.0±0.2	6.3±0.1	35±2	-2.2±0.1	4.5±0.4	3.0±0.3	0.56±0.05	2.0±0.7	89±2
731	540.7±0.1	2.53±0.15	5.9±0.3	5.9±0.2	44±2	-2.3±0.1	6.0±0.6	3.8±0.4	0.71±0.07	5.2±0.7	90±2
732	540.7±0.1	2.45±0.16	4.9±0.3	5.9±0.2	39±3	-2.3±0.1	6.1±0.9	3.3±0.5	0.59±0.08	3.9±0.6	89±3
733	539.9±0.2	2.29±0.16	3.0±0.2	5.9±0.3	21±4	-2.5±0.2	4.3±1.4	1.8±0.6	0.29±0.09	1.2±0.5	93±4
734	541.1±0.1	1.10±0.05	6.2±0.4	5.7±0.1	63±2	-1.8±0.1	7.6±0.5	5.1±0.4	1.15±0.08	7.9±0.8	90±2
735	540.7±0.2	1.08±0.05	5.0±0.3	5.6±0.1	51±2	-2.0±0.1	10.1±0.7	4.5±0.3	0.79±0.05	5.6±0.5	89±2
736	540.5±0.1	1.10±0.04	4.0±0.2	5.7±0.[illegible]	40±2	-2.1±0.1	10.5±0.9	3.7±0.3	0.56±0.05	3.7±0.7	90±2
737	541.7±0.1	0.87±0.04	6.0±0.3	5.8±0.1	66±1	-1.7±0.1	4.7±0.3	4.3±0.3	1.31±0.08	5.7±0.4	87±2
738	541.7±0.1	0.87±0.05	5.0±0.3	5.8±0.[illegible]	57±1	-1.8±0.1	6.2±0.5	4.4±0.3	0.98±0.06	5.4±0.8	87±2

Table 10.2.6 (*continued*) Benzene SCWO Φ variation data measured at T=540°C, P=246 bar, $[C_6H_6]_0$=0.6 mM

Run No.	T (°C)	Φ	τ (s)	$[C_6H_6]_0$ 10^{-7} mol/mL	Conversion (%)	ln k'	$[C_6H_5OH]$ 10^{-9} mol/mL	[CO] 10^{-7} mol/mL	$[CO_2]$ 10^{-6} mol/mL	$[CH_4]$ 10^{-8} mol/mL	Carbon Balance (%)
741	540.8±0.1	1.06±0.03	6.1±0.4	5.6±0.1	66±1	-1.8±0.1	6.8±0.3	4.8±0.2	1.18±0.06	8.5±0.5	88±2
742	540.9±0.1	1.04±0.03	5.0±0.3	5.5±0.1	56±1	-1.8±0.1	7.8±0.4	4.3±0.3	0.88±0.05	6.0±0.5	87±2
743	540.8±0.1	1.05±0.03	4.0±0.2	5.6±0.1	45±1	-1.9±0.1	8.2±0.5	3.7±0.3	0.65±0.04	4.4±0.8	88±2
749	540.7±0.1	0.90±0.02	3.0±0.2	6.1±0.1	30±2	-2.1±0.1	5.0±0.6	2.5±0.3	0.46±0.06	1.7±0.3	91±2
750	540.0±0.1	0.89±0.02	4.0±0.2	6.1±0.1	43±2	-2.0±0.1	8.7±0.8	3.7±0.3	0.68±0.05	3.7±0.3	89±2
751	540.0±0.1	0.48±0.02	7.0±0.4	5.8±0.2	79±1	-1.5±0.1	2.2±0.1	3.2±0.4	1.9±0.1	4.4±1.0	86±3
752	540.0±0.2	0.48±0.02	6.0±0.4	5.8±0.2	72±1	-1.6±0.1	3.0±0.2	4.0±0.4	1.6±0.1	5.4±1.6	88±2
753	540.0±0.1	0.48±0.02	4.0±0.2	5.8±0.2	53±2	-1.7±0.1	7.0±0.8	4.0±0.5	0.91±0.08	3.7±0.8	86±3
754	540.0±0.1	0.48±0.02	3.0±0.2	5.9±0.2	35±2	-1.9±0.1	7.4±0.9	2.7±0.4	0.52±0.06	1.4±0.2	89±3
788	541.0±0.1	0.89±0.04	6.0±0.4	5.9±0.2	62±3	-1.8±0.1	5.5±0.6	4.4±0.4	1.3±0.1	4.5±2.1	90±3
789	541.4±0.1	0.90±0.04	4.0±0.2	6.0±0.2	44±2	-2.0±0.1	5.8±0.96	3.8±0.4	0.78±0.07	3.3±1.0	91±2
790	539.4±0.2	0.86±0.03	4.0±0.2	5.8±0.1	21±2	-2.8±0.1	0.32±0.05	0.9±0.2	0.36±0.06	0.07±0.01	92±2
791	536.9±0.5	0.87±0.04	3.0±0.2	5.8±0.1	15±3	-2.9±0.2	0	0.7±0.3	0.24±0.08	0.04±0.4	94±3
792	541.6±0.1	0.85±0.04	6.0±0.4	5.8±0.1	65±1	-1.7±0.1	4.8±0.4	4.7±0.2	1.46±0.07	6.1±0.5	93±2
793	541.9±0.1	0.85±0.04	4.0±0.2	5.8±0.1	43±1	-2.0±0.1	6.8±0.8	4.1±0.3	0.82±0.05	3.9±0.5	95±2

Table 10.2.7 Benzene SCWO Φ variation data measured at T=550°C, P=246 bar, $[C_6H_6]_0$=0.6 mM

Run No.	T (°C)	Φ	τ (s)	$[C_6H_6]_0$ 10^{-7} mol/mL	Conversion (%)	ln k'	$[C_6H_5OH]$ 10^{-9} mol/mL	[CO] 10^{-7} mol/mL	$[CO_2]$ 10^{-6} mol/mL	$[CH_4]$ 10^{-8} mol/mL	Carbon Balance (%)
770	550.2±0.1	1.05±0.04	6.0±0.4	6.0±0.1	79±1	-1.3±0.1	4.5±0.2	5.2±0.2	1.98±0.09	10.5±0.7	94±2
771	549.2±0.2	1.09±0.04	5.0±0.3	6.2±0.1	71±1	-1.4±0.1	6.4±0.4	5.8±0.4	1.57±0.09	9.7±0.9	91±2
772	550.6±0.0	1.10±0.07	3.0±0.2	6.2±0.3	44±3	-1.7±0.1	10.0±1.5	4.6±0.7	0.8±0.1	4.9±1.0	92±4
776	550.4±0.1	0.48±0.01	7.0±0.4	5.9±0.1	93±0	-1.0±0.1	0.69±0.08	2.1±0.4	2.9±0.1	7.0±0.9	96±4
777	550.7±0.1	0.48±0.01	5.0±0.3	5.9±0.1	82±0	-1.1±0.1	3.3±0.3	4.4±0.5	2.2±0.1	8.5±2.0	96±4
778	550.7±0.1	0.48±0.01	3.0±0.2	5.9±0.1	56±1	-1.3±0.1	10.1±0.9	5.1±0.4	1.13±0.08	5.2±0.9	94±2
779	550.2±0.2	2.38±0.10	7.0±0.4	5.8±0.2	60±2	-2.0±0.1	7.5±0.5	5.6±0.4	1.08±0.08	11.9±1.8	92±2
780	550.7±0.1	2.37±0.09	5.0±0.3	5.8±0.1	49±2	-2.0±0.1	10.3±0.7	5.1±0.3	0.78±0.06	8.3±0.9	93±2
781	550.9±0.1	2.38±0.09	3.0±0.2	5.8±0.1	32±2	-2.1±0.1	11.0±1.2	3.3±0.4	0.41±0.04	4.1±0.6	93±2

Table 10.2.8 Benzene SCWO concentration variation data measured at T=540°C, P=246 bar, Φ=0.9±0.1

Run No.	T (°C)	Φ	τ (s)	$[C_6H_6]_0$ 10^{-7} mol/mL	Conversion (%)	ln k^*	$[C_6H_5OH]$ 10^{-9} mol/mL	[CO] 10^{-7} mol/mL	$[CO_2]$ 10^{-6} mol/mL	$[CH_4]$ 10^{-8} mol/mL	Carbon Balance (%)
737	541.7±0.1	0.87±0.04	6.0±0.3	5.8±0.1	66±1	-1.7±0.1	4.7±0.3	4.3±0.3	1.31±0.08	5.7±0.4	87±2
738	541.7±0.1	0.87±0.05	5.0±0.3	5.8±0.1	57±1	-1.8±0.1	6.2±0.5	4.4±0.3	0.98±0.06	5.4±0.8	87±2
741	540.8±0.1	1.06±0.03	6.1±0.4	5.6±0.1	66±1	-1.8±0.1	6.8±0.3	4.8±0.2	1.18±0.06	8.5±0.5	88±2
742	540.9±0.1	1.04±0.03	5.0±0.3	5.5±0.1	56±1	-1.8±0.1	7.8±0.4	4.3±0.3	0.88±0.05	6.0±0.5	87±2
743	540.8±0.1	1.05±0.03	4.0±0.2	5.6±0.1	45±1	-1.9±0.1	8.2±0.5	3.7±0.3	0.65±0.04	4.4±0.8	88±2
749	540.7±0.1	0.90±0.02	3.0±0.2	6.1±0.1	30±2	-2.1±0.1	5.0±0.6	2.5±0.3	0.46±0.06	1.7±0.3	91±2
750	540.0±0.1	0.89±0.02	4.0±0.2	6.1±0.1	43±2	-2.0±0.1	8.7±0.8	3.7±0.3	0.68±0.05	3.7±0.3	89±2
755	541.1±0.2	0.95±0.04	7.0±0.4	12.2±0.3	56±1	-2.1±0.1	12.6±0.8	7.0±0.6	2.3±0.2	5.1±3.0	87±2
756	541.5±0.3	0.95±0.04	6.0±0.4	12.2±0.3	51±1	-2.1±0.1	13.9±1.1	7.5±0.6	2.1±0.3	6.0±2.2	90±4
757	541.7±0.2	0.95±0.04	5.0±0.3	12.2±0.3	41±2	-2.2±0.1	20.4±1.8	6.3±0.6	1.3±0.1	4.1±0.5	88±2
758	540.9±0.2	0.91±0.05	4.0±0.2	12.0±0.2	29±2	-2.5±0.1	6.4±0.7	3.6±0.5	0.9±0.1	0.8±0.1	89±2
759	540.8±0.2	0.94±0.06	3.0±0.2	12.1±0.2	20±2	-2.6±0.1	5.8±1.0	2.3±0.5	0.50±0.08	0.40±0.06	90±2
760	541.1±0.1	0.83±0.04	6.9±0.4	3.9±0.1	77±1	-1.6±0.1	2.5±0.4	3.1±0.5	1.0±0.1	6.1±0.9	85±5
761	541.3±0.1	0.83±0.04	5.9±0.3	3.9±0.1	66±1	-1.7±0.1	5.9±0.4	3.6±0.2	0.74±0.05	6.4±0.6	85±2
762	541.2±0.1	0.83±0.05	5.0±0.3	3.9±0.1	58±2	-1.8±0.1	7.3±0.7	3.4±0.3	0.55±0.05	5.0±0.6	84±2
763	541.0±0.1	0.88±0.03	4.0±0.2	3.8±0.1	47±2	-1.8±0.1	3.9±0.3	2.9±0.2	0.53±0.05	3.5±0.3	91±3
764	540.7±0.2	0.88±0.04	3.0±0.2	3.9±0.1	32±2	-2.1±0.1	5.0±0.6	2.2±0.3	0.32±0.04	2.2±0.3	94±2
782	540.2±0.1	0.90±0.02	7.0±0.4	12.0±0.3	50±2	-2.3±0.1	11.2±1.3	7.1±0.8	2.3±0.2	4.7±1.0	94±3
783	540.8±0.1	0.90±0.03	5.0±0.3	12.0±0.3	35±3	-2.5±0.1	11.0±1.9	6.1±1.0	1.4±0.2	3.6±1.4	95±3
784	541.1±0.1	0.90±0.03	3.0±0.2	12.0±0.3	15±4	-2.9±0.3	8.0±3.1	2.6±1.1	0.5±0.2	0.6±0.2	97±4
788	541.0±0.1	0.89±0.04	6.0±0.4	5.9±0.2	62±3	-1.8±0.1	5.5±0.6	4.4±0.4	1.3±0.1	4.5±2.1	90±3
789	541.4±0.1	0.90±0.04	4.0±0.2	6.0±0.2	44±2	-2.0±0.1	5.8±0.96	3.8±0.4	0.78±0.07	3.3±1.0	91±2
792	541.6±0.1	0.85±0.04	6.0±0.4	5.8±0.1	65±1	-1.7±0.1	4.8±0.4	4.7±0.2	1.46±0.07	6.1±0.5	93±2
793	541.9±0.1	0.85±0.04	4.0±0.2	5.8±0.1	43±1	-2.0±0.1	6.8±0.8	4.1±0.3	0.82±0.05	3.9±0.5	95±2

Table 10.2.9 Benzene SCWO concentration variation data measured at T=550°C, P=246 bar, Φ=1.0±0.1

Run No.	T (°C)	Φ	τ (s)	$[C_6H_6]_0$ 10^{-7} mol/mL	Conversion (%)	ln k'	$[C_6H_5OH]$ 10^{-9} mol/mL	[CO] 10^{-7} mol/mL	$[CO_2]$ 10^{-6} mol/mL	$[CH_4]$ 10^{-8} mol/mL	Carbon Balance (%)
766	550.6±0.1	1.00±0.02	7.0±0.4	5.9±0.1	88±0	-1.2±0.1	3.1±0.1	4.3±0.2	2.16±0.07	12.5±1.0	89±2
767	550.5±0.1	0.98±0.06	7.1±0.4	12.1±0.6	84±1	-1.4±0.1	8.9±0.8	8.1±0.7	4.5±0.3	16.5±1.8	92±4
768	550.5±0.1	1.04±0.05	5.1±0.3	12.7±0.4	69±1	-1.5±0.1	17.7±1.4	10.4±0.7	3.0±0.2	13.4±1.2	88±2
769	550.3±0.1	1.09±0.09	3.0±0.2	12.9±0.2	38±1	-1.9±0.1	25.5±1.8	5.9±0.5	1.05±0.08	4.0±0.9	86±2
770	550.2±0.1	1.05±0.04	6.0±0.4	6.0±0.1	79±1	-1.3±0.1	4.5±0.2	5.2±0.2	1.98±0.09	10.5±0.7	94±2
771	549.2±0.2	1.09±0.04	5.0±0.3	6.2±0.1	71±1	-1.4±0.1	6.4±0.4	5.8±0.4	1.57±0.09	9.7±0.9	91±2
772	550.6±0.0	1.10±0.07	3.0±0.2	6.2±0.3	44±3	-1.7±0.1	10.0±1.5	4.6±0.7	0.8±0.1	4.9±1.0	92±4
773	550.7±0.1	0.99±0.08	7.0±0.4	3.7±0.1	91±0	-1.1±0.1	1.29±0.06	2.5±0.2	1.50±0.07	8.3±0.9	91±3
774	550.5±0.1	0.99±0.08	5.0±0.3	3.7±0.1	75±1	-1.3±0.1	3.1±0.2	3.7±0.2	1.02±0.05	7.3±0.6	93±2
775	550.2±0.0	0.99±0.08	3.0±0.2	3.7±0.1	50±2	-1.5±0.1	5.1±0.5	3.2±0.3	0.52±0.04	4.2±0.3	91±2

Table 10.2.10 Benzene SCWO experiments conducted for detecting single- and multi-ringed aromatic species at P=246 bar

Run No.	T (°C)	Φ	τ (s)	$[C_6H_6]_0$ 10^{-7} mol/mL	Conversion (%)	ln k'	$[C_6H_5OH]$ 10^{-9} mol/mL	[CO] 10^{-7} mol/mL	$[CO_2]$ 10^{-6} mol/mL	$[CH_4]$ 10^{-8} mol/mL	Carbon Balance (%)
632	577.8±0.3	1.2±0.3	6.1±0.1	5.2±0.2	92.4±0.6	-0.87±0.03	2.5±0.5	4.5±0.6	2.3±0.2	18.2±1.9	102±5
633	527.6±0.2	1.1±0.4	6.1±0.1	4.9±0.2	23±4	-3.1±2	1.4±1.2	1.3±0.4	0.19±0.06	0.7±0.2	89±4
636	625.1±0.4	1.0±0.3	6.1±0.1	5.0±0.2	95.4±0.3	-0.68±0.02	0	1.1±0.2	2.7±0.2	13.5±1.3	102±5
637	625.9±0.4	1.3±0.3	6.0±0.1	5.2±0.2	90.9±0.6	-0.92±0.03	2.0±0.2	2.3±0.2	2.3±0.2	15.9±1.8	94±4
638	624.9±0.5	0.9±0.3	6.1±0.1	5.3±0.2	97±5	-0.39±0.02	0	0.35±0.04	2.9±0.2	11.2±1.1	97±5

10.3 Data Used in the Development of the SCWO Benzene Mechanism

The following section presents data used in the development of the supercritical water benzene oxidation mechanism. Section 10.3.1 summarizes the input data necessary to perform the QRRK calculations by CHEMACT or CHEMDIS for reactions for which pressure dependent rate constants were calculated. In Section 10.3.2 the thermodynamic data used in the model calculations is presented. Lastly, the full mechanism is presented in Section 10.3.3.

10.3.1 Data used in the QRRK analysis of specific reactions as implemented by CHEMDIS or CHEMACT

Lennard-Jones parameters for water (Dean *et al.*, 1991):
σ = 2.605 A, ε/k_B = 572. K, ΔE_{avg}(cal/mol) = 1425.

$H+O_2 \Leftrightarrow HO_2 \Leftrightarrow OH+O$

High-pressure rate constants used in the CHEMACT analysis

No.	Reaction	A (cm^3-mol-s)	n	E_a (cal/mol)
1	$H+O_2 \Leftrightarrow HO_2$	4.52×10^{13}	0.	0.
-1	$HO_2 \Leftrightarrow H+O_2$	5.51×10^{13}	0.	48800.
2	$HO_2 \Leftrightarrow OH+O$	2.34×10^{14}	0.	65600.

geometric mean frequency (HO_2) = 1738 cm^{-1} (Cobos *et al.*, 1985), σ = 3.458 A, ε/k_B = 107.4 K

Notes on sources of rate constants:
The rate constant k_1 is taken from Cobos *et al.* (1985). The reverse rate constant k_{-1} is calculated from microscopic reversibility using thermodynamic data given in Chapter 7. To obtain a value for k_2, the reverse rate constant k_{-2} was set equal to the forward rate constant for $OH+O=H+O_2$ as recommended by Cobos *et al.* (1985). The value of k_{-2} is taken from Baulch *et al.* (1992) and k_2 is calculated by microscopic reversibility.

Calculated rate constants by CHEMACT at 246 bar for T=298-1000 K

No.	Reaction	A (cm^3-mol-s)	n	E_a (cal/mol)
1	$H+O_2 \Leftrightarrow HO_2$	2.07×10^{18}	-1.691	890.
2	$H+O_2 \Leftrightarrow OH+O$	2.10×10^{15}	-0.3	20200.

$OH+OH \Leftrightarrow H_2O_2$

High-pressure rate constants used in the CHEMACT analysis

No.	Reaction	A (cm^3-mol-s)	n	E_a (cal/mol)
1	$OH+OH \Leftrightarrow H_2O_2$	1.99×10^{27}	-4.85	2760.
-1	$H_2O_2 \Leftrightarrow OH+OH$	9.05×10^{13}	0.	48100.

geometric mean frequency (H_2O_2) = 2052 cm^{-1} (Brouwer *et al.*, 1987), σ = 3.458 A, ε/k_B = 107.4 K

Notes on sources of rate constants:
The forward rate constant k_1 is a fit to the values of k_∞ at 210, 298, 406, 510, 614 and 694 K given in Fulle *et al.* (1996). The reverse rate constant k_{-1} is calculated from microscopic reversibility.

Calculated rate constants by CHEMACT at 246 bar for T=298-1000 K

No.	Reaction	A (cm^3-mol-s)	n	E_a (cal/mol)
1	$OH+OH \Leftrightarrow H_2O_2$	2.96×10^{28}	-5.262	2980.

$C_2H_2+H \Leftrightarrow C_2H_3$

High-pressure rate constants used in the CHEMACT analysis

No.	Reaction	A (cm^3-mol-s)	n	E_a (cal/mol)
1	$C_2H_2+H \Leftrightarrow C_2H_3$	1.73×10^{14}	0.	1640.
-1	$C_2H_3 \Leftrightarrow C_2H_2+H$	2.0×10^{14}	0.	39740.

geometric mean frequency (C_2H_3) = 2052 cm^{-1}, σ =4.1 A, ε/k_B = 209. K

Notes on sources of rate constants:
The reverse rate constant k_{-1} was reported by Warnatz (1984). The forward rate constant k_1 is calculated from microscopic reversibility.

Calculated rate constants by CHEMACT at 246 bar for T=298-1000 K

No.	Reaction	A (cm^3-mol-s)	n	E_a (cal/mol)
1	$C_2H_2+H \Leftrightarrow C_2H_3$	7.85×10^{14}	-.224	1770.

$CO+O \Leftrightarrow CO_2$

High-pressure rate constants used in the CHEMACT analysis

No.	Reaction	A (cm^3-mol-s)	n	E_a (cal/mol)
1	$CO+O \Leftrightarrow CO_2$	1.80×10^{10}	0.	2400.
-1	$CO_2 \Leftrightarrow CO+O$	7.5×10^{12}	0.	128800.

geometric mean frequency (CO_2) = 1089 cm^{-1}, σ = 3.763 A, ε/k_B = 244. K

Notes on sources of rate constants:
The forward rate constant is taken from Troe (1974). Westmoreland *et al.* (1986) also used the high-pressure value of Troe in his CHEMACT analysis of this reaction where he found good agreement between the CHEMACT predictions and the experimental data. The reverse rate constant k_{-1} is calculated from microscopic reversibility.

This reaction was found to be at its high-pressure limit at 246 bar at temperatures ≤1000 K. The high-pressure rate constant was used in the mechanism.

$C_6H_5+O_2 \Leftrightarrow C_6H_5OO \Leftrightarrow C_6H_5O+O$

High-pressure rate constants used in the CHEMDIS analysis

No.	Reaction	A (cm^3-mol-s)	n	E_a (cal/mol)
1	$C_6H_5+O_2 \Leftrightarrow C_6H_5OO$	6.022×10^{12}	0.	-320.
-1	$C_6H_5OO \Leftrightarrow C_6H_5+O_2$	1.47×10^{18}	-1.01	42126.
2	$C_6H_5OO \Leftrightarrow C_6H_5O+O$	6.72×10^{12}	0.15	32225.

C_6H_5OO (frequency (cm^{-1})/degeneracy): 546.9/14.97 1350.7/12.14 3198.3/5.89 calculated using CPFIT to fit the heat capacity data as described in (Ritter *et al.*, 1990; Bozzelli *et al.*, 1997)
σ = 5.75 A, ε/k_B = 450. K

Notes on sources of rate constants:
The value of k_1 is from Yu and Lin (1994) and k_{-1} is calculated from microscopic reversibility. The rate constant k_2 is estimated by assuming k_{-2} has a preexponential factor for diffusion controlled reactions ($A=10^{12}$ $cm^3mol^{-1}s^{-1}$) and no energy barrier for reaction (E_a=0) and calculating k_2 from microscopic reversibility.

Calculated rate constants by CHEMDIS at 246 bar for T=400-1000 K

No.	Reaction	A (cm^3-mol-s)	n	E_a (cal/mol)
1	$C_6H_5+O_2 \Leftrightarrow C_6H_5OO$	1.85×10^{13}	-0.15	-159.
2	$C_6H_5+O_2 \Leftrightarrow C_6H_5O+O$	2.57×10^{-29}	12.73	-5699.
3	$C_6H_5OO \Leftrightarrow C_6H_5O+O$	4.27×10^{15}	-0.7	33027.

10.3.2 Thermochemical data

Thermodynamic data for species used in the analysis of the reduced and full benzene oxidation mechanism

SPECIES	ΔH_f(298)	S(298)	C_p(300)	C_p(400)	C_p(500)	C_p(600)	C_p(800)	C_p(1000)	C_p(1500)	Source
	kcal/mol	cal/mol K	Kcal/mol	Kcal/mol	Kcal/mol	Kcal/mol	Kcal/mol	Kcal/mol	Kcal/mol K	
C12H10	43.50	93.41	66.69	71.96	76.84	81.34	89.29	95.98	108.16	
C6H6	19.81	64.37	19.92	27.09	33.25	38.38	45.87	51.05	58.31	
C6H6OH	10.17	84.11	25.51	33.94	40.94	46.17	54.13	59.52	68.54	a
C6H5	79.44	69.83	21.01	27.06	32.43	37.05	43.90	47.77	53.26	a
C6H5O	10.36	74.89	24.79	31.31	37.08	42.01	49.25	53.28	58.98	a
C6H5OH	-23.06	75.39	24.86	32.53	38.71	43.65	50.76	55.62	62.81	b
C5H5O	42.94	72.73	20.60	27.20	32.60	36.99	43.44	47.73	54.07	c
C5H4OH	16.88	75.23	21.69	28.61	34.08	38.38	44.34	48.04	53.24	c
C5H6	31.26	65.50	18.23	24.76	30.15	34.59	41.25	45.81	52.50	c
C6H	213.17	74.12	22.14	25.22	27.67	29.53	31.81	33.27	35.88	
C5H4O	7.40	66.71	19.50	25.73	30.87	34.78	40.31	44.27	49.40	c
C5H5	57.17	63.58	17.86	24.30	29.47	33.58	39.46	43.26	48.68	c
C4H6	34.97	68.17	18.80	22.74	26.39	29.69	35.17	39.30	45.45	
C4H4	73.63	66.65	17.57	21.18	24.19	26.68	30.49	33.17	37.33	
CH2CHCCH2	74.11	69.81	19.69	23.74	27.10	29.88	34.09	37.04	41.67	
CH2CHCHCH	83.99	69.05	19.06	23.57	27.22	30.15	34.45	37.38	42.05	c
C6H4OH	32.90	70.91	22.37	28.97	34.45	38.98	45.80	50.49	57.38	i
C5H5(L)	84.11	72.81	21.05	25.53	29.31	32.50	37.48	41.10	46.78	d
H2CCCCH	111.33	72.96	20.24	22.43	24.44	26.23	29.10	30.93	33.68	
C4H2	111.71	59.79	17.74	20.03	21.85	23.24	25.10	26.61	28.96	
C3H4	47.70	54.91	14.14	17.19	19.80	22.01	25.51	28.07	31.99	
H2CCCH	83.05	61.49	15.84	17.74	19.47	21.01	23.43	25.00	27.55	
C3H2	106.53	56.22	13.21	15.25	16.95	18.32	20.25	21.63	24.12	
C3H6	4.89	61.52	15.46	19.27	22.73	25.80	30.78	34 52	40.14	
C2H	134.01	49.57	8.92	9.61	10.21	10.72	11.56	12.18	13.29	
C2H2	54.20	48.02	10.62	11.99	13.08	13.95	15.27	16.31	18.27	
C2H3	68.42	55.33	9.57	11.19	12.78	14.31	16.98	18.75	21.26	
C2H4	12.54	52.38	10.23	12.79	14.94	16.83	20.05	22.51	26.22	
CH4	-17.90	44.47	8.43	9.84	11.14	12.41	15.00	17.25	20.63	
C2	200.24	47.64	10.27	9.49	8.94	8.60	8.45	8.62	8.93	
CH2CO	-12.40	57.79	12.43	14.17	15.67	16.91	18.79	20.24	22.44	
HCCO	42.45	60.74	12.65	13.47	14.23	14.92	16.07	16.83	17.98	
HCO	10.40	53.66	8.24	8.78	9.28	9.77	10.74	11.52	12.56	
H2O	-57.80	45.10	8.00	8.23	8.44	8.67	9.22	9.87	11.26	
H2O2	-32.53	55.66	10.41	11.44	12.34	13.11	14.29	15.21	16.85	
H2	.00	31.21	6.90	6.96	7.00	7.02	7.07	7.21	7.73	
O	59.56	38.47	5.23	5.14	5.08	5.05	5.02	5.00	4.98	
HO2	3.00	54.73	8.34	8.95	9.49	9.97	10.78	11.39	12.45	
O2	.00	49.01	7.01	7.22	7.44	7.65	8.07	8.35	8.72	
OH	9.32	43.88	7.15	7.10	7.07	7.06	7.13	7.33	7.87	
*H	52.10	27.39	4.97	4.97	4.97	4.97	4.97	4.97	4.97	
CH3O	3.90	54.61	9.08	10.79	12.43	13.98	16.63	18.60	21.51	

Thermodynamic data for species used in the analysis of the reduced and full benzene oxidation mechanism (*continued*)

SPECIES	$\Delta H_f(298)$	$S(298)$	$C_p(300)$	$C_p(400)$	$C_p(500)$	$C_p(600)$	$C_p(800)$	$C_p(1000)$	$C_p(1500)$	Source
	kcal/mol	cal/mol K	cal/mol K	cal/mol K	cal/mol K	cal/mol K	cal/mol K	cal/mol K	cal/mol K	
CH3	34.82	46.38	9.23	10.09	10.83	11.52	12.87	14.12	16.27	
CH2O	-27.70	52.25	8.40	9.50	10.50	11.47	13.36	14.88	16.97	
CH	142.01	43.72	6.95	7.00	7.05	7.11	7.37	7.78	8.75	
CH2	101.51	45.10	8.07	8.30	8.60	8.98	9.85	10.61	11.83	
CO	-26.42	47.21	6.95	7.03	7.14	7.27	7.61	7.95	8.41	
CO2	-94.06	51.08	8.91	9.86	10.65	11.31	12.32	12.99	13.93	
BENZYNE	121.78	69.55	18.61	24.33	29.19	33.19	38.90	42.81	48.24	
C6H5(L)	140.60	84.28	26.90	31.87	36.27	40.04	45.65	48.93	53.93	
C6H2	169.68	70.94	24.63	27.76	30.26	32.18	34.76	36.81	39.90	
C6H3	158.46	76.31	24.27	28.01	31.14	33.69	37.35	40.04	43.91	
C7H7	47.80	75.58	25.45	33.50	40.38	46.07	54.30	60.02	67.99	j
C7H8	11.95	76.46	24.88	33.30	40.62	46.78	55.95	62.35	71.37	j
C8H10	4.30	84.16	30.24	39.95	48.53	55.92	67.31	75.54	84.82	
C10H8	36.00	79.63	31.84	42.96	52.41	60.16	71.20	78.67	88.85	i
C5H2	165.25	63.70	19.90	23.26	25.97	28.07	30.84	32.81	35.39	
C5H3	135.42	70.54	21.05	24.28	27.00	29.23	32.47	34.91	38.45	
HCCHCCH	129.89	69.07	18.02	20.82	23.29	25.41	28.56	30.46	33.46	
C4H	155.09	60.90	14.10	15.37	16.56	17.66	19.59	21.15	23.44	
H2C4O	54.60	66.44	17.27	19.62	21.79	23.73	26.81	28.73	31.51	
C3H5	40.75	63.02	14.96	18.61	21.75	24.43	28.67	31.74	36.33	c
C3H4P	45.80	54.91	14.14	17.19	19.80	22.01	25.51	28.07	31.99	
C2H5	28.02	60.14	11.32	13.60	15.95	18.29	22.58	25.50	29.56	
C2H6	-20.04	54.73	12.58	15.69	18.62	21.30	25.82	29.30	34.61	
C2O	68.51	55.68	10.31	11.09	11.72	12.24	13.06	13.66	14.64	
HCCOH	20.43	58.71	13.22	14.78	16.16	17.35	19.15	20.30	22.29	
CH3OH	-48.06	57.28	10.51	12.40	14.25	16.01	19.07	21.40	25.02	
CH2OH	-4.10	58.88	11.32	12.94	14.38	15.62	17.54	18.79	20.95	
HCH	92.49	46.72	8.25	8.55	8.88	9.23	9.93	10.57	11.74	
C	171.31	37.76	4.98	4.98	4.97	4.97	4.97	4.97	4.97	
C7H8O	-23.90	87.41	28.13	37.00	44.55	50.94	60.84	67.76	77.42	e
C8H8	35.40	82.41	29.00	38.25	45.91	52.22	61.69	68.16	77.52	e
C8H6	73.81	75.11	25.78	33.70	40.24	45.62	53.67	59.21	67.49	d
C10H7	93.91	78.11	28.41	37.96	46.17	53.20	64.28	72.21	83.90	i
C6H7	47.97	73.09	24.00	30.88	37.09	42.53	50.87	55.78	62.79	
C6H6D	78.38	77.37	34.56	36.83	38.94	40.89	44.36	47.29	61.52	
C6H6F	50.59	67.83	34.56	36.83	38.94	40.89	44.36	47.29	61.52	
C6H813 RAS	25.41	72.50	22.74	30.88	37.73	43.48	52.30	58.48	67.44	f
C6H814 RAS	26.05	70.82	22.70	30.71	37.48	43.19	52.03	58.28	67.36	f
C6H4	115.71	71.51	21.84	26.59	30.50	33.71	38.54	41.94	47.37	d
*AR	.00	36.98	4.97	4.97	4.97	4.97	4.97	4.97	4.97	
C5H5O1_2	23.14	75.73	20.84	27.24	32.35	36.29	42.39	46.69		g
C=CC.C=COH	7.18	85.00	25.04	32.22	38.11	42.79	49.59	54.34	61.52	g
COC=CKET	-31.02	84.13	28.43	34.43	39.29	42.26	46.62	49.94	54.31	c
C=CC=C=O	1.82	71.96	21.62	26.23	30.23	32.64	36.20	39.20	43.21	c
C6H4O2	-29.37	79.62	26.04	32.20	37.67	42.27	48.87	53.42	59.48	h

Thermodynamic data for species used in the analysis of the reduced and full benzene oxidation mechanism (*continued*)

SPECIES	$\Delta H_f(298)$	$S(298)$	$C_p(300)$	$C_p(400)$	$C_p(500)$	$C_p(600)$	$C_p(800)$	$C_p(1000)$	$C_p(1500)$	Source
	kcal/mol	cal/mol K	Kcal/mol	Kcal/mol	Kcal/mol	Kcal/mol	Kcal/mol	Kcal/mol	Kcal/mol K	
C5H4	111.07	70.89	20.93	25.14	28.52	31.23	35.29	38.35	42.92	h
C6H5OO	37.04	85.62	26.76	34.25	40.07	44.82	51.76	56.48		a
C6H5OOH	0.94	85.40	28.81	37.09	43.62	48.91	56.48	61.45		a

a: (Lay *et al.*, 1996); b: (Burcat *et al.*, 1985); c: (Zhong and Bozzelli, 1998); d: estimated by Shandross (1996) using MOPAC (Stewart, 1990); e: (Emdee *et al.*, 1992); f: estimated by Shandross (1996) using THERM (Ritter and Bozzelli, 1990); g: (Zhong and Bozzelli, 1997); h: (Alzueta *et al.*, 1998) (taken from Burcat and McBride, 1995 and updates); i: (Zhang and McKinnon, 1995); j: (Gardiner, 1984).

10.3.3 Full Mechanism

```
 ELEMENTS H O C AR END
!
        SPECIES
        AR C6H6 C6H5OH C6H5O C6H5 C5H6 C5H5O  C5H4OH  C5H5
        C5H4O C4H6 CH2CHCHCH C4H4  H2CCCCH C4H2  C3H4 H2CCCH C3H2
        C2H4 C2H3 C2H2 CH2CO  C2H HCCO CH4 CH3O CH3 CH2O  CH2 CH
        CO2 CO H2O H2 H2O2 HCO HO2  H OH O2 O C6H4OH C6H4
        C5H3 C5H2 CH2CHCCH2  HCCHCCH C4H H2C4O
        C3H6 C3H5 C3H4P C2H6 C2H5 HCCOH C2O CH3OH CH2OH HCH C
        C6H3 C7H7 C7H8 C6H7 C2 C6H5OO C6H5OOH
        C5H5O1_1 C=CC.C=COH COC=CKET C=CC=C=O
        C6H4O2 C5H4 C6H3O2 C6H3O3 C6H6O  C5H5CHO  C5H4CHO
        END

REACTIONS
! 1. Revised ZM model, i.e. from Shandross (1995) thesis and later work.
! 2. THIS VERSION has been "depressurized," for use at 246 bar and
!    about 800-900 K, with a bath gas of H2O. Reactions which were
!    previously calc'd with QRRK or RRKM and do not now have a comment
!    like "QRRKras246bar are high-pressure limits. They should be
!    indicated with a note like "HighP."
!
!    N.B. This only includes reactions for which QRRK or RRKM had
!        been used to calculate pressure dependence. At this
!        stage, low-pressure limit reactions ("+M") have been left
!         in the low-pressure limit.
!
!    Notation:  !** = change to high pressure.
!
!***REACTIONS USED IN THE REDUCED MECHANISM***

!H2/O2 reactions:
H+O2=HO2                    2.07E+18        -1.69     890 !Chemact by jld@246 bar
HO2+HO2=H2O2+O2     2.22E+11  0.0  -1629.0 !Hippler ea fit to single exponential
H2O2+OH=H2O+HO2   7.829E+12        0.        1331.4
OH+OH=H2O2          1.00E+29        -5.452   3070.0 !Chemact by jld@246 bar
OH+HO2=H2O+O2             1.905E+16        -1.0      0.0       !value of Kim et al, 1994
H+O2=OH+O                 2.1E+15-0.3      20200.0 !Chemact by jld@246 bar
OH+OH=O+H2O         1.504E+09        1.14      99.4 !
O+HO2=OH+O2         3.250E+13        0.        0.0

!C6H6 reactions:
OH+C6H6=C6H5OH+H      1.34E+13      0.0    10592 !He et al., HighP
OH+C6H6=C6H5+H2O      1.63E+08       1.42     1454 !Baulch et al. 1992
O+C6H6=C6H5O+H          2.40E+13   0   4668 !Ko et al. (1991)

!C6H5OH Reactions
```

```
H+C6H5O=C6H5OH 2.50E+14 0.0 0.0 !He et al. high p (1988)
OH+C6H5OH=H2O+C6H5O 1.39E+08 1.43 -962 !Shandross (1995)
C6H5OH+O=C6H5O+OH 1.28E13 0 2891 !Frank
C6H5OH+HO2=C6H5O+H2O2 3.00E13 0.0 15000.0 !c
C6H5OH+CH2CHCHCH=C4H6+C6H5O 6.00E12 0.0 0.0 !a
C6H5OH+CH2CHCCH2=C4H6+C6H5O 6.00E12 0.0 0.0 !a
C6H5OH+C6H5=C6H6+C6H5O 4.91E12 0.0 4400.0 !a

!C6H5 and C6H5OO Reactions
C6H5+O=C5H5+CO 9E13 0.0 0.0 !Frank
!Chemact C6H5O2 Reactions:
C6H5 + O2 = C6H5OO 1.85E+13 -.15 -159.
C6H5 + O2 = C6H5O + O 2.57E-29 12.73 -5699.
C6H5OO= C6H5O + O 4.27E+15 -0.7 33027.
C6H5OO=C6H4O2+H 4.0E+8 0.0 0.0 !treated as adjustable parameter
C6H5OO=C5H5+CO2 1.2E+8 0.0 0.0 !treated as adjustable parameter
!Estimated C6H5OO reactions
C6H5OO+H=C6H5OOH 2.5E+14 0.0 0.0 !Same as C6H5O+H=C6H5OH
C6H5O+OH=C6H5OOH 1.0E+12 0.0 0.0 !Diffusion controlled
C6H5OO+HO2=C6H5OOH+O2 1.867E+12 0.0 1540 !(HO2+HO2=H2O2+O2)
C6H5OO+C6H5OH=C6H5OOH+C6H5O 1.0E+12 0.0 6961 !estimated
C6H5O+HO2=C6H5OO+OH 1.50E+14 0.0 23650 !from CO+HO2=CO2+OH

!C6H5O reactions
C6H5O+C5H6=C5H5+C6H5OH 3.16E11 0.0 8000.0 !a
C6H5O+O=C6H4O2+H 3E13 0.0 0.0 !Frank
C6H5O=C5H5+CO 7.40E11 0.0 43853 !Frank HighP 25th comb symp

!C6H4O2 submodel (Alzueta)
!C6H4O2=C5H4O+CO 3.7E11 0.0 59000 !Alzueta
C6H4O2=C5H4+CO2 3.5E12 0.0 67000 !Alzueta
C6H4O2+H=>C5H5O+CO 2.5E13 0.0 4700 !Alzueta
C6H4O2+H=>C6H3O2+H2 2.0E12 0.0 8100 !Alzueta
C6H4O2+OH=>C6H3O2+H2O 1.0E6 2.0 4000 !Alzueta
C6H4O2+O=>C6H3O3+H 1.5E13 0.0 4530 !Alzueta
C6H4O2+O=>C6H3O2+OH 1.4E13 0.0 14700 !Alzueta

!C6H3O2 submodel (Alzueta)
C6H3O2+H=>C2H2+C2H2+CO+CO 1E14 0.0 0.0 !Alzueta
C6H3O2+O=>C2H2+HCCO+CO+CO 1E14 0.0 0.0 !Alzueta
C6H3O3=>C2H2+HCCO+CO+CO 1E12 0.0 50000 !Alzueta
!
!
!Bozzelli's C5H5/C5H6 mechanism
C5H6 + H = C2H2 + C3H5 7.14E-34 15.06 14617
C5H6 + O = C5H5O1_2 + H 1.00E+15 -0.61 3669
C5H6 + OH = C=CC.C=COH 4.39E+10 0.82 2914
C5H5 + H = C5H6 3.21E+14 0 0
C5H5 + O = C5H5O 5.17E+30 -5.96 3445
C5H5 + O = C5H4O + H 4.25E+15 -0.56 1230
C5H5 + O = CH2CHCHCH + CO 1.45E+01 3.76 2213
```

```
C5H5 + O2 = COC=CKET + H 4.35E+07 1.08 16737
C5H5 + O2 = C=CC=C=O + HCO 1.31E-03 4.41 16472
C5H5 + HO2 = C5H5O + OH 6.19E-31 13.81 -4130
C5H5 + HO2 = C5H4O + H2O 9.46E-32 13.13 -4803
C5H5 + OH = C5H4OH + H 3.63E-48 18.18 -3853
C5H6+H=C5H5+H2   1.2E5  2.5  1492 !Abstraction
C5H6+OH=C5H5+H2O          3.08E6  2.0  0.0 !Abstraction
C5H6+HCO=C5H5+CH2O        1.08E8  1.9  16000 !Abstraction
C5H6+C6H5=C6H6+C5H5     0.1E0  4.0  0.0 !Abstraction
C5H6+C3H5=C5H5+C3H6     0.2E0  4.0  0.0 !Abstraction
C5H6+CH3=C5H5+CH4         0.18E0 4.0 0.0 !Abstraction
C5H6+HO2=C5H5+H2O2    1.10E04  2.6  12900.0 !Abstraction
C5H6+O2=C5H5+HO2          4.00E13     0.00 37150 !Abstraction
C5H6+O=C5H5+OH  4.77E04  2.71  1106.0 !Abstraction
C5H6+C2H3=C5H5+C2H4  0.12E0  4.0  0.0 !Abstraction
C5H6+CH2CHCHCH=C5H5+C4H6  0.12E0  4.0  0.0 !Abstraction
C5H6+CH2CHCCH2=C5H5+C4H6 6.00E12     0.0       0.0 !Emdee

!C5H5O reactions
C5H5O=CH2CHCHCH+CO    7.4E11  0.0  43900

!C5H4O reactions
C5H4O=C4H4+CO          1E12 0.0 0.0 !Frank
C5H4O=CO+C2H2+C2H2  1.00E15     0.0   78000.0 !a, Alzueta
C5H4O+O=C4H4+CO2     1E13 0.0 2000  !Alzueta
C5H4O+H=CH2CHCCH2+CO  2.5E13 0.0 4700  !Alzueta
C5H4OH=C5H4O+H           2.13E13  0.0  48000 !Emdee High P

!C5H4 reactions
C5H4+H=C5H3+H2  1E6 [illegible]0 !Alzueta
C5H4+O=C5H3+OH  1E[illegible] 2.5  3000  !Alzueta
C5H4+OH=C5H3+H2O  1E7  2.0  0.0  !Alzueta

!C5H3 reactions
C5H3+O2=C2H2+HCCO+CO  1E12  0.0  0.0  !Alzueta

!C7H7 reactions
C7H8+OH=C7H7+H2O        1.26E13     0.0    2583.0 !a72
C5H5+C2H2=C7H7          3.72E11     0.0      8300 !!! CST-new-HighP

!C4 reactions
CH2CHCCH2+O2=C4H4+HO2    1.20E11    0.00       0.0 !a
C4H4+OH=H2CCCCH+H2O      7.50E06     2.0   5000.0 !b174

!C2 reactions
C2H3+O2=CH2O+HCO         4.00E12     0.0   -250.0 !b105
C2H2+H=C2H3   7.85E+14  -0.224  1770 !Chemact by jld@246 bar

!C1 reactions
CH2O+OH=HCO+H2O        3.43E09    1.18     -447.0  !b74&a
HCO+M=H+CO+M           2.50E14     0.0    16802.0  !b79
```

```
CO+O=CO2  1.8E+10  0.0  2438.0 !jld HP Limit Troe, 1974
CO+OH=CO2+H          3.09E11    0.0     735.0  !72DFX
!
!***REACTIONS NOT INCLUDED IN THE REDUCED MECHANISM WHICH
!    WERE INCLUDED IN THE FULL MECHANISM OF SHANDROSS***
!
!C6H6 reactions
C6H6+O=C6H5+OH                2.0E+13  0.0  14694    !
C6H6+O2=C6H5+HO2   6.3E+13  0.0  60000.   !

!C6H5 reactions
C6H5+OH=C6H5O+H           5.0E+13  0.0  0.0      !

!C6H4OH reactions
OH+C6H5OH=H2O+C6H4OH   1.41E+13     0.00    4571 !Shandross (1995)
H+C6H5OH=H2+C6H4OH     1.67E+14     0.00   16000 !Shandross (1995)
C5H5+CO=C6H4OH         8.39E07     0.0     49910 !! HighP!

!   C4H6 = CH2CH-CHCH2: 1,3-Butadiene reactions
C4H6+H2CCCH=CH2CHCCH2+C3H4 1.00E13   0.0   22501.0 !88KER/SIN
C4H6+O=C2H4+CH2CO        1.00E12     0.0       0.0 !88HAR/WEI
C4H6+O=C3H4+CH2O         1.00E12     0.0       0.0 !88HAR/WEI
C4H6+OH=C3H5+CH2O        1.00E12     0.0       0.0 !88HAR/WEI
C4H6+OH=C2H5+CH2CO       1.00E12     0.0       0.0 !88HAR/WEI
C4H6+H=CH2CHCHCH+H2      3.00E07     2.0    6000.0 !b210&209

!   C4H5 = CH2CHCHCH & CH2CHCCH2 : Butadienyl reactions
CH2CHCCH2+M=C4H4+H+M     2.00E15     0.0   42000.0 !b216
CH2CHCHCH+M=C4H4+H+M     1.00E14     0.0   30000.0 !b217
CH2CHCHCH+O2=C4H4+HO2    1.20E11    0.00       0.0 !a
CH2CHCHCH+H=CH2CHCCH2+H  1.00E14     0.0       0.0 !b213
CH2CHCHCH+OH=C4H4+H2O    2.00E07     2.0     1000. !b185
CH2CHCHCH+H=C4H4+H2      3.00E07     2.0    1000.0 !b186
CH2CHCHCH+C2H3=C6H6+H2   2.80E-7    5.63   -1890.0 !89WES/DEA
2C2H3=CH2CHCCH2+H        4.00E13     0.0       0.0 !b109
CH2CHCCH2+OH=C4H4+H2O    2.00E07     2.0     1000. !b185GUESS
CH2CHCCH2+H=C4H4+H2      3.00E07     2.0    1000.0 !b186GUESS

!   C4H4 = H-CC-CHCH2 : Vinyl acetylene reactions
HCCHCCH+H+M=C4H4+M        1.00E15     0.0       0.0 !87FRE/WAR
H2CCCCH+H+M=C4H4+M        1.00E15     0.0       0.0 !87FRE/WAR
!**  H2CCCCH+H=C4H4          1.30E23   -3.39    13208 !! QRRKras
H2CCCCH+H=C4H4          2.80E13  -.4282     9367 !! HighP
C4H4+C2H=H2CCCCH+C2H2    4.00E13     0.0       0.0 !88HAR/WEI
C4H4+C2H=HCCHCCH+C2H2    4.00E13     0.0       0.0 !87FRE/WAR
C4H4+H=H2CCCCH+H2        3.00E07     2.0    5000.0 !b184
C4H4+H=HCCHCCH+H2        2.00E07     2.0   15000.0 !b175
H2CCCH+HCH=C4H4+H        4.00E13     0.0       0.0 !b171
C4H4+C2H3=C2H4+H2CCCCH   5.00E11     0.0   16300.0 !88HAR/WEIU
C4H4+C2H3=C2H4+HCCHCCH   5.00E11     0.0   16300.0 !88HAR/WEIU
C4H4+C2H=C4H2+C2H3       1.00E13     0.0       0.0 !87FRE/WAR
```

```
!**  C2H3+C2H=C4H4          3.05E25  -3.52    4551 !! QRRKras
C2H3+C2H=C4H4          1.00E14    0.0      0.0 !! HighP
C2H4+C2H=C4H4+H        1.21E13    0.0      0.0 !86TSA/HAM

!    C4H3 = H2CCCCH & HCCHCCH reactions
HCCHCCH+H=H2CCCCH+H      1.0E14    0.0      0.0 !b177
H2CCCCH+M=C4H2+H+M      2.00E15    0.0  48000.0 !b214
HCCHCCH+M=C4H2+H+M       1.00E14    0.0  30000.0 !b215
H2CCCCH+O=CH2CO+C2H     2.00E13    0.0      0.0 !b180
H2CCCCH+O=H2C4O+H       2.00E13    0.0      0.0 !b181
H2CCCCH+O2=CH2CO+HCCO   1.00E12    0.0      0.0 !b178
H2CCCCH+OH=C4H2+H2O     3.00E13    0.0      0.0 !b179
H2CCCCH+H=C4H2+H2       5.00E13    0.0      0.0 !b182
H2CCCCH+H2=C2H2+C2H3    5.01E10    0.0  20000.0 !86COL
H2CCCCH+HCH=C3H4+C2H    2.00E13    0.0      0.0 !b183
!**  C2H2+C2H=HCCHCCH       4.76E33  -6.40    7801 !! QRRKras
C2H2+C2H=HCCHCCH       1.00E13    0.0      0.0 !! HighP
H2CCCH+CH=H2CCCCH+H     7.00E13    0.0      0.0 !b172&3
H2CCCH+CH=HCCHCCH+H     7.00E13    0.0      0.0 !b172&3
C2H2+C2H2=HCCHCCH+H     1.00E13    0.0    45888 !!! CST
C3H2+HCH=H2CCCCH+H      3.00E13    0.0      0.0 !b164

!    C4H2 = H-CC-CC-H : Diacetylene reactions. C4H, butadiynyl
C4H2+O=C3H2+CO         1.20E12    0.0      0.0 !b202
2C3H2=C4H2+C2H2        2.00E13    0.0  85000.0 !92KER/XIE
C2H2+C2H=C4H2+H        3.00E13    0.0      0.0 !b124
C4H2+M=C4H+H+M          3.5E17    0.0  80065.0 !87FRE/WAR
C4H2+C2H=C4H+C2H2      2.00E13    0.0      0.0 !87FRE/WAR

!    C3H6 = Propylene reactions
C3H6+HO2=C3H5+H2O2      9.64E03    2.6  13910.0 !91TSA
C3H6+CH3=C3H5+CH4       2.21E00    3.5   5675.0 !91TSA
C3H6+O=C3H5+OH         6.03E10    0.7   7633.0 !91TSA
C3H6+O=C2H5+HCO         1.21E11    0.1   8960.0 !91TSA
C3H6+O2=C3H5+HO2        6.03E13    0.0  47593.0 !91TSA
C3H6+CH2OH=C3H5+CH3OH   6.03E01    2.95 11989.0 !91TSA
C3H6+CH3O=C3H5+CH3OH    9.00E01    2.95 11987.0 !91TSA
C3H6+C2H=C3H4P+C2H3     1.21E13    0.0      0.0 !91TSA
C3H6+CH2=C3H5+CH3       7.23E11    0.0   6192.0 !91TSA
C3H6+HCO=C3H5+CH2O      1.08E07    1.9  17006.0 !!! CST-new
C3H6+C2H5=C3H5+C2H6     2.23E00    3.5   6637.0 !91TSA
C3H6+C2H3=C3H5+C2H4     2.21E00    3.5   4682.0 !91TSA
C3H5+HCO=C3H6+CO        6.03E13    0.0      0.0 !91TSA
C3H5+CH2OH=C3H6+CH2O    1.81E13    0.0      0.0 !91TSA
C3H5+CH3O=C3H6+CH2O     3.01E13    0.0      0.0 !91TSA
C3H5+C2H3=C3H6+C2H2     4.82E12    0.0      0.0 !91TSA
C3H5+C2H5=C3H6+C2H4     2.59E12    0.0   -131.0 !91TSA
2C3H5=C3H4+C3H6         8.43E10    0.0   -262.0 !91TSA
CH2+C2H5=C3H6+H         9.03E12    0.0      0.0 !!! CST-new
CH2+C2H4=C3H6           9.03E13    0.0      0.0 !!! CST-new
```

```
!   C3H5 = H2CCHCH2 :  ally radical reactions
C3H4+H=C3H5              1.20E11   0.69   3007.0 !92TSA/WAL
C3H5+OH=C3H4+H2O          6.03E12    0.0      0.0 !91TSA
CH3+C2H2=C3H5            2.43E46  -10.9   19974. !87DEA/WES
C3H5+CH2=C4H6+H           3.01E13    0.0      0.0 !91TSA
C2H+C3H5=C2H2+C3H4        1.50E-1    0.0      0.0 !91TSA
C2H+C3H5=C2H3+H2CCCH      2.00E01    0.0      0.0 !91TSA
C3H5+C2H3=C3H4+C2H4       2.41E12    0.0      0.0 !91TSA
C3H5+C2H5=C3H4+C2H6       9.64E11    0.0   -131.0 !91TSA
C2H3+CH2OH=C3H5+OH        1.21E13    0.0      0.0 !87TSA
C2H4+HCH=C3H5+H           3.19E12    0.0   5285.4 ! CST


!**  C3H4=C3H4P             1.01E+28  -4.632  63183.0 !!! CSTuniQRRKras
C3H4=C3H4P               2.00E13    0.0    62000 !!! CST-HighP
C3H4+C3H2=3C2H2           1.70E13    0.0  15000.0 !92KER/XIE
C3H4P+C3H2=3C2H2          1.70E13    0.0  15000.0 !92KER/XIE
C3H4+O=CO+C2H4            1.50E13    0.0   2103.0 !88HAR/WEI
C3H4+OH=HCO+C2H4          1.00E12    0.0      0.0 !88HAR/WEI
C3H4+M=H2CCCH+H+M         1.00E17    0.0  70000.0 !92KER/XIE
C3H4P+M=H2CCCH+H+M        1.00E17    0.0  70000.0 !92KER/XIE
C3H4+CH3=H2CCCH+CH4       2.00E12    0.0   7700.0 !92KER/XIE
C3H4P+CH3=H2CCCH+CH4      2.00E12    0.0   7700.0 !92KER/XIE
C3H4+H=C2H2+CH3           2.00E13    0.0   2400.0 !92KER/XIE
!**  C2H+CH3=C3H4P          4.16E33   -6.61    33537 !! QRRKras
C2H+CH3=C3H4P            2.01E07   1.639    24089 !! HighP
HCH+C2H2+M=C3H4+M         1.20E13    0.0   6600.0 !92BAU/COB
C2H2+CH2+M=C3H4P+M        2.23E14    0.0      0.0 !92BAU/COB
C2H3+HCH=C3H4+H           3.00E13    0.0      0.0 !b107
C2H2+CH2+M=C3H4+M         2.23E14    0.0      0.0 !92BAU/COB
C3H4P+C2H=C2H2+H2CCCH     1.00E13    0.0      0.0 !92KER/XIE
C3H4+C2H=C2H2+H2CCCH      1.00E13    0.0      0.0 !92KER/XIE
C3H4+O=CH2O+C2H2          9.00E12    0.0   1870.0 !!! CST-new
C3H4+O=HCO+C2H3           9.00E12    0.0   1870.0 !!! CST-new
C3H4P+O=CH2O+C2H2         7.50E12    0.0   2102.0 !!! CST-new
C3H4P+O=HCO+C2H3          7.50E12    0.0   2102.0 !!! CST-new
C3H4+OH=CH2CO+CH3         3.37E12    0.0   -304.0 !!! CST-new
C3H4P+OH=CH2CO+CH3        4.28E11    0.0   -843.0 !!! CST-new

!   H2CCCH  reactions
H2CCCH+O=C3H2+OH          3.20E12    0.0      0.0 !88HAR/WEI
CH3+C2H=H2CCCH+H          2.41E13    0.0      0.0 !86TSA/HAM
C2H+CH2OH=H2CCCH+OH       1.21E13    0.0      0.0 !87TSA
C2H+C2H5=CH3+H2CCCH       1.81E13    0.0      0.0 !86TSA/HAM
C2H2+HCCO=H2CCCH+CO       1.10E11    0.0   3000. !b125
H2CCCH+O2=CH2CO+HCO       3.00E10    0.0   2868.0 !b167

!   C3H2 propynylidene reactions
C3H2+O=C2H+HCO            6.80E13    0.0      0.0 !88HAR/WEI
!!!  C3H2+OH=C2H2+HCO         5.00E13    0.0      0.0 !b163  CST-rem
```

```
!   H2C4O reactions
H2C4O+H=C2H2+HCCO        5.00E13    0.0   3000.0 !b165
H2C4O+OH=CH2CO+HCCO      1.00E07    2.0   2000.0 !b166

!   C2H6 ethane reactions
C2H6+CH3=C2H5+CH4        5.50E-1    4.0   8300.0 !b88
C2H6+H=C2H5+H2           5.40E02    3.5   5210.0 !b89
C2H6+O=C2H5+OH           3.00E07    2.0   5115.0 !b90
C2H6+OH=C2H5+H2O         8.70E09    1.05  1810.0 !b91
C2H6+O2=C2H5+HO2         1.00E13    0.0  51000.0 !88HAR/WEI
C2H6+HO2=C2H5+H2O2       3.00E11    0.0  11500.0 !88HAR/WEI
HCO+C2H5=C2H6+CO         1.21E14    0.0      0.0 !86TSA/HAM
C2H4+C2H5=C2H3+C2H6      6.32E02    3.13 18010.0 !86TSA/HAM
2CH3+M=C2H6+M            3.18E41   -7.0   2762.0 !b22
H2/2.0/  CO/2.0/  CO2/3.0/  H2O/5.0/
H2/2.0/  CO/2.0/  CO2/2.0/  H2O/5.0/          !!! CST
CH2+C2H6=CH3+C2H5        1.20E14    0.0      0.0 !138
C2H6+HCO=C2H5+CH2O       4.70E04    2.7  18233.0 !!! CST-new
2C2H5=C2H6+C2H4          1.39E12    0.0      0.0 !!! CST-new
C2H3+C2H5=C2H6+C2H2      4.82E11    0.0      0.0 !!! CST-new
C2H2+C2H5=C2H6+C2H       2.71E11    0.0  23446.0 !!! CST-new

!   C2H5 ethyl reactions
C2H5+O=C2H4+OH           5.00E13    0.0      0.0 !d
C2H5+O=CH2O+CH3          1.61E13    0.0      0.0 !86TSA/HAM
HO2+C2H5=C2H4+H2O2       3.01E11    0.0      0.0 !86TSA/HAM
HCH+CH3=C2H5             2.53E20   -3.49  2030.0 !86WESTMORELAND
CH3+C2H5=C2H4+CH4        1.95E13   -0.5     0.0 !86TSA/HAM
CH3+CH2=C2H5             1.11E19   -3.20  1780.0 !86WESTMORELAND
C2H+C2H5=C2H2+C2H4       1.81E12    0.0      0.0 !86TSA/HAM
C2H5+H=C2H4+H2           1.81E12    0.0      0.0 !d
C2H5+H=CH3+CH3           1.00E14    0.0      0.0 !b97
C2H5+O2=C2H4+HO2         8.43E11    0.0   3875.0 !b98
C2H4+H+M=C2H5+M          6.37E27   -2.8    -54.0 !b96
2C2H4=C2H5+C2H3          4.82E14    0.0  71539.0 !86TSA/HAM
C2H5+OH=C2H4+H2O         2.41E13    0.0      0.0 !d
C2H5+HO2=CH3+CH2O+OH     2.40E13    0.0      0.0 !d
CH2+C2H5=C2H4+CH3        9.03E12    0.0      0.0 !!! CST-new
HCH+C2H5=CH3+C2H4        1.81E13    0.0      0.0 !!! CST-new

!   C2H4 ethylene reactions
C2H4+M=C2H2+H2+M         2.60E17    0.0  79297.0 !d
H2/2.5/  H2O/16.0/  CO/1.9/  CO2/3.8/  CH4/16.0/
C2H4+M=C2H3+H+M          1.40E16    0.0  82360.0 !b207
C2H4+O=CH2O+CH2          2.51E13    0.0   5000.0 !d
C2H4+H=C2H3+H2           1.33E06    2.53 12241.0 !b92
2HCH=C2H4                1.11E20   -3.43  2070.0 !86WESTMORELAND
HCH+CH3=C2H4+H           4.20E13    0.0      0.0 !86WESTMORELAND
CH3O+C2H3=CH2O+C2H4      2.41E13    0.0      0.0 !d51
CH2CO+CH2=C2H4+CO        1.60E14    0.0      0.0 !b151
C2H3+CH2O=C2H4+HCO       5.43E3     2.81  5862.0 !86TSA/HAM
```

```
C2H3+CH2OH=C2H4+CH2O   3.01E13    0.0     0.0 !87TSA
CH3+CH2=C2H4+H         4.94E13   -.076   94.0 !86WESTMORELAND
CH+CH4=C2H4+H          6.00E13    0.0     0.0 !b60
C2H4+O=CH3+HCO         1.60E09    1.2     746. !b93
C2H4+OH=C2H3+H2O       2.02E13    0.0    5955.0 !b94
C2H4+OH=CH3+CH2O       1.05E12    0.0    -916.0 !!! CST
C2H4+O2=C2H3+HO2       4.22E13    0.0   57594.0 !d
C2H4+CH3=C2H3+CH4      4.16E12    0.0   11127.2 !92BAU/COB
C2H4+O=OH+C2H3         1.51E07    1.91   3736.0 !87MAH/MAR
C2H4+C2H2=2C2H3        2.41E13    0.0   68360. !86TSA/HAM
C2H3+HCO=C2H4+CO       9.04E13    0.0     0.0 !86TSA/HAM

!   C2H3 vinyl radical or ethenyl reactions
C2H2+H2=C2H3+H         4.02E15   -.56  65800.0 !86WESTMORELAND
C2H3+O=CH2CO+H         3.00E13    0.0     0.0 !b104
C2H3+O=C2H2+OH         3.00E13    0.0     0.0 !92BAU/COB
C2H3+O=CO+CH3          3.00E13    0.0     0.0 !92BAU/COB
CH+HCH=C2H3            3.09E14   -1.98   620.0 !Westmorelandpaper
CH+CH3=C2H3+H          3.00E13    0.0     0.0 !b59
CH2+CH2=C2H3+H         2.00E13    0.0     0.0 !84FAR/JUS(1.6-2.3)
2HCH=C2H3+H            7.12E21   -3.9   2460.0 !86WESTMORELAND
CH2OH+C2H2=C2H3+CH2O   7.30E11    0.0   9004.0 !87TSA
C2H3+O=HCO+CH2         3.00E13    0.0     0.0 !92BAU/COB
C2H3+O2=C2H2+HO2       7.51E14   -1.04   2376. !93BOZ/DEA
C2H3+OH=C2H2+H2O       2.00E13    0.0     0.0 !b106
C2H3+C2H=2C2H2         3.00E13    0.0     0.0 !b108
C2H3+CH=HCH+C2H2       5.00E13    0.0     0.0 !b110
C2H3+CH3=C2H2+CH4      3.92E11    0.0     0.0 !86TSA/HAM
C2H3+CH2=CH3+C2H2      1.81E13    0.0     0.0 !86TSA/HAM
HCH+C2H3=CH3+C2H2      1.81E13    0.0     0.0 !!! CST

!   C2H2 acetylene reactions
C2H2+M=C2H+H+M         4.20E16    0.0   107000. !b205
C2H2+O2=C2H+HO2        1.2E13     0.0   74475.0 !d
C2H2+H=CH+CH2          1.02E16    0.0   125076.0 !LEE93
C2H+H2=C2H2+H          4.09E05    2.39    864.0 !b101
C2H2+OH=C2H+H2O        3.37E07    2.0    14000. !b111
C2H2+OH=HCCOH+H        5.04E5     2.3    13500. !b112
C2H2+OH=CH2CO+H        2.18E-4    4.5    -1000. !b113
C2H2+OH=CH3+CO         4.83E-4    4.0    -2000. !b114
CH3OH+C2H=CH3O+C2H2    1.21E12    0.0     0.0 !87TSA
CH3OH+C2H=CH2OH+C2H2   6.03E12    0.0     0.0 !87TSA
C2H+CH4=C2H2+CH3       1.81E12    0.0    497.0 !86TSA/HAM
HCCO+CH=C2H2+CO        5.00E13    0.0     0.0 !b129
HCCO+HCCO=C2H2+2CO     1.00E13    0.0     0.0 !b130
HO2+C2H2=CH2CO+OH      6.03E09    0.0   7949.0 !86TSA/HAM
HCO+C2H=C2H2+CO        6.03E13    0.0     0.0 !86TSA/HAM
C+CH3=C2H2+H           5.00E13    0.0     0.0 !b63
CH2+C2H2=HCH+C2H2      4.00E13    0.0     0.0 !b 144
CH2+CH2=C2H2+H2        3.01E13    0.0     0.0 !!! CST
CH3O+C2H=CH2O+C2H2     2.41E13    0.0     0.0 !d52
```

```
2HCH=C2H2+2H          4.97E12   0.19   -150.0 !86WESTMORELAND
2HCH=C2H2+H2          4.02E14  -0.47    480.0 !86WESTMORELAND
CH+HCH=C2H2+H          2.50E12  -3.68   4190.0 !Westmorelandpaper
C2H+CH2OH=C2H2+CH2O    3.61E13    0.0      0.0 !87TSA
C2H+C2H=C2H2+C2        1.81E12    0.0      0.0 !86TSA/HAM
C2H+CH2=CH+C2H2        1.81E13    0.0      0.0 !86TSA/HAM
C2H2+O=C2H+OH          3.16E15   -0.6    15000. !b116
C2H2+O=HCH+CO          1.40E06   2.09    1562.0 !a
C2H2+O=HCCO+H          5.80E6    2.09    1562.0 !a
HCH+C2H=CH+C2H2        1.81E13    0.0      0.0 !!! CST-new

!   CH2CO reactions
CH2CO+M=HCH+CO+M       3.60E15    0.0   59235.0 !d&b122
H2/2.5/ H2O/16.0/ CO/1.9/ CO2/3.8/ CH4/16.0/ CH3OH/5.0/
CH2CO+O=HCO+HCO        2.00E13    0.0    2293.0 !d
CH2CO+O=CH2+CO2        1.75E12    0.0    1350.0 !b117
CH2CO+H=HCCO+H2        5.00E13    0.0    8000.0 !b119
 CH2CO+O=HCCO+OH       1.00E13    0.0    8000.0 !b120
CH2O+CH=CH2CO+H        9.46E13    0.0    -515.0 !b56
!**  CH2+CO=CH2CO        6.125E08 -0.002      0.0 !! QRRKras
CH2+CO=CH2CO          6.03E08    0.0      0.0 !! HighP
CH2CO+OH=HCCO+H2O      7.50E12    0.0    2000.0 !b121
CH2CO+OH=CH2O+HCO      2.80E13    0.0      0.0 !d
CH2CO+OH=CH3O+CO       2.80E13    0.0      0.0 !92BAU/COB
HCCOH+H=CH2CO+H        1.00E13    0.0      0.0 !b115

!   HCCO Ketyl reactions
HCCO+H=CH2+CO          1.00E14    0.0      0.0 !b126
HCCO+O=2CO+H           1.00E14    0.0      0.0 !b127
!**  HCCO+H=HCCOH         7.544E38 -8.345     6449 !! QRRKras
HCCO+H=HCCOH           1.00E14    0.0      0.0 !! HighP
HCCO+OH=C2O+H2O        3.00E13    0.0      0.0 !b131
HCCO+O2=2CO+OH         1.46E12    0.0    2500. !a
HO2+C2H=HCCO+OH        1.81E13    0.0      0.0 !86TSA/HAM
C2H+O2=HCCO+O          5.00E13    0.0    1500.0 !92BAU/COB
C2H+OH=HCCO+H          2.00E13    0.0      0.0 !b150

!   C2H ethynyl reactions
C2H+M=C2+H+M           4.68E16    0.0  124000.0 !86COL
C2H+O=CO+CH            5.00E13    0.0      0.0 !b152
C2H+O2=HCO+CO          2.41E12    0.0      0.0 !d122
C2H+O2=H+CO+CO         3.52E13    0.0      0.0 !b123
C2H+OH=CH2+CO          1.81E13    0.0      0.0 !86TSA/HAM
C2H+OH=C2+H2O          4.00E07    2.0    8000.0 !b154
C+HCH=C2H+H            5.00E13    0.0      0.0 !b64
CH+HCH=C2H+2H          5.49E22   -2.41   11520.0 !Westmorelandpaper
C2+H2=C2H+H           4.00E05    2.4    1000.0 !b155

!   C2O & C2  reactions
C2O+H=CH+CO            5.00E13    0.0      0.0 !b132
C2O+O=CO+CO            5.00E13    0.0      0.0 !b133
```

```
C2O+OH=CO+CO+H          2.00E13    0.0      0.0 !b134
C2O+O2=2CO+O            2.00E13    0.0      0.0 !b135
C2+OH=C2O+H             5.00E13    0.0      0.0 !b157
C2+O2=2CO               5.00E13    0.0      0.0 !b156

!   CH4 Methane reactions
CH4+O2=CH3+HO2          7.94E13    0.0  56000.0 !b24
CH4+H=CH3+H2            5.47E07   1.97  11210.0 !a
CH4+OH=CH3+H2O          5.72E06   1.96   2639.0 !a
CH4+HO2=CH3+H2O2        1.81E11    0.0  18580.0 !a

!   CH3OH methanol reactions
CH3OH+M=CH3+OH+M        3.50E16    0.0  66444.0 !!! CST
CH3OH+M=CH2OH+H+M       1.75E15    0.0  66444.0 !!! CST
CH3OH+M=CH2+H2O+M       7.00E15    0.0  66444.0 !!! CST-new
CH3OH+CH3=CH2OH+CH4     3.19E01   3.17   7172.0 !d165
CH3OH+CH3=CH3O+CH4      1.45E01   3.10   6935.0 !d166
CH3OH+HO2=H2O2+CH2OH    9.64E10    0.0  12579.0 !Corrected, ras
CH3OH+O=OH+CH2OH        3.80E05    2.5   3080.0 !d160
CH3OH+O=OH+CH3O         1.00E13    0.0   4684.0 !84WAR(.3-1.0)
CH3OH+O2=CH2OH+HO2      2.05E13    0.0  44717.0 !d163
CH3OH+OH=H2O+CH2OH      1.00E13    0.0   1697.0 !!! CST
CH3OH+OH=H2O+CH3O       1.00E13    0.0   1697.0 !!! CST
CH3OH+CH2OH=CH3OH+CH3O  7.83E09    0.0  12062.0 !87TSA
CH3OH+H=CH2OH+H2        3.98E13    0.0   6095.0 !!! CST
CH3OH+H=CH3O+H2         3.98E13    0.0   6095.0 !!! CST
CH3OH+HCH=CH2OH+CH3     1.58E12    0.0   5736.0 !!! CST-new

!   CH3O methoxy radical reactions[CH3O C2H5O-> alkoxy radicals]
CH3O+M=CH2O+H+M         9.37E24   -2.7  30590.0 !a
CH3O+H=CH2O+H2          2.00E13    0.0      0.0 !b38
CH3O+OH=CH2O+H2O        1.00E13    0.0      0.0 !b40
CH3O+O=CH2O+OH          1.00E13    0.0      0.0 !b42
CH3O+O2=CH2O+HO2        6.30E10    0.0   2600.0 !b44&a
CH3O+HO2=CH2O+H2O2      3.01E11    0.0      0.0 !d48
CH3O+CO=CH3+CO2         1.57E13    0.0  11797.0 !d49 Correct typo

!   CH2OH hydroxymethyl Rxns [CH2OH CH3CHOH->hydroxyalkyl radicals]
CH2OH+M=CH2O+H+M        1.67E24   -2.5  34190.0 !a
CH2OH+O=CH2O+OH         1.00E13    0.0      0.0 !b43
CH2OH+O2=CH2O+HO2       2.41E14    0.0   5000.0 !a
CH2OH+OH=CH2O+H2O       1.00E13    0.0      0.0 !b41
CH2OH+H=CH2O+H2         2.00E13    0.0      0.0 !b39
CH2OH+HO2=CH2O+H2O2     1.20E13    0.0      0.0 !d170
CH2OH+HCO=CH3OH+CO      1.20E14    0.0      0.0 !d171
CH2OH+CH2O=CH3OH+HCO    5.54E03   2.81   5682.0 !d173
2CH2OH=CH3OH+CH2O       4.82E12    0.0      0.0 !!! CST
CH2OH+HCO=2CH2O         1.81E14    0.0      0.0 !87TSA

!   CH3 methyl reactions
CH3+M=CH+H2+M           6.90E14    0.0  82500.0 !92BAU/COB
```

```
CH3+H(+M)=CH4(+M)      1.00E17   -0.8    315.0 !!! CST
LOW /7.00E33 -4.88 9.310/
TROE /0.7086 134.0 1784.0 5740.0/
H2/2.0/ CO/1.5/ CO2/2.0/ H2O/6.0/ CH4/2.0/ C2H6/3.0/ AR/0.7/
CH3+HO2=CH3O+OH       2.00E13    0.0    1076.0 !a
CH3+O=CH2O+H          6.03E13    0.0       0.0 !71DEA/KIS
CH3+O=CH3O            1.78E14   -2.14    603.0 !87DEA/WES
CH3+O2=CH3O+O         7.26E11    0.39  27363.0 !87DEA/WES
CH3+O2=CH2OH+O        1.29E13    0.0   26900.0 !92GLA
CH3+OH=CH3OH          1.24E43   -9.49  10471.0 !87DEA/WES
CH3+OH=CH2OH+H        1.09E11    0.4    -708.0 !!! CST-new
CH3+OH=CH3O+H         8.93E11   -0.02  13073.0 !87DEA/WES
CH3+OH=HCH+H2O        7.50E06    2.0    5000.0 !!! CST-new
CH3+OH=CH2O+H2        3.98E10   -0.02   8765.0 !87DEA/WES
CH3+HO2=CH2OH+OH      2.00E13    0.0       0.0 !92GLA
CH3+HCO=CH4+CO        1.20E14    0.0       0.0 !a
CH3+CH2OH=CH4+CH2O    2.41E12    0.0       0.0 !87TSA
CH3+CH3O=CH4+CH2O     2.41E13    0.0       0.0 !86TSA/HAM
CH3+CH2O=CH4+HCO      5.54E03    2.81   5863.0 !a

!   Triplet Methylene reactions
HCH+H+M=CH3+M         2.40E31   -4.38     0.0 !92GLA
HCH+H=CH+H2           1.00E18   -1.56     0.0 !b46
HCH+O=CO+2H           5.00E13    0.0      0.0 !b66
HCH+O=CO+H2           3.00E13    0.0      0.0 !b67
HCH+O2=CO2+2H         1.60E12    0.0   1000.0 !b68
HCH+O2=CH2O+O         5.00E13    0.0   9000.0 !b69
HCH+O2=CO2+H2         6.90E11    0.0    500.0 !b70
HCH+O2=CO+H2O         1.90E10    0.0  -1000.0 !b71
HCH+O2=CO+OH+H        8.60E10    0.0   -500.0 !b72
HCH+O2=HCO+OH         4.30E10    0.0   -500.0 !b73
HCH+OH=CH+H2O         1.13E07    2.0   3000.0 !b47
HCH+OH=CH2O+H         2.50E13    0.0      0.0 !b48
HCH+CO2=CH2O+CO       1.10E11    0.0   1000.0 !b65
CH2+M=HCH+M           1.00E13    0.0      0.0 !b136
H/0.0/  H2O/0.0/  C2H2/0.0/
HCH+HCO=CH3+CO        1.81E13    0.0      0.0 !!! CST-new
HCH+CH3O=CH3+CH2O     1.81E13    0.0      0.0 !!! CST-new

!   Singlet Methylene reactions
CH2+CH4=2CH3          4.00E13    0.0      0.0 !b137
CH2+H2=CH3+H          7.00E13    0.0      0.0 !140
CH2+H2O=HCH+H2O       3.00E13    0.0      0.0 !b142
CH2+H=HCH+H           2.00E14    0.0      0.0 !b145
CH2+O=H+H+CO          3.00E13    0.0      0.0 !b146
CH2+O=H2+CO           7.83E12    0.0      0.0 !!! CST
CH2+O2=CO2+2H         7.83E12    0.0      0.0 !!! CST
CH2+O2=O+CH2O         7.83E12    0.0      0.0 !!! CST
CH2+O2=H2+CO2         7.83E12    0.0      0.0 !!! CST
CH2+O2=H+CO+OH        7.83E12    0.0      0.0 !!! CST
CH2+OH=CH2O+H         3.01E13    0.0      0.0 !b147
```

```
CH2+H=CH+H2          3.01E13    0.0       0.0 !b148
CH2+CO2=CH2O+CO       3.00E12    0.0       0.0 !b149
CH2+HO2=CH2O+OH       3.01E13    0.0       0.0 !d
CH2+H2O2=CH3O+OH      3.01E13    0.0       0.0 !d
CH2+HCO=CO+CH3        1.81E13    0.0       0.0 !d
CH2+CH2O=HCO+CH3      1.20E12    0.0       0.0 !d
CH2+O=CH+OH          3.00E14    0.0    11923. !84FAR/JUS(.9-2.3K)

!   CH2O formaldehyde reactions
CH2O+H=HCO+H2         2.19E08    1.8    3000.0 !b75 & f2
CH2O+M=HCO+H+M        3.31E16    0.0   81000.0 !b76
CH2O+O=HCO+OH         1.80E13    0.0    3080.0 !b77&a
CH2O+O2=HO2+HCO       1.23E06    3.0   52000.0 !f6
CH2O+HO2=HCO+H2O2     4.40E06    2.0   12000.0 !f9

!    CH methine & C reactions
CH+O=C+OH            1.52E13    0.0    4732.0 !86MUR/ROD
CH+O=CO+H            5.70E13    0.0       0.0 !b50
CH+O2=CO+OH           3.30E13    0.0       0.0 !92BAU/COB
CH+O2=HCO+O           3.30E13    0.0       0.0 !b49
CH+OH=HCO+H           3.00E13    0.0       0.0 !b51
CH+OH=C+H2O           4.00E07    2.0    3000.0 !b52
CH+CO2=HCO+CO         3.40E12    0.0     690.0 !b53
CH+H=C+H2            1.50E14    0.0       0.0 !b54
CH+H2O=CH2O+H         1.17E15   -0.75      0.0 !b55
CH+H2O=CH2OH          5.71E12    0.0    -755.0 !88ZAB/FLE3
C+O2=CO+O            2.00E13    0.0       0.0 !b61
C+OH=CO+H            5.00E13    0.0       0.0 !b62

!HCO aldehyde reactions
HCO+O=CO2+H           3.00E13    0.0       0.0 !b82
HCO+O2=CO2+OH         3.31E12   -0.4       0.0 !92BAU/COB
HCO+HO2=CO2+OH+H      3.00E13    0.0       0.0 !d
HCO+CH3O=CH3OH+CO     9.04E13    0.0       0.0 !86TSA/HAM
2HCO=CH2O+CO          4.50E13    0.0       0.0 !g
HCO+O2=CO+HO2         3.3E13    -0.4       0.0 !b83
HCO+OH=CO+H2O         3.02E13    0.0       0.0 !a
HCO+H=CO+H2           2.00E14    0.0       0.0 !e
HCO+O=CO+OH           3.00E13    0.0       0.0 !b81
2HCO=2CO+H2           3.01E12    0.0       0.0 !!! CST-new

!CO & CO2  reactions
CO+O2=CO2+O           2.51E12    0.0   47690.0 !a
CO+HO2=CO2+OH         1.50E+14  0.0  23650. !Tan 1994

!References
!    a : Emdee,J.I., K. Brezinsky, and I. Glassman, A Kinetic Model for The
!    Oxidation of Toluene Near 1200K, J. Phys. Chem., 96(5), 2151-2161 (1992).
!
!    b : Miller,J.A., and C.F. Melius, Kinetic and Thermodynamic Issues
!    in the Formation of Aromatic Compounds in Flames of Aliphatic Fuels,
```

```
!       Combustion and Flame, 91:21-39 (1992).
!
!   c : Bittker, D.A., Detailed Mechanism for Oxidation of Benzene,
!       Combust. Sci. and Tech., Vol.79, 49-72 (1991).
!
!   d is the paper from Dr. McKinnon.(Oxidation of CH4)
!
!   e : Chang, W.D., Karra, S.B., and Senkan, S. M.(1987). A computational
!   study of chlorine inhibition of CO flames. Combust. Flame 69, 113.
!
!   f : Hidaka,Y., T. Taniguchi, H. Tanaka, T. Kamesawa, K. Inami, and
!     H. Kawano, Shock-Tube Study of CH2O Pyrolysis and Oxidation,
!           Combustion and Flame 92: 365-376 (1993).
!
!   g  : Baggott,J.E., Frey, H.M., Lightfoot,P.D., Walsh, R.,
!           Chem. Phys. Lett. 132:225 (1986).
!
!   h  : Kern, R.D., C.H. WU, G.B. Skinner, V.S. RAO, J.H. Kiefer, J.A. Towers,
!      and L.J. Mizerka, Collaborative Shock Tube Studies of Benzene Pyrolysis,
!       20th Symposium (International) on Combustion, 789-797 (1984).
!
!   i : Vandooren, J., and J. Bian, Vialidation of H2/O2 Reaction Mechanisms by
!      Comparison with the Experimental Structure of a Rich Hydrogen-Oxygen Flame,
!       23rd Symposium (International) on Combustion, 341-346 (1990).
!
!   LEE93     : K.Y.LEE,M.H.YANG and I.K.PURI, Combustion and Flame
!           92:419-439 (1993).  [CH3CL/CH4/Air flame]
!
!   84FRE/CLA : Frenklach, M., D.W. Clary, W.C. Gardiner,Jr., S.E. Stein, Detailed
!      Kinetic Modeling of Soot Formation in Shock-Tube Pyrolysis of Acetylene,
!           20th Symp. (Int.) on Combustion, 887-901(1984).
!
!   84WAR     : Warnatz,J., Rate Coefficients in the C/H/O system,
!     Combustion Chemistry (ed.W.C. Gardiner,Jr.), Springer-Verlag, N.Y. 197(1984)
!
!   85KIE/WEI : Kiefer,J.H., Wei,H.C., Kern,R.D., and Wu, C.H.,
!      The High Temperature Pyrolysis of 1,3-Butadiene: Heat of Formation and
!      Rate of Dissociation of Vinyl Radical, Int. J. Chem. Kinet., Vol.17,
!      225(1985).
!
!   85KIE/FIZ : Kiefer,J.H., L.J. Mizerka, M.R. Patel, and H.-C. Wei, A Shock tube
!      Investigation of Major Pathways in the High-Temperature Pyrolysis of
!       Benzene, J. Phys. Chem. 89(10), 2013-2019(1985).
!
!   86COL     : Colket,M.B.,III, The Pyrolysis of Acetylene and Vinlacetylene in a
!       Single-Pulse Shock Tube, 21st Symp. (Int.) on Combustion,851-864(1986).
!
!   86TSA/HAM : Tsang,W., and Hampson, R.F., Chemical Kinetic Data Base for
!      Combustion Chemistry. Part I. Methane and Related Compounds,
!       J. Phys. Chem. Ref. Data, Vol.15, 1087 (1986).
!
```

! 86MUR/ROD : Murrell,J.N., and J.A. Rodriguez, Predicted Rate Constants for the
! Exothermic Reactions of Ground State Oxygen Atoms and CH Radicals,
! J. Molec. Struct. (Theochem), 139, 267(1986).
!
! 87DEA/WES : Dean, A.M., and P.R. Westmoreland, Bimolecular QRRK Analysis of
! Methyl Radical Reactions,
! International Journal of Chemical Kinetics, Vol.19, 207-228 (1987).
!
! 87FRE/WAR : Frenklach,M., and J. Warnatz, Detailed Modeling of PAH Profiles
! In a Sooting Low-Pressure Acetylene Flame.
! Combust. Sci. and Tech. Vol.51, 265-283(1987).
!
! 87MAH/MAR :Mahmud,K., P. Marshall, and A.Fontijn, A High-Temperature
! Photochemistry Kinetics Study of the Reaction of O(3p) Atoms
! with Ethylene from 290 to 1568K, J. Phys. Chem., 91, 1568(1987).
!
! 87TSA :Tsang,W., Chemical Kinetic Data Base for Combustion Chemistry. Part 2.
! Methanol, J. Phys. Chem. Ref. Data, Vol.16, 471(1987).
!
! 87WU/KER : Wu, C.H., and R.D. Kern, Shock-Tube Study of Allene Pyrolysis,
! J. Phys. Chem., 91(24), 6291-6296(1987).
!
! 88BRA/FRA : Braun-Unkhoff,M. , P.Frank, and Th. Just, A Shock Tube Study on the
! Thermal Decomposition of Toluene and of the Phenyl, Radical, at High
! Temperature, 22nd Symposium (Int.) on Combustion, 1053-1061(1988).
!
! 88BRU/GEE : Bruinsma,O.S.L., R.S. Geertsma, P. Bank, and J.A. Moulijn, Gas Phase
! Pyrolysis of Coal-Related Aromatic Compounds in a Coiled Tube Flow Reactor,
! Fuel, Vol.67, 327(1988)
!
! 88DUR/AMO :Duran,R.P., V.T. Amorebieta, and A.J. Colussi, Is the Homogeneous
! Thermal Dimerization of Acetylene a Free-Radical Chain Reaction?
! Kinetic and Thermochemical Analysis, J. Phys. Chem.,72, 91(1988).
!
! 88GHI/COL : Ghibaudi, E. and A.J. Colussi, Kinetics and Thermochemistry
! of the equilibrium 2 (acetylene)= vinylacetylene. Direct Evidence against
! a chaim mechanism, J. Phys. Chem., 92, 5839(1988).
!
! 88HAR/WEI :Harris,S.H., A.M. Weiner, and R.J. Blint, Formation of Small Aromatic
! Molecules in a Sooting Ethylene Flame,
! Combustion and Flame 72:91-109 (1988).
!
! 88KER/SIN : Kern, R.D., H.J. Singh, and C.H. Wu, Thermal Decomposition of
! 1,2 Butadienl, Int. J. Chem. Kinet., Vol.20, 731(1988).
!
! 89WES/DEA : Westmoreland, P.R., A.M. Dean, J.B. Howard, and J.P. Longwell,
! Forming Benzene in Flames by Chemically Activated Isomerization,
! J. Phys. Chem.,93(25) 8171-8180(1989).
!
! 90DEA : Dean,A.M., Detailed Kinetic Modeling of Autocatalysis in Methane
! Pyrolysis, J. Phys. Chem., 94(4), 1432-1439(1990).

```
!
!   91CHE/WAR : Chevalier, C. and J. Warnatz, A Tentative Detailed Chemical
!       Scheme for the Oxidation of Benzene-Air Mixtures,
!       Div. of Fuel Chemistry, ACS, New York, 36(4), 1486-93 (1991).
!
!   91KO/ADU  : Ko, T., G.Y. Adusei, and A. Fontijn, Kinetics of the O(3P)+C6H6
!       Reaction over a Wide Temperature Range,
!       J. Phys. Chem., 95(22), 8745-8748(1991).
!
!   91TSA     : Tsang, W., Chemical Kinetic Data Base for Combustion Chemistry.
!       Part V. Propane, J. Phys. Chem. Ref. Data, Vol.20, 221-274(1991).
!
!   92BAU/COB :Baulch,D.L., C.J. Cobos, R.A. Cox, C. Esser, P. Frank, Th. Just,
!       J.A. Kerr, M.J. Pilling, J. Troe, R.W. Walker, and J. Warnatz,
!       Evaluated Kinetic Data for Combustion Modelling,
!       J. Phys. Chem. Ref. Data, 21(3), 411(1992).
!
!   92BEN     : Benson, S.W., Radical Processes in the Pyrolysis of Acetylene,
!       Int. J. Chem. Kinet., 24, 217-237(1992).
!
!   93BOZ/DEA : Bozzelli, J.W., and A.M. Dean, Hydrocarbon Radical Reaction with
!           O2: Comparison of Ally, Formyl, and Vinyl to Ethyl.
!           J. Phys. Chem., 97(17), 4427-4441(1993).
!
!   92GLA     : Glarborg, P., A Reduced Mechanism For Nitrogen Chemistry in
!       Methane Combustion, 24th Symposium (Int.) on Combustion, 889-898(1992).
!
!   92HID/MAS : Hidaka, Y., H. Masaoka, H. Oshita, T. Nakamura, K. Tanaka, and
!       H. Kawano, Thermal Decomposition of Vinylacetylene in Shock Waves.
!       Int. J. Chem. Kinet., Vol. 24, 871-885(1992).
!
!   92KER/XIE : Kern,R.D., K. Xie, and H. Chen, The Reactions of Propargyl Chloride
!       and 1,5 Hexadiyne Behind reflected Shock Waves,
!       **********, 1423-
!
!   92TRE/MEN : Trevino,C., and F. Mendez, Reduced Kinetic Mechanism for Methane
!       Ignition, 24th Symposium (Int.) on Combustion, 121-127(1992).
!
!   92WES     : Westmoreland, P.R., Thermochemistry and Kinetics of C2H3+O2
!           Reactions, Combust. Sci. and Tech., Vol.82, 151-168 (1992).
END
```

10.4 REFERENCES

Alzueta, M.U., M. Oliva and P. Glarborg, "Parabenzoquinone pyrolysis and oxidation in a flow reactor." *Int. J. Chem. Kin.* **30**, 683 (1998).

Baulch, D.L., C.J. Cobos, R.A. Cox, C. Esser, P. Frank, T. Just, J.A. Kerr, M.J. Pilling, J. Troe, R.W. Walker and J. Warnatz, "Evaluated kinetic data for combustion modelling." *J. Phys. Chem. Ref. Data* **21**(3), 411 (1992).

Bozzelli, J.W., A.Y. Chang and A.M. Dean, "Molecular density of states from estimated vapor phase heat capacities." *Int. J. Chem. Kin.* **29**(3), 161 (1997).

Brouwer, L., C.J. Cobos, J. Troe, H.-R. Dübal and F.F. Crim, "Specific rate constants $k(E,J)$ and product state distributions in simple bond fission reactions. II. Application to HOOH→OH+OH." *J. Chem. Phys.* **86**(11), 6171 (1987).

Burcat, A. and B. McBride, "Ideal gas thermodynamic data for combustion and air-pollution use." Aerospace Engineering Report TAE 732, Israel Institute of Technology, Technian (1995 and updates).

Burcat, A., F.J. Zeleznik and B.J. McBride, "Ideal gas thermodynamic properties for the phenyl, phenoxy and *o*-biphenyl radicals." NASA Technical Memorandum 83800, (1985).

Cobos, C.J., H. Hippler and J. Troe, "High-pressure falloff curves and specific rate constants for the reactions H + O_2 = HO_2 = HO + O." *J. Phys. Chem.* **89**, 342 (1985).

Dean, A.M., J.W. Bozzelli and E.R. Ritter, "CHEMACT: A computer code to estimate rate constants for chemically-activated reactions." *Combust. Sci. Technol.* **80**, 63 (1991).

Emdee, J.L., K. Brezinsky and I. Glassman, "A kinetic model for the oxidation of toluene near 1200 K." *J. Phys. Chem.* **96**, 2151 (1992).

Fulle, D., H.F. Hamann, H. Hippler and J. Troe, "High-pressure range of the addition of HO to HO. III. Saturated laser-induced fluorescence measurements between 200 and 700 K." *J. Chem. Phys.* **105**(3), 1001 (1996).

Gardiner, W.C., Ed. (1984). Combustion Chemistry. New York, Springer-Verlag.

Lay, T.S., J.W. Bozzelli and J.H. Seinfeld, "Atmospheric photochemical oxidation of benzene: benzene + OH and the benzene-OH adduct (hydroxyl-2,4-cyclohexadienyl) + O_2." *J. Phys. Chem.* **100**, 6543 (1996).

Ritter, E.R. and J.W. Bozzelli, "THERM: Thermodynamic property estimation of gas phase radicals and molecules." *Proceedings of 12th Int. CODATA Conf.*, July 15-19 (1990).

Ritter, E.R., J.W. Bozzelli and A.M. Dean, "Kinetic study on thermal decomposition of chlorobenzene diluted in H_2." *J. Phys. Chem.* **94**(6), 2493 (1990).

Shandross, R.A., "Experimental and theoretical study of hydrogen and benzene destruction chemistries." Ph.D. Thesis, Department of Chemical Engineering, Massachusetts Institute of Technology, Cambridge, MA (1996).

Stewart, J.J.P., "MOPAC." Quantum Chemistry Program Exchange, Indiana University Chemistry Department, (1990).

Troe, J., "Thermal dissociation and recombination of polyatomic molecules." in *Fifteenth Symposium (International) on Combustion*, The Combustion Institute, Pittsburgh, 667 (1974).

Warnatz, J., "Rate coefficients in the C/H/O system." in *Combustion Chemistry*, W. C. Gardiner, Ed., Springer-Verlag, New York, 197 (1984).

Westmoreland, P.R., J.B. Howard, J.P. Longwell and A.M. Dean, "Prediction of rate constants for combustion and pyrolysis reactions by bimolecular QRRK." *AIChE Journal* **32**(12), 1971 (1986).

Yu, T. and M.C. Lin, "Kinetics of the $C_6H_5 + O_2$ reaction at low temperatures." *J. Am. Chem. Soc.* **116**, 9571 (1994).

Zhang, H.-Y. and J.T. McKinnon, "Elementary reaction modeling of high-temperature benzene combustion." *Combust. Sci. Technol.* **107**, 261 (1995).

Zhong, X. and J.W. Bozzelli, "Thermochemical and kinetic analysis on the addition reactions of H, O, OH, and HO_2 with 1,3 cyclopentadiene." *Int. J. Chem. Kin.* **29**, 893 (1997).

Zhong, X. and J.W. Bozzelli, "Thermochemical and kinetic analysis of the H, OH, HO_2, O, and O_2 association reactions with cyclopentadienyl radical." *J. Phys. Chem.* **102**, 3537 (1998).